



HAL
open science

Synthesis and physical properties of helical nanosized quinoline-based foldamers: structure, dynamics and photoinduced electron transport

Xuesong Li

► **To cite this version:**

Xuesong Li. Synthesis and physical properties of helical nanosized quinoline-based foldamers: structure, dynamics and photoinduced electron transport. Organic chemistry. Université de Bordeaux; Université de Liège, 2016. English. NNT : 2016BORD0013 . tel-01326993

HAL Id: tel-01326993

<https://theses.hal.science/tel-01326993>

Submitted on 6 Jun 2016

HAL is a multi-disciplinary open access archive for the deposit and dissemination of scientific research documents, whether they are published or not. The documents may come from teaching and research institutions in France or abroad, or from public or private research centers.

L'archive ouverte pluridisciplinaire **HAL**, est destinée au dépôt et à la diffusion de documents scientifiques de niveau recherche, publiés ou non, émanant des établissements d'enseignement et de recherche français ou étrangers, des laboratoires publics ou privés.

THÈSE COTUTELLE PRÉSENTÉE
POUR OBTENIR LE GRADE DE
DOCTEUR DE
L'UNIVERSITÉ DE BORDEAUX
ET L'UNIVERSITÉ DE LIÈGE

ÉCOLE DOCTORALE DES SCIENCES CHIMIQUES UB
ÉCOLE DOCTORALE DE SCIENCES (CHIMIE) ULg
SPÉCIALITÉ : CHIMIE ORGANIQUE

Par **Xuesong LI**

**Synthesis and Physical Properties of Helical Nanosized
Quinoline-based Foldamers**
– Structure, dynamics and photoinduced electron transport

Sous la direction de : Ivan HUC
et de : Anne-Sophie DUWEZ

Soutenue le 28 Janvier 2016

Membres du jury :

M. LIMA, J. C.	Associate Professor, Universidade Nova de Lisboa	Rapporteur
M. GAN, Q.	Full Professor, Huazhong Univ. of Sci. & Tech.	Rapporteur
M. LECOMMANDOUX, S.	Full Professor, Bordeaux INP	Président
Mme. JIANG, N.	Associate Professor, Nanjing Medical University	Examineur
M. HUC, I.	Directeur de Recherche, CNRS	Directeur de thèse
Mme. DUWEZ, A.-S.	Full Professor, Université de Liège	Directrice de thèse
M. MAURIZOT, V.	Chargé de recherche, CNRS	Membre invité

穷则独善其身，达则兼济天下

-- 孟子

As troubled, improve yourself firstly;

as valued, benefit the world then.

-- Mencius

Résumé de ma thèse

Les foldamères sont des architectures moléculaires artificielles inspirées de la structure et de la fonction des polymères naturels (e.g. ADN et protéines). Pour mimer les fonctions de tels polymères naturels, des foldamères de grande taille et de poids moléculaire importants sont requis. La synthèse de foldamères de taille nanométrique possédant une structure secondaire bien définie reste cependant un challenge. En effet, la synthèse des foldamères oligoamide aromatique développée dans notre groupe se heurte à la faible réactivité de l'amine aromatique, particulièrement encombrés du fait du repliement de ces molécules.

Les principaux travaux de thèse ont consisté en la synthèse de ces nano-objets, les foldamères d'amide aromatiques, possédant un squelette quinoline et une taille nanométrique. Dans un premier temps une méthode de synthèse de ces composés a été élaborée et une étude de multi bromation one-pot de ces oligomères a été réalisée permettant d'observer un accroissement de la solubilité de ces foldamères permettant d'accéder à des composés possédant jusqu'à 96 unités. Après avoir obtenu ces différents oligoamides de quinoline de taille nanométrique, la caractérisation des propriétés physico-chimiques des foldamères a été étudiée en solution et en phase gazeuse.

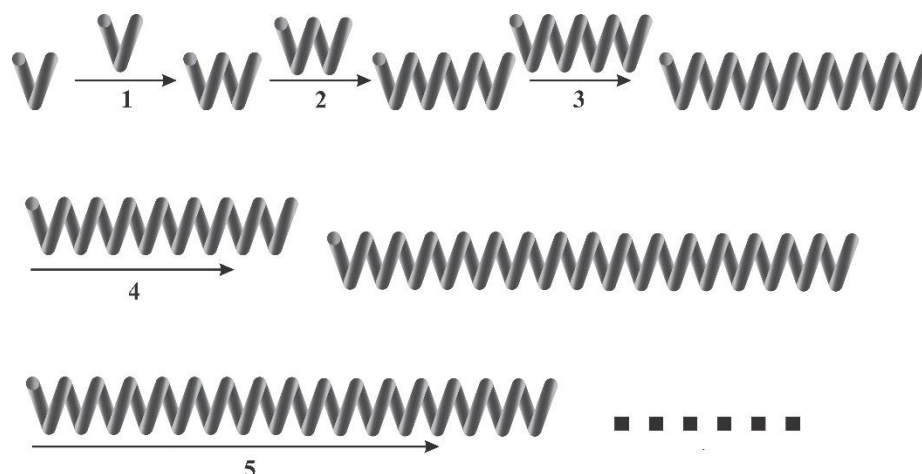


Figure I Schéma de la stratégie de doublement de segment

Pour synthétiser ces nano foldamères aromatiques, une stratégie de doublement de segment a été utilisée. Deux réactifs (chlorure d'acide et amine) de tailles équivalentes sont couplés à haute concentration pour donner un produit dont la taille est double à celle des réactifs initiaux (Figure I). Par exemple, un chlorure d'acide et l'amine d'un foldamère de 8 unités (8mer) peuvent être couplés pour former un foldamère de 16 unités. Cette réaction simple, en théorie, se heurte cependant à des difficultés importantes de purification du produit désiré. En effet, la formation d'un sous-produit, un anhydride, formé par la réaction entre le chlorure d'acide et son acide correspondant est la plupart du temps observée. Or cet anhydride possède une polarité similaire au produit désiré. Afin de permettre une synthèse convergente et possédant des purifications plus aisées, nous avons cherché des conditions permettant d'hydrolyser le

sous-produit anhydride dans le milieu réactionnel. Nous avons découvert qu'une hydrolyse propre de ces anhydrides repliés en hélice pouvait être réalisée en chauffant au reflux le mélange produits, réactifs en excès et sous-produits, dans un mélange pyridine/eau. De plus, pour s'affranchir des séparations chromatographiques difficiles entre le produits de couplage et l'amine de départ n'ayant pas réagi, un excès de chlorure d'acide a été utilisé. Avec cette stratégie de doublement de segment et les conditions appropriées, une série de nano foldamères a été synthétisée possédant jusqu'à 64 unités. Pour ce composé un problème de solubilité a été observé

La bromation one-pot de ces foldamères a été étudiée et appliquée avec succès pour des 8mer, 16mer et même 32mer. L'atome H de la position 5 du cycle quinoline a été substitué par des atomes Br, grâce à l'utilisation d'un excès de N-bromosuccinimide (NBS) pour donner un produit bromé unique (Figure II). De façon intéressante, ces foldamères bromés montrent une solubilité accrue par rapport à leurs homologues non bromés. Cela a permis la synthèse de foldamères plus longs que 64 unités. Ainsi après bromation des précurseurs réactionnels, de longs foldamères bromés ont été préparés (jusqu'à 96mer) et ont tous montré une bonne solubilité

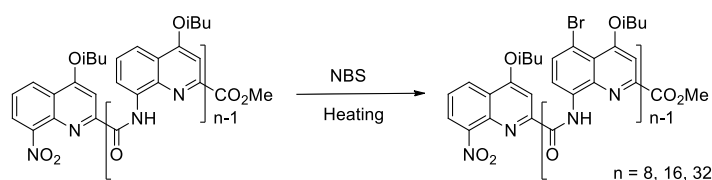


Figure II Schéma de la bromation one-pot des foldamères de quinoline

Les propriétés physico-chimiques en solution et en phase gazeuse de ces nano foldamères ont été explorées en collaboration avec d'autres groupes. Avec les Dr. Frédéric Rosu et Dr. Valérie Gabelica à l'IECB à Bordeaux (France), la spectrométrie de masse de mobilité ionique a été utilisée pour explorer la conformation de ces foldamères en phase gazeuse. Les résultats expérimentaux et issus de modélisation révèlent que la conformation hélicoïdale des foldamères (bromés ou non) est suffisamment rigide et conservée en phase gaz. Il a également été montré que la bromation n'affecte pas cette conformation hélicoïdale. Trois conformations de foldamères anhydrides bromés ont été observées en phase gazeuse, ce qui est probablement dû à la flexibilité de la liaison anhydride. En coopération avec le Prof. Aldrik H. Veders à l'université de Wageningen (Pays-Bas), la diffusion translationnelle des foldamères en solution a été étudiée par RMN DOSY (Figure III). Un mélange de différents foldamères peut-être séparé sur un spectre grâce à leurs coefficients de diffusion translationnels. Il est montré qu'il existe une dépendance entre les racines cubiques des coefficients de diffusion du poids moléculaire des foldamères et le nombre d'unités de quinoline dans leur séquence. Les rayons hydrodynamiques résultants des foldamères en solution augmentent en effet avec le nombre d'unités quinoline dans la séquence. En collaboration avec le Prof. Jean Duhamel à l'université de Waterloo (Canada), des résultats préliminaires de spectroscopie de fluorescence d'anisotropie ont montré qu'en solution, il y avait aussi

une diffusion rotationnelle des foldamères. Pour ce faire, une série de foldamères possédant une fonction perylene liée de façon rigide au squelette de l'oligomère a été préparée. Ces composés ont montré une anisotropie mesurable dans le toluène et l'alcool benzylique. Les temps de corrélation de rotation des foldamères ont aussi été obtenus dans différents solvants.

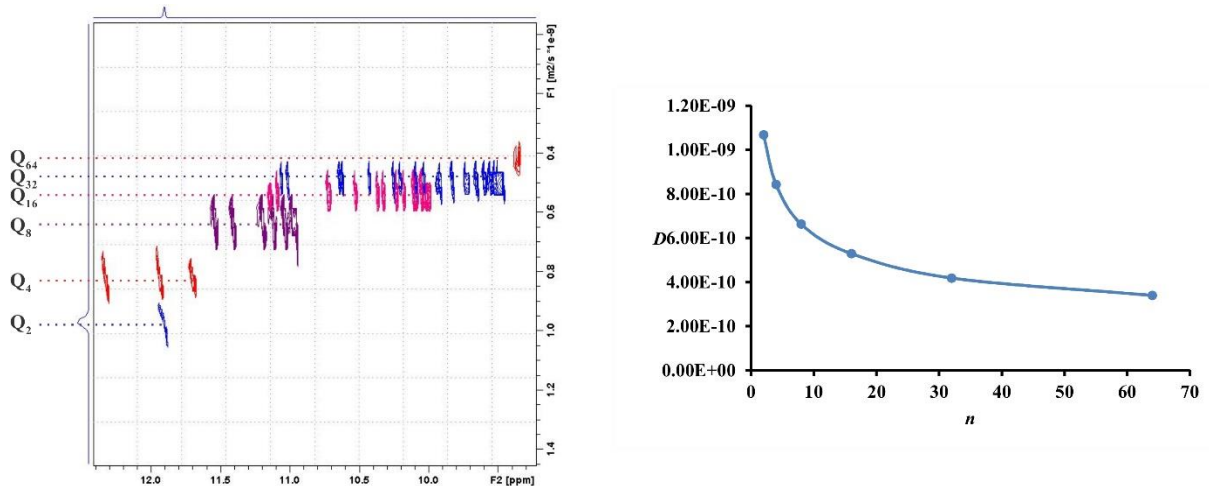


Figure III Les différents foldamères séparés spectralement par leurs coefficients de diffusion translationnelle.

Des études mécaniques à l'échelle de la molécule unique ont été menées sur les foldamères par AFM-SMFS (spectroscopy-based single molecule force spectroscopy, spectroscopie à force atomique, Figure IV a). Pour cette étude des foldamères de différentes tailles et possédant à chaque extrémités des fonctions permettant leur greffage sur une surface d'or d'un côté par l'intermédiaire d'une fonction thiol et une chaîne ethyleneglycol de l'autre pour s'adsorber à la surface du tip d'AFM ont été synthétisés. Lors de l'extension de ces foldamères par une force de traction exercée par le tips de l'AFM on obtient une courbe de force. Cette courbe montre un plateau dont la longueur est proportionnelle à la longueur de l'oligomère. Ce plateau a été attribué à la rupture successive des forces non covalentes maintenant la structure hélicoïdale du foldamère. Les résultats obtenus dans la DMF fraîchement distillé (anhydre) diffèrent de ceux dans la DMF contenant de l'eau. Cela suggère que le solvant a un effet important sur la structure et la stabilité de ces structures secondaires repliés.

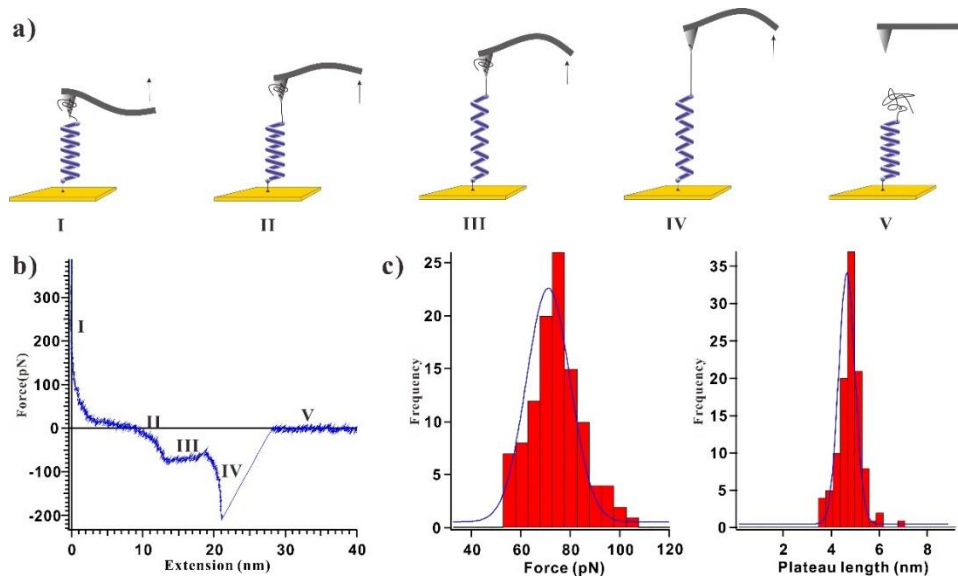


Figure IV Force de molécule unique spectroscopie de l'foldamère (17mer) dans du DMF fraîchement distillé l'interprétation de la séquence des événements qui ont lieu au cours de la traction (a), le profil résultant force-extension (b) et les histogrammes correspondants (c) de la rupture la force et la longueur du plateau ($n = 108$).

En collaboration avec les Dr. Sergey Denisov et Nathan D. McClenaghan à l'ISM à Bordeaux (France), ces nano foldamères ont été appliqués à un transfert d'électrons photo-induit (Figure V). Après avoir été fonctionnalisés par un donneur d'électrons (oligo *p*-phenylene vinylene – OPV) et un accepteur d'électrons (perylene bisimide – PB) à chaque extrémité, les foldamères (Q_n) deviennent des ponts pour le système de transfert d'électrons. Les analyses des données expérimentales de l'extinction de la fluorescence montrent que la vitesse de séparation de charge de ces systèmes OPV- Q_n -PB est rapide (de l'ordre de la nanoseconde) et que la recombinaison de ces charges est extrêmement lente (de l'ordre de la microseconde). Les données d'extinction de fluorescence et de spectroscopie d'absorption transitoire (TRABS) révèlent que le mécanisme général de transfert d'électrons menant à un état de séparation de charge dans ces systèmes OPV- Q_n -PB peut être décrit par un principe multi-étapes, appelé mécanisme de hopping.

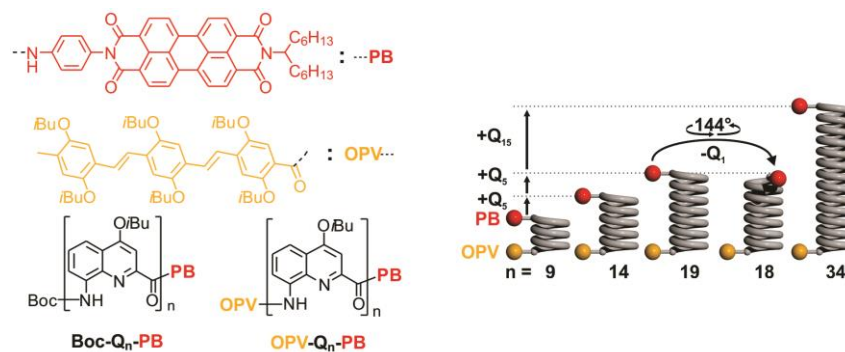


Figure V Transfert d'électrons photo-induit par nano foldamères

Comme précédemment cité la construction de molécules de grande taille et de haut poids moléculaire est un prérequis essentiel afin d'obtenir des objets moléculaires pouvant mimer les fonctions des biopolymères tels que les protéines. Lors de ma thèse, nous avons développé la synthèse de nano foldamères aromatiques et après avoir étudié leurs propriétés physico-chimiques nous avons pu les utiliser en tant que matériaux moléculaires pour conduire des électrons. La poursuite des recherches sur ces nano foldamères nous permettra aussi de mieux comprendre comment la nature fonctionne et d'obtenir plus d'idées concernant les fonctions / applications de ces foldamères aromatiques. La construction d'édifices moléculaires plus complexes comprenant non seulement des structures hélicoïdales mais aussi des structures de types feuillets et la combinaison de ces deux structures secondaires pourra de plus être envisagée.

Acknowledgement

Even though I wrote this thesis, a number of people have contributed to its production. Without the help from them, I cannot complete my thesis. I express my sincerest gratitude to these people who helped and encouraged me during my PhD study.

I owe my supervisors, Dr. Ivan Huc, Prof. Anne-Sophie Duwez and Dr. Victor Maurizot, a great debt of gratitude for your excellent guidance on my research. You have provided me the great research surroundings which allowed me to learn and understand deeply the field of chemistry. What I have learned from you undoubtedly influences me and my academic life. I am grateful to Dr. Ivan Huc for offering me a chance to study in Europe and for training me with his kind patience and erudite knowledge. I have learned a lot from you professionally as well as personally. I am appreciative of all the support from Prof. Anne-Sophie Duwez that has helped me a lot. I would like to ventilate my thankfulness to Dr. Victor Maurizot who has been always standing by me, provided me a wonderful research support and always encouraged me! One simply cannot wish for a supervisor friendlier than you. I really appreciate and cherish our friendship built during my PhD study.

Traveling and studying between France and Belgium, I have been aided by many other people: thank Dr. Yann Ferrand, Dr. Lucile Fischer, Dr. Eric Meriet, Dr. Nicolas Willet and Dr. Perrine Lussis for your favors with and valuable suggestions to the related research.

I would like to thank all my collaborators: Dr. Markandeya Nagula, Dr. Sergey Denisov, Dr. Nathan D. McClenaghan, Dr. Frédéric Rosu, Dr. Valérie Gabelica, Prof. Aldrik H. Velders and Prof. Jean Duhamel. Without your help, I cannot finish such a thesis full of broad research topics. Collaborations with all of you has offered me awe-inspiring opportunities to learn those interesting knowledge and research fields, which has extended my view of science and knowledge of fields beyond organic/supramolecular chemistry.

I would also like to thank Maïle Vallade, Michael Singleton, Christos Tsiamantas, Weixia Zhang, Ji Liu, Nan Jiang, Xiang Wang, Xiaobo Hu, Jinhua Wang, Julie Enert, Antoine Jacquet, Antoine Meunier, Soumen De, Subrata Saha, Damien Sluysmans, Floriane Devaux, and Marie Asano. I really appreciate the encouragement and help from all of you when I was depressed and lost my confidence. And meanwhile, I address my thanks to the group members in Ivan

Huc's group and Anne-Sophie Duwez's group. The time spent together is memorable.

Thank Institut Européen de Chimie et Biologie, University of Bordeaux and Department of Chemistry at University of Liege to provide the related support and equipment that I needed to carry out my experiments and complete my thesis. Also thank the International Doctor School in Functional Materials and the financial support of the Erasmus Mundus scholarship.

Last but not the least, I sincerely thank my parents and family to support me these years. I can always obtain the most heart-warming support from you!

List of abbreviations

- AFM:** atomic force spectroscopy
- AFM-SMFS:** atomic force microscopy-based single molecule force spectroscopy
- BzOH:** benzyl alcohol
- Boc:** *tert*-butyloxycarbonyl
- C5₂-PB:** *N,N* Bis(3-pentyl)perylene bisimide
- CCS:** collision cross section
- CD:** circular dichroism
- CHCl₃:** chloroform
- CDCl₃:** deuterated chloroform
- CR:** charge recombination
- CS:** charge separation
- D-B-A:** donor-bridge-acceptor
- DCM:** dichloromethane
- DDS:** dodecyl sulfide
- DIPEA:** diisopropylethylamine
- DMF:** *N,N*-dimethylformamide
- DOSY:** diffusion ordered spectroscopy
- DTIMS:** drift tube ion mobility spectrometry
- ESI:** electrospray ionization
- Ghosez reagent:** 1-chloro-*N,N*,2-trimethyl propenylamine
- GSB:** ground state-bleaching
- GPC:** gel permeation chromatography
- HOMO:** highest occupied molecular orbital
- HRMS:** high resolution mass spectroscopy
- i*BuOH:** isobutanol
- IMS:** ion mobility spectrometry
- IMS-MS:** ion mobility spectrometry-Mass spectrometry
- LUMO:** lowest unoccupied molecular orbital

MALDI: matrix-assisted laser desorption/ionization

Me: methyl

MeOH: methanol

MS: Mass spectrometry

M.W.: molecular weight

NBS: N-bromosuccinimide

NMR: nuclear magnetic resonance

NOESY: nuclear overhauser effect spectroscopy

OPV: oligo *p*-phenylene vinylene

PB: perylene bisimide

PB-Q_n: perylene bisimide functionalized foldamer containing *n* quinoline units

PEG: poly(ethylene glycol)

ppm: parts per million

PyBOP: benzotriazol-1-yl-oxytripyrrolidinophosphonium hexafluorophosphate

PA: projection approximation

PSA: projection superposition approximation

PET: photo-induced electron transfer

Q_n: quinoline-based foldamer containing *n* quinoline units

^mBrQ_n: quinoline-based foldamer containing *n* quinoline units and *m* bromines on the backbone

quant.: quantitative

ROESY: rotating-frame Overhauser spectroscopy

rt: room temperature

SOMO: singly occupied molecular orbital

T: temperature

TFA: trifluoroacetic acid

THF: tetrahydrofuran

TLC: thin layer chromatography

TM: trajectory model

TRABS: transient absorption spectroscopy

Contents

I Introduction	1
1 Foldamer and synthesis of long foldamers.....	1
1.1 Foldamer.....	1
1.2 Synthesis of nanosized foldamers and its current challenge	5
2 Characterization of supramolecular structures of foldamers.....	6
3 The objectives of my thesis	8
4 Reference.....	11
II Segment doubling synthesis of nano-sized foldamers	19
1 Introduction	19
2 Synthesis.....	22
3 Results and discussion.....	24
4 Conclusion.....	48
5 Experimental Section.....	49
5.1 Methods of NMR.....	49
5.2 Methods of X-Ray Crystallography	49
5.3 Summary of X-Ray Crystallography.....	52
5.4 Methods of Chemical Synthesis	53
6 References	73
III Assessment of helix rigidity in solution and in gas phrase	77
1 Introduction	77
2 Ion mobility spectrometry-Mass spectrometry (IMS-MS).....	81
2.1 Introduction	81
2.2 Results and discussion.....	85
2.3 Conclusion.....	90
2.4 Experimental section	90
3 Diffusion-ordered spectroscopy (DOSY).....	92
3.1 Introduction	92
3.2 Results and discussion.....	96
3.3 Conclusion.....	103
3.4 Experimental section	103

4 Fluorescence anisotropy spectroscopy	104
4.1 Introduction	104
4.2 Results and discussion	106
4.3 Conclusion	112
4.4 Experimental section	112
5 General conclusion	115
6 Reference	116
IV Mechanochemistry of foldamers	120
1 Introduction	120
2 Synthesis and basic principle of AFM-SMFS	123
2.1 Synthesis	123
2.2 Basic principle of AFM-SMFS	124
3 Results and Discussion	126
4 Conclusion and perspectives	134
5 Experimental Section	136
5.1 Methods of NMR	136
5.2 Methods of Chemical Synthesis	136
5.3 Measurement of AFM-SMFS	139
6 Reference	141
V Photophysics of Foldamers	145
1 Introduction	145
2 Synthesis and Measurements	148
2.1 Synthesis	148
2.2 Measurement	151
3 Results and discussion	152
4 Conclusion	163
5 Experiments	164
5.1 Methods of NMR	164
5.2 Methods of Chemical Synthesis	164
6 References	178
VI Conclusion and perspective	182

I Introduction

1 Foldamer and synthesis of long foldamers

1.1 Foldamer

Supramolecular chemistry, beyond the conventional research domain of molecules, is related to the chemical systems comprised of diverse number of discrete molecular subunits, assembled or organized by special force(s) varying from weak non-covalent forces (hydrogen bonding, metal-ligand coordination, electrostatics, *etc.*) to strong covalent bonds. Even though the word ‘supramolecular’ had emerged in biology since 1930¹, its appearance in chemistry field was in 1970s, described by Jean-Marie Lehn²:

“Just as there is a field of molecular chemistry based on the covalent bond, there is a field of supramolecular chemistry, the chemistry of molecular assemblies and of the intermolecular bond.”

He later defined the concept of supramolecular chemistry as:³

“Supramolecular chemistry may be defined as “chemistry beyond the molecule,” bearing on the organized entities of higher complexity that result from the association of two or more chemical species held together by intermolecular forces.”

In the last decades, the field of supramolecular chemistry has been developed intensively, from molecular recognition, molecular devices to bionics. As a growing popular branch of supramolecular chemistry, foldamer chemistry, mimicking the structural and functional abilities of natural biopolymers (like proteins, nucleic acids and polysaccharides), has been attracting more and more attention from all over the world.⁴ Foldamer can be defined as artificial folded molecular architectures inspired by the structures and functions of biopolymers.⁵ Over the last approx. twenty years, the field of foldamer has aggrandized itself from initial mimicry of natural biopolymers with similar building blocks to extensive investigation by using various designed monomers that are obviously different from those in Nature (Figure 1). In Nature, limited

building blocks have been utilized to build up well-defined folded architectures: 20 standard amino acids in proteins¹ and 5 canonical nucleobases in DNA and RNA. In contrast, building blocks in foldamer initially emerged as natural amino acid (α -) analogues, for example, β -, γ - and δ - amino acids, which are 'biotic' and are based on aliphatic chains (Figure 1a-d). With further development of foldamer chemistry, 'abiotic' aromatic building blocks (Figure 1e-g) were designed and introduced into foldameric backbones. These aromatic foldamers, especially aromatic amide oligomers, are becoming more and more popular and important due to their special advantages: stability of folded structure, predictability of folding modes, propensity of crystallization and relative ease of synthesis.⁵ Besides difference in chemical structure, for abiotic aromatic foldamers, principles of folding also differ from those for biotic aliphatic foldamers. Hybrids, which are built up by biotic aliphatic and abiotic aromatic building blocks, appear as the third type of foldamer in which some unsuspected characters are able to be realized. A brief introduction of these three types of foldamers are presented as follow.

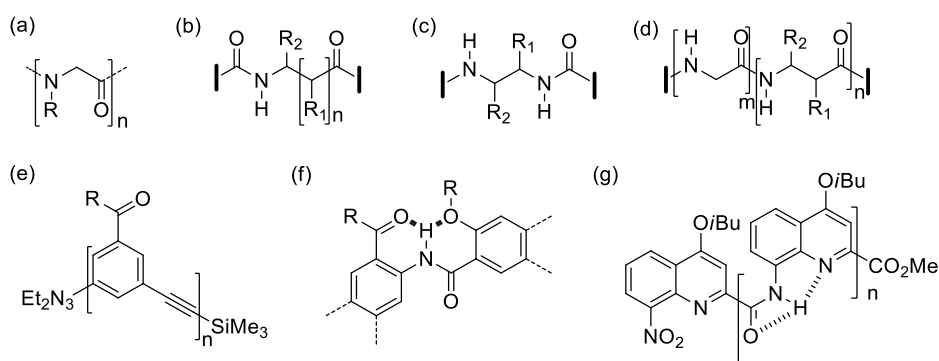


Figure 1 Representative backbones used in foldamer chemistry: a) peptoid, b) biotic peptides based on β - ($n = 1$), γ - ($n = 2$) and δ - ($n = 3$) amino acids, c) oligourea, d) α/β peptide, e) m-phenylene ethynylene oligomer, (f) oligomer based on *p*-phenylenediamine/*p*-phthalic acid and (g) quinoline-based oligomer.

For biotic aliphatic foldamers that basically mimic the structures and biological properties of natural peptides and nucleic acids, their building blocks include but non-limit un-natural amino acids⁶ (Figure 1c). β -peptides were firstly investigated as foldamer inspired by their natural analogue α -peptide. Helices formed by these β -peptides foldamers showed a stronger stability than α -peptide (Figure 1b).^{6a, 6b} Heterogeneous oligomers composed of various aliphatic

¹ Up to now, 23 proteinogenic amino acids have been found, including 20 standard amino acids and 3 non-standard amino acids which are involved by some special translation mechanisms: selenocysteine, pyrrolysine and N-formylmethionine.

building blocks (biotic and abiotic) has also been prepared in order to offer more potential. Generally, there are two approaches to construct heterogeneous foldamers: the ‘block’ oligomer and the ‘interspersed’ oligomer. The former is comprised of several homogeneous segments of peptides that combine with each other, and the later consists of several types of subunits (amino acids) that intersperse in a regular pattern through the peptide sequence. Varied approach can offer different peptides with diverse characters, even though the number and type of subunits (amino acids) are totally the same. Gellman and his coworkers pioneered foldamers composed of heterogeneous sequences by combining α -amino acid and β -amino acids and systematically studied them (Figure 1d).⁷ In addition to un-natural amino acids, peptide nucleic acids (PNAs)⁸, N-substituted oligoglycines (peptoids)⁹ and N,N'-linked urea¹⁰ have been also used as building block to construct abiotic foldamers (Figure 1).

For abiotic aromatic foldamers, existence of aryl groups ensures the stability in structure, and also alters the principles of folding formation.⁵ Hydrogen bonding and hydrophobic interaction play key role in the folding of aliphatic foldamers. They do the same in the structuration of aromatic foldamer. Meanwhile, so too have π - π stacking and geometry of monomer strong influence upon the resulting conformation of aromatic foldamers. In the case of oligoamide aromatic foldamers, hydrogen bonding only take place locally among the neighboring monomers rather than the ‘long-range’ ones that are not close to each other, which differs from the ‘long-range’ H-bond interactions in aliphatic foldamers, avoiding appearance of the complicated alternative conformations.¹¹ Main backbones of aromatic foldamers include phenylene ethynylene¹², aza-heterocycles¹³ Benzoylurea¹⁴ and aromatic (benzyl¹⁵ and heterocyclic¹⁶) amides.¹⁷ Compared with the aliphatic foldamers, all aromatic foldamers exhibit more invariable folded structures due to existence of the π - π stacking and the rigidity of designed monomers. Because of the predictability of the conformation of aromatic oligoamide foldamer, use of heterogeneous sequence that are built up by varied aromatic monomers gives access to construction of more sophisticated structure, For example, the programmed combination of aromatic heterocyclic residues like pyridine-, quinoline- and anthracene-monomers is able to not only generate nanosized helical foldamers (Figure 2a), but also provide molecular containers of variable internal cavities with controllable volumes¹⁸ (Figure 2b). These forming cavities, in which central residues construct a large space and terminal ones

work as cap, are able to encapsulate special guest molecules, for example saccharides¹⁹, with high selection of chirality²⁰ (Figure 2d), and also able to shuffle through a aliphatic rod as molecular machine²¹ (Figure 2c). These aromatic foldamers with well-disciplined sequences have allowed the host-guest interactions to illustrate their special functions which are beyond those of biopolymers.^{19b-d, 21a}

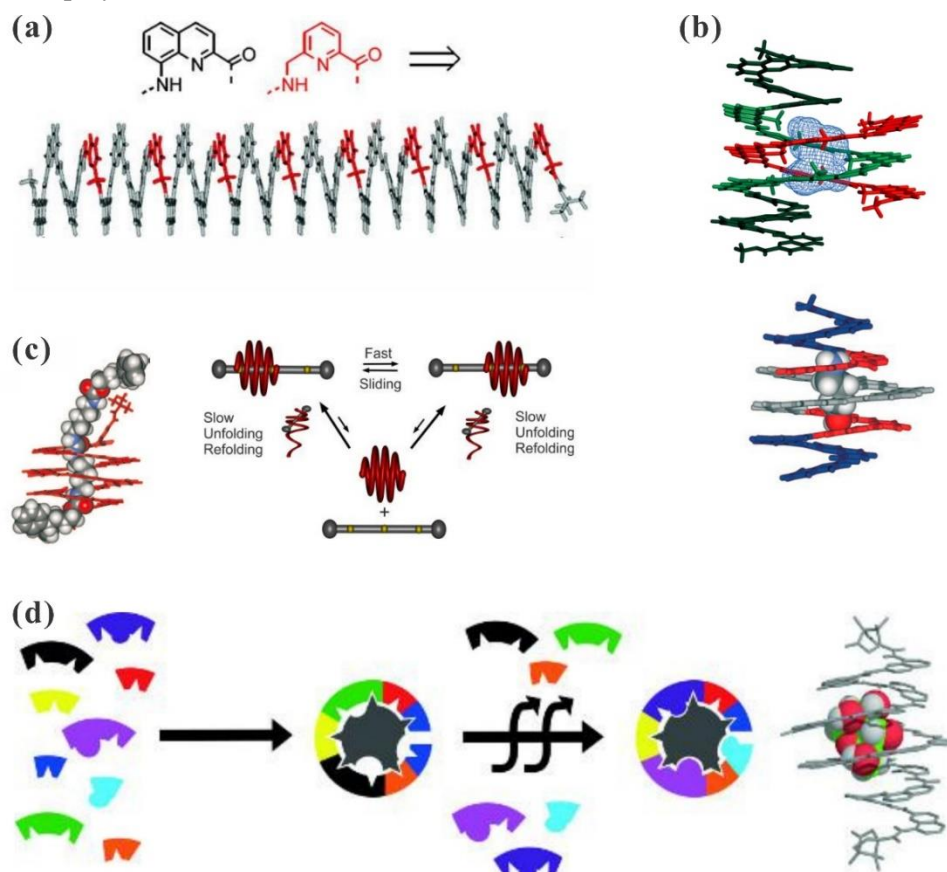


Figure 2 Crystal structures of (a) 5.6 nm aromatic foldamer with 40 units, (b) foldamer capsules with diverse inner volumes, (c) foldamer-based molecular device and (d) helically folded aromatic oligoamide sequence for the selective encapsulation of fructose.

Hybrid foldamers composed of biotic aliphatic and abiotic aromatic monomers have also been prepared recently and show unconventional structures. Aliphatic and aromatic N, N'-urea-based foldamers formed a large variety of secondary structures including sheet, turn, helix and duplex and these structures have been demonstrated at atomic level.²² Foldamer based on α -aliphatic and α -aromatic amino acids can present strand-like conformation and could be converted into duplex with disulfide crosslink in aqueous media (Figure 3a).²³ Mimicry of protein quaternary structures through intermolecular interaction was also explored by macrocyclic β -sheet peptide of β -aliphatic and α -aromatic amino acids (Figure 3c).²⁴ Helical

conformation can also be obtained depending on the nature of the aromatic unit that is used. When a sequence composed of one natural α -amino acid and two 2-8 amino acid quinolone units²⁵ was synthesized, a helical shape was formed but when the sequence was an alternation of only one of the different units a zip-zag tape conformation occurred (Figure 3b).²⁶

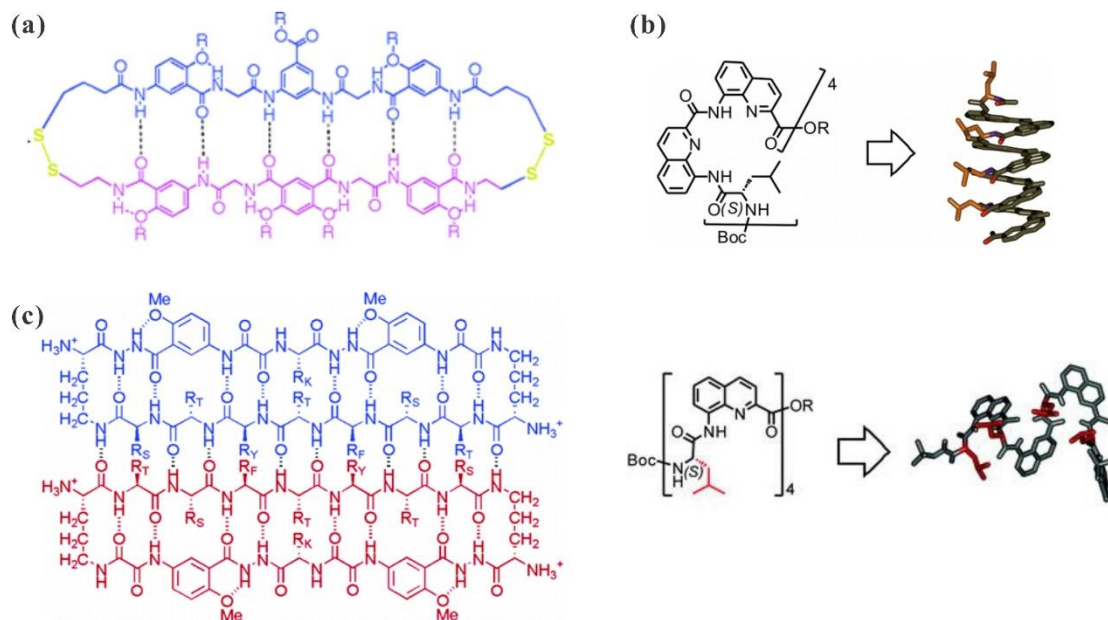


Figure 3 Examples of hybrid foldamers composed of aliphatic and aromatic monomers: (a) disulfide cross-linked duplexes, (b) varied conformations with diverse order of natural α -amino acid and α -aromatic acids and (c) macrocyclic β -sheet peptide of β -aliphatic and α -aromatic amino acids.

Besides design of foldamers, structure, function and application of foldamers have also been extensively investigated.^{6d, 6e, 7, 11c, 27} Even though derived from biological molecules, the research of foldamer now has gone beyond biology, and expanded to other fields: materials chemistry²⁸, nanoscience²⁹, photophysics³⁰, and other branches in supramolecular chemistry.^{4c,}

5, 11a, 17, 27b

1.2 Synthesis of nanosized foldamers and its current challenge

The objects of interest in foldamer chemistry can be in angstrom scale, but also in nano- and even micro-meter regions, which depends on the chemical composition of foldamer molecules and how the resulting molecules interact with each other.⁵ The size of foldamer molecules, in turn, have a mightily effect on the relative structures, properties and even functions.¹⁷ For foldamers composed of *m*-phenylene ethynylene, a random coil structure was probed when the

number of repeating unit was less than 8 and the helical conformation, comprised of six repeating units in each turn, appeared when the number was up to 8.³¹ In general, functions of biopolymers could be realized only by large tertiary and quaternary folded motifs.⁵ By analogy to biopolymer, foldamers of large sizes akin to biopolymers (e.g. protein) become a prerequisite to express related functions. To obtain the protein-sized foldamers, the most crucial challenge lies in the advancement of synthesis methods. Stepwise synthesis that usually is used in organic synthesis only could afford molecules with limited molecular weights.^{28, 32} polymer chemistry is a way that can provide folded molecules of large molecular weight and size^{27, 33}, such as polyisocyanates, polyacetylenes, polyguanidines, polymethacrylates, polyisocyanides, polysilanes and poly(quinoxalin-2,3-diyl)s, but polydispersity of their molecular weights makes the resulting structure and functions difficult to be handled precisely.^{27b} Tools in molecular biology, for example polymerase³⁴, provide access to generating foldamers comprised natural amino acids and nucleic acid, or their analogues (xeno-nucleic acids, XNA). The foldamers whose subunits are apparently differ from those of biopolymers, however, still escaped.

In order to find out an appropriate way of synthesizing foldamer of large size (protein-sized/nanosized), during my PhD study, an approach, the segment doubling strategy, has been developed and was employed to synthesize nanosized aromatic foldamer based on quinoline unit, an aromatic building block differing totally from the natural amino acids or nucleic acids.

2 Characterization of supramolecular structures of foldamers

With the achievements of understanding chemical structures, the design and synthesis of building blocks for foldamers have not appeared as challenging as before in foldamer chemistry. But deep insight into the structural dynamics of these foldamers still represent an issue for researchers, especially for the abiotic family of foldamer. Many techniques/tools, which are generally used in chemistry, biology and even materials science, have been successfully employed to characterize the structure and dynamics of foldamers.

NMR spectroscopy is the most commonly used technique for characterization of foldamers, especially ¹H NMR.³⁵ This technique illustrates the exact chemical information of structures for the relative monomers, intermediates and the final oligomers. 2D NMR also show its ability

to assign signals of both aliphatic³⁶ and aromatic³⁷ foldamers in low-field region where signals of hydrogen atoms from hydrogen-bonded amides shifted to lower region, which indicates the formation of intramolecular hydrogen-bonding (Figure 4). The strength of hydrogen bonding in peptide was determined with hydrogen–deuterium exchange experiments as well.³⁸ But, NMR cannot always work for characterization of foldamers, especially when foldamer molecules aggregate with each other and their characteristic signals overlap to form the broad multiple peaks.¹²

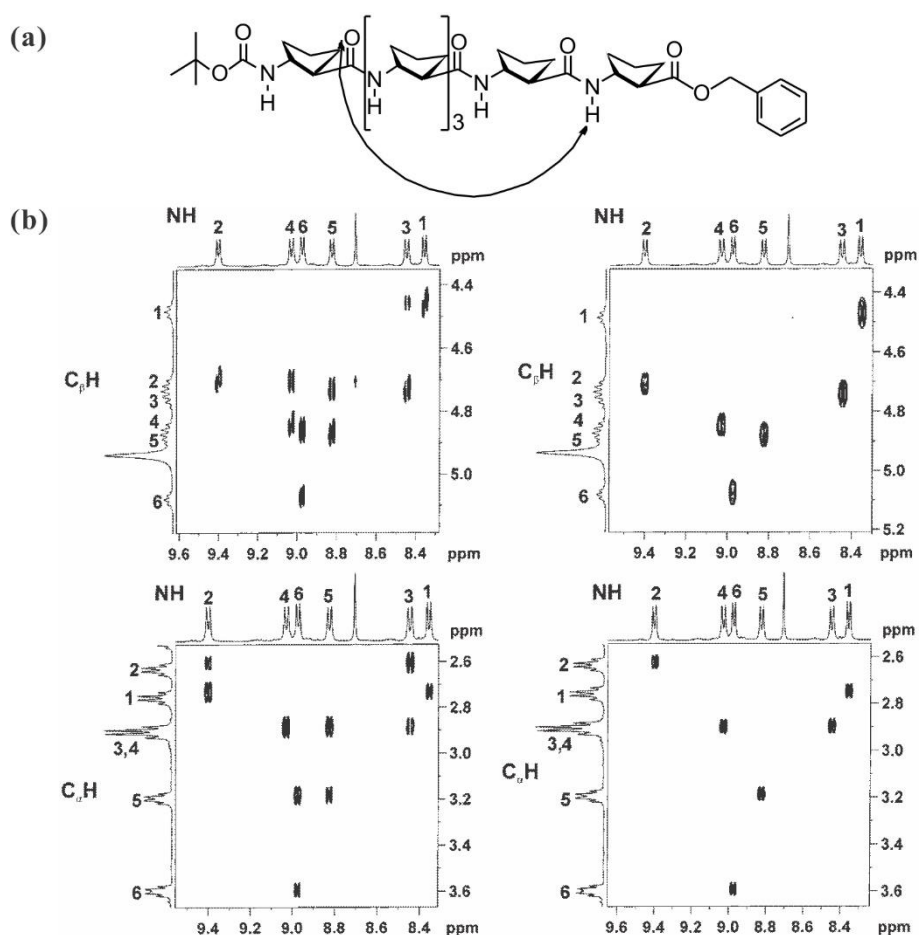


Figure 4 2D NMR applied to assign the signals of hydrogen atoms of amide in aliphatic helical foldamers: (a) chemical structures of helix composed of *trans*-2-aminocyclopentanecarboxylic acid and (b) ROESY (the left two) and TOCSY (the right two) spectra of this aliphatic helix in pyridine-*d*5. The top two spectra represent the ROESY and TOCSY spectra for the NH- $C_{\beta}H$ region; the bottom two clarify the NH- $C_{\alpha}H$ region.

UV/Vis spectroscopy is another technique for foldamer characterization, especially for abiotic foldamers in which aromatic interactions occurred. Some region of absorption spectra could

shift bathochromically due to the strengthened coplanarity of abiotic backbones resulting from the intramolecular π - π stacking.³⁹ For some aromatic foldamers, for example oligoanthranilamide,^{39b} the more is the number of repeat units the more is the red-shift of characteristic peak. This technique also was applied to identify the formation of folded helical structure for oligophenylacetylene¹² and to investigate molecular recognition⁴⁰ and thermodynamic property of β -turn^{39a} of foldamers consisting of m-phenylene ethynylene.

Crystallography is crucial for characterization of foldamers at atomic level, and able to offer significant detailed structural information of folding at solid state. X-ray diffraction of single crystals has revealed to support the structural information of foldamers in solution. Conformations of peptide and aromatic oligoamide at solid state have been found to match well with those characterized by 2D NMR in solution.^{36a, 37} Sometimes, crystallography also has ability to disclose the structure variance at solid phase and in solution.⁴¹ For example, it occurred that one conformation appeared at solid state and two conformations were resolved in solution. The α/β -peptides gave one helix defined by $i, i+3$ C=O...H-N backbone hydrogen bonds at solid phase, rather than two helices (defined by $i, i+3$ C=O...H-N and $i, i+4$ C=O...H-N hydrogen bonds) in solution.^{41d}

Besides techniques mentioned above, fluorescence spectroscopy^{31a}, IR^{41a, 42}, MS⁴³, electron microscopy⁴⁴, AFM image^{27b, 33, 45}, CD^{40-41, 42, 46}, theoretical calculation^{36b, 41a, 42, 47} and electron spin resonance^{31b} are also used in foldamer chemistry to character the supramolecular structures of foldamer molecules. In addition, these techniques are able to provide some other information about structures, like molecular weight, formation of duplex, triplex and quadruple, morphology, chirality and even the number of repeat unit in one turn.^{5, 6d, 6e, 7, 11a, 11c, 17, 27}

3 The objectives of my thesis

In my thesis, the main task is aimed at synthesis of helical nanosized foldamers by using 8-amino-2-quinolinecarboxylic acid as starting monomer and segment doubling strategy (Figure

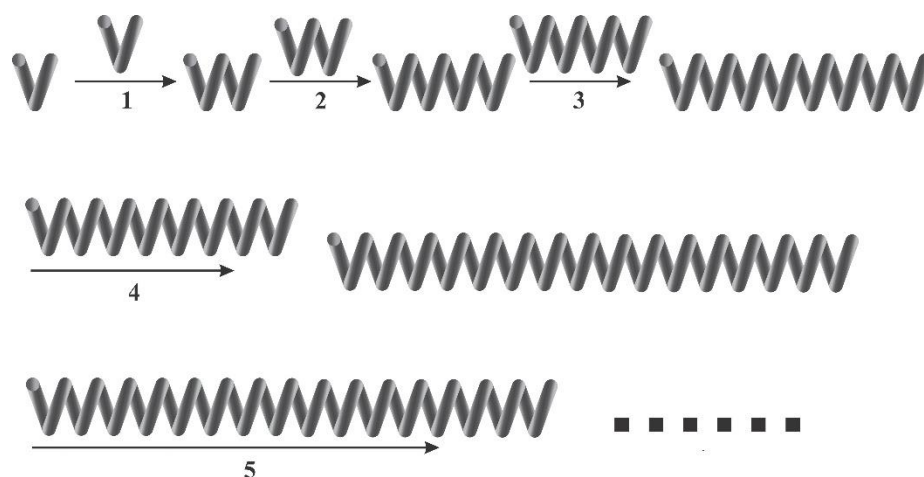


Figure 5 Scheme of synthesis of nanosized helical foldamer with the double segment strategy.

5). After functionalization of the nanosized foldamers with an anchoring group and flexible polymer at terminals, mechanochemistry of these foldamers was investigated by employing atom force spectroscopy-based single molecule force spectroscopy (AFM-SMFS) (Figure 6a). In cooperation with another groups, physicochemical properties of the nanosized foldamers have been explored with ion mobility spectroscopy-mass spectroscopy (IMS-MS, collaboration with Dr. Frédéric Rosu and Dr. Valérie Gabelica) in order to get information about the

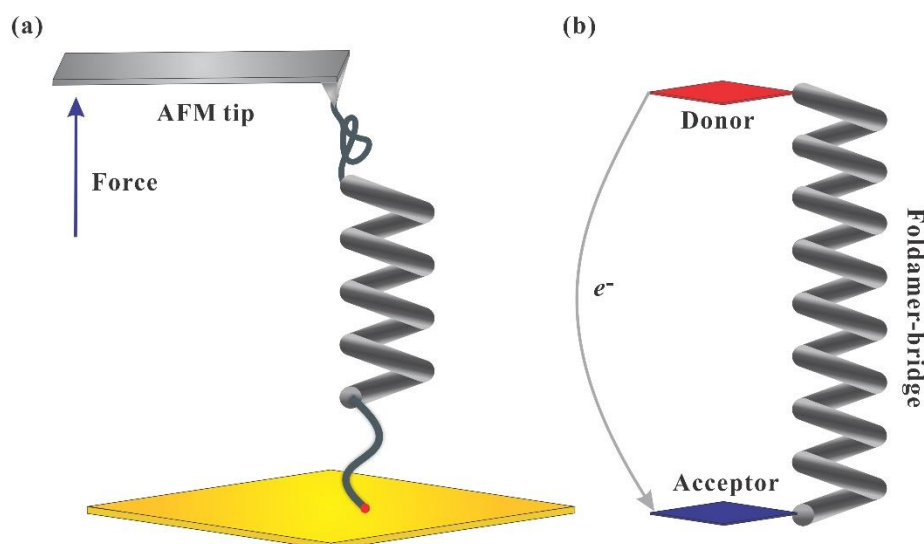


Figure 6 Schemes of (a) mechanochemistry of foldamer with AFM-SMFS and (b) photoinduced electron transfer through rigid nanosized foldamers.

conservation of foldamer conformation and the rigidity of foldamers in gas phase, diffusion ordered spectroscopy (DOSY, collaboration with Prof. Aldrik H. Velders) to determine the translational diffusion of foldamers and the related hydrodynamic sizes in solution and discrimination of diverse foldamers of a homogeneous series in mixture, and fluorescence anisotropy (collaboration with Prof. Jean Duhamel) to obtain rotational diffusion of foldamers and the rigidity of foldamer molecules in solution. The application of the nanosized foldamers in photophysics (photo-induced electron transfer) was then studied by labelling foldamers with electron donor and electron acceptor at terminals, in collaboration with Dr. Nathan D. McClenaghan (Figure 6b).

4 Reference

- 1 (a) Baas-Becking, L. G.; Galliher, E. W., Wall Structure and Mineralization in Coralline Algae. *The Journal of Physical Chemistry* **1930**, *35* (2), 467-479; (b) Palade, G. E., A SMALL PARTICULATE COMPONENT OF THE CYTOPLASM. *The Journal of Biophysical and Biochemical Cytology* **1955**, *1* (1), 59-68; (c) Mitchell, P., Coupling of Phosphorylation to Electron and Hydrogen Transfer by a Chemi-Osmotic type of Mechanism. *Nature* **1961**, *191* (4784), 144-148; (d) Luria, S. E., Molecular Biology: Past, Present, Future. *BioScience* **1970**, *20* (24), 1289-1296.
- 2 Lehn, J.-M., Cryptates: inclusion complexes of macropolycyclic receptor molecules. *Pure and applied Chemistry* **1978**, *50* (9-10), 871-892.
- 3 Lehn, J.-M., Supramolecular chemistry—Scope and perspectives: Molecules—Supermolecules—Molecular devices. *Journal of inclusion phenomena* **1988**, *6* (4), 351-396.
- 4 (a) Gellman, S. H., Foldamers: a manifesto. *Accounts of Chemical Research* **1998**, *31* (4), 173-180, and references therein; (b) Sanford, A. R.; Gong, B., Evolution of helical foldamers. *Current Organic Chemistry* **2003**, *7* (16), 1649-1659; (c) Hecht, S.; Huc, I., *Foldamers: structure, properties and applications*. John Wiley & Sons: 2007, and references therein.
- 5 Guichard, G.; Huc, I., Synthetic foldamers. *Chemical Communications* **2011**, *47* (21), 5933-5941, and references therein.
- 6 (a) Seebach, D.; Overhand, M.; Kühnle, F. N. M.; Martinoni, B.; Oberer, L.; Hommel, U.; Widmer, H., β -Peptides: Synthesis by Arndt-Eistert homologation with concomitant peptide coupling. Structure determination by NMR and CD spectroscopy and by X-ray crystallography. Helical secondary structure of a β -hexapeptide in solution and its stability towards pepsin. *Helvetica Chimica Acta* **1996**, *79* (4), 913-941; (b) Appella, D. H.; Christianson, L. A.; Karle, I. L.; Powell, D. R.; Gellman, S. H., β -Peptide foldamers: robust helix formation in a new family of β -amino acid oligomers. *Journal of the American Chemical Society* **1996**, *118* (51), 13071-13072; (c) Seebach, D.; Matthews, J., [small beta]-Peptides: a surprise at every turn. *Chemical Communications* **1997**, (21), 2015-2022; (d) Gellman, S. H., Foldamers: A Manifesto. *Accounts of Chemical Research* **1998**, *31* (4), 173-180; (e) Cheng, R. P.; Gellman, S. H.; DeGrado, W. F., β -Peptides: From Structure to Function. *Chemical Reviews* **2001**, *101* (10), 3219-3232.

-
- 7 Horne, W. S.; Gellman, S. H., Foldamers with Heterogeneous Backbones. *Accounts of Chemical Research* **2008**, *41* (10), 1399-1408, and references therein.
- 8 Nielsen, P. E.; Egholm, M.; Berg, R. H.; Buchardt, O., Sequence-selective recognition of DNA by strand displacement with a thymine-substituted polyamide. *Science* **1991**, *254* (5037), 1497-1500.
- 9 Simon, R. J.; Kania, R. S.; Zuckermann, R. N.; Huebner, V. D.; Jewell, D. A.; Banville, S.; Ng, S.; Wang, L.; Rosenberg, S.; Marlowe, C. K., Peptoids: a modular approach to drug discovery. *Proceedings of the National Academy of Sciences* **1992**, *89* (20), 9367-9371.
- 10 Semetey, V.; Rognan, D.; Hemmerlin, C.; Graff, R.; Briand, J. P.; Marraud, M.; Guichard, G., Stable Helical Secondary Structure in Short - Chain N, N' - Linked Oligoureas Bearing Proteinogenic Side Chains. *Angewandte Chemie* **2002**, *114* (11), 1973-1975.
- 11 (a) Huc, I., Aromatic Oligoamide Foldamers. *European Journal of Organic Chemistry* **2004**, *2004* (1), 17-29, and references therein; (b) Li, Z.-T.; Hou, J.-L.; Li, C.; Yi, H.-P., Shape-Persistent Aromatic Amide Oligomers: New Tools for Supramolecular Chemistry. *Chemistry – An Asian Journal* **2006**, *1* (6), 766-778, and references therein; (c) Goodman, C. M.; Choi, S.; Shandler, S.; DeGrado, W. F., Foldamers as versatile frameworks for the design and evolution of function. *Nat Chem Biol* **2007**, *3* (5), 252-262, and references therein.
- 12 Nelson, J. C.; Saven, J. G.; Moore, J. S.; Wolynes, P. G., Solvophobic Driven Folding of Nonbiological Oligomers. *Science* **1997**, *277* (5333), 1793-1796.
- 13 Bassani, D. M.; Lehn, J.-M.; Baum, G.; Fenske, D., Designed Self-Generation of an Extended Helical Structure From an Achiral Polyheterocyclic Strand. *Angewandte Chemie International Edition in English* **1997**, *36* (17), 1845-1847.
- 14 Rodriguez, J. M.; Hamilton, A. D., Benzoylurea Oligomers: Synthetic Foldamers That Mimic Extended α Helices. *Angewandte Chemie International Edition* **2007**, *46* (45), 8614-8617.
- 15 (a) Hamuro, Y.; Geib, S. J.; Hamilton, A. D., Oligoanthranilamides. Non-Peptide Subunits That Show Formation of Specific Secondary Structure. *Journal of the American Chemical Society* **1996**, *118* (32), 7529-7541; (b) Zhu, J.; Parra, R. D.; Zeng, H.; Skrzypczak-Jankun, E.; Zeng, X. C.; Gong, B., A New Class of Folding Oligomers: Crescent Oligoamides. *Journal of the American Chemical Society* **2000**, *122* (17), 4219-4220.
- 16 (a) Berl, V.; Huc, I.; Houry, R. G.; Krische, M. J.; Lehn, J.-M., Interconversion of single and double helices formed from synthetic molecular strands. *Nature* **2000**, *407* (6805), 720-723; (b)

-
- Jiang, H.; L ger, J.-M.; Huc, I., Aromatic δ -peptides. *Journal of the American Chemical Society* **2003**, *125* (12), 3448-3449.
- 17 Zhang, D.-W.; Zhao, X.; Hou, J.-L.; Li, Z.-T., Aromatic Amide Foldamers: Structures, Properties, and Functions. *Chemical Reviews* **2012**, *112* (10), 5271-5316, and references therein.
- 18 (a) Bao, C.; Kauffmann, B.; Gan, Q.; Srinivas, K.; Jiang, H.; Huc, I., Converting Sequences of Aromatic Amino Acid Monomers into Functional Three-Dimensional Structures: Second-Generation Helical Capsules. *Angewandte Chemie International Edition* **2008**, *47* (22), 4153-4156; (b) Singleton, M. L.; Pirotte, G.; Kauffmann, B.; Ferrand, Y.; Huc, I., Increasing the Size of an Aromatic Helical Foldamer Cavity by Strand Intercalation. *Angewandte Chemie International Edition* **2014**, *53* (48), 13140-13144.
- 19 (a) Ferrand, Y.; Kendhale, A. M.; Kauffmann, B.; Gr ard, A.; Marie, C.; Blot, V.; Pipelier, M.; Dubreuil, D.; Huc, I., Diastereoselective Encapsulation of Tartaric Acid by a Helical Aromatic Oligoamide. *Journal of the American Chemical Society* **2010**, *132* (23), 7858-7859; (b) Ferrand, Y.; Chandramouli, N.; Kendhale, A. M.; Aube, C.; Kauffmann, B.; Gr ard, A.; Laguerre, M.; Dubreuil, D.; Huc, I., Long-Range Effects on the Capture and Release of a Chiral Guest by a Helical Molecular Capsule. *Journal of the American Chemical Society* **2012**, *134* (27), 11282-11288; (c) Lautrette, G.; Kauffmann, B.; Ferrand, Y.; Aube, C.; Chandramouli, N.; Dubreuil, D.; Huc, I., Structure Elucidation of Host-Guest Complexes of Tartaric and Malic Acids by Quasi-Racemic Crystallography. *Angewandte Chemie International Edition* **2013**, *52* (44), 11517-11520; (d) Lautrette, G.; Aube, C.; Ferrand, Y.; Pipelier, M.; Blot, V.; Thobie, C.; Kauffmann, B.; Dubreuil, D.; Huc, I., Tuning the Guest-Binding Ability of a Helically Folded Capsule by In Situ Modification of the Aromatic Oligoamide Backbone. *Chemistry – A European Journal* **2014**, *20* (6), 1547-1553.
- 20 Chandramouli, N.; Ferrand, Y.; Lautrette, G.; Kauffmann, B.; Mackereth, C. D.; Laguerre, M.; Dubreuil, D.; Huc, I., Iterative design of a helically folded aromatic oligoamide sequence for the selective encapsulation of fructose. *Nat Chem* **2015**, *7* (4), 334-341.
- 21 (a) Gan, Q.; Ferrand, Y.; Bao, C.; Kauffmann, B.; Gr ard, A.; Jiang, H.; Huc, I., Helix-Rod Host-Guest Complexes with Shuttling Rates Much Faster than Disassembly. *Science* **2011**, *331* (6021), 1172-1175; (b) Ferrand, Y.; Gan, Q.; Kauffmann, B.; Jiang, H.; Huc, I., Template-Induced Screw Motions within an Aromatic Amide Foldamer Double Helix. *Angewandte Chemie International*

Edition **2011**, 50 (33), 7572-7575.

- 22 Fischer, L.; Guichard, G., Folding and self-assembly of aromatic and aliphatic urea oligomers: Towards connecting structure and function. *Organic & Biomolecular Chemistry* **2010**, 8 (14), 3101-3117.
- 23 Li, M.; Yamato, K.; Ferguson, J. S.; Gong, B., Sequence-Specific Association in Aqueous Media by Integrating Hydrogen Bonding and Dynamic Covalent Interactions. *Journal of the American Chemical Society* **2006**, 128 (39), 12628-12629.
- 24 Khakshoor, O.; Demeler, B.; Nowick, J. S., Macrocyclic β -Sheet Peptides That Mimic Protein Quaternary Structure through Intermolecular β -Sheet Interactions. *Journal of the American Chemical Society* **2007**, 129 (17), 5558-5569.
- 25 Kudo, M.; Maurizot, V.; Kauffmann, B.; Tanatani, A.; Huc, I., Folding of a Linear Array of α -Amino Acids within a Helical Aromatic Oligoamide Frame. *Journal of the American Chemical Society* **2013**, 135 (26), 9628-9631.
- 26 Kudo, M.; Maurizot, V.; Masu, H.; Tanatani, A.; Huc, I., Structural elucidation of foldamers with no long range conformational order. *Chemical Communications* **2014**, 50 (70), 10090-10093.
- 27 (a) Nakano, T.; Okamoto, Y., Synthetic Helical Polymers: Conformation and Function. *Chemical Reviews* **2001**, 101 (12), 4013-4038, and references therein; (b) Yashima, E.; Maeda, K.; Iida, H.; Furusho, Y.; Nagai, K., Helical polymers: synthesis, structures, and functions. *Chemical reviews* **2009**, 109 (11), 6102-6211, and references therein.
- 28 Sánchez-García, D.; Kauffmann, B.; Kawanami, T.; Ihara, H.; Takafuji, M.; Delville, M.-H.; Huc, I., Nanosized Hybrid Oligoamide Foldamers: Aromatic Templates for the Folding of Multiple Aliphatic Units. *Journal of the American Chemical Society* **2009**, 131 (24), 8642-8648.
- 29 (a) Yoo, S. H.; Eom, T.; Kwon, S.; Gong, J.; Kim, J.; Cho, S. J.; Driver, R. W.; Lee, Y.; Kim, H.; Lee, H.-S., Foldecture as a Core Material with Anisotropic Surface Characteristics. *Journal of the American Chemical Society* **2015**, 137 (6), 2159-2162; (b) Kwon, S.; Kim, B. J.; Lim, H.-K.; Kang, K.; Yoo, S. H.; Gong, J.; Yoon, E.; Lee, J.; Choi, I. S.; Kim, H.; Lee, H.-S., Magnetotactic molecular architectures from self-assembly of [β]-peptide foldamers. *Nat Commun* **2015**, 6; (c) Eom, J.-H.; Gong, J.; Kwon, S.; Jeon, A.; Jeong, R.; Driver, R. W.; Lee, H.-S., A Hollow Foldecture with Truncated Trigonal Bipyramid Shape from the Self-Assembly of an 11-Helical Foldamer. *Angewandte Chemie International Edition* **2015**, 54 (45), 13204-

-
- 13207; (d) Kwon, S.; Shin, H. S.; Gong, J.; Eom, J.-H.; Jeon, A.; Yoo, S. H.; Chung, I. S.; Cho, S. J.; Lee, H.-S., Self-Assembled Peptide Architecture with a Tooth Shape: Folding into Shape. *Journal of the American Chemical Society* **2011**, *133* (44), 17618-17621; (e) Kwon, S.; Jeon, A.; Yoo, S. H.; Chung, I. S.; Lee, H.-S., Unprecedented Molecular Architectures by the Controlled Self-Assembly of a β -Peptide Foldamer. *Angewandte Chemie International Edition* **2010**, *49* (44), 8232-8236.
- 30 (a) Wolffs, M.; Delsuc, N.; Veldman, D.; Anh, N. V.; Williams, R. M.; Meskers, S. C. J.; Janssen, R. A. J.; Huc, I.; Schenning, A. P. H. J., Helical Aromatic Oligoamide Foldamers as Organizational Scaffolds for Photoinduced Charge Transfer. *Journal of the American Chemical Society* **2009**, *131* (13), 4819-4829; (b) Zeidan, T. A.; Wang, Q.; Fiebig, T.; Lewis, F. D., Molecular Wire Behavior in π -Stacked Donor-Bridge-Acceptor Tertiary Arylureas. *Journal of the American Chemical Society* **2007**, *129* (32), 9848-9849; (c) Marcos Ramos, A.; Meskers, S. C. J.; Beckers, E. H. A.; Prince, R. B.; Brunsveld, L.; Janssen, R. A. J., Supramolecular Control over Donor-Acceptor Photoinduced Charge Separation. *Journal of the American Chemical Society* **2004**, *126* (31), 9630-9644.
- 31 (a) Prince, R. B.; Saven, J. G.; Wolynes, P. G.; Moore, J. S., Cooperative Conformational Transitions in Phenylene Ethynylene Oligomers: Chain-Length Dependence. *Journal of the American Chemical Society* **1999**, *121* (13), 3114-3121; (b) Matsuda, K.; Stone, M. T.; Moore, J. S., Helical Pitch of m-Phenylene Ethynylene Foldamers by Double Spin Labeling. *Journal of the American Chemical Society* **2002**, *124* (40), 11836-11837.
- 32 (a) Miller, J. S.; Kennedy, R. J.; Kemp, D. S., Solubilized, Spaced Polyalanines: A Context-Free System for Determining Amino Acid α -Helix Propensities. *Journal of the American Chemical Society* **2002**, *124* (6), 945-962; (b) Price, J. L.; Horne, W. S.; Gellman, S. H., Discrete Heterogeneous Quaternary Structure Formed by α/β -Peptide Foldamers and α -Peptides. *Journal of the American Chemical Society* **2007**, *129* (20), 6376-6377; (c) Delsuc, N.; Massip, S.; L  ger, J.-M.; Kauffmann, B.; Huc, I., Relative Helix-Helix Conformations in Branched Aromatic Oligoamide Foldamers. *Journal of the American Chemical Society* **2011**, *133* (9), 3165-3172; (d) Byrne, L.; Sol   J.; Boddaert, T.; Marcelli, T.; Adams, R. W.; Morris, G. A.; Clayden, J., Foldamer - Mediated Remote Stereocontrol: > 1, 60 Asymmetric Induction. *Angewandte Chemie* **2014**, *126* (1), 155-159.

-
- 33 Yashima, E.; Maeda, K.; Furusho, Y., Single- and double-stranded helical polymers: synthesis, structures, and functions. *Accounts of chemical research* **2008**, *41* (9), 1166-1180, and references therein.
- 34 Pinheiro, V. B.; Taylor, A. I.; Cozens, C.; Abramov, M.; Renders, M.; Zhang, S.; Chaput, J. C.; Wengel, J.; Peak-Chew, S.-Y.; McLaughlin, S. H.; Herdewijn, P.; Holliger, P., Synthetic Genetic Polymers Capable of Heredity and Evolution. *Science* **2012**, *336* (6079), 341-344.
- 35 Cubberley, M. S.; Iverson, B. L., ¹H NMR Investigation of Solvent Effects in Aromatic Stacking Interactions. *Journal of the American Chemical Society* **2001**, *123* (31), 7560-7563.
- 36 (a) Barchi, J. J.; Huang, X.; Appella, D. H.; Christianson, L. A.; Durell, S. R.; Gellman, S. H., Solution Conformations of Helix-Forming β -Amino Acid Homooligomers. *Journal of the American Chemical Society* **2000**, *122* (12), 2711-2718; (b) Hetényi, A.; Mándity, I. M.; Martinek, T. A.; Tóth, G. K.; Fülöp, F., Chain-Length-Dependent Helical Motifs and Self-Association of β -Peptides with Constrained Side Chains. *Journal of the American Chemical Society* **2005**, *127* (2), 547-553.
- 37 Dolain, C.; Gréard, A.; Laguerre, M.; Jiang, H.; Maurizot, V.; Huc, I., Solution Structure of Quinoline - and Pyridine - Derived Oligoamide Foldamers. *Chemistry-A European Journal* **2005**, *11* (21), 6135-6144.
- 38 Steffel, L. R.; Cashman, T. J.; Reutershan, M. H.; Linton, B. R., Deuterium Exchange as an Indicator of Hydrogen Bond Donors and Acceptors. *Journal of the American Chemical Society* **2007**, *129* (43), 12956-12957.
- 39 (a) Cary, J. M.; Moore, J. S., Hydrogen Bond-Stabilized Helix Formation of a *m*-Phenylene Ethynylene Oligomer. *Organic Letters* **2002**, *4* (26), 4663-4666; (b) Wu, Z.-Q.; Jiang, X.-K.; Zhu, S.-Z.; Li, Z.-T., Hydrogen bond-induced rigid oligoanthranilamide ribbons that are planar and straight. *Organic letters* **2004**, *6* (2), 229-232.
- 40 Prince, R. B.; Barnes, S. A.; Moore, J. S., Foldamer-Based Molecular Recognition. *Journal of the American Chemical Society* **2000**, *122* (12), 2758-2762.
- 41 (a) Yang, D.; Zhang, Y.-H.; Li, B.; Zhang, D.-W.; Chan, J. C.-Y.; Zhu, N.-Y.; Luo, S.-W.; Wu, Y.-D., Effect of Side Chains on Turns and Helices in Peptides of β 3-Aminoxy Acids. *Journal of the American Chemical Society* **2004**, *126* (22), 6956-6966; (b) Choi, S. H.; Guzei, I. A.; Gellman, S. H., Crystallographic Characterization of the α/β -Peptide 14/15-Helix. *Journal of the American*

-
- Chemical Society* **2007**, *129* (45), 13780-13781; (c) Choi, S. H.; Guzei, I. A.; Spencer, L. C.; Gellman, S. H., Crystallographic Characterization of Helical Secondary Structures in α/β -Peptides with 1:1 Residue Alternation. *Journal of the American Chemical Society* **2008**, *130* (20), 6544-6550; (d) Choi, S. H.; Guzei, I. A.; Spencer, L. C.; Gellman, S. H., Crystallographic Characterization of Helical Secondary Structures in 2:1 and 1:2 α/β -Peptides. *Journal of the American Chemical Society* **2009**, *131* (8), 2917-2924; (e) Choi, S. H.; Guzei, I. A.; Spencer, L. C.; Gellman, S. H., Crystallographic Characterization of 12-Helical Secondary Structure in β -Peptides Containing Side Chain Groups. *Journal of the American Chemical Society* **2010**, *132* (39), 13879-13885.
- 42 Pendem, N.; Douat, C.; Claudon, P.; Laguerre, M.; Castano, S.; Desbat, B.; Cavagnat, D.; Ennifar, E.; Kauffmann, B.; Guichard, G., Helix-Forming Propensity of Aliphatic Urea Oligomers Incorporating Noncanonical Residue Substitution Patterns. *Journal of the American Chemical Society* **2013**, *135* (12), 4884-4892.
- 43 Hartley, C. S.; Elliott, E. L.; Moore, J. S., Covalent Assembly of Molecular Ladders. *Journal of the American Chemical Society* **2007**, *129* (15), 4512-4513.
- 44 Zhu, J.; Dong, Z.; Lei, S.; Cao, L.; Yang, B.; Li, W.; Zhang, Y.; Liu, J.; Shen, J., Design of Aromatic Helical Polymers for STM Visualization: Imaging of Single and Double Helices with a Pattern of π - π Stacking. *Angewandte Chemie* **2015**, *127* (10), 3140-3144.
- 45 Banno, M.; Yamaguchi, T.; Nagai, K.; Kaiser, C.; Hecht, S.; Yashima, E., Optically Active, Amphiphilic Poly(meta-phenylene ethynylene)s: Synthesis, Hydrogen-Bonding Enforced Helix Stability, and Direct AFM Observation of Their Helical Structures. *Journal of the American Chemical Society* **2012**, *134* (20), 8718-8728.
- 46 (a) Brunsveld, L.; Meijer, E. W.; Prince, R. B.; Moore, J. S., Self-Assembly of Folded m-Phenylene Ethynylene Oligomers into Helical Columns. *Journal of the American Chemical Society* **2001**, *123* (33), 7978-7984; (b) Farrera-Sinfreu, J.; Zaccaro, L.; Vidal, D.; Salvatella, X.; Giralt, E.; Pons, M.; Albericio, F.; Royo, M., A New Class of Foldamers Based on cis- γ -Amino-1-proline_{1,2}. *Journal of the American Chemical Society* **2004**, *126* (19), 6048-6057; (c) Longhi, G.; Abbate, S.; Lebon, F.; Castellucci, N.; Sabatino, P.; Tomasini, C., Conformational Studies of Phe-Rich Foldamers by VCD Spectroscopy and ab Initio Calculations. *The Journal of Organic Chemistry* **2012**, *77* (14), 6033-6042.

47 Wu, Y.-D.; Han, W.; Wang, D.-P.; Gao, Y.; Zhao, Y.-L., Theoretical Analysis of Secondary Structures of β -Peptides. *Accounts of Chemical Research* **2008**, *41* (10), 1418-1427, and references therein.

II Segment doubling synthesis of nano-sized foldamers

1 Introduction

Presently much interest is developed and many efforts is devoted to artificial folded molecular architectures, so-called foldamers.¹ A large variety of synthetic organic backbones that are able to adopt folded conformations in space has been explored and described, opening the prospect to mimic, and sometimes possibly go beyond, biopolymeric structures and functions.² However, functions of biopolymers (in particular, of proteins) are generally achieved by large tertiary or quaternary folded motifs.³ In order to possess the capability to have both the related structures and the resulting functions of biopolymers, foldamers with adequately massive molecular weights and sufficiently large folded structures become essential and prerequisite. Foldameric molecules produced by stepwise synthesis most often consist of relatively small objects in the 1-5 kDa range.⁴ For instance, based on these synthesized helical structures, α/β peptides imitating gp41, a HIV membrane protein, effectively prevented the HIV from fusing into cells, showed a less susceptibility to proteolytic degradation.⁵ Using up-bottom approach⁶, another α/β peptides derived from Z-domain peptide targeting vascular endothelial growth factor hindered the proteolytic degradation of these α/β -peptides, and meanwhile, proposed a versatile method.⁷ Therefore, a major challenge in foldamer synthesis thus lies in the development of methods to prepare substantially larger folded structures that would give access to more elaborate functions. For this purpose, a long term strategy is to adapt or to evolve molecular biology tools so that they accommodate non-natural monomers. For example, the tolerance of DNA polymerases to non-natural nucleobases is being enhanced⁸, and the ribosome machinery shown to accept monomers different from the natural α -amino-acids.⁹ Yet, abiotic backbones that much differ from biopolymers still escape this approach, and their preparation rests solely on stepwise synthetic chemistry.

Great achievements have been reported in the chemical total synthesis of large peptidic chains (>300 amino acids)¹⁰ through the combination of solid phase synthesis and native chemical ligation methods.¹¹ Related strategies are being applied to oligonucleotide synthesis.¹²

mixtures, precluding the routine synthesis of long sequences, despite the generally required acid chloride strong activation of the terminal carboxylic groups.¹⁶

Strategies to circumvent these difficulties have been proposed. For example, the insertion of removable alkoxy-benzyl amine substituents resulted in the formation of tertiary amides that locally disrupt folding and alleviate steric hindrance during synthesis.¹⁶ Alternatively, including some reactive monomers bearing e.g. aliphatic instead of aromatic amines, allowed the use of standard peptide coupling agents, and gave easy access to large foldamers that retained their compact structure despite the flexibility imparted by the aliphatic linkages, the aromatic units dictating the overall folding behavior.¹⁷ As shown in the following, the recourse to these strategies may be avoided as direct couplings between large folded segments can in fact be carried out efficiently.

We recently reported the chromatography-free large scale synthesis of octameric strand **5a**.¹⁸ This compound can be prepared by coupling dimer acid chloride **2d** with hexamer amine **4b** that is from coupling reaction of dimer acid chloride **2d** with tetramer amine **3b** (Figure 1). The preparation of **5a** did not employ the coupling reaction of tetramer acid chloride and tetramer amine due to the fact the appearance of anhydride caused by tetramer acid chloride in the presence of water sharply decreases the yield of octamer **5a**. This compound, octamer **5a**, has been shown previously to fold in a helix spanning over three turns, with a pitch of 3.5 Å that was characterized both in the solid state and in solution.¹⁹ The large available quantity of **5a** prompted us to use this octamer as a starting material and to attempt the synthesis of much longer oligomers. In the following, I describe the gram scale preparation of quinoline-based helical nanosized/protein-sized oligoamide foldamers having up to 64 units (15.6 kDa) and the tens milligrams scale synthesis of foldamers with more than 10 nm of the helical length, up to 96 units (25.7 kDa) *via* a segment doubling approach. We show that combining pure reagents, high reaction concentration, and long reaction times allow us to carry out high yielding iterative couplings between long folded segments.

2 Synthesis

Taking quinoline-based octamer **5a** as the starting material, longer foldamers 16mer **6a**, 32mer **8a** and 64mer **10** have been successfully prepared by employing segment doubling synthesis strategy in large scale, as shown in Figure 2. More details are available in the coming Results and Discussion part.

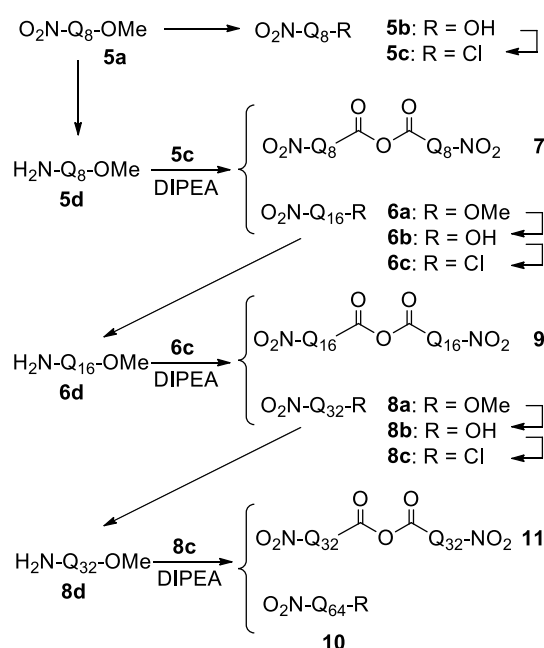


Figure 2 Segment doubling synthesis of long oligomers by using quinoline-based octamer as the starting materials.

Based on the experience in our group that bromination of foldamer backbone provided the possibility to separate the resulting 16mer (with 7 bromines) from the corresponding anhydride (from brominated octamer, with 14 bromines. More details available in Results and Discussion part), bromination was introduced into the long foldamers and we realized that this reaction could be done just in one pot with high yield and that the resulting brominated oligomers display better solubility in chlorated solvents than the non-brominated ones. This advantage paves the way of the resolution issue of long (nanosized) foldamers. A new series of foldamer was designed as shown in Figure 3. More relative details are available in the following Results and Discussion part.

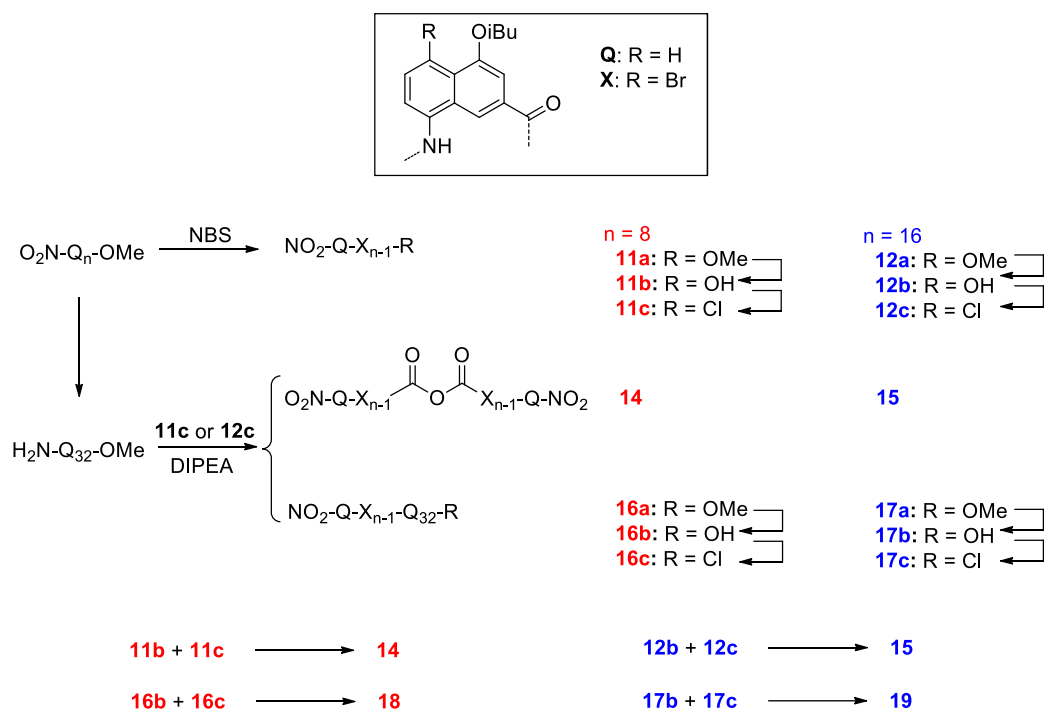


Figure 3 Incremental synthesis of bromo-substituted long foldamers.

3 Results and discussion

The saponification of the terminal methyl ester of **5a** to give acid **5b** (Figure 4a) and the hydrogenation of the N-terminal nitro group to give amine **5d** (Figure 4c) both require relatively harsh conditions due to the hindrance of these groups associated with folding. Compound **5a** was saponified to produce its corresponding acid **5b** under strong base condition: NaOH in a THF/MeOH mixture; conversion of **5b** to its acid chloride was done with oxalyl chloride to provided acid chloride **5c** quantitatively (Figure 4b). The hydrogenation of **5a** yielded amine **5d** by using Pd/C, NH_4VO_3 and NH_4HCO_2 by refluxing in ethyl acetate and ethanol mixture. The coupling of **5c** and **5d** was relatively slow unless high concentrations were used (see Figure 2 d and e as examples of incomplete and complete consumption of **5d**).

In order to have fast coupling, concentration should be in the range of 0.15 M range which, due to the high molecular weight of the reagents (approx. 2 kDa), represent around $0.3 \text{ g}\cdot\text{mL}^{-1}$ and require sufficiently high solubility. Under such conditions, this reaction yielded a mixture containing the expected product 16mer **6a**, and variable amounts of anhydride **7** and remaining

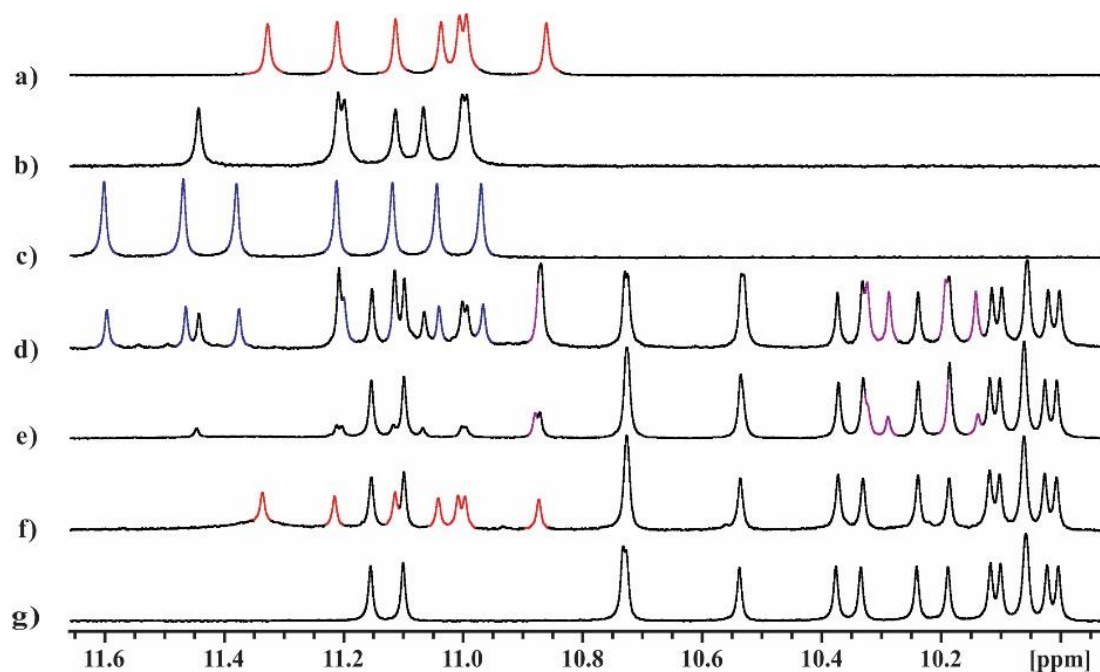


Figure 4 Excerpt of ^1H NMR (300 MHz) spectra showing amide NH region of a) octamer acid **5b**, b) octamer acid chloride **5c**, c) octamer amine **5d**, d) reaction mixture after coupling, showing **5d**, **6a** and **7**, e) reaction mixture after adding excess **5c**, including **6a** and variable amount of **5c** and **7**, f) results after refluxing in pyridine/ H_2O , a mixture of **5b** and **6a** and g) pure **6a** after chromatographic purification.

Signals of anhydride **7** in d) and e) was colorized as purple; red signals belong to **5b** and blue to **5d**.

amine **5d** (Figure 2 and 4d). As shown by ^1H NMR spectra in Figure 4, the amide protons where the block building repeat units (quinoline) combine with one another and that are involved in intramolecular hydrogen bonds, are shifted downfield, appearing as the sharp signals, as expected for quinolone-based foldamers.^{19a, 20} The number of sharp signals is equal to that of amide protons, that is to say, one less than the number of the block building repeat units (quinoline), for example, octamer (eight (8) quinoline units in the sequence) has seven (7) sharp signals between 10.8 ~ 11.6 ppm (Figure 4). These sharp signals shift upfield as the lengths of foldamers increase because of an increase of ring current effects associated with aromatic stacking in the helical structure.^{15, 18, 20} To clarify the ^1H NMR spectra of these complicated compounds and simplify the related spectra description, only just the signals of amide protons are shown and discussed in the following text if not specially mentioned.

The formation of anhydrides such as **7** reflects the greater reactivity of acid **5b** as compared to amine **5d** towards acid chloride **5c** in the presence of base, and the hydrolysis of the acid chloride to carboxylic acid during the course of the coupling reaction due to the presence of water which is difficult to avoid. Because of the folded structure and the position of anhydride bond (center of the folded structure), the resulting anhydride is particularly stable and does not react readily with water or methanol at ambient atmosphere. Multiple attempts also showed that the anhydride constitute a recurrent by-product: rigorously anhydrous conditions that would prevent acid chloride hydrolysis and the subsequent anhydride formation can rarely be achieved. The separation of **5d**, **6a** and **7** by chromatographic methods proved to be extremely delicate, if feasible at all, and in any case incompatible with large scales. As described below, these difficulties were overcome as follows.

The first solution was carried out by a former post-doctor, Dr. Kolupula Srinivas, in our group. He had explored the conversion of octmer **5a** into heptabromo analogue by using excess N-bromo succinimide (NBS) in 1,2-dichloroethane (Figure 5a), and observed that these two compounds possess remarkably different retention coefficients (R_f) on silica gel. This observation suggested that when heptabromo-octamer acid chloride **20c**, resulting from saponification and subsequent activation of heptabromo-octamer, reacted with octamer amine

5d, the resulting anhydride with fourteen bromines, the resultant 16mer **21a** bearing seven bromines and the remaining starting material **5d** (without bromine) could display different polarities from one another, which makes the purification relatively easy by using classic chromatographic methods. This approach finally vouchsafes permission to incremental elongation of bromo-substituted oligomers (up to 24mer bearing seven bromines) *via* iterative couplings with octamer amine **5d** and a resulting anhydride-form 48mer **23** bearing fourteen bromines.

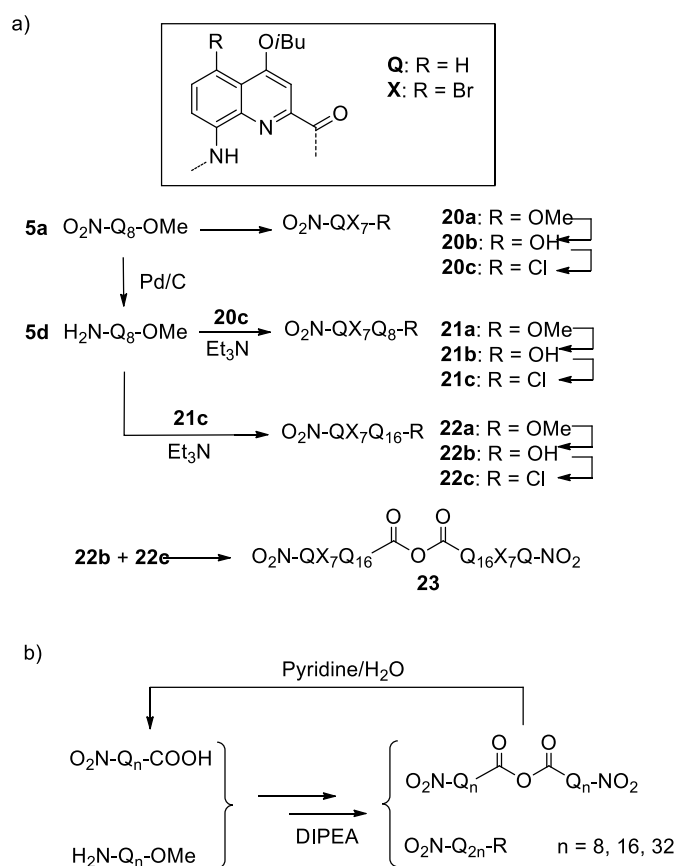


Figure 5 Scheme of a) synthesis of brominated foldamers carried out by Dr. Kolupula Srinivas and b) hydrolysis of anhydrides by refluxing in pyridine and water.

The second approach was to implement a more convergent and higher yielding synthesis. We thus sought for conditions to hydrolyze recurrent anhydride by-products and eventually recycle the recovered carboxylic acids. We found that clean hydrolysis of the helically folded anhydrides could be achieved upon refluxing them in a pyridine/H₂O mixture (Figure 5b). This treatment was then included in the work-up of coupling reactions. In addition, in order to avoid difficult chromatographic separation between the coupling products and the unreacted starting

material amine, we included a control by NMR of the presence of remaining amine and its elimination by adding excess acid chloride until it had completely disappeared (Figure 4). Following this procedure allows us to produce 16mer **6a** in approx. 80% isolated yield, following an relatively easy purification procedure, as the main by-product was the starting acid **5a** which is easy to remove and recycle by chromatographic purification on silica gel.

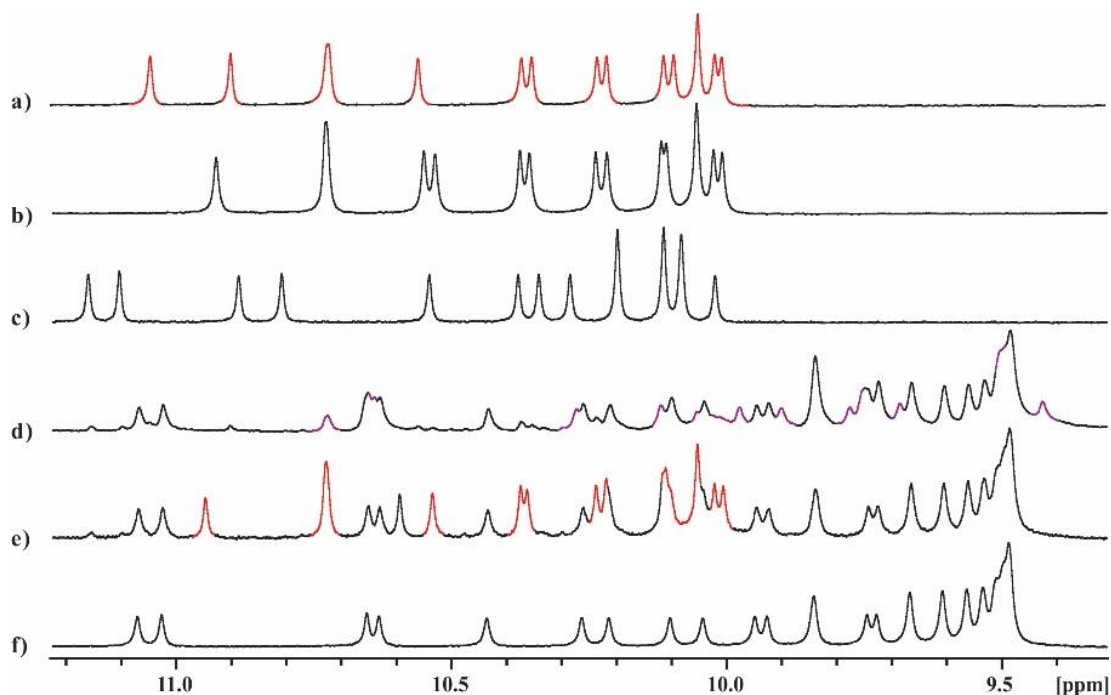


Figure 6 Representative ^1H NMR spectra (300 MHz) showing amide NH region of a) 16mer acid **6b**, b) 16mer acid chloride **6c**, c) 16mer amine **6d**, d) reaction mixture of **6c** and **6d**, e) results after refluxing the reaction mixture in a pyridine/water mixture and f) pure 32mer **8a** after chromatographic purification. Signals of **6b** are marked as red colour and signals of anhydride **9** as purple.

Similarly, the 16mer **6a** was taken as the starting material for production of 32mer **8a**. The methyl ester group of **6a** was saponified using ground powder NaOH in a THF/MeOH mixture (9/1, v/v), almost quantitatively giving 16mer acid **6b** (Figure 6a). The activation of **6b** via excess oxalyl chloride afforded quantitatively 16mer acid chloride **6c** (Figure 6b). The complete conversion of the acid was controlled by NMR. In the presence of Pd/C, NH_4VO_3 and NH_4HCO_2 , the hydrogenation of 16mer **6a** was performed under refluxing at 95 °C overnight in ethyl acetate/ethanol mixture, yielding 16mer amine **6d** (Figure 6c). Noteworthy is that this reaction should be kept under its own atmosphere which can prevent NH_3 from escaping out of the reaction flask, and avoid forming formic acid that can react with the product amine to give

the formamide compound byproduct. Meanwhile, immediate workup should be performed once the reaction mixture is cooled down to room temperature. Coupling of **6c** (2 equiv.) and **6d** took place in the presence of DIPEA and generated a mixture of expected 32mer **8a** and unavoidable anhydride **9** (Figure 6d). Refluxing of this reaction mixture in pyridine/H₂O mixture allowed the hydrolysis of anhydride **9** into its polar starting material 16mer acid **6b** (Figure 6e). Then, the resulting crude was purified by silica gel column to afford pure 32mer **8a** (Figure 6f). It has to be noted that as the sizes of 16mer and 32mer reach up to nanometer range, their solubility in dichloromethane that is used for the syntheses of shorter oligomers, for example, hexamer and octamer, becomes poor. Another solvent in which these nano-sized oligomers can be easily dissolved to keep them at a high concentration has to be found and employed. Eventually, chloroform was found and used as the solvent of this reaction.

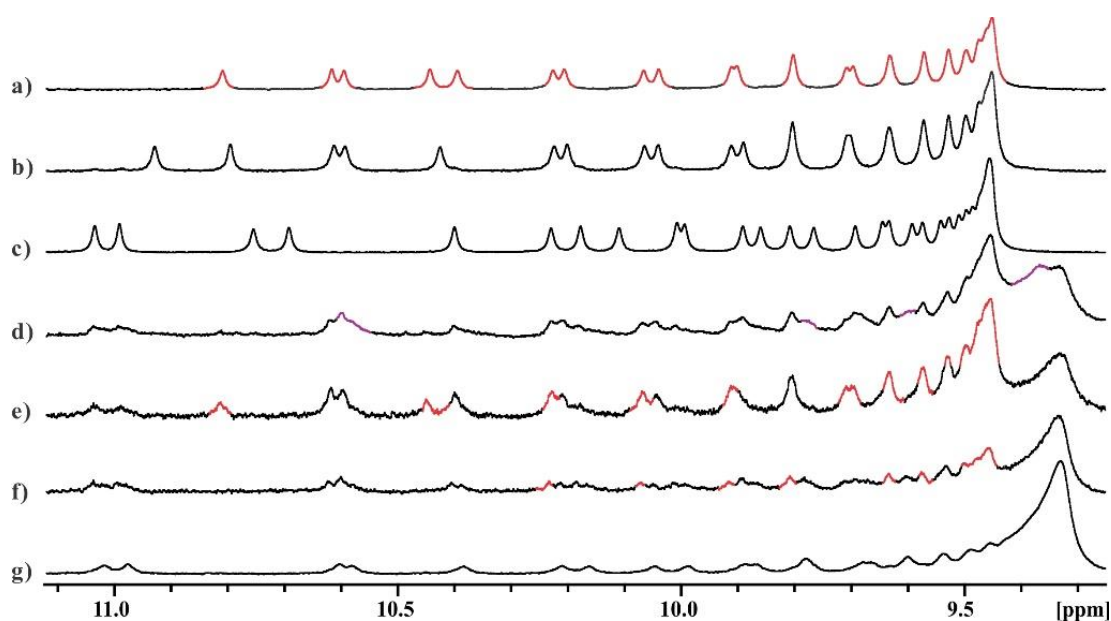


Figure 7 Excerpt of ¹H NMR spectra (300 MHz) of synthesis of 64mer: a) 32mer acid **8b**, b) 32mer acid chloride **8c**, c) 32mer amine **8d**, d) reaction crude of **8c** and **8d**, e) result of refluxing in pyridine/H₂O, f) result of purification by chromatographic methods in toluene and g) pure 64mer **10** after recycling GPC. Herein, signals of 32mer **8b** are showed in red and these of anhydride **11** in purple.

The 64mer oligomer **10** was synthesized using similar coupling condition between 32mer acid chloride **8c** and 32mer amine **8d** in the presence of DIPEA (Figure 7). Similarly to the synthesis of 32mer, in order to keep the reaction at high concentration, an appropriate solvent that is able to afford great solubility for 32mer acid and amine, toluene, was found and chosen for this

reaction. Considering that the lengths of the two starting materials **8c** and **8d** reach up to protein size (approx. 5 nm) and the corresponding reactive sites (acid chloride group of **8c** and amino group of **8d**) stand ulterior in these folded nano-sized structures, the activity of coupling these two nano-sized starting materials to form longer foldamer indisputably decreased, compared with formation of 16mer, or even 32mer. The resulting oligomer 64mer possesses a very large folded structure (approx. 10 nm) that becomes problematic to be separated from its nano-sized starting materials. Many efforts have been already devoted to purify this nanorod-like oligomer. Even though toluene was able to dissolve this reaction crude, composed of a mixture of the expected 64mer **10** and starting material 32mer **8b** acid, attempt to isolate 64mer **10** via chromatographic methods in toluene showed extremely tricky. By successive use of chromatography, partial quantity of starting material 32mer acid **8b** could be removed but pure 64mer **10** was still unobtainable (Figure 7f). This resultant impure 64mer (some 32mer acid involved) was injected into a recycling GPC system, by which compounds of different size could be separated, using chloroform as eluent -- it can dissolve small quantity of this mixture (approx. 1 mg/mL), yielding only ~ 500 μg of pure 64mer each time (Figure 7g and 8). All in all, even though the separation of 64mer is tough, the coupling reaction of forming 64mer is demonstrated to be fine and accessible. Because of the solubility issue of 64mer, insufficient quantity of this compound could be isolated for further elongation of this series of foldamer,

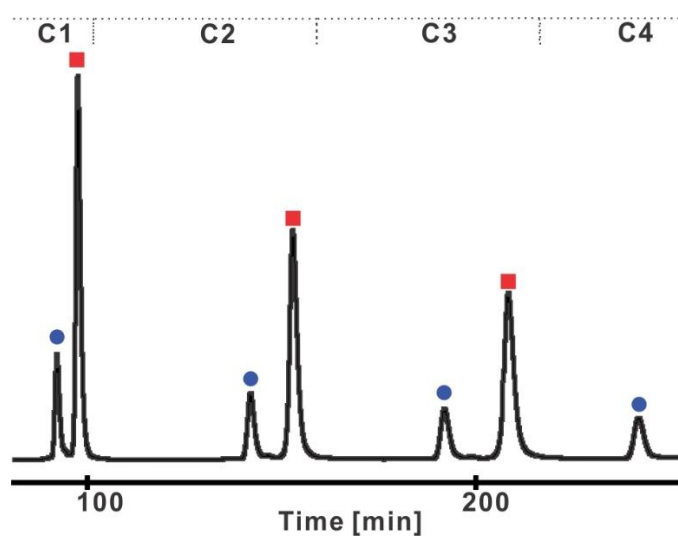


Figure 8 Curve of recycling GPC of 64mer purification. The peaks marked with blue circle stand for appearance of 64mer **10** and the ones with red square for 32mer acid **8b**.

As mentioned above that the former postdoc Dr. Kolupula Srinivas had explored to brominate the backbones of quinoline-based octamer, this bromination has positive impact on separating its resulting expected products from other by-products. In order to give access to longer foldamers, bromination of backbones of nanosized quinoline-based foldamers was explored (Figure 9).

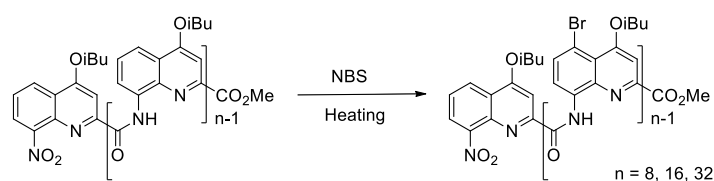


Figure 9 Synthetic scheme of bromination of quinolone-based foldamers.

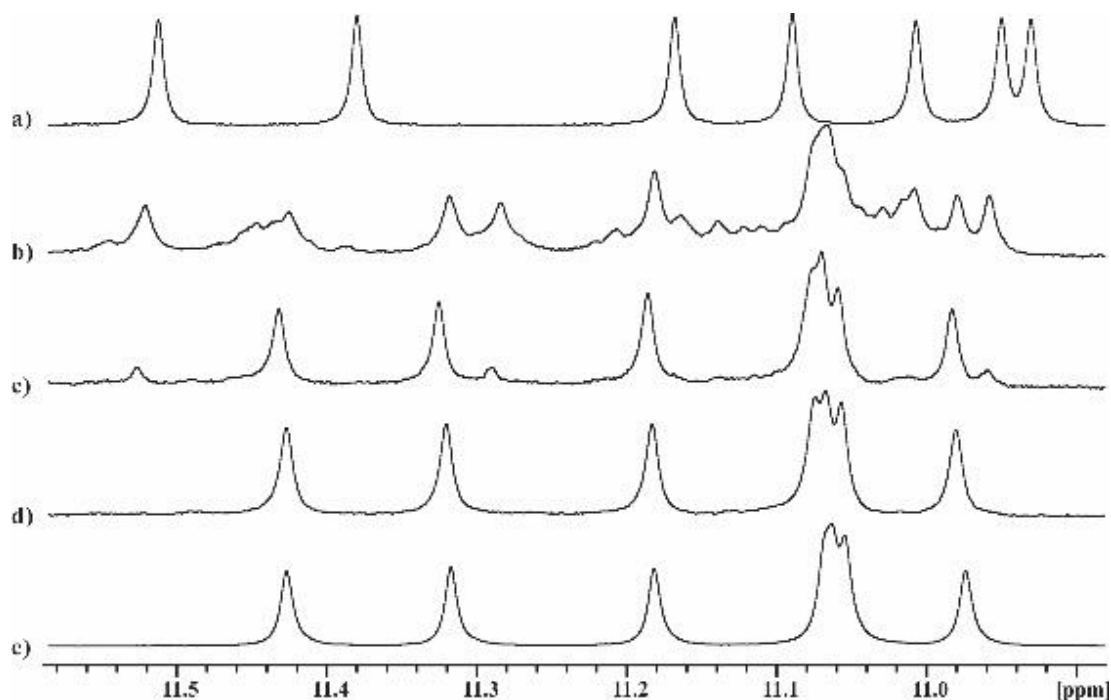


Figure 10 Excerpt of ^1H NMR spectra (300 MHz) of synthesis of $^7\text{BrQ}_8$ at $45\text{ }^\circ\text{C}$: a) starting material bromine-free octamer **5a**, b) reaction after overnight, c) reaction after two days, d) reaction crude after four days and e) pure $^7\text{BrQ}_8$ **12a** after flash silica gel column.

First of all, octamer **5a** (Q_8) was brominated into its heptabromo analogue $^7\text{BrQ}_8$ **12a** with excess quantity of NBS in 1,2-dichloroethane. By controlling reaction temperature and reaction time and with excess quantity of NBS, this reaction can yield almost unique heptabromo-octamer

(Figure 10) of which HRMS data confirmed the clean conversion (Figure 11). More interestingly, its solubility in classic solvents, like chloroform, is much better than its corresponding bromine-free compound, which seems to provide a positive favor to the synthesis of longer quinoline-based foldamers since the solubility of longer quinoline-based foldamers generally decrease with the increment of backbone length.

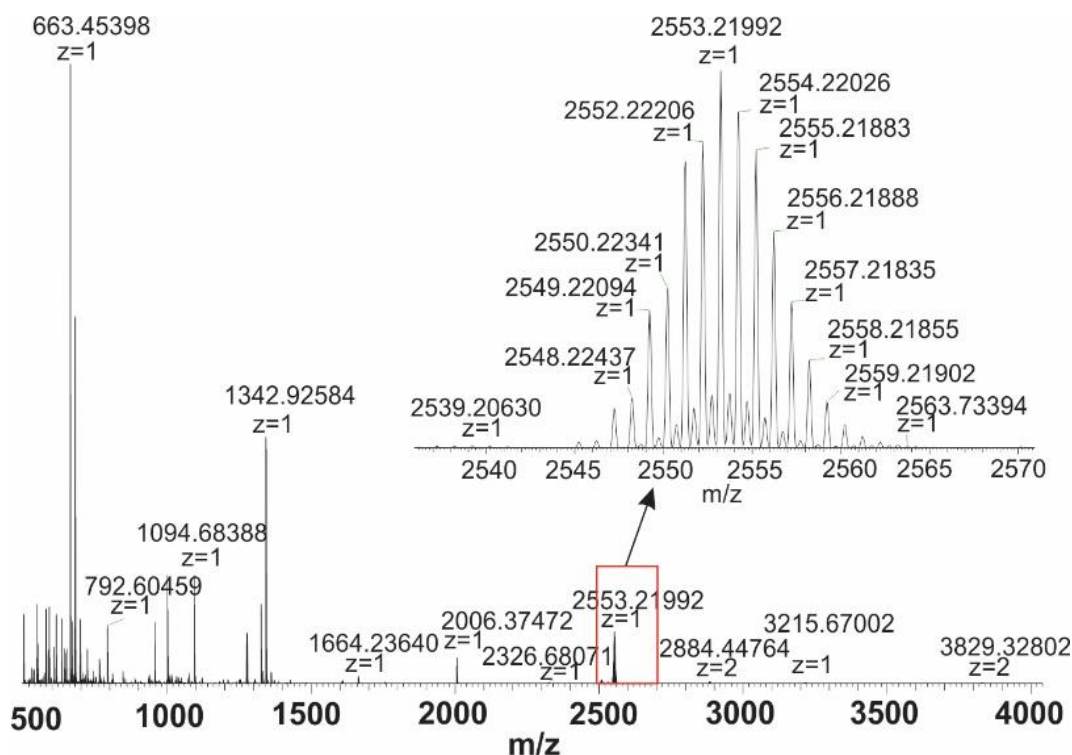


Figure 11 Full spectra of HRMS of brominated octamer ${}^7\text{BrQ}_8$ **12a** and its representative section. This sample is measured with a condition of FTMS & p ESI. The symmetrical branched spectra of $[\text{}^7\text{BrQ}_8+\text{H}]^+$ results from isotopes of bromine.

In fact, reaction temperature, reaction time and quantity of NBS have a direct influence upon the bromination reaction. When using a saturated solution NBS, if the reaction temperature is changed from 40 to 70 °C the reaction kinetic is greatly accelerated (from 7 days to approx. 2 days for completion). As the reaction temperature was set to 70 °C, changes of reaction time and/or quantity of NBS can make it possible to detect ‘intermediate’ products that contain different numbers of bromine on their backbones. The number of these octamer intermediates is shown in table 1. Initially, a reaction with 1 equiv. octamer and 1 equiv. NBS was set up at 70 °C. After 12 h of reaction, approx. 50 to 100 μL reaction sample was then picked up from the reaction mixture for the ${}^1\text{H}$ NMR and HRMS data collection, after which, 2 more equiv.

NBS was added into the reaction. By reiterating this procedure, diverse reaction samples with different reaction time and NBS quantity were picked up and measured with ^1H NMR and HRMS after certain time (24 h, 36 h, 48 h, 60 h, 72 h, 96 h, 120 h, 144 h, 168 h and 192 h).

Table 1 Intermediates after different reaction time and varied quantity of NBS

Reaction time	12 h	24 h	36 h	48 h	60 h	72 h	96 h	120 h	144 h	168 h
NBS quantity ¹	1	3	5	7	9	11	13	15	17	19
Intermediates ²	0Br, 1Br, 2Br	0Br, 1Br, 2Br, 3Br	0Br, 1Br, 2Br, 3Br, 4Br	2Br, 3Br, 4Br, 5Br	3Br, 4Br, 5Br, 6Br, 7Br	3Br, 4Br, 5Br, 6Br, 7Br, 4Br+Cl, 5Br+Cl	6Br, 7Br, 4Br+2Cl, 5Br+Cl, 6Br+Cl	6Br, 7Br, 5Br+Cl, 6Br+Cl	5Br, 7Br, 8Br, 5Br+2Cl, 6Br+Cl	5Br, 7Br, 8Br, 5Br+2Cl, 6Br+Cl

¹The quantity of NBS here is the one added before and used for the data collection, not including the 2 more equiv. added after picking up the reaction sample for data collection.

² $n\text{Br}$ means one intermediate with n bromine atoms; $n\text{Br}+m\text{Cl}$ means one intermediate with n bromine atoms and m chlorine atoms.

As shown in MS spectra in Figure 12, after reacting for 12 h with 1 equiv. of NBS, starting material (octamer with zero bromine) and intermediate with one bromine are the main products and some oligomers with two bromines and few with three bromines appeared as well. After adding 2 more equiv. of NBS and lasting another 12 h, quantity of starting material decreased, intermediates with one bromine and two bromines became the main products and meanwhile quantity of intermediate with three bromines grew up as well. When 2 more equiv. of NBS and lasted for 36 h, starting material has almost been consumed, main intermediates were with two and three bromines and compounds with four bromines showed up. As reaction time increased and more NBS was added, intermediates with less bromines faded away and meantime, intermediates with more bromines came out until up to the final product -- heptabromo-octamer. While the reaction went by and especially when reaction lasted for long time (up to 144 h), some unexpected side-products appeared: one or two chlorines were replacing bromine, or a product with eight bromines was detected. Partial chlorination of foldamers was perhaps caused by the exchange between Br^- and Cl^- which is caused by the decomposition of solvent 1,2-

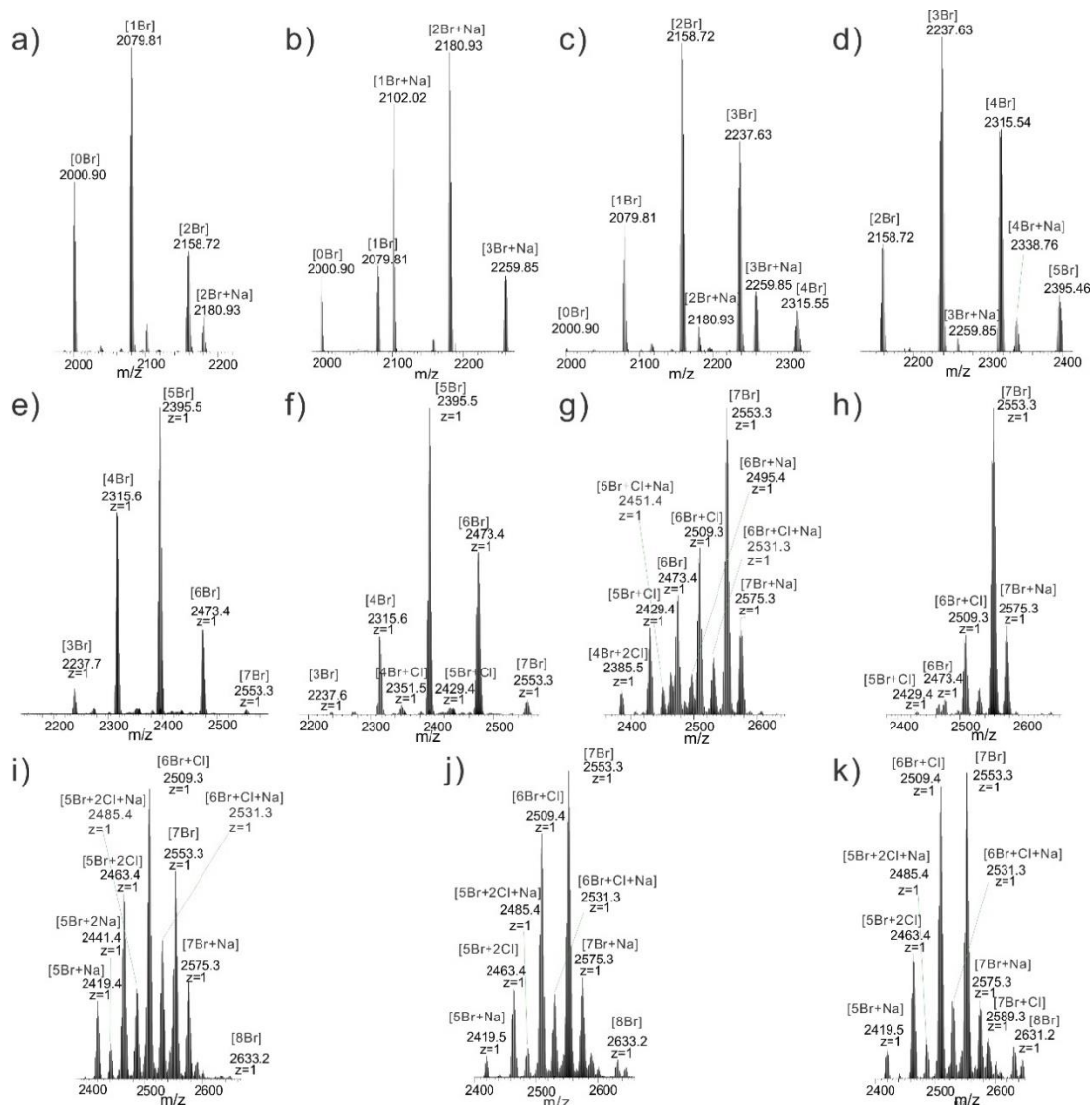


Figure 12 Mass spectroscopies of different intermediates of brominated octamer under varied reaction time and different quantity of NBS at 70 °C: a) after 12 h and 1 equiv. NBS; b) 24 h and 3 equiv. NBS; c) 36 h and 5 equiv. NBS; d) 48 h and 7 equiv. NBS; e) 60 h and 9 equiv. NBS; f) 72 h and 11 equiv. NBS; g) 96 h and 13 equiv. NBS; h) 120 h and 15 equiv. NBS; i) 144 h and 17 equiv. NBS; j) 168 h and 17 equiv. NBS and k) 192 h and 17 equiv. NBS.

dichloroethane. Over-bromination phenomenon of foldamers resulting on the formation of the oligomer with 8 Br can be explain by the substitution of one of the H at 6 position of some quinoline ring.²¹ Table 1 summarizes the number of intermediates observed in each sample. Because the number of intermediates is too large, it is impossible to distinguish them using ¹HNMR, Only when the reaction is finish and only the final product becomes the major compound in the reaction crude NMR show sharp and recognizable signals (Figure 13). The crystalline structure of this 8mer demonstrated the place of Br at 5th position of quinoline ring and presented a perfect helical folded structure. (Figure 14).

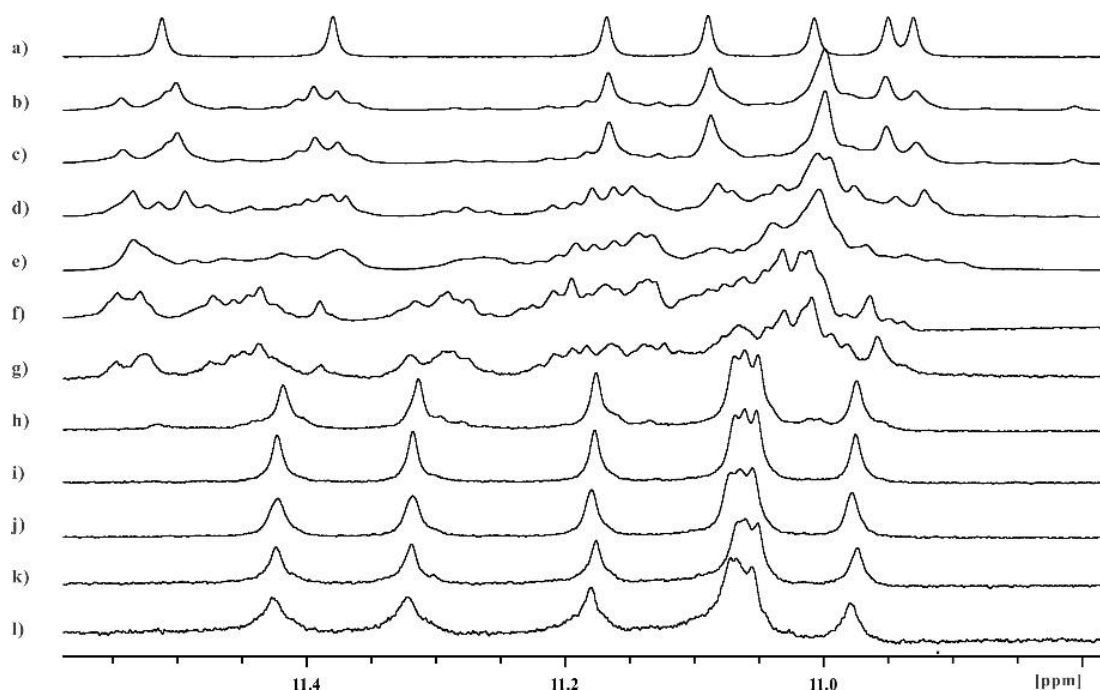


Figure 13 Excerpt of ^1H NMR spectra (300 MHz) of intermediates of bromination of octamer at $70\text{ }^\circ\text{C}$ in 1,2-dichloroethane by changing reaction time and quantity of NBS: a) starting material octamer; b) after 12 h and 1 equiv. NBS; c) 24 h and 3 equiv. NBS; d) 36 h and 5 equiv. NBS; e) 48 h and 7 equiv. NBS; f) 60 h and 9 equiv. NBS; g) 72 h and 11 equiv. NBS; h) 96 h and 13 equiv. NBS; i) 120 h and 15 equiv. NBS; j) 144 h and 17 equiv. NBS; k) 168 h and 17 equiv. NBS and l) 192 h and 17 equiv. NBS.

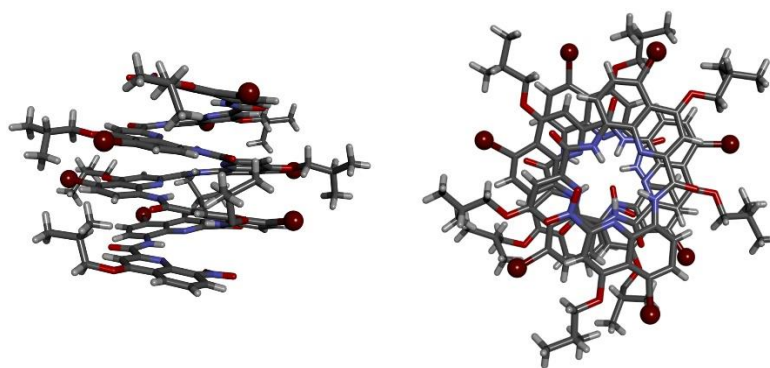


Figure 14 Crystalline structure of $^7\text{BrQ}_8$ (Br atoms are emphasized as ball with deep red in the structure; left: side view; right: top view).

As shown in Figure 14, saponification of $^7\text{BrQ}_8$ with NaOH in THF/MeOH gave the corresponding acid $^7\text{BrQ}_8\text{-COOH}$ **12b** like the octamer Q_8 does. Because of the p - π conjugation between bromine atom and quinoline ring which strengthens density of electrons among carboxyl group, reactivity of the acid was decreased and conversion to its corresponding acid chloride took more time than the corresponding bromine-free foldamer acids. Overnight reaction was required to convert $^7\text{BrQ}_8\text{-COOH}$ **12b** with oxalyl chloride to $^7\text{BrQ}_8\text{-COCl}$ **12c**.

Combining **12b** with **12c** gave the anhydride 16mer $^{14}\text{BrQ}_{16}$ **14** which displayed a good solubility, even in dichloromethane (Figure 15).

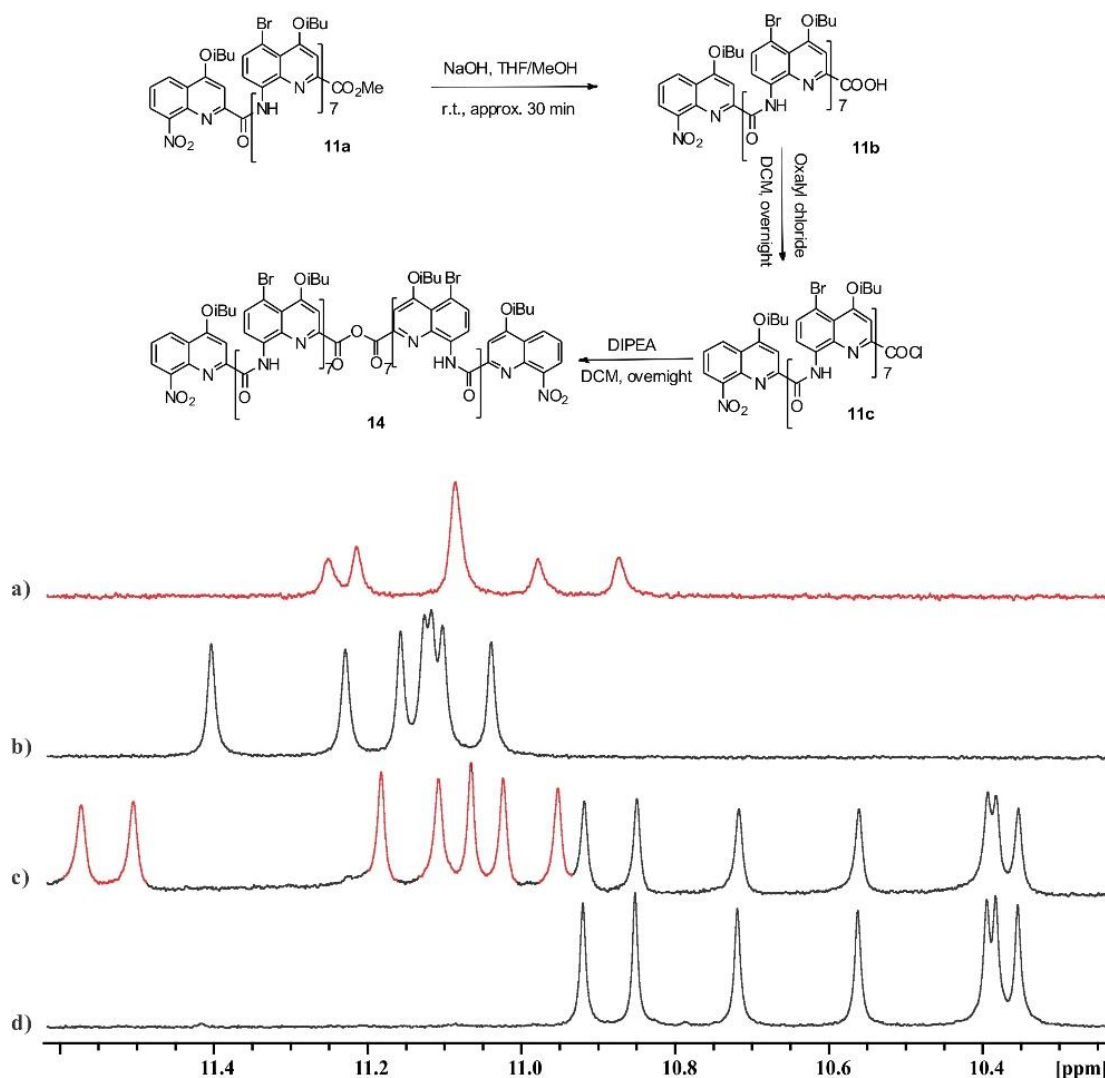


Figure 15 Synthetic scheme of $^{7}\text{BrQ}_8$ -based compounds (top) and their representative NMR spectra (300 MHz) (down): a) brominated octamer acid $^{7}\text{BrQ}_8\text{-COOH}$ **12b**, b) acid chloride $^{7}\text{BrQ}_8\text{-COCl}$ **12c**, c) reaction crude and d) purified 16mer $^{14}\text{BrQ}_{16}$ **14**. Compared with initial octamer acid $^{7}\text{BrQ}_8\text{-COOH}$, the peaks of octamer acid in reaction crude c) (red peaks) shifted because of the presence of base DIPEA.

According to the beneficial profit on solubility of the bromination of the octamer backbone and on the conversion to a unique perbrominated product, bromination of longer foldamers was worthy of exploring to extend the possibility of obtaining only one main product that possesses good solubility. As mentioned above, the reaction time, the reaction temperature and the quantity of NBS are able to influence the results of bromination. As the quantity of NBS is set,

the reaction temperature has a positive relation with the reaction time: the lower the temperature is, the longer the time is. 16mer Q₁₆ **8a** with excess NBS in 1,2-dichloroethane at 70 °C could provide unique final product ¹⁵BrQ₁₆ **12a** in 6 days (Figure 16). The resulting crude could then be easily purified by silica gel column, giving pure product ¹⁵BrQ₁₆ in 92% yield (Figure 16 and 17). If the reaction temperature was set at 55 °C, more time (12 days) could be needed to complete the bromination of Q₁₆ **8a** than the reaction at 70 °C does (6 days). As calculated (Table 2), the number of pentadecabromo 16mer ¹⁵BrQ₁₆ is only one; the number of possible 16mer containing 14 bromine (¹⁴BrQ₁₆) or 1 bromine (¹BrQ₁₆) is 15. While the number of incompletely-brominated intermediates containing various number of bromines vary from 100 to 6 435. The number of these intermediates is so large that it is impossible to distinguish them on the ¹H NMR spectra leading to broad signals. Meanwhile, as the reaction time increases, side product containing Cl instead of Br atom may appear as previously presented. It has to be noted that this side products are impossible to separate from the target product. So the reaction duration became crucial for the success of Q₁₆ bromination. Reaction must be stopped once no obvious intermediates can be observed in ¹H NMR data.

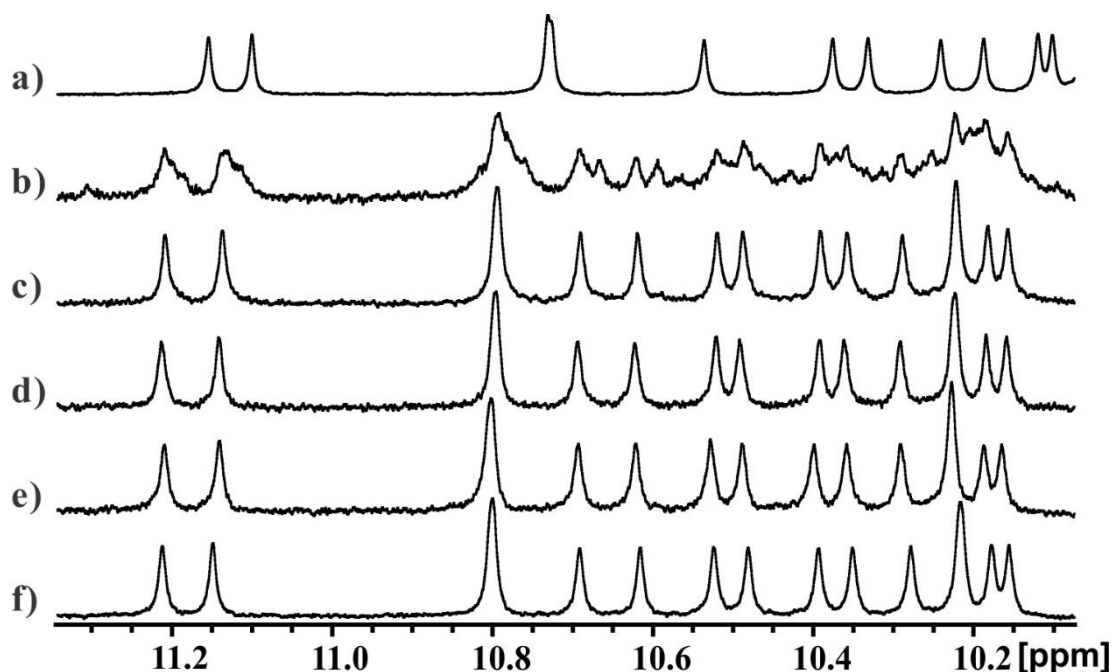


Figure 16 Excerpt of ¹H NMR spectra (300 MHz) of synthesis of ¹⁵BrQ₁₆ at 70 °C: a) starting material bromine-free 16mer, b) reaction crude after 12 h, c) after 3 days, d) after 5 days, e) after 6 days, f) after purification with flash silica gel column.

Table 2 The number of foldamers with varied number of bromine atoms

		1 Br	2 Br	3 Br	4 Br	5 Br	6 Br	7 Br	8 Br	9 Br	10 Br	11 Br	12 Br	13 Br	14 Br	15 Br
8mer	1	7	21	35	35	21	7	1								
16mer	1	15	105	455	1365	3003	5005	6435	6435	5005	3003	1365	455	105	15	1
32mer	1	31	465	4495	31465	169911	736281	2629575	7888725	20160075	44352165	84672315	141120525	206253075	265182525	300540195
32mer*	31 Br	30 Br	29 Br	28 Br	27 Br	26 Br	25 Br	24 Br	23 Br	22 Br	21 Br	20 Br	19 Br	18 Br	17 Br	16 Br
	1	31	465	4495	31465	169911	736281	2629575	7888725	20160075	44352165	84672315	141120525	206253075	265182525	300540195

*The numbers of Q_{32} foldamers with 16 – 31 bromines on the backbones in this row are equal to the numbers of those Q_{32} ones with 15 – 0 bromines in the former row, namely, the number of $^{(31-x)Br}Q_{32}$ = the number of $^{xBr}Q_{32}$, where $x = 0, 1, 2, \dots, 31$. For the number y of foldamers with varied bromines towards all these three series of foldamers (with n quinoline units, $n = 8, 16$ and 32), a generalized formula could be expressed as $y^{(n-x-1)Q_n} = y^{(x)Q_n} = \frac{(n-1)!}{(n-x-1)!x!} = \frac{(n-1)(n-2)(n-3)\dots(n-x)}{x(x-1)(x-2)\dots 1}$, where $n = 8, 16$ or 32 ; $x = 0, 1, 2, \dots, n-1$.

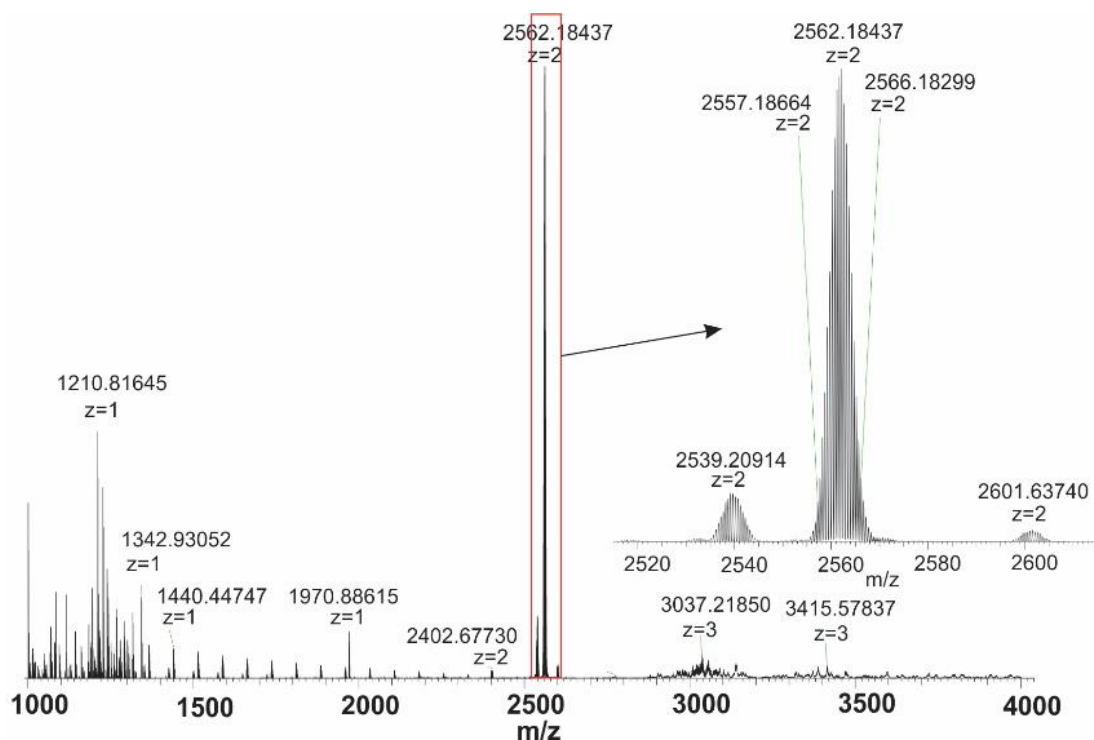


Figure 17 HRMS full spectra of brominated 16mer $^{15}\text{BrQ}_{16}$ and its representative section. This sample is measured with a condition of FTMS & *p* ESI. In the small HRMS curve, that two series of small peaks appeared is caused by the substitution of one chlorine atom and fourteen bromine atoms (m/z is around 2539, $z=2$), and the one more bromine atom substitution on foldamer, namely, a 16mer with 16 Bromines, not expected 15 Bromines. Both are caused by long reaction time and can be avoided using short time and higher temperature.

The corresponding anhydride 32mer $^{30}\text{BrQ}_{32}$ **15** was then synthesized. After saponification of brominated 16mer **12a** $^{15}\text{BrQ}_{16}$ into its acid **12b** (Figure 18a), subsequent activation of this acid **12b** generated the corresponding acid chloride **12c** (Figure 18b). In the presence of DIPEA, **12c** was added into **12b**, and reaction was allowed to last overnight and finally provided the target product 32mer $^{30}\text{BrQ}_{32}$ **15** (Figure 18d). It must be noted here that this triacontabromo 32mer $^{30}\text{BrQ}_{32}$ exhibits very good solubility, effortlessly dissolving in chloroform, toluene and even dichloromethane, which was not possible for the bromine-free foldamers of 32 quinoline units. The existence of bromine on the backbone of this anhydride 32mer **15** gives access to a good solubility, even better than its starting material, brominated 16mer **12a**.

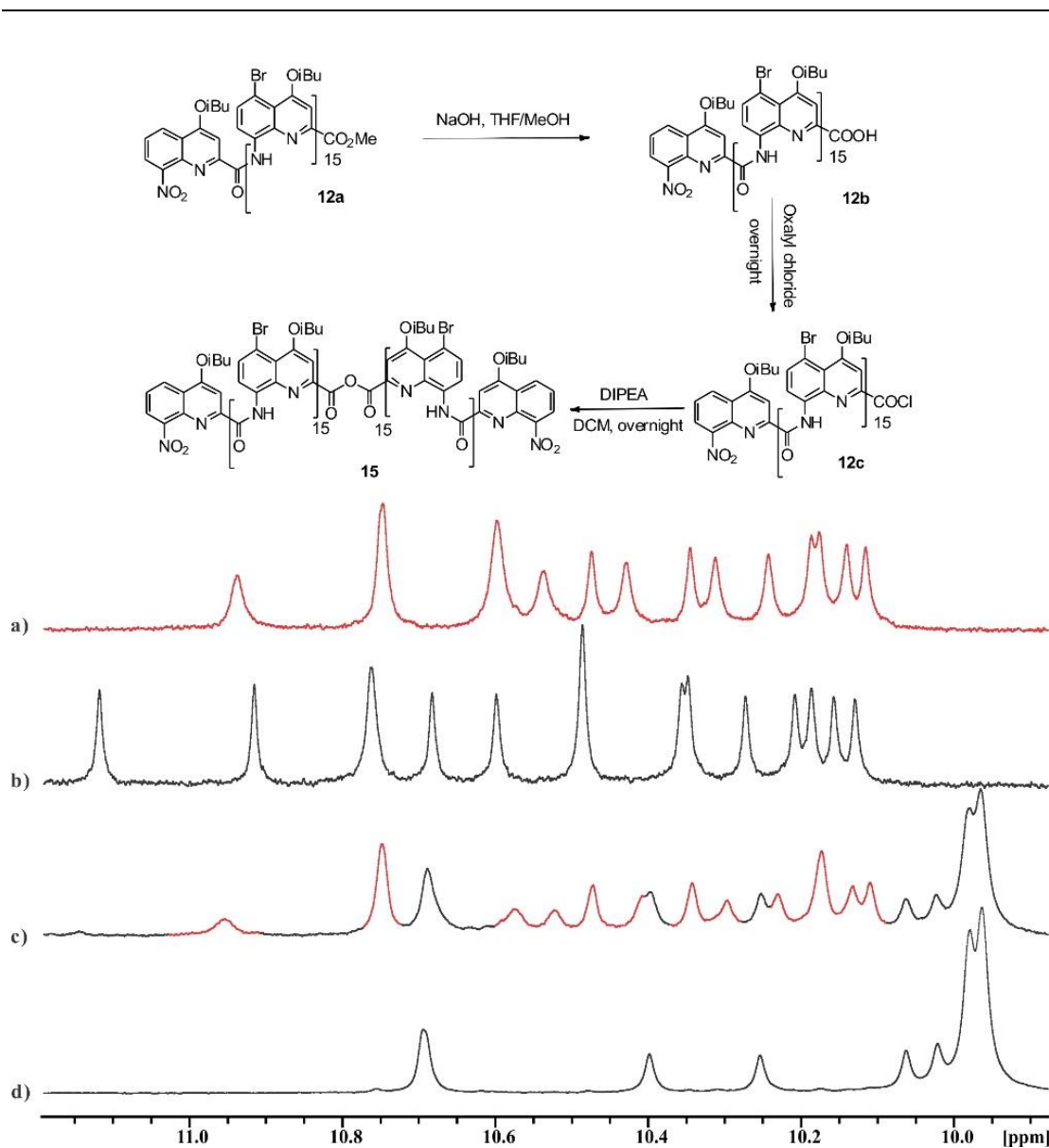


Figure 18 Representative section of ^1H NMR spectra (300 MHz) of preparation for 32mer $^{30}\text{BrQ}_{32}$: a) brominated 16mer acid $^{15}\text{BrQ}_{16}\text{-COOH}$, b) acid chloride $^{15}\text{BrQ}_{16}\text{-COCl}$, c) reaction crude after overnight and d) purified 32mer $^{30}\text{BrQ}_{32}$ after recycling gel permeation chromatography. Peaks marked as red in c) stands for $^{15}\text{BrQ}_{16}\text{-COOH}$.

Since bromination of octamer **5a** and 16mer **6a** have shown that they can produce clean and unique oligomers by controlling the reaction temperature and reaction time, respectively, bromination of the longer oligomer, 32mer **Q₃₂** **8a**, was tested. At first, bromination of 32mer was started using similar reaction condition as those for octamer **5a** and 16mer **6a**: the same concentration of 32mer and saturated NBS in 1,2-dichloroethane. Unfortunately, it was found that it is difficult to complete bromination because of the poor solubility of 32mer **8a** in 1,2-dichloroethane. The low concentration of 32mer undoubtedly caused long reaction time, which,

subsequently, resulted in the chlorination of compound **8a** caused by the decomposition of solvent 1,2-dichloroethane during a long reaction time. Considering the huge number of intermediates (Table 2) and the presence of side reaction, bromination of 32mer in 1,2-dichloroethane seems to be problematic. To avoid the presence of by-product, the solvent used for the bromination of 32mer should have a good solubility for compound **8a** and meanwhile, the reaction should finish in an appropriate time. Many efforts have thus been made, for example, change of the reaction temperature and exploration of alternative solvents (tetrachloromethane, 1,2-dibromoethane, dioxane, toluene and their mixtures). Unfortunately, obtaining the unique expected product, $^{31}\text{BrQ}_{32}$, in a time frame that is acceptable for routine synthesis like couple of weeks (maximum) was extremely difficult. To prepare the expected brominated 32mer $^{30}\text{BrQ}_{32}$, a reaction operated in bromobenzene after around 80 days at 70 °C gave the good result (Figure 19). HNMR result showed the sharp signal around amide region (Figure 19f), and the subsequent HRMS results exactly confirmed that the resulting compound was the expected product, 32mer with thirty one (31) bromines on the backbone (Figure 20).

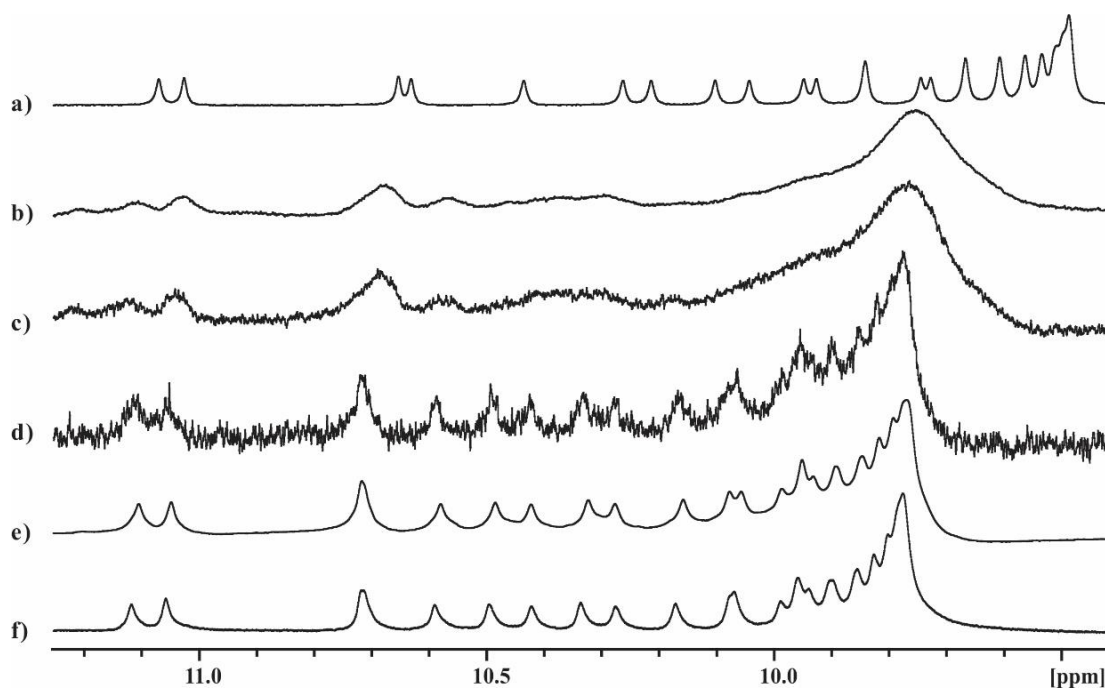


Figure 19 Excerpt of ^1H NMR spectra (300 MHz) of synthesis of $^{31}\text{BrQ}_{32}$: a) starting material bromine-free Q_{32} , b) reaction result after 2.5 days, c) after 10 days, d) after approx. 30 days, e) after more than 60 days and f) after approx. 80 days.

Nevertheless, the bromination of 32mer is proven to work, even though the reaction time is long.

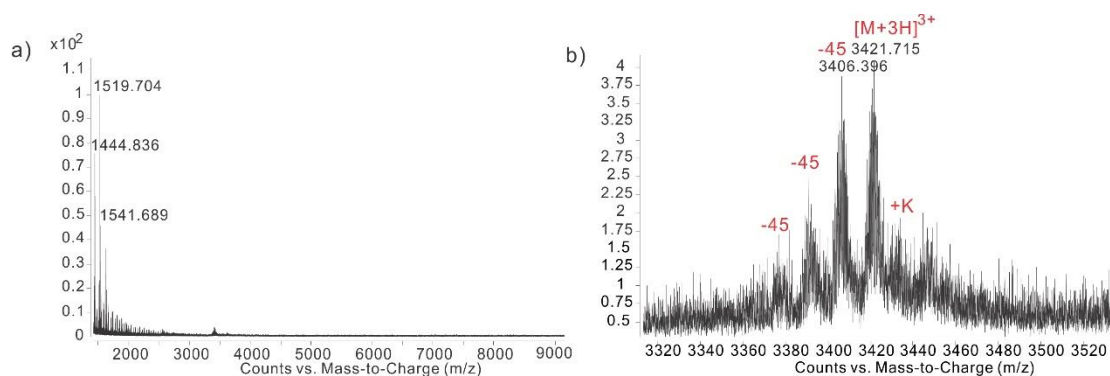


Figure 20 HRMS spectrum of brominated 32mer, measured with a condition of FTMS & *p* ESI. The main peaks stands for the desired product with 31 bromines ($^{31}\text{BrQ}_{32}$, see $[M+3H]^{3+}$ peak in b)). The three peaks on the left of the main peak $[M+3H]^{3+}$ are compounds of partial chlorination (from right to left): $(1\text{Cl}+30\text{Br})\text{Q}_{32}$, $(2\text{Cl}+29\text{Br})\text{Q}_{32}$ and $(3\text{Cl}+28\text{Br})\text{Q}_{32}$, respectively. The peak on the right of the main peak $[M+3H]^{3+}$ is the target fragment plus K^+ .

Given these experiments and data mentioned above, a one-pot multi-bromination of nanosized foldamer backbones has been realized, and this reaction is able to provide only one unique final product after certain reaction time and temperature with excess quantity of NBS. Upon the final unique product, hydrogen atom at 5th position of each quinoline unit of foldameric molecules can be distinctively substituted by bromine atom, apart from the N-terminal quinoline unit where the nitro group, an electron withdrawing group, probably has a negative effect on electrophilic aromatic substitution of quinoline unit.

Considering that the brominated oligomer possesses a better solubility in organic solvents than the corresponding bromine-free one, it was expected that longer hybrid foldamers that are derived from the combination of brominated foldamers with bromine-free foldamers would propably have the enhanced solubility. If so, this improved solubility provides us the possibility to explore the synthesis of oligomers longer than 64mer, and the possibility to separate these resulting oligomers from their starting materials. Two asymmetrical quinoline-based foldamers **16a** and **17a** then were designed and synthesized by using $^7\text{BrQ}_8$ **11a** and $^{15}\text{BrQ}_{16}$ **12a** as starting materials, respectively(Figure 21). In the presence of DIPEA coupling of bromine-free 32mer

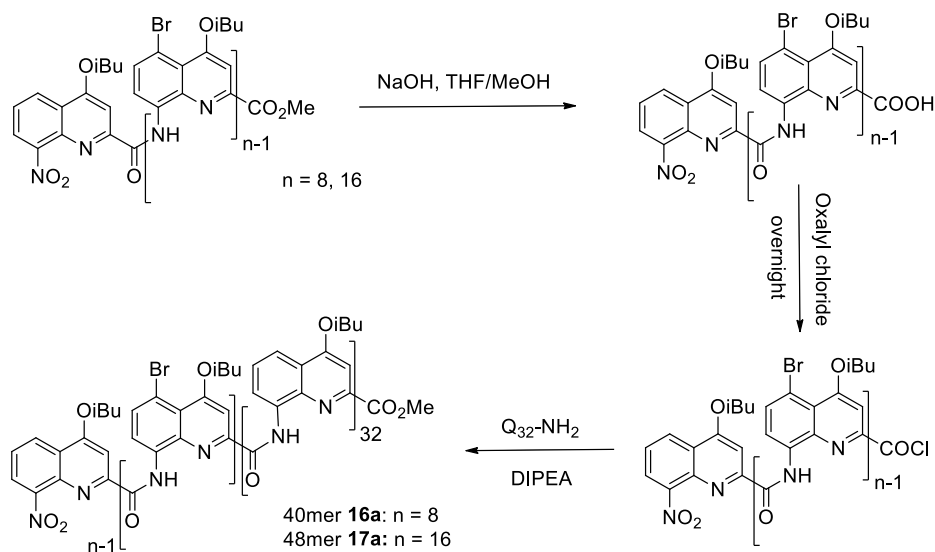


Figure 21 Synthetic scheme of asymmetrical foldamers 40mer **16a** and 48mer **17a**.

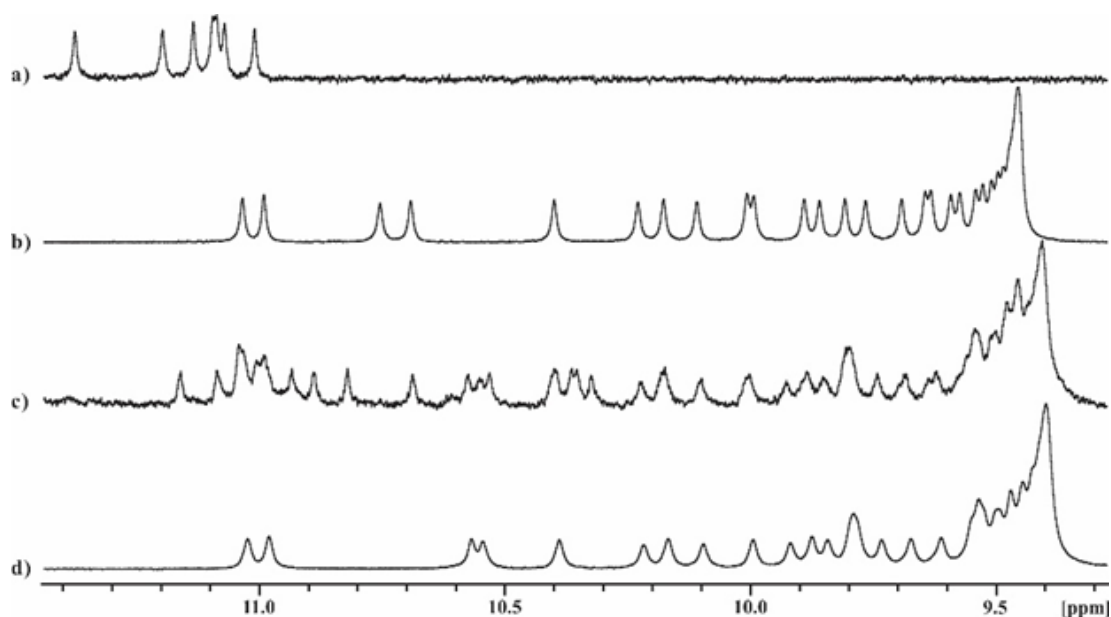


Figure 22 Representative ^1H NMR spectra (300 MHz) of syntheses of asymmetrical 40mer **16a**: a) brominated octamer acid chloride $^{7\text{Br}}\text{Q}_8\text{-COCl}$, b) 32mer amine $\text{Q}_{32}\text{-NH}_2$, c) reaction crude and d) pure 40mer $^{7\text{Br}}\text{Q}_{40}$.

amine **8d** and excess of brominated 8mer acid chloride $^{7\text{Br}}\text{Q}_8\text{-COCl}$ **11c** that resulted from activation of **11b** with oxalyl chloride generated crude mixture containing 40mer **16a**, variable amount of anhydride **14** and Q_{32} amine **8d**. Purification was achieved by using recycling GPC, and finally provided pure 40mer $^{7\text{Br}}\text{Q}_{40}$ **16a** (Figure 22). By the same token, pure 48mer $^{15\text{Br}}\text{Q}_{48}$ **17a** was synthesized by combining bromine-free 32mer amine **8d** and excess of brominated

16mer acid chloride $^{15}\text{BrQ}_{16}\text{-COCl}$ **12c**, and by being purified with recycling GPC (Figure 23). As expected, both of these two nanosized hybrid foldamers displayed respectable solubility in general solvents, e. g. chloroform. One common feature of these two nano-sized foldamers lies in their asymmetrical constitution including an solubilizing fragment at one terminal. These two asymmetrical foldamers 40mer **16a** and 48mer **17a** exhibit a better solubility in chloroform than the shorter bromine-free 32mer. It dicloses that bromination of even a partial fragment of foldamer still can increase the solubility of the whole foldamer molecule, which permits us to employ them as starting materials for the elongation of foldamer, preparing nanosized foldamers longer than the bromine-free 64mer.

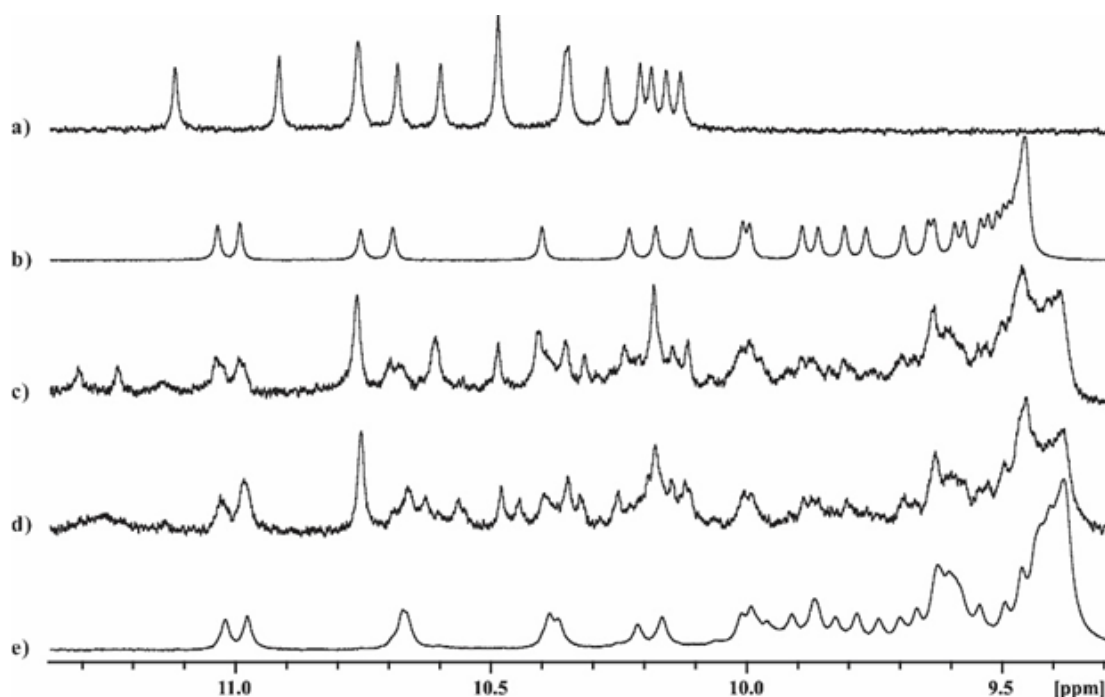


Figure 23 Representative section of ^1H NMR spectra (300 MHz) of syntheses of asymmetrical 48mer **17a**: a) brominated 16mer acid chloride $^{15}\text{BrQ}_{16}\text{-COCl}$, b) 32mer amine $\text{Q}_{32}\text{-NH}_2$, c) reaction crude, d) crude after refluxing in pyriding/water and e) pure 48mer $^{15}\text{BrQ}_{48}$.

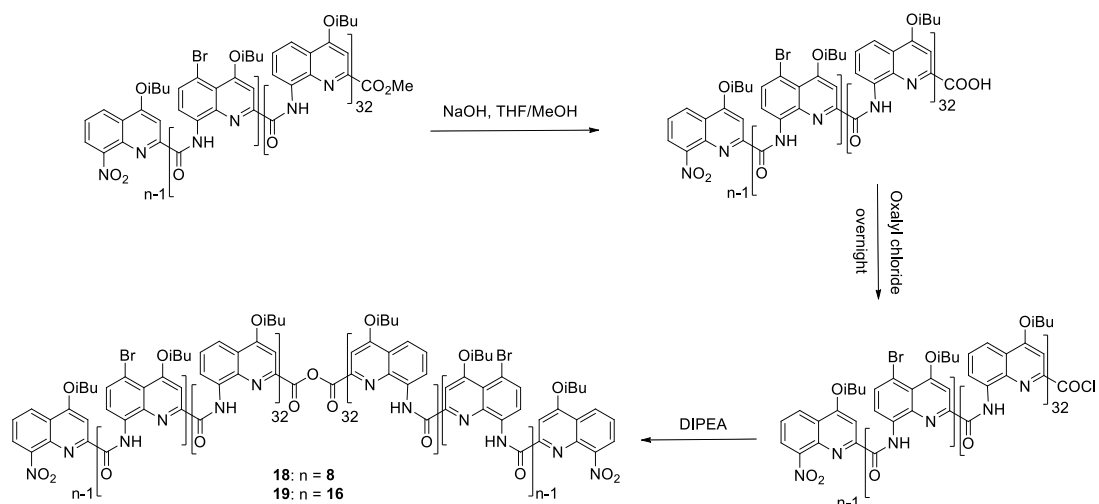


Figure 24 Synthetic scheme of anhydride-form foldamers 80mer **18** and 96mer **19** which are based on asymmetrical, partially brominated oligomers **16a** and **17a**, respectively.

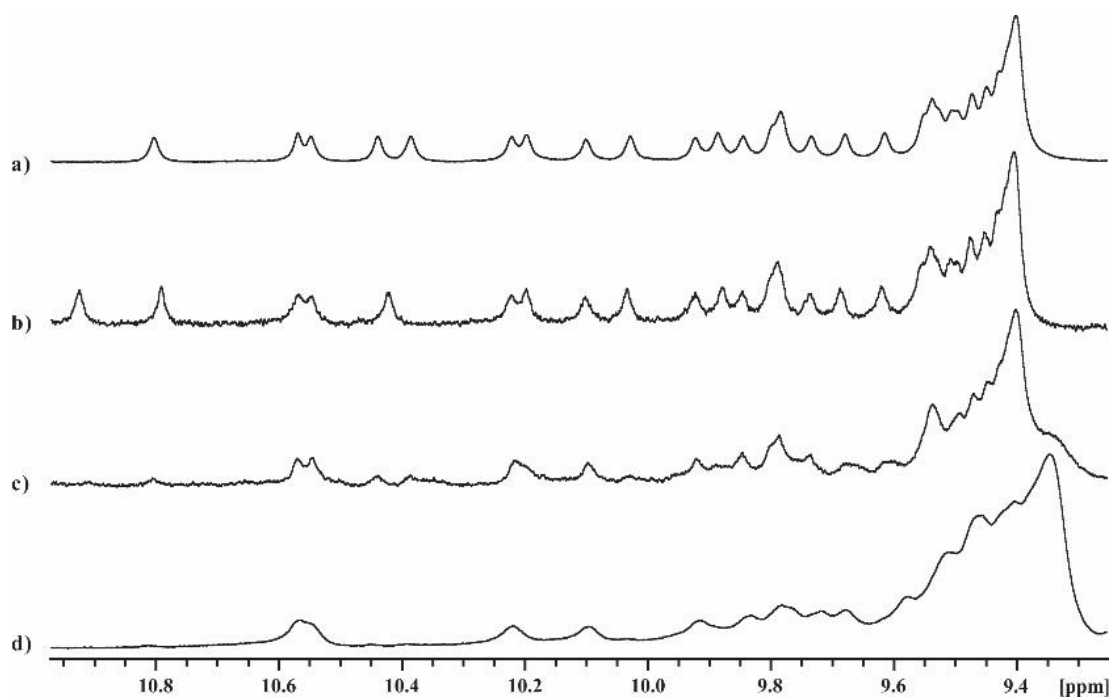


Figure 25 Excerpt of ^1H NMR spectra (300 MHz) of syntheses of 80mer **18**: a) 40mer acid $^7\text{BrQ}_{40}\text{-COOH}$, b) 40mer acid chloride $^7\text{BrQ}_{40}\text{-COCl}$, c) reaction crude and d) pure 80mer $^{14}\text{BrQ}_{80}$ from recycling GPC.

The saponification of 40mer **16a** with NaOH in THF/MeOH provided its acids **16b**. After activation to its acid chloride **16c** by using oxalyl chloride, this reactive acid chloride was coupled to its corresponding acids **16b**, yielding the anhydride 80mer **18** (Figure 24 and 25). Even though this symmetrical anhydride foldamer possesses huge folded structure (approx. 12 nm in length) and high molecular weight (approx. 20.7 kDa) that are larger than the ones of

bromine-free 64mer, it still displays comparable solubility in chloroform (Figure 25). Thanks to the great solubility, this nanosized foldamer can be easily purified by using the recycling GPC. As presented in Figure 26a, the product 80mer **18** can be separated completely from the starting material **16b** only after 2 cycles.

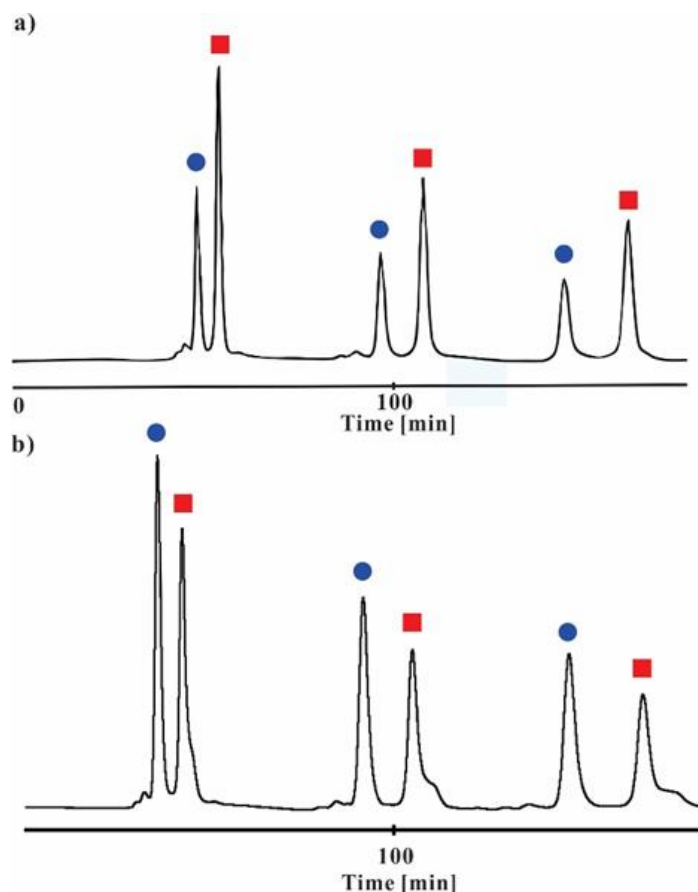


Figure 26 Curves of purification of a) 80mer **18** and b) 96mer **19** with recycling GPC: peaks marked with blue circles stand for target products 80mer or 96mer; peaks marked with red square mean the starting materials 40mer acid **16b** or 48mer acid **17b**.

A longer anhydride foldamer 96mer **19** was also synthesized by coupling 48mer acid **17b** and its corresponding acid chloride **17c** (Figure 24). This foldamer molecule, 96mer **19**, of approx. 14 nm in helical length and about 25.7 kDa molecular weight even exhibits a better solubility in chloroform than the shorter 80mer **18**, which is probably caused by the presence of more bromine atoms on the backbone. Bromine atoms increase the interaction between foldamer molecule and the solvent molecule, and further strengthens the solubility of foldamer. The

recycling GPC (Figure 26b) was employed again here to separate this huge nanosized oligomer **19** from its starting material 48mer acid **17b** (Figure 27).

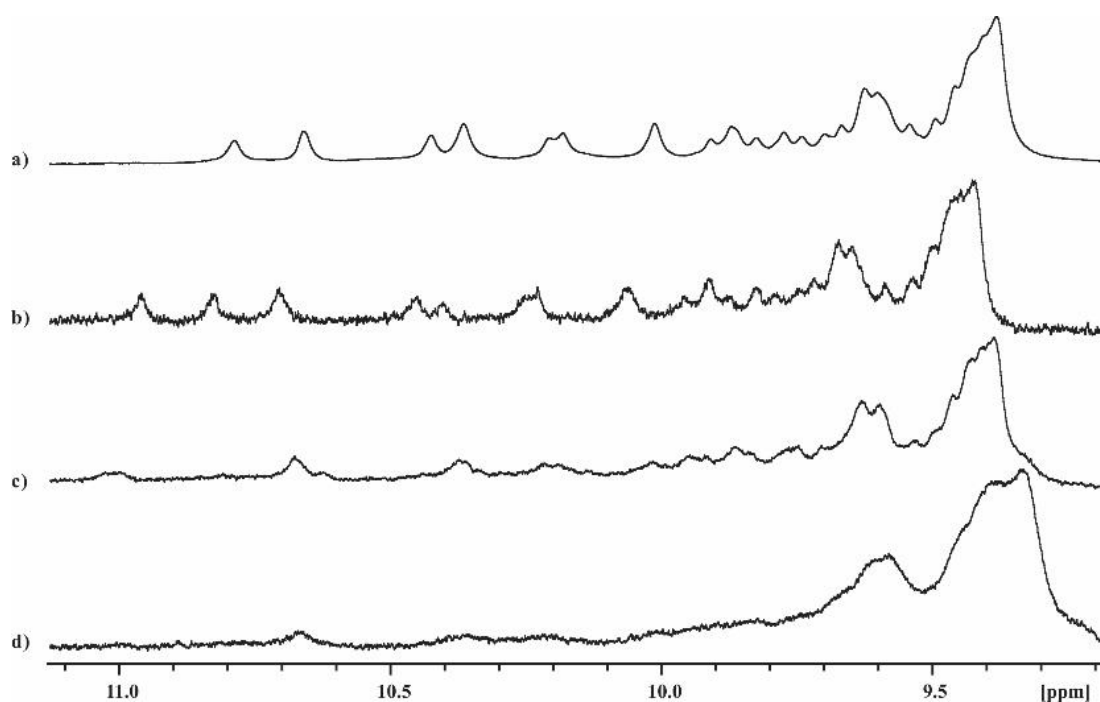


Figure 27 Excerpt of ^1H NMR spectra (300 MHz) of syntheses of 96mer **19**: a) 48mer acid $^{15}\text{BrQ}_{48}\text{-COOH}$, b) 40mer acid chloride $^{15}\text{BrQ}_{48}\text{-COCl}$, c) reaction crude and d) pure 96mer $^{30}\text{BrQ}_{96}$ from recycling GPC.

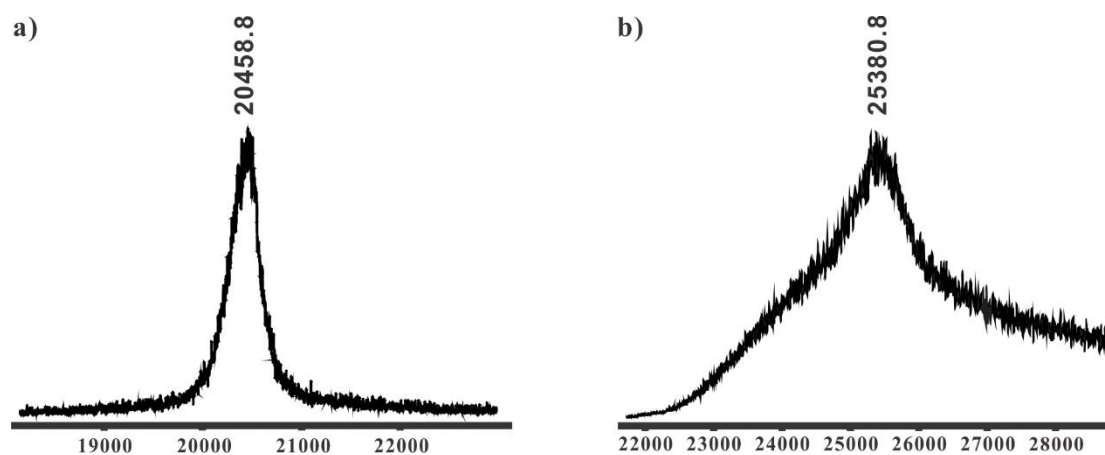


Figure 28 MALDI mass spectra of nanosized foldamers: 80mer (a) and 96mer (b).

Since the molecules **18** and **19** are so huge, the HNMR signals of these two huge molecules would overlap severely, leading to the difficult assignment of singals. As shown in Figure 25d and 27d, overlap of amide region of these two foldamers occurred and the appearance of broad

signals replaces the presence of sharp peaks. Mass spectrum provides an approach to identify the molecules as expected. Figure 28 shows the MALDI results of these two huge foldamer molecules.

4 Conclusion

Based on the chromatography-free large scale synthesis of quinolone-based octameric helix, longer nanosized aromatic helical oligomers have been synthesized. When segment doubling strategy was employed to synthesize these nanosized foldamers by coupling the oligomeric acid chloride with its corresponding amine, the formation of anhydride and the presence of remaining amine made the purification of product problematic. Introduction into the workup of a protocol that hydrolyzed anhydride into acid by refluxing the reaction crude in pyridine/H₂O mixture, and that an excess quantity of acid chloride was used to avoid the presence of some unreacted of amine, allowed us to prepare the nanosized aromatic foldamers (up to 64mer **10**, approx. 9nm, 15.6 kDa). The poor solubility of 64mer, however, limits the further elongation of this series of oligomer.

We found that one-pot bromination of backbone of quinoline-based foldamers can be achieved by monitoring the reaction temperature and the reaction time with excess quantity of NBS. More importantly, bromination gives access to the growing solubility of brominated foldamers. Substitution of H atom at position 5 of quinoline ring with Br atom can dramatically expand the solubility of the resulting brominated foldamers (e.g., **14** and **15**). As combining these brominated foldamers with the bromine-free oligomer, the resulting macromolecules (**16a** and **17a**) also display good solubility, which permits us to explore synthesis of longer foldamers. The longer oligomers, anhydride 80mer **18** and 96mer **19**, that originate from **16a** and **17a** have been synthesized, and even exhibit better solubility than the short but bromine-free foldamer (i.e. 64mer **10**) in organic solvent. Thanks to the increasing solubility, pure huge oligomers with well-defined helical structures, 80mer **18** (~12 nm) and 96mer **19** (~14 nm) have been prepared and purified *via* using recycling GPC.

5 Experimental Section

5.1 Methods of NMR

NMR data were recorded at 300 MHz using an Avance II NMR spectrometer (Bruker Biospin) with a vertical 7.05T narrow-bore/ultrashield magnet operating at 300 MHz for ^1H observation and 75 MHz for ^{13}C observation by means of a 5-mm direct BBO H/X probe with Z gradient capabilities. All chemical shifts are quoted in parts per million (ppm, δ) relative to the ^1H residual signal of the deuterated solvent used (CDCl_3 at 7.26 ppm). ^1H NMR splitting patterns with observed first-order coupling are designated as singlet (s), doublet (d), double doublet (dd), triplet (t), or quartet (q). Splitting patterns that could not be interpreted or easily visualized are designated as multiplet (m) or broad (br). Coupling constants (J) are reported in hertz. Samples were not degassed. Data processing was performed with Topspin 2.0 software.

5.2 Methods of X-Ray Crystallography

Crystallographic data for compound heptabromo 8mer 2a were collected at the IECB x-ray facility (UMS 3033 – UMS001) on a Rigaku FRX rotating anode (2.9 kW). Data were collected at the copper $\text{k}\alpha$ wavelength with a partial chi goniometer. The x-ray source is equipped with high flux Osmic Varimax mirrors and a Dectris Pilatus 200K detector.

Crystallographic data for compound Y were collected at the PROXIMA 1 (SOLEIL) beamline at 0.855 Å. Phi-scans were performed and data recorded with a large ADSC Q315r CCD detector. The Rigaku CrystalClear suite2 was used to index and integrate the home source data with a multiscan absorption correction. Data collected at the synchrotron were processed with the XDS package3. All structures were solved by direct methods with Shelxd3 and refined by full-matrix least-squares methods with shelxl4 using WinGX5 software. The SQUEEZE procedure6 implemented in WinGX was used for all structures in order to treat the regions with highly disordered solvent molecules (mainly chloroform, water, and methanol). The positions of the H atoms were deduced from coordinates of the non-H atoms and confirmed by Fourier synthesis. The non-H atoms were refined with anisotropic temperature parameters. H atoms

were included for structure factor calculations but not refined. SHELX SIMU and DELU restraints were used in the refinement strategy in order to reduce the anisotropic displacement parameters of the lateral chains. DFIX instructions were used to geometrically restraint most of these side chains too.

The final cif files were checked using IUCR's checkcif algorithm. Due to the characteristics of the crystals mentioned above (large volume fractions of disordered solvent molecules and side chains for the sk48, weak diffraction intensity, incompleteness of the data and moderate resolution), a number of A - level and B - level alerts remain in the check cif file. These alerts are explicitly listed below and have been divided into two groups. They are inherent to the data and refinement procedures and do not reflect errors. Rather, they illustrate the limited practicality of the checkcif tool for medium size molecule crystallography.

The functional group O12-C11-O13 is a methyl ester group whose methyl is not defined in a discrete position. The mean length of the Csp2-O bonds indicate a disordered and fractional occupancy of this methyl group between both oxygen atoms.

GROUP 1 ALERTS

Alert level A

CHEMW03_ALERT_2_A ALERT: The ratio of given/expected molecular weight as calculated from the _atom_site* data lies outside

PLAT043_ALERT_1_A Calculated and Reported Mol. Weight Differ by .. Check

PLAT051_ALERT_1_A Mu(calc) and Mu(CIF) Ratio Differs from 1.0 by . %

PLAT602_ALERT_2_A VERY LARGE Solvent Accessible VOID(S) in Structure ! Info

Alert level C

PLAT041_ALERT_1_C Calc. and Reported SumFormula Strings Differ Please Check

PLAT068_ALERT_1_C Reported F000 Differs from Calcd (or Missing)... Please Check

All these alerts are due to the squeeze procedure where calculated solvent molecules are added

to the SFAC and UNIT instructions of the squeezed structure.

GROUP 2 ALERTS

Alert level A

THETM01_ALERT_3_A The value of $\sin(\theta_{\max})/\lambda$ is less than 0.550

Alert level B

RFACR01_ALERT_3_B The value of the weighted R factor is > 0.35

PLAT084_ALERT_3_B High wR_2 Value (i.e. > 0.25) Report

PLAT341_ALERT_3_B Low Bond Precision on C-C Bonds 0.0195 Ang.

PLAT220_ALERT_2_B Large Non-Solvent C $U_{\text{eq}}(\max)/U_{\text{eq}}(\min)$ Range 6.4 Ratio

PLAT222_ALERT_3_B Large Non-Solvent H $U_{\text{iso}}(\max)/U_{\text{iso}}(\min)$... 7.3 Ratio

PLAT230_ALERT_2_B Hirshfeld Test Diff for O90 -- C83 .. 7.2 su

PLAT234_ALERT_4_B Large Hirshfeld Difference C35 -- C37 .. 0.28 Ang.

PLAT242_ALERT_2_B Low U_{eq} as Compared to Neighbors for C35 Check

PLAT369_ALERT_2_B Long C(sp²)-C(sp²) Bond C59 - C62 .. 1.59 Ang.

Alert level C

RFACG01_ALERT_3_C The value of the R factor is > 0.10

R factor given 0.149

PLAT026_ALERT_3_C Ratio Observed / Unique Reflections too Low 45 %

PLAT082_ALERT_2_C High R_1 Value 0.15 Report

PLAT213_ALERT_2_C Atom C6 has ADP max/min Ratio 3.2 prolat

PLAT213_ALERT_2_C Atom C74 has ADP max/min Ratio 3.6 prolat

PLAT230_ALERT_2_C Hirshfeld Test Diff for... .. 6.5 su

PLAT234_ALERT_4_C Large Hirshfeld Difference 0.17 Ang.

PLAT241_ALERT_2_C High U_{eq} as Compared to Neighbors for N11 Check

PLAT242_ALERT_2_C Low U_{eq} as Compared to Neighbors for O14 Check

All these alerts in fact point to the same and unique problem which is the overall weak quality of the data and refinement statistics if compared to that expected for small molecule structures

from highly diffracting

Most of the other alerts are related to geometrical and atomic displacement parameters problems, all concerning disordered side chains. Many of these alerts are redundant: for example, a “unusually high $U(\text{eq})$ as compared with bonded neighbors” generally goes with one or several “unusually low $U(\text{eq})$ as compared with bonded neighbors”.

Because of too many disordered side chains, their atom site occupancies have been constrained rather than using FVAR values.

5.3 Summary of X-Ray Crystallography

Identification code	Compound 11a
Empirical formula	C114 H105 Br7 Cl9 N16 O19
Formula weight	2881.56
Temperature	153(2) K
Wavelength	1.54178 Å
Crystal system	Monoclinic
Space group	P21/n
Unit cell dimensions	$a = 19.423(4) \text{ \AA}$, $\alpha = 90^\circ$ $b = 23.548(5) \text{ \AA}$, $\beta = 98.09(3)^\circ$ $c = 30.226(6) \text{ \AA}$, $\gamma = 90^\circ$
Volume	$13686(5) \text{ \AA}^3$
Z	4
Density (calculated)	1.398 Mg/m^3
Absorption coefficient	4.607 mm^{-1}
F(000)	5804
Crystal size	$0.12 \times 0.10 \times 0.08 \text{ mm}^3$
Theta range for data collection	2.97 to 68.66°
Index ranges	$-23 \leq h \leq 23$, $-28 \leq k \leq 21$, $-35 \leq l \leq 36$
Reflections collected	77653
Independent reflections	24823 [R(int) = 0.0813]
Completeness to theta = 68.66°	98.1 %
Absorption correction	Semi-empirical from equivalents
Max. and min. transmission	0.7092 and 0.6076
Refinement method	Full-matrix least-squares on F^2

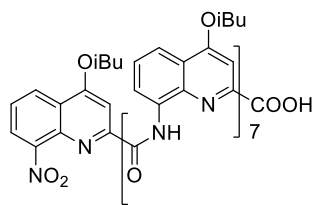
Data / restraints / parameters	24823 / 160 / 1390
Goodness-of-fit on F^2	1.500
Final R indices [$I > 2\sigma(I)$]	R1 = 0.1486, wR2 = 0.3486
R indices (all data)	R1 = 0.1830, wR2 = 0.3609
Largest diff. peak and hole	1.777 and -0.588 e. \AA^{-3}

5.4 Methods of Chemical Synthesis

All reactions were carried out under a dry nitrogen environment. Chemicals and reagents were used as commercially supplied without any further purification unless otherwise stated. Dichloromethane (DCM), Tetrahydrofuran (THF) and Toluene were dried over alumina columns under nitrogen. Chloroform, triethylamine (Et_3N) and diisopropylethylamine (DIEA) were distilled over calcium hydride (CaH_2) prior to use. Reactions were monitored by thin layer chromatography (TLC) on Merck silica gel 60-F254 plates and observed under UV light (254 and 365 nm). Column chromatography was carried out on Merck GEDURAN Si60 (40-63 μm). Circular chromatography purifications were carried out on Chromatotron® with silica gel, Merck grade 7749, TLC grade with binder and fluorescent indicator. Analytical and semi-preparative GPC was carried out on Shimadzu Recycling GPC system equipped with LC-20 AD pump, SPD-M20A UV detector and a set of 1H, 1.5H, 2.5H and 3H columns (size: 20×600 mm) in chloroform/0.5~1% ethanol as eluent with a flow rate of 3.5 mL/min. ESI and MALDI mass spectra were obtained on a Waters LCT Premier and a Bruker Reflex III spectrometers respectively, from the Mass Spectrometry Laboratory at the European Institute of Chemistry and Biology (UMS 3033 - IECB), Pessac, France and a Voyager DE-STR mass spectrometer from AB Sciex, Les Ulis, France.

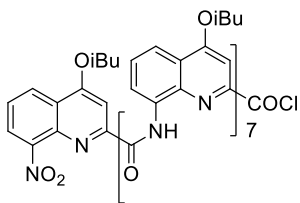
Dimer and its acid/amine, tetramer and its acid/amine, hexamer and its acid/amine and octamer from 4-isobutoxyl-8-amino-2-quinolinecarboxyl acid were synthesized by using the published procedures.¹⁸

5.4.1 Synthesis of 16-mer



Octamer acid (Q₈-COOH) 5b. Octamer **5a** (13 g, 6.5 mmol) was dissolved in 500mL THF/MeOH (9/1, v/v) and then ground NaOH (5.2 g, 130 mmol) was added. This mixture was stirred at room temperature for around 0.5 h and monitored with TLC

(cyclohexane/ethyl acetate = 7/3) until the reaction completed. 0.1 M HCl was used to neutralize the base and acidify the solution to approximate 5 (pH value). After removal of organic solvents, the resultant mixture was dissolved in CHCl₃, washed with H₂O and brine and dried with anhydrous Na₂SO₄, filtrated and concentrated to yield acid **5b** quantitatively as a yellowish solid. ¹H NMR(300 MHz, CDCl₃): δ 11.30 (s, 1H), 11.18 (s, 1H), 11.08 (s, 1H), 11.01 (s, 1H), 10.98 (s, 1H), 10.96 (s, 1H), 10.83 (s, 1H), 8.32 (dd, *J* = 8.3, 1.5 Hz, 1H), 8.23 (dd, *J* = 7.7, 1.2 Hz, 2H), 8.18 (dd, *J* = 4.2, 1.3 Hz, 1H), 8.16 (dd, *J* = 3.6, 1.3 Hz, 1H), 8.12 (dd, *J* = 8.3, 1.3 Hz, 1H), 8.05 (dd, *J* = 7.7, 1.2 Hz, 1H), 7.91 (dd, *J* = 3.0, 1.3 Hz, 1H), 7.90 – 7.85 (m, 2H), 7.84 (s, 1H), 7.81 (s, 1H), 7.66 (dd, *J* = 7.7, 1.3 Hz, 1H), 7.54 (dd, *J* = 7.6, 1.2 Hz, 1H), 7.44 (td, *J* = 8.0, 4.2 Hz, 2H), 7.35 – 7.21 (m, 6H), 7.19 – 7.12 (m, 1H), 7.06 (s, 1H), 7.02(s, 1H), 6.98 (d, *J* = 8.0 Hz, 1H), 6.80 (s, 1H), 6.69 (s, 1H), 6.52 (s, 1H), 6.48 (s, 1H), 6.45 (s, 1H), 6.15 (s, 1H), 4.18 – 4.04 (m, 3H), 4.04 – 3.81 (m, 10H), 3.74 (d, *J* = 6.4 Hz, 2H), 3.66 (dd, *J* = 9.1, 7.4 Hz, 1H), 2.51 (m, 2H), 2.44 – 2.25 (m, 5H), 2.25 – 2.18 (m, 1H), 1.38 – 1.33 (m, 8H), 1.27 – 1.10 (m, 40H). ¹³C NMR (CDCl₃, 75 MHz): δ 163.16, 163.13, 162.91, 162.76, 162.73, 162.66, 162.46, 162.31, 161.86, 160.80, 160.53, 160.38, 160.06, 159.68, 159.23, 159.19, 153.00, 149.87, 149.02, 148.62, 148.25, 148.21, 144.66, 144.02, 138.62, 138.09, 137.84, 137.74, 137.55, 137.51, 137.19, 137.15, 134.13, 133.60, 133.03, 132.80, 132.72, 132.62, 132.40, 127.88, 127.72, 127.02, 126.90, 126.34, 125.87, 125.63, 125.49, 123.74, 123.53, 122.49, 122.36, 122.23, 122.22, 121.95, 121.76, 121.61, 117.90, 117.39, 116.88, 116.65, 116.49, 116.33, 116.26, 116.10, 115.94, 115.91, 115.55, 99.81, 99.48, 99.05, 98.53, 98.40, 98.18, 97.90, 97.73, 77.27, 75.51, 75.33, 75.23, 75.02, 30.35, 28.21, 28.19, 28.14, 28.11, 28.09, 28.04, 27.95, 19.61, 19.57, 19.53, 19.48, 19.46, 19.38, 19.36, 19.32, 19.22, 19.12. MS (ES⁺): *m/z* calcd for C₁₁₂H₁₁₂N₁₆O₁₉ [M+H]⁺ 1986.8 found 1986.8.



Octamer acid chloride (Q8-COCl) 5c. Dry **5b** (13 g, 6.5 mmol)

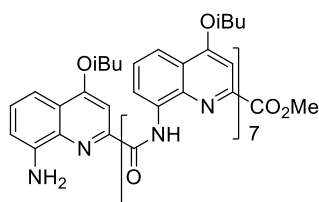
was dissolved in 50 mL CHCl_3 . Oxalyl chloride (5.6 mL) was put into the mixture dropwise under nitrogen at 0°C . The reaction was

warmed up to room temperature and lasted for approx. 3h. After

complete, the mixture was dried under vacuum for approx. 5 h to remove solvent and remaining

oxalyl chloride to yield **5c** quantitatively as a pale yellowish solid. ^1H NMR (300 MHz, CDCl_3):

δ 11.44 (s, 1H), 11.21 (s, 1H), 11.20 (s, 1H), 11.11 (s, 1H), 11.07 (s, 1H), 11.00 (s, 2H), 8.35 (d, $J = 3.57$ Hz, 1H), 8.28 – 8.14(m, 5H), 8.08 (d, $J = 3.66$ Hz, 1H), 7.94 – 7.90 (m, 3H), 7.84 – 7.79 (m, 2H), 7.69 (d, $J = 3.63$ Hz, 1H), 7.57 (d, $J = 3.63$ Hz, 1H), 7.51 – 7.44 (m, 2H), 7.39 – 7.19 (m, 7H), 7.08 – 7.01 (m, 3H), 6.79 (s, 1H), 6.71 (s, 1H), 6.57 (s, 1H), 6.48 (s, 1H), 6.32 (s, 1H), 6.19 (s, 1H), 4.21 – 3.70 (m, 16H), 2.60 – 2.21 (m, 8H), 1.42 – 1.14 (m, 48H).



Octamer amine (Q8-NH₂) 5d. To the solvents of 250 mL

EtOAc and EtOH (4/1, v/v) were added octamer (9.0 g, 4.5 mmol), Pd/C (0.90 g, 10% w/w,) and ammonium metavanadate

(catalyst quantity) at room temperature. After this mixture was

heated up to 95°C , ammonium formate (12.8 g, in 15mL H_2O) was added into the mixture in 5

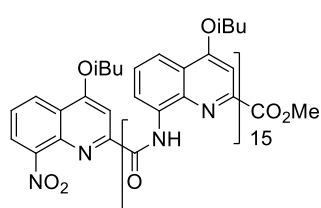
intervals (~20min per interval). The reaction mixture was stirred overnight at 95°C , filtered

through celite, washed with H_2O and brine, dried with Na_2SO_4 , filtered again concentrated to

give the product **5d** as a yellowish solid (8.73 g, 98.5% yield). ^1H NMR(300 MHz, CDCl_3): δ

11.56 (s, 1H), 11.43 (s, 1H), 11.34 (s, 1H), 11.18 (s, 1H), 11.08 (s, 1H), 11.01 (s, 1H), 10.94 (s, 1H), 8.24 (dd, $J = 7.7, 1.1$ Hz, 1H), 8.15 (dd, $J = 5.1, 1.2$ Hz, 1H), 8.14 – 8.08 (m, 2H), 8.06 (dd, $J = 7.6, 1.1$ Hz, 1H), 7.94 – 7.85 (m, 3H), 7.83 (dd, $J = 8.4, 1.2$ Hz, 1H), 7.75 (td, $J = 8.4, 1.2$ Hz, 3H), 7.64 (dd, $J = 7.6, 1.1$ Hz, 1H), 7.45 (t, $J = 8.0$ Hz, 1H), 7.38 (t, $J = 8.0$ Hz, 1H), 7.33 – 7.28 (m, 5H), 7.20 – 7.17 (m, 1H), 6.99 (t, $J = 8.0$ Hz, 1H), 6.95 (s, 1H), 6.89 (s, 1H), 6.80 (t, $J = 8.0$ Hz, 1H), 6.68 (s, 1H), 6.64 (s, 1H), 6.53 (s, 2H), 6.38 (s, 1H), 6.18 (s, 1H), 5.67 (dd, $J = 7.4, 1.0$ Hz, 1H), 4.14 (td, $J = 9.2, 6.4$ Hz, 3H), 4.01 – 3.94 (m, 4H), 3.92 – 3.79 (m, 6H), 3.68 (d, $J = 6.4$ Hz, 2H), 3.65 – 3.57 (m, 1H), 3.13 (s, 2H), 3.02 (s, 3H), 2.56 – 2.45 (m, 2H), 2.43 – 2.24 (m, 5H), 2.22 – 2.15 (m, 1H), 1.35 (m, 8H), 1.18 (m, 40H). ^{13}C NMR (CDCl_3 , 75 MHz): δ 163.71, 163.07, 162.88, 162.83, 162.73, 162.66, 162.48, 162.29, 161.94, 161.48,

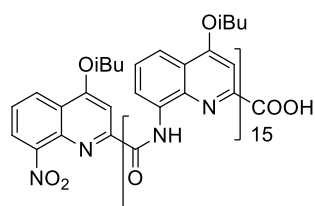
161.15, 161.09, 160.65, 159.46, 159.33, 158.95, 149.59, 149.15, 149.06, 148.82, 148.76, 148.04, 145.10, 142.93, 138.73, 138.06, 137.90, 137.64, 137.60, 137.44, 135.92, 133.67, 133.60, 133.51, 133.34, 133.03, 132.94, 132.56, 127.45, 126.88, 126.73, 126.56, 126.36, 126.00, 125.85, 122.67, 122.44, 122.31, 122.26, 121.91, 121.63, 121.44, 121.39, 116.85, 116.79, 116.62, 116.17, 116.03, 115.91, 115.64, 115.55, 115.25, 109.81, 109.25, 100.05, 99.21, 98.92, 98.70, 98.59, 98.31, 97.65, 97.45, 77.24, 75.02, 75.21, 75.08, 75.02, 74.91, 74.73, 51.96, 28.29, 28.18, 28.15, 28.12, 28.08, 28.04, 27.98, 19.65, 19.58, 19.51, 19.47, 19.45, 19.42, 19.31, 19.25, 19.18. MS (ES⁺): m/z calcd for C₁₁₃H₁₁₇N₁₆O₁₇ [M+H]⁺ 1970.881 found 1970.886.



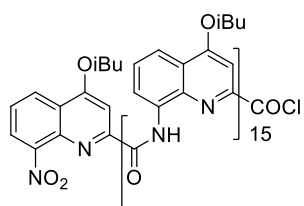
16-mer (Q₁₆) 6a. To a solution of **5d** (8.73 g, 4.43 mmol) and DIPEA (2.3 mL, 13.3 mL) in CHCl₃ (30 mL) was added dropwise a solution of **5c** in CHCl₃ (42 mL) at 0 °C. The reaction was warmed up to room temperature, stirred overnight and monitored by ¹H NMR until reaction completed. More time or/and **5c** could be necessary if the reaction was incomplete after overnight. The mixture was evaporated under reduced pressure to remove solvent and then refluxed in pyridine/H₂O (100 mL / 20 mL) overnight to hydrolyze by-product anhydride **7**. Then pyridine and H₂O were azeotroped with toluene and the residue was purified by silica gel chromatography eluting with dichloromethane/ethyl acetate (pure dichloromethane ~ 200/5 (v/v)) to obtain the product **6a** as a yellowish solid (13.25g, 76% yield). ¹H NMR (300 MHz, CDCl₃): δ 11.12 (s, 1H), 11.07 (s, 1H), 10.70 (s, 2H), 10.51 (s, 1H), 10.34 (s, 1H), 10.30 (s, 1H), 10.21 (s, 1H), 10.16 (s, 1H), 10.08 (s, 1H), 10.07 (s, 1H), 10.02 (s, 2H), 9.99 (s, 1H), 9.97 (s, 1H), 8.17 (dd, *J* = 8.1, 1.4 Hz, 1H), 7.95 (dd, *J* = 7.6, 1.0 Hz, 1H), 7.89 (dd, *J* = 3.1, 1.1 Hz, 1H), 7.88 – 7.85 (m, 1H), 7.82 (d, *J* = 1.0 Hz, 1H), 7.81 – 7.77 (m, 2H), 7.77 – 7.74 (m, 1H), 7.72 (dd, *J* = 6.2, 1.2 Hz, 1H), 7.70 – 7.52 (m, 10H), 7.24 (s, 2H), 7.23 – 7.20 (m, 2H), 7.20 – 7.09 (m, 5H), 7.09 – 6.73 (m, 22H), 6.42 (s, 1H), 6.38 (s, 1H), 6.21 (s, 1H), 6.16 (s, 1H), 6.15 (s, 1H), 5.91 (s, 1H), 5.87 (d, *J* = 0.9 Hz, 2H), 5.82 – 5.67 (m, 6H), 3.92 (dd, *J* = 15.1, 8.2 Hz, 4H), 3.82 – 3.45 (m, 28H), 2.83 (s, 3H), 2.42 – 2.02 (m, 16H), 1.26 – 1.00 (m, 96H). ¹³C NMR (101 MHz, CDCl₃): δ 163.63, 162.63, 162.51, 162.45, 162.31, 162.29, 162.14, 162.06, 161.79, 161.74, 161.70, 160.84, 160.50, 160.38, 159.85, 159.31, 158.92, 158.90, 158.69, 158.66, 158.63, 158.61, 158.54, 158.47, 158.43, 152.88, 149.74, 148.70, 148.48, 148.44,

148.41, 148.10, 148.01, 147.95, 147.90, 147.86, 144.86, 144.49, 138.54, 138.50, 137.78, 137.70, 137.44, 137.08, 137.05, 136.99, 136.84, 136.80, 136.76, 136.73, 136.70, 133.84, 133.44, 133.38, 133.04, 132.43, 132.39, 132.35, 132.31, 132.29, 132.24, 132.18, 132.13, 132.09, 127.86, 127.39, 126.66, 126.56, 126.01, 125.73, 125.55, 125.51, 125.36, 125.30, 125.22, 125.06, 125.04, 123.62, 123.44, 122.12, 122.02, 121.96, 121.88, 121.74, 121.63, 121.55, 121.49, 121.39, 121.30, 121.11, 117.06, 116.80, 116.65, 116.59, 116.52, 116.47, 116.40, 116.30, 115.94, 115.85, 115.76, 115.66, 115.61, 115.38, 115.33, 115.30, 115.25, 99.90, 99.78, 99.47, 98.61, 98.39, 98.28, 98.16, 98.14, 97.83, 97.42, 97.20, 77.37, 75.42, 75.14, 75.03, 74.87, 74.82, 74.64, 51.89, 28.17, 28.12, 28.05, 27.97, 19.68, 19.65, 19.63, 19.59, 19.56, 19.46, 19.43, 19.37, 19.35, 19.34, 19.30, 19.26, 19.22, 19.18. MS (ES⁺): *m/z* calcd for C₂₂₅H₂₂₈N₃₂O₃₅ [M+2H]²⁺ 1969.8 found 1969.7.

5.4.2 Synthesis of 32-mer 8a

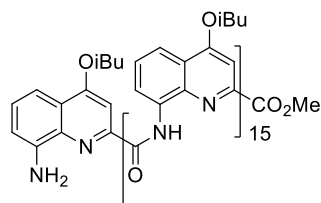


16-mer acid (Q₁₆-COOH) 6b. Compound **6a** (730 mg, 185 μ mol) was dissolved in 30 mL THF/MeOH (9/1, v/v) and then ground NaOH (148 mg, 3.7 mmol) was added. This mixture was allowed to proceed at room temperature for around 4 h and monitored with TLC until the reaction completed. 0.1 M HCl was used to neutralize the base and protonate the product. After removal of organic solvents with rotary evaporator, the residue was dissolved in CHCl₃, washed with H₂O and brine and dried with anhydrous Na₂SO₄, filtrated and concentrated to yield acid **6b** as a yellowish solid (725 mg, 99.7% yield). ¹H NMR(300 MHz, CDCl₃): δ 10.93 (s, 1H), 10.73 (s, 2H), 10.56 (s, 1H), 10.54 (s, 1H), 10.38 (s, 1H), 10.36 (s, 1H), 10.24 (s, 1H), 10.22 (s, 1H), 10.17 – 9.94 (m, 6H), 8.21 (dd, J = 8.1, 1.5 Hz, 1H), 8.08 – 7.98 (m, 2H), 7.91 (dd, J = 7.3, 0.9 Hz, 1H), 7.88 – 7.57 (m, 15H), 7.28 – 6.74 (m, 31H), 6.59 (s, 1H), 6.49 (s, 1H), 6.36 (s, 1H), 6.16 (s, 1H), 6.13 (s, 1H), 5.97 – 5.88 (m, 3H), 5.85 – 5.76 (m, 5H), 5.75 (s, 1H), 4.01 – 3.48 (m, 32H), 2.45 – 2.10 (m, 16H), 1.42 – 0.95 (m, 96H). MS (ES⁺): *m/z* calcd for C₂₂₄H₂₂₄N₃₂O₃₅ [M]⁺ 3924.68 found 3924.69.



16-mer acid chloride (Q₁₆-COCl) 6c. Oxalyl chloride (0.081 mL, 924 μmol) was put dropwise into the solution of dry **6b** (0.725 g, 185 μmol) in 4 mL CHCl₃ under nitrogen at 0 °C. Then the reaction was warmed up to room temperature and lasted for approx. 3h.

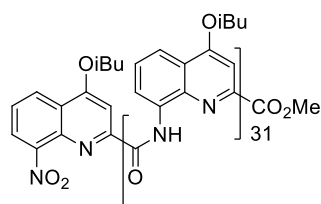
After complete, the mixture was dried under vacuum for approx. 5 h to remove solvent and remaining oxalyl chloride to produce **6c** quantitatively as a pale yellowish solid. ¹H NMR (300 MHz, CDCl₃): δ 11.01 (s, 1H), 10.87 (s, 1H), 10.69 (s, 2H), 10.53 (s, 1H), 10.34 (s, 1H), 10.32 (s, 1H), 10.20 (s, 1H), 10.19 (s, 1H), 10.08 (s, 1H), 10.06 (s, 1H), 10.02 (s, 2H), 9.99 (s, 1H), 9.98 (s, 1H), 8.18 – 8.16 (m, 1H), 8.02 – 7.95 (m, 2H), 7.88 – 7.86 (m, 1H), 7.82 – 7.58 (m, 16H), 7.29 – 6.75 (m, 30H), 6.51 (s, 1H), 6.44 (s, 1H), 6.13 (d, 2H), 6.09 (s, 1H), 5.91 (s, 1H), 5.87 (d, 2H), 5.80 (s, 1H), 5.79 (s, 1H), 5.77 (s, 1H), 5.76 (s, 1H), 5.75 (s, 1H), 5.71 (s, 1H), 3.97–3.46 (m, 32H), 2.40 – 2.07 (m, 16H), 1.25 – 1.02 (m, 96H).



16-mer amine (Q₁₆-NH₂) 6d. To the solvents of EtOAc and EtOH (25 mL, 4/1, v/v) were added compound **6a** (0.5 g, 127 μmol), Pd/C (50 mg, 10% w/w) and ammonium metavanadate (catalyst quantity) at room temperature. After this mixture was heated up to 95 °C, ammonium formate (0.5 g, in 1.2 mL H₂O) was added into the mixture in 3~5 intervals (~10min per interval). The reaction mixture was allowed to stirred overnight at 95 °C, filtered through celite, washed with H₂O and brine, dried with Na₂SO₄, filtered again concentrated to give the product **6d** as a yellowish solid (0.444 g, 90 % yield). ¹H NMR(300 MHz, CDCl₃): δ 11.13 (s, 1H), 11.07 (s, 1H), 10.85 (s, 1H), 10.77 (s, 1H), 10.51 (s, 1H), 10.35 (s, 1H), 10.31 (s, 1H), 10.25 (s, 1H), 10.16 (s, 2H), 10.08 (s, 2H), 10.05 (s, 2H), 9.99 (s, 1H), 7.96 (d, J = 7.2 Hz, 1H), 7.88 (d, J = 6.9 Hz, 1H), 7.85 – 7.71 (m, 5H), 7.71 – 7.52 (m, 11H), 7.33 – 7.30 (m, 2H), 7.22 – 7.16 (m, 3H), 7.13 (dd, J = 8.2, 2.1 Hz, 3H), 7.10 – 6.74 (m, 20H), 6.71 – 6.64 (m, 3H), 6.42 (s, 1H), 6.39 (s, 1H), 6.25 – 6.12 (m, 3H), 5.91 (s, 3H), 5.81 – 5.72 (m, 6H), 5.50 (d, J = 6.6 Hz, 1H), 4.02 – 3.37 (m, 34H), 2.84 (s, 3H), 2.48 – 1.97 (m, 16H), 1.35 – 0.93 (m, 96H). ¹³C NMR (CDCl₃, 75 MHz): δ 173.38, 163.55, 162.73, 162.55, 162.37, 162.28, 162.22, 162.07, 162.03, 161.95, 161.93, 161.73, 161.64, 161.11, 160.80, 160.77, 160.30, 158.86, 158.82, 158.70, 158.64, 158.78, 158.55, 158.50, 158.48, 158.44, 158.40, 158.36, 152.15, 149.29,

148.82, 1148.62, 148.38, 148.33, 148.17, 148.04, 147.96, 147.86, 147.79, 147.10, 144.78, 142.69, 140.33, 139.30, 138.46, 137.71, 137.44, 137.04, 137.01, 136.98, 136.95, 136.78, 136.74, 136.72, 136.70, 136.65, 135.90, 135.70, 133.36, 133.27, 133.13, 132.98, 132.53, 132.46, 132.30, 132.27, 132.22, 132.15, 132.08, 131.19, 130.05, 127.31, 126.56, 126.37, 126.33, 125.91, 125.65, 125.43, 125.30, 125.22, 125.06, 124.79, 124.48, 124.00, 122.48, 121.96, 121.89, 121.74, 121.67, 121.56, 121.52, 121.49, 121.31, 121.22, 121.03, 119.12, 116.57, 116.42, 116.32, 115.87, 115.78, 115.59, 115.52, 115.30, 114.09, 109.70, 109.06, 99.83, 99.06, 98.56, 98.49, 98.31, 98.25, 98.15, 98.10, 97.35, 97.13, 77.25, 75.09, 74.95, 74.90, 74.79, 74.74, 74.57, 64.65, 51.79, 36.54, 34.90, 34.54, 34.32, 33.84, 31.95, 31.69, 31.46, 31.05, 30.33, 30.22, 29.72, 29.61, 29.53, 29.47, 29.38, 29.29, 29.18, 28.98, 28.67, 28.57, 28.10, 28.04, 27.94, 27.89, 25.94, 24.83, 24.53, 22.71, 19.58, 19.51, 19.45, 19.35, 19.27, 19.19, 19.13, 19.10, 14.14, 1.04.

MS (ES⁺): *m/z* calcd for C₂₂₅H₂₃₀N₃₂O₃₃ [M+2H]²⁺ 1954.868 found 1954.867.

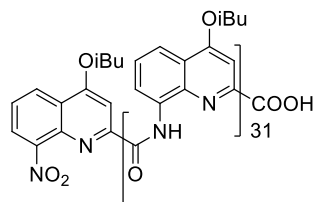


32-mer (Q₃₂) 8a. To a solution of **6d** (0.444 g, 0.114 mmol) and DIPEA (0.0936 mL, 0.568 mmol) in CHCl₃ (2 mL) was added dropwise a solution of **6c** in CHCl₃ (3 mL) under nitrogen at 0°C.

The reaction was warmed up to room temperature, stirred overnight and monitored by ¹H NMR until reaction completed. More time or/and **6c** could be necessary if the reaction was incomplete after overnight. The mixture was evaporated under reduced pressure to remove solvent and then refluxed in pyridine/H₂O (20 mL / 2 mL) overnight, hydrolyzing the resulting by-product anhydride **9**. Then pyridine and H₂O were evaporated with toluene, forming an azeotrope and the residue was purified by silica gel chromatography eluting with dichloromethane/ethyl acetate (pure dichloromethane ~ 200/5 (v/v)) and cyclohexane/ethyl acetate (10/1 to 2/1) to gain the product **8a** as a yellowish solid (0.725 g, 81.4% yield). ¹H NMR (300 MHz, CDCl₃): δ 11.03 (s, 1H), 10.99 (s, 1H), 10.61 (s, 1H), 10.59 (s, 1H), 10.40 (s, 1H), 10.22 (s, 1H), 10.18 (s, 1H), 10.06 (s, 1H), 10.01 (s, 1H), 9.91 (s, 1H), 9.89 (s, 1H), 9.80 (s, 2H), 9.71 (s, 1H), 9.69 (s, 1H), 9.63 (s, 2H), 9.57 (s, 2H), 9.53 (s, 2H), 9.50 (s, 2H), 9.45 (s, 8H), 8.11 (d, J = 7.5 Hz, 1H), 7.87 (d, J = 6.9 Hz, 1H), 7.80 (t, J = 7.5 Hz, 2H), 7.74 – 7.28 (m, 32H), 7.20 – 6.42 (m, 62H), 6.32 (d, J = 6.7 Hz, 2H), 6.20 – 5.98 (m, 3H), 5.85 – 5.69 (m, 3H), 5.68 – 5.54 (m, 5H), 5.65 – 5.39 (m, 17H), 4.06 – 3.03 (m, 64H), 2.77 (s,

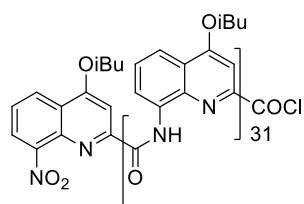
3H), 2.32 – 1.94 (m, 32H), 1.19 – 0.89 (m, 192H). MS (ES⁺): *m/z* calcd for C₄₄₉H₄₅₃N₆₄O₆₇ [M+3H]³⁺ 2605.5 found 2605.7.

5.4.3 Synthesis of 64-mer 10



32-mer acid (Q₃₂-COOH) 8b. Compound **8a** (0.4 g, 51.2 μmol) was dissolved in 15 mL THF/MeOH (9/1, v/v) and then ground NaOH (0.041g, 102 μmol) was added. This mixture was allowed to proceed at room temperature overnight and monitored with

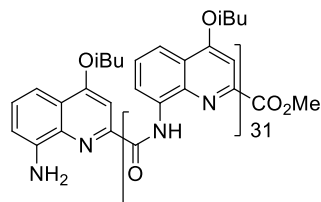
TLC until the reaction completed. 0.1 M HCl was used to neutralize the base and protonate the product. After removal of organic solvents with rotary evaporator, the residue was dissolved in CHCl₃, washed with H₂O and brine and dried with anhydrous Na₂SO₄, filtrated and concentrated to yield acid **8b** as a pale yellowish solid (370 mg, 93% yield). ¹H NMR(300 MHz, CDCl₃): δ 10.81 (s, 1H), 10.61 (s, 1H), 10.59 (s, 1H), 10.44 (s, 1H), 10.39 (s, 1H), 10.22 (s, 1H), 10.20 (s, 1H), 10.06 (s, 1H), 10.04 (s, 1H), 9.91 (s, 1H), 9.90 (s, 1H), 9.80 (s, 2H), 9.71 (s, 1H), 9.70 (s, 1H), 9.63 (s, 2H), 9.57 (s, 2H), 9.53 (s, 2H), 9.50 (s, 2H), 9.45 (s, 8H), 8.11 (dd, *J* = 8.0, 1.3 Hz, 1H), 7.91 (dd, *J* = 11.8, 7.4 Hz, 2H), 7.79 (d, *J* = 7.3 Hz, 1H), 7.75 – 7.28 (m, 32H), 7.23 – 6.41 (m, 62H), 6.37 (s, 1H), 6.26 (s, 1H), 6.00 (d, *J* = 2.0 Hz, 2H), 5.85 – 5.71 (m, 3H), 5.71 – 5.55 (m, 5H), 5.55 – 5.26 (m, 17H), 3.90 – 3.17 (m, 64H), 2.32 – 1.96 (m, 32H), 1.16 – 0.91 (m, 192H). MS (ES⁺): *m/z* calcd for C₄₄₈H₄₅₁N₆₄O₆₇ [3M+3H]³⁺ 7803.40 found 7803.41.



32-mer acid chloride (Q₃₂-COCl) 8c. Oxalyl chloride (0.17 mL, 474 μmol) was put dropwise into the solution of dry **8b** (370 mg, 47.4 μmol) in 1.5 mL anhydrous toluene under nitrogen at 0 °C.

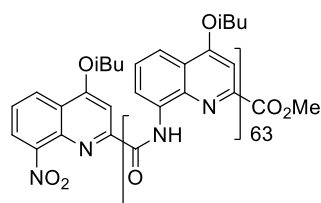
Then the reaction was warmed up to room temperature and lasted for approx. 4h. After complete, the mixture was dried under vacuum for approx. 5 h to remove solvent and remaining oxalyl chloride to produce **8c** quantitatively as a pale yellowish solid. ¹H NMR (300 MHz, CDCl₃): δ 10.96 (s, 1H), 10.83 (s, 1H), 10.65 (s, 1H), 10.63 (s, 1H), 10.46 (s, 1H), 10.26 (s, 1H), 10.24 (s, 1H), 10.10 (s, 1H), 10.08 (s, 1H), 9.95 (s, 1H), 9.93 (s, 1H), 9.84 (s, 2H), 9.74 (s, 2H), 9.67 (s, 2H), 9.61 (s, 2H), 9.56 (s, 2H), 9.53 (s, 2H), 9.51 – 9.49 (m, 8H), 8.15 (d, *J* = 3.7 Hz, 1H), 7.98 (d, *J* = 3.76 Hz, 1H), 7.92 (d, *J* = 3.56 Hz, 1H), 7.83 (d, *J* = 3.63 Hz, 1H), 7.73 – 6.50 (m, 93H), 6.46 (s, 1H), 6.41 (s, 1H), 6.11 (s, 2H), 6.06 (s, 1H), 6.04 (s,

1H), 5.84 (s, 1H), 5.81 (s, 1H), 5.78 (s, 1H), 5.71 (s, 1H), 5.66 (s, 1H), 5.65 (s, 1H), 5.64 (s, 1H), 5.61 (s, 1H), 5.54 (s, 3H), 5.53 (s, 1H), 5.49 (s, 2H), 5.47 (s, 2H), 5.46 (s, 2H), 5.44 – 5.43 (m, 8H), 3.90 – 3.30 (m, 64H), 2.33 – 2.06 (m, 32H), 1.29 – 0.98 (m, 192H).



32-mer amine (Q₃₂-NH₂) 8d. To the solvents of EtOAc and EtOH (20 mL, 4/1, v/v) were added compound **8a** (0.15 g, 19.2 μmol), Pd/C (15 mg, 10% w/w) and ammonium metavanadate (catalyst quantity) at room temperature. After this mixture was heated up

to 95 °C, ammonium formate (57.7 mg, in 0.5 mL H₂O) was added into the mixture in 3~5 intervals (~10min per interval). The reaction mixture was allowed to stirred at 95 °C overnight, filtered through celite, washed with H₂O and brine, dried with Na₂SO₄, filtered again concentrated to give the product **8d** as a yellowish solid (145 mg, 97.3% yield). ¹H NMR (300 MHz, CDCl₃): δ 11.04 (s, 1H), 10.99 (s, 1H), 10.76 (s, 1H), 10.69 (s, 1H), 10.40 (s, 1H), 10.23 (s, 1H), 10.18 (s, 1H), 10.11 (s, 1H), 10.01 (s, 1H), 9.99 (s, 1H), 9.89 (s, 1H), 9.86 (s, 1H), 9.81 (s, 1H), 9.77 (s, 1H), 9.69 (s, 1H), 9.64 (s, 1H), 9.63 (s, 1H), 9.59 (s, 1H), 9.57 (s, 1H), 9.54 (s, 1H), 9.53 (s, 1H), 9.51 (s, 1H), 9.50 (s, 1H), 9.46 (s, 8H), 7.88 (d, J = 7.2 Hz, 1H), 7.81 (d, J = 7.2 Hz, 1H), 7.77 – 7.28 (m, 33H), 7.22 – 6.39 (m, 62H), 6.34 (s, 1H), 6.31 (s, 1H), 6.15 (s, 1H), 6.08 (s, 1H), 6.04 (s, 1H), 5.88 – 5.72 (m, 3H), 5.69 – 5.54 (m, 5H), 5.54 – 5.27 (m, 18H), 3.94 – 3.11 (m, 64H), 2.77 (s, 5H), 2.29 – 1.96 (m, 32H), 1.16 – 0.91 (m, 192H). MS (ES⁺): *m/z* calcd for C₄₄₉H₄₅₅N₆₄O₆₅ [M+3H]³⁺ 2595.81 found 2595.82.



64-mer (Q₆₄) 10. To a solution of **8d** (0.184 g, 23.7 μmol) and DIPEA (0.012 mL, 71.1 μmol) in toluene (1 mL) was added dropwise a solution of **8c** in toluene (3 mL) under nitrogen at 0 °C.

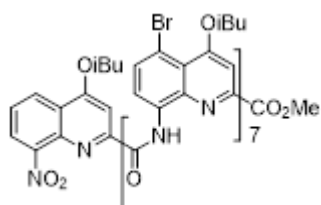
The reaction was warmed up to room temperature, stirred overnight and monitored by ¹H NMR until reaction completed. More time or/and **8c** could be necessary if the reaction was incomplete after overnight. The mixture was evaporated under reduced pressure to remove solvent and then refluxed in pyridine/H₂O (8 mL / 0.5 mL) overnight to hydrolyze the formed anhydride **11**. Then pyridine and H₂O were evaporated with toluene, forming an azeotrope. Silica gel chromatography and chromatotron eluting with toluene/ethyl acetate (pure toluene ~ 200/5 (v/v)) were firstly employed to remove main part of

starting material Q₃₂-COOH, and then recycling GPC with CHCl₃/0.5~1% ethanol as eluent was used to eliminate the remaining Q₃₂-COOH, producing the pure product **10** as a pale yellowish solid (312 mg, 85% yield). ¹H NMR (700 MHz, CDCl₃) δ 11.08 – 10.91 (m, 3H), 10.60 (s, 1H), 10.57 (s, 1H), 10.38 (s, 2H), 10.26 – 10.11 (m, 3H), 10.11 – 9.94 (m, 3H), 9.88 – 9.86 (m, 3H), 9.77 (s, 3H), 9.67 – 9.66 (m, 3H), 9.59 (s, 3H), 9.53 (s, 3H), 9.48 (s, 3H), 9.45 (s, 3H), 9.32 (s, 29H), 8.09 (s, 2H), 7.96 – 7.76 (m, 5H), 7.75 – 7.30 (m, 34H), 7.23 – 6.21 (m, 144H), 6.21 – 5.97 (m, 7H), 5.90 – 5.70 (m, 6H), 5.70 – 5.08 (m, 58H), 3.90 – 3.06 (m, 128H), 2.76 (s, 3H), 2.24 – 1.95 (m, 64H), 1.14 – 0.82 (m, 384H). MS: *m/z* calcd for C₈₉₇H₉₀₄N₁₂₈O₁₃₁ [M+6H]⁶⁺ 2595.3 found 2595.7.

5.4.4 Synthesis of brominated octamer **11a**, 16-mer **12a** and 32-mer **13**

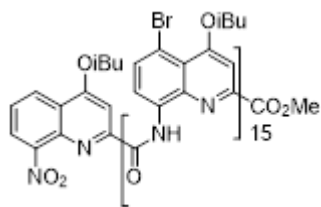
General method of brominated octamer **11a**, 16-mer **12a** and 32-mer **13**

To a sealed pressure tube was added a mixture of foldamer, N-bromosuccinimide (NBS) and solvent (1,2-dichloroethane or bromobenzene). This mixture was allowed to stir at 70 °C and monitored by ¹H NMR until the reaction completed. Silica gel chromatography was employed to purify the product, a yellowish solid.



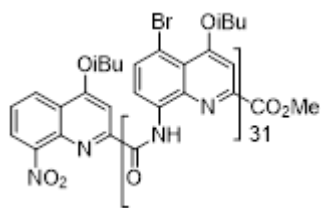
Brominated octamer (⁷BrQ₈) **11a.** According to the general method, 100 mg octamer **5a** (50 μmol) and 303 mg NBS (1.7 mmol) was mixed with 0.75 mL 1,2-dichloroethane. The reaction lasted around 4 days, and after purification, produced 116 mg **11a** (91% yield). ¹H NMR (300 MHz, CDCl₃): δ 11.43 (s, 1H), 11.32 (s, 1H), 11.18 (s, 1H), 11.06 (s, 2H), 11.05 (s, 1H), 10.97 (s, 1H), 8.32 (dd, *J* = 3.44, 4.84 Hz, 1H), 8.14 (d, *J* = 4.18 Hz, 1H), 8.06 (d, *J* = 4.21 Hz, 1H), 7.85 – 7.71 (m, 4H), 7.59 – 7.12 (m, 12H), 6.66 (s, 1H), 6.63 (s, 1H), 6.58 (s, 1H), 6.51 (s, 1H), 6.50 (s, 1H), 6.19 (s, 1H), 4.30 – 3.66 (m, 16H), 3.13 (s, 3H), 2.65 – 2.22 (m, 8H), 1.49 – 1.17 (m, 48H). ¹³C-NMR (CDCl₃, 75 MHz): δ 164.3, 163.9, 163.9, 163.7, 163.5, 163.4, 162.9, 162.9, 162.6, 160.6, 160.3, 160.1, 159.9, 159.0, 158.4, 158.3, 152.7, 149.6, 148.2, 148.1, 147.8, 147.6, 144.8, 144.4, 139.7, 139.2, 139.2, 138.5, 138.4, 138.4, 134.5, 134.1, 133.6, 133.2, 133.2, 133.1, 132.9, 132.8, 132.5, 132.0, 131.9, 131.7, 127.2, 125.4, 123.9, 123.4, 120.4, 119.9, 119.8, 119.8, 119.7, 119.6, 119.2, 116.4, 116.3, 116.2, 116.0, 115.0, 115.0, 114.9, 109.2, 109.1, 108.8, 108.6, 107.9, 107.9, 100.8, 100.7, 100.6, 99.9, 98.9, 98.7, 98.3, 97.8, 77.1,

76.7, 76.3, 76.3, 76.0, 75.6, 51.9, 29.5, 29.5, 28.1, 28.1, 28.0, 27.9, 27.8, 19.8, 19.7, 19.6, 19.5, 19.4, 19.4, 19.3, 19.2, 19.1. MS (ES⁺): *m/z* calcd for C₁₁₃H₁₀₇Br₇N₁₆O₁₉ [M+H]⁺ 2553.2 found 2553.2.



Brominated 16-mer 12a. As stated in the General method above, 16-mer **6a** (300 mg, 75 μ mol), NBS (461 mg, 2.58 mmol) and 1.5 mL 1,2-dichloroethane were mixed in a sealed pressure tube. The reaction was stirred at 70 °C and controlled by ¹H NMR. After

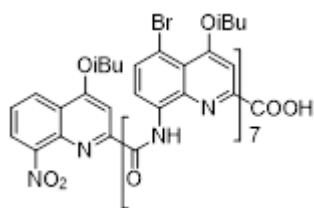
purified by silica gel chromatography, the reaction yielded **12a** as a yellowish solid (353 mg, 92% yield). ¹H NMR (300 MHz, CDCl₃): δ 11.16 (s, 1H), 11.08 (s, 1H), 10.75 (s, 1H), 10.74 (s, 1H), 10.64 (s, 1H), 10.57 (s, 1H), 10.47 (s, 1H), 10.45 (s, 1H), 10.34 (s, 1H), 10.32 (s, 1H), 10.25 (s, 1H), 10.18 (s, 1H), 10.17 (s, 1H), 10.14 (s, 1H), 10.11 (s, 1H), 8.19 (dd, *J* = 3.38, 4.82 Hz, 1H), 7.90 (d, *J* = 5.02 Hz, 1H), 7.87 (d, *J* = 5.09 Hz, 1H), 7.64 – 7.56 (m, 4H), 7.36 – 6.75 (m, 28H), 6.47 (s, 1H), 6.42 (s, 1H), 6.41 (s, 1H), 6.23 (s, 2H), 6.04 (s, 1H), 5.98 (s, 2H), 5.96 (s, 1H), 5.94 (s, 1H), 5.93 (s, 1H), 5.92 (s, 1H), 5.91 (s, 1H), 5.86 (s, 1H), 4.06 – 3.50 (m, 32H), 2.99 (s, 3H), 2.45 – 2.21 (m, 16), 1.37 – 1.10 (m, 96H). ¹³C-NMR (CDCl₃, 75 MHz): δ 164.15, 163.71, 163.64, 163.61, 163.57, 163.51, 163.43, 163.39, 163.35, 163.04, 162.94, 162.71, 160.46, 160.24, 160.05, 159.84, 158.83, 158.14, 158.04, 157.99, 157.93, 157.90, 152.73, 149.49, 147.99, 147.77, 147.57, 147.54, 147.52, 147.47, 147.18, 147.10, 144.79, 144.40, 139.79, 139.14, 139.04, 138.96, 138.34, 138.21, 138.12, 138.04, 137.93, 137.89, 137.15, 134.56, 134.12, 133.64, 133.16, 133.09, 132.94, 132.80, 132.69, 132.53, 131.77, 131.66, 131.59, 131.55, 131.49, 131.45, 131.41, 127.31, 125.40, 123.92, 120.23, 119.71, 119.68, 119.57, 119.45, 119.41, 119.36, 119.31, 119.29, 119.25, 119.21, 119.05, 116.31, 116.15, 115.99, 114.91, 114.77, 114.69, 114.61, 114.54, 114.39, 109.10, 108.97, 108.72, 108.70, 108.45, 108.25, 108.22, 108.17, 108.15, 108.09, 108.02, 107.93, 107.84, 100.90, 100.57, 99.96, 98.54, 98.32, 97.67, 77.26, 76.31, 76.17, 76.01, 75.67, 72.13, 63.10, 52.06, 34.92, 32.84, 31.94, 30.94, 30.33, 29.71, 29.68, 29.46, 29.38, 29.29, 28.67, 28.56, 28.44, 28.17, 28.13, 28.03, 27.95, 27.87, 23.41, 22.71, 21.85, 19.83, 19.74, 19.69, 19.57, 19.52, 19.47, 19.40, 19.36, 19.34, 19.28, 19.18, 18.14, 14.14, 1.03. MS (ES⁺): *m/z* calcd for C₂₂₅H₂₁₁Br₁₅N₃₂O₃₅ [M+2H]⁺ 5124.3 found 5124.4.



Brominated 32-mer 13. A mixture of 32-mer **8a** (50 mg, 6.4 μmol), NBS (300 mg, 1.7 mmol) and bromobenzene (0.9 mL) was allowed to proceed at 70 °C and monitored by ^1H NMR until the reaction came to the end. The resulting residue was purified

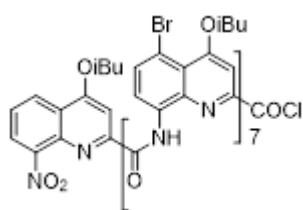
by silica gel chromatography and gives the product as a yellowish solid. ^1H NMR (300 MHz, CDCl_3): δ

5.4.5 Synthesis of brominated 16-mer ($^{14}\text{BrQ}_{16}$) **14**



Synthesis of brominated octamer acid ($^{7}\text{BrQ}_8\text{-COOH}$) **11b. To a mixture of compound **11a** ($^{7}\text{BrQ}_8$) (100 mg, 39.2 μmol) and 9 mL solvents (THF/MeOH, 9/1, v/v) was added the ground NaOH (31.4 mg, 784 μmol). The reaction was allowed to stir at room**

temperature and monitored by TLC (cyclohexane/DCM = 1/5). Once the reaction was complete, the 0.1 M HCl was poured inside to pH around 5. After evaporation of organic solvents, the residue was dissolved into DCM, washed with H_2O and brine, dried with Na_2SO_4 , filtered and concentrated to provide product **11b** a yellowish solid quantitatively. ^1H NMR (300 MHz, CDCl_3): δ 10.98 (s, 1H), 10.92 (s, 1H), 10.88 (s, 1H), 10.82 (s, 1H), 10.75 (s, 1H), 10.63 (s, 1H), 10.60 (s, 1H), 8.26 (dd, $J = 3.47, 4.73$ Hz, 1H), 7.85 (d, $J = 4.13$ Hz, 1H), 7.75 (d, $J = 3.82$ Hz, 1H), 7.68 – 7.64 (m, 2H), 7.56 (d, $J = 4.19$ Hz, 1H), 7.49 (d, $J = 4.16$ Hz, 1H), 7.41 – 7.13 (m, 9H), 7.08 (s, 1H), 7.01 – 6.97 (m, 2H), 6.56 (s, 1H), 6.34 (s, 1H), 6.25 (s, 1H), 6.17 (s, 1H), 6.13 (s, 1H), 6.07 (s, 1H), 4.16 – 3.54 (m, 16H), 2.55 – 2.23 (m, 8H), 1.39 – 1.17 (m, 48H). ^{13}C -NMR (CDCl_3 , 100 MHz): δ 164.82, 164.43, 164.34, 164.19, 164.04, 163.45, 162.04, 161.07, 160.75, 160.20, 160.04, 159.44, 158.72, 153.15, 150.06, 149.01, 148.46, 148.14, 147.92, 147.85, 145.28, 144.12, 139.67, 139.36, 139.16, 138.94, 138.87, 138.81, 138.73, 135.34, 134.82, 134.16, 133.67, 133.45, 133.31, 133.12, 132.95, 132.31, 132.22, 132.02, 127.84, 125.98, 125.21, 124.46, 123.94, 120.85, 120.34, 120.25, 120.15, 120.04, 119.89, 117.42, 117.14, 116.90, 116.58, 115.53, 115.23, 109.73, 109.66, 109.35, 109.02, 108.79, 108.42, 101.11, 100.34, 99.92, 99.40, 99.24, 99.12, 98.89, 98.68, 77.63, 76.82, 76.12, 32.35, 32.04, 30.72, 30.11, 29.85, 29.78, 28.58, 28.48, 28.37, 23.11, 20.23, 20.13, 20.09, 20.02, 19.58, 19.87, 19.73, 19.62, 14.55. MS (ES^+): m/z calcd for $\text{C}_{122}\text{H}_{106}\text{Br}_7\text{N}_{16}\text{O}_{19}$ [$\text{M}+\text{H}$] $^+$ 2538.2 found 2539.2.

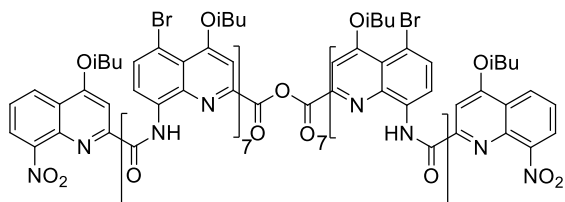


Synthesis of brominated octamer acid chloride (${}^7\text{BrQ}_8\text{-COCl}$)

11c. The oxalyl chloride (65.8 μL , 749 μmol) was added dropwise into the solution of **11b** (190 mg, 74.9 μmol) in 1.5 mL CHCl_3 . The reaction was allowed to proceed overnight and then dried by pump for approx. 7 h after it completed, yielding pure **11c** as a pale yellowish solid quantitatively. ${}^1\text{H}$ NMR (300 MHz, CDCl_3): δ 11.37 (s, 1H), 11.19 (s, 1H), 11.13 (s, 1H), 11.09 (s, 1H), 11.08 (s, 1H), 11.07 (s, 1H), 11.01 (s, 1H), 8.34 – 8.31 (m, 1H), 8.19 (d, $J = 4.26$ Hz, 1H), 8.15 (d, $J = 4.13$ Hz, 1H), 7.86 – 7.78 (m, 4H), 7.58 – 7.32 (m, 8H), 7.21 (s, 1H), 7.22 – 6.98 (m, 3H), 6.70 (s, 2H), 6.58 (s, 1H), 6.47 (s, 1H), 6.42 (s, 1H), 6.21 (s, 1H), 4.22 – 3.67 (m, 16H), 2.62 – 2.30 (m, 8H), 1.49 – 1.19 (m, 48H).

Synthesis of brominated 16-mer (${}^{14}\text{BrQ}_{16}$) 14. The solution of **11c** in 2 mL CHCl_3 was added dropwise into the mixture of compound **11b** (19.0 mg, 3.94 μmol) and DIPEA (13.0 μL , 74.9 μmol) in 1 mL CHCl_3 at 0°C . The reaction mixture was allow to warm up to room temperature and monitored by ${}^1\text{H}$ NMR. Once compound **11c** was consumed totally, the reaction mixture was washed with H_2O , 0.1 M HCl and brine, dried with Na_2SO_4 , filtered and concentrated. The resulting residue was purified by recycling GPC with CHCl_3 (including ~1% EtOH) as eluent

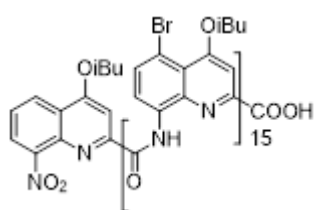
and gave the product **14** as a yellowish solid.



${}^1\text{H}$ NMR (300 MHz, CDCl_3): δ 10.88 (s, 2H), 10.81 (s, 2H), 10.68 (s, 2H), 10.52 (s, 2H), 10.35 (s, 2H), 10.34 (s, 2H), 10.31 (s, 2H), 8.21 (dd, $J = 3.38, 4.83$ Hz, 2H), 7.66 (d, $J = 4.18$ Hz, 2H), 7.54 (d, $J = 4.17$ Hz, 2H), 7.33 (s, 1H), 7.32 (s, 1H), 7.306 (s, 1H), 7.295 (s, 1H), 7.25 – 6.96 (m, 24H), 6.90 (s, 1H), 6.88 (s, 1H), 6.69 (s, 1H), 6.66 (s, 1H), 6.26 (s, 2H), 6.16 (s, 2H), 6.12 (s, 2H), 6.08 (s, 2H), 6.03 (s, 2H), 5.95 (s, 2H), 4.07 – 3.49 (m, 32H), 2.50 – 2.27 (m, 16H), 1.37 – 1.11 (m, 96H). ${}^{13}\text{C}$ -NMR (CDCl_3 , 75 MHz): δ 164.25, 163.72, 163.65, 163.56, 163.01, 162.84, 162.30, 160.44, 160.27, 159.08, 159.03, 158.90, 157.97, 157.88, 156.33, 152.73, 149.55, 147.76, 147.54, 147.43, 147.35, 147.18, 144.87, 142.75, 139.18, 139.12, 138.40, 138.29, 128.24, 138.04, 137.62, 133.64, 133.57, 133.18, 133.12, 132.92, 132.80, 132.42, 132.38, 131.77, 131.51, 131.46, 130.69, 127.33, 125.43, 124.02, 123.95, 123.48, 120.32, 119.74, 119.60, 119.38, 118.94, 118.45,

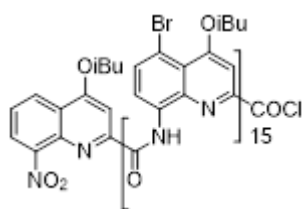
118.17, 116.37, 115.96, 115.21, 114.87, 114.73, 114.48, 109.63, 109.10, 108.87, 108.76, 108.43, 107.90, 107.76, 100.76, 100.55, 99.89, 99.27, 98.69, 98.62, 98.49, 98.43, 77.24, 76.34, 76.24, 75.67, 30.95, 28.18, 28.12, 28.07, 28.00, 27.95, 27.86, 19.97, 19.89, 19.78, 19.74, 19.69, 19.65, 19.63, 19.61, 19.59, 19.49, 19.45, 19.43, 19.40, 19.36, 19.28, 19.16. HRMS (ES⁺): *m/z* calcd for C₂₂₄H₂₀₈Br₁₄N₃₂O₃₇ [M+2]⁺ 2530.2 found 2530.3.

5.4.6 Synthesis of brominated 32-mer (³⁰BrQ₃₂) **15**



Synthesis of brominated 16-mer acid (¹⁵BrQ₁₆-COOH) **12b**. To

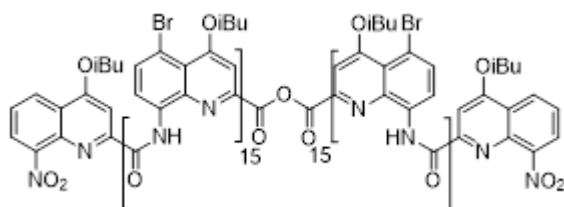
a mixture of compound **12a** (¹⁵BrQ₁₆) (293 mg, 57.2 μmol) and 10 mL solvents (THF/MeOH, 9/1, v/v) was added the ground NaOH (45.8 mg, 1.14 mmol). The reaction was allowed to stir at room temperature and monitored by TLC (cyclohexane/DCM = 1/2). Once the reaction was complete, the 0.1 M HCl was poured inside to pH around 5. After evaporation of organic solvents, the residue was dissolved into CHCl₃, washed with H₂O and brine, dried with Na₂SO₄, filtered and concentrated to provide product **12b** a yellowish solid (278 mg, 95% yield). ¹H NMR (300 MHz, CDCl₃): δ 10.96 (s, 1H), 10.76 (s, 2H), 10.62 (s, 2H), 10.56 (s, 1H), 10.48 (s, 1H), 10.44 (s, 1H), 10.35 (s, 1H), 10.32 (s, 1H), 10.25 (s, 1H), 10.19 (s, 1H), 10.18 (s, 1H), 10.15 (s, 1H), 10.12 (s, 1H), 8.21 (dd, *J* = 3.43, 4.81 Hz, 1H), 7.96 – 7.88 (m, 2H), 7.67 – 7.57 (m, 5H), 7.36 – 6.75 (m, 27H), 6.51 (s, 1H), 6.48 (s, 1H), 6.45 (s, 1H), 6.22 (s, 1H), 6.20 (s, 1H), 6.04 (s, 1H), 5.98 (s, 1H), 5.98 (s, 1H), 5.97 (s, 1H), 5.95 (s, 1H), 5.93 (s, 1H), 5.92 (s, 1H), 5.92 (s, 1H), 5.86 (s, 1H), 4.07 – 3.51 (m, 32H), 2.47 – 2.29 (m, 16H), 1.36 – 1.12 (m, 96H). MS (ES⁺): *m/z* calcd for C₂₂₄H₂₁₁Br₁₅N₃₂O₃₅ [2M+2H]²⁺ 5109.35 found 5109.34.



Synthesis of brominated 16-mer acid chloride (¹⁵BrQ₁₆-COCl) **12c**. The

oxalyl chloride (6.70 μL, 78.3 μmol) was added dropwise into the solution of **12b** (80 mg, 15.7 μmol) in 1 mL CHCl₃. The reaction was allowed to proceed overnight and then dried by pump for approx. 7 h after it completed, yielding pure **12c** as a pale yellowish solid quantitatively. ¹H NMR (300 MHz, CDCl₃): δ 11.12 (s, 1H), 10.97 (s, 1H), 10.91 (s, 1H), 10.85 (s, 1H), 10.76 (s, 2H), 10.68 (s, 1H), 10.60 (s, 1H), 10.49 (s, 2H), 10.36 (s, 1H), 10.35 (s, 1H), 10.27 (s, 1H), 10.21 (s, 1H), 10.19 (s, 1H), 10.16 (s, 1H), 10.13 (s, 1H), 8.22 – 8.20 (m, 1H), 8.02 (d, *J* = 4.23

Hz, 1H), 7.92 (d, $J = 4.18$ Hz, 1H), 7.70 – 7.57 (m, 5H), 7.37 – 6.76 (m, 27H), 6.53 (s, 1H), 6.50 (s, 1H), 6.34 (s, 1H), 6.25 (s, 1H), 6.21 (s, 1H), 6.05 (s, 1H), 5.99 (s, 2H), 5.98 (s, 1H), 5.96 (s, 1H), 5.94 (s, 1H), 5.93 (s, 1H), 5.92 (s, 1H), 5.87 (s, 1H), 4.08 – 3.52 (m, 36H), 2.51 – 2.24 (m, 16H), 1.38 – 1.20 (m, 96H).

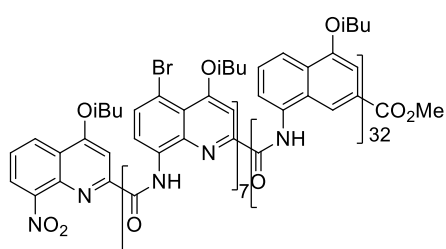


Synthesis of brominated 32-mer ($^{30}\text{BrQ}_{32}$)

15. DIPEA (6.67 μL , 39.2 μmol) was added dropwise into the solution of **12c** in 1.3 mL CHCl_3 at 0°C . The reaction was allowed to warm up to room temperature and monitored by ^1H NMR. The reagent **12c** could react with the tiny H_2O in the reaction atmosphere to form **12b** with which **12c** can couple to generate **15**. Once compound **12c** was consumed totally, the reaction mixture was washed with H_2O , 0.1 M HCl and brine, dried with Na_2SO_4 , filtered and concentrated. The resulting residue was purified by recycling GPC with CHCl_3 (including ~1% EtOH) as eluent and gave the product **15** as a yellowish solid. ^1H NMR (300 MHz, CDCl_3): δ 10.69 (m, 4H), 10.40 (s, 2H), 10.25 (s, 2H), 10.06 (s, 2H), 10.02 (s, 2H), 9.98 (s, 8H), 9.96 (s, 10H), 8.16 (dd, $J = 3.34, 4.74$ Hz, 2H), 7.59 (d, $J = 4.14$ Hz, 2H), 7.52 (d, $J = 4.09$ Hz, 2H), 7.30 – 6.58 (m, 54H), 6.53 (d, $J = 1.42$ Hz, 2H), 6.50 (d, $J = 1.35$ Hz, 2H), 6.44 (d, $J = 4.10$ Hz, 2H), 6.35 (d, $J = 4.08$ Hz, 2H), 5.98 (s, 2H), 5.97 (s, 2H), 5.89 (s, 2H), 5.88 (s, 2H), 5.86 (s, 2H), 5.84 (s, 2H), 5.83 (s, 2H), 5.79 (s, 2H), 5.78 (s, 2H), 5.72 (s, 2H), 5.71 (s, 2H), 5.69 (s, 2H), 4.04 – 3.47 (m, 64H), 2.47 – 2.17 (m, 32H), 1.33 – 1.02 (m, 192H). MS (ES^+): m/z calcd for $\text{C}_{448}\text{H}_{419}\text{Br}_{30}\text{N}_{64}\text{O}_{69}$ [$\text{M}+3\text{H}$] $^{3+}$ 3400.55 found 3400.57.

5.4.7 Synthesis of 40-mer ($^{7}\text{BrQ}_{40}$) **16a**

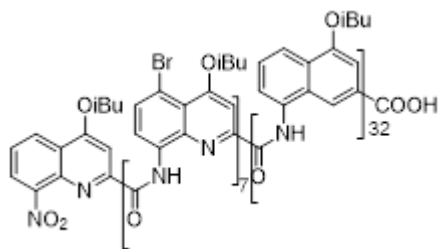
To a mixture of compound **8d** ($\text{Q}_{32}\text{-NH}_2$) (136 mg, 17.5 μmol) and DIPEA (15 μL , 87.4 μmol) in 1 mL toluene was added dropwise the solution of compound **11c** ($^{7}\text{BrQ}_8\text{-COCl}$) (88.7 mg, 34.9 μmol) at 0°C under argon. The reaction was warmed up to room temperature, stirred



overnight and controlled by ^1H NMR. After completed, the reaction was washed by H_2O , 0.1 M HCl, dried by Na_2SO_4 , filtered, concentrated and

purified by recycling GPC to give the product **16a** as a yellowish solid (72 mg, 40% yield). ¹H NMR (300 MHz, CDCl₃): δ 11.02 (s, 1H), 10.98 (s, 1H), 10.57 (s, 1H), 10.55 (s, 1H), 10.39 (s, 1H), 10.22 (s, 1H), 10.17 (s, 1H), 10.10 (s, 1H), 9.99 (s, 1H), 9.92 (s, 1H), 9.87 (s, 1H), 9.84 (s, 1H), 9.79 (s, 3H), 9.73 (s, 1H), 9.67 (s, 1H), 9.61 (s, 1H), 9.53 (m, 5H), 9.50 (m, 2H), 9.47 (s, 2H), 9.45 (s, 2H), 9.40 (m, 12H), 8.13 – 8.10 (m, 1H), 7.87 (d, *J* = 3.73 Hz, 1H), 7.81 (d, *J* = 3.64 Hz, 1H), 7.70 – 6.42 (m, 111H), 6.33 (s, 1H), 6.31 (s, 1H), 6.15 (s, 1H), 6.06 (s, 1H), 6.03 (s, 1H), 5.87 (s, 1H), 5.80 (s, 1H), 5.75 (s, 1H), 5.68 (s, 1H), 5.64 (s, 1H), 5.62 (s, 1H), 5.60 (s, 1H), 5.55 (s, 1H), 5.54 (s, 1H), 5.51 (s, 1H), 5.50 (s, 1H), 5.48 (s, 1H), 5.47 (s, 1H), 5.465 (m, 2H), 5.42 (m, 3H), 5.40 (m, 2H), 5.37 (m, 4H), 5.35 (m, 10H), 3.94 – 3.22 (m, 80H), 2.77 (s, 3H), 2.35 – 1.98 (m, 40H), 1.29 – 0.90 (m, 240H). MS (ES⁺): *m/z* calcd for C₅₆₁H₅₅₉Br₇N₈₀O₈₃ [M+4H]⁴⁺ 2577.16 found 2577.17.

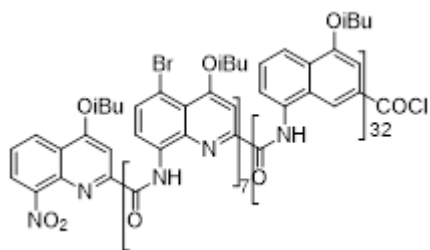
5.4.8 Synthesis of 80-mer 18



Synthesis of 40-mer acid (⁷BrQ₄₀-COOH) 16b. To a solution of compound **16a** (72 mg, 6.99 μmol) in 2 mL THF/MeOH (9/1, v/v) was added ground NaOH (5.6 mg, 139.8 μmol). The reaction was stirred at room temperature overnight and monitored by TLC

(CHCl₃/EtOAc = 200/5) until complete (if not, more time and/or NaOH could be needed). 0.1 M HCl was used to protonate the product until pH value of reaction went to approx. 5. The reaction was evaporated to remove organic solvents and the resulting residue was dissolved into CHCl₃, washed by H₂O and brine, dried by Na₂SO₄, filtered and concentrated to provide the product **16b** as a yellowish solid (50 mg, 70%). ¹H NMR (300 MHz, CDCl₃): δ 10.80 (s, 1H), 10.57 (s, 1H), 10.55 (s, 1H), 10.44 (s, 1H), 10.39 (s, 1H), 10.22 (s, 1H), 10.20 (s, 1H), 10.10 (s, 1H), 10.03 (s, 1H), 9.92 (s, 1H), 9.89 (s, 1H), 9.84 (s, 1H), 9.78 (s, 3H), 9.73 (s, 1H), 9.68 (s, 1H), 9.61 (s, 1H), 9.54 (m, 4H), 9.50 (m, 2H), 9.47 (s, 2H), 9.45 (s, 2H), 9.40 (m, 11H), 8.12 (dd, *J* = 3.40, 4.53 Hz, 1H), 7.94 – 7.91 (m, 1H), 7.90 – 7.87 (m, 1H), 7.70 – 6.45 (m, 112H), 6.37 (s, 1H), 6.26 (s, 1H), 6.00 (s, 1H), 5.99 (s, 1H), 5.87 (s, 1H), 5.80 (s, 1H), 5.76 (s, 1H), 5.68 (s, 1H), 5.65 (s, 1H), 5.62 (s, 1H), 5.60 (s, 1H), 5.55 (s, 1H), 5.54 (s, 1H), 5.52 (s, 1H), 5.49 (s, 1H), 5.48 (s, 1H), 5.47 (s, 2H), 5.46 (s, 1H), 5.44 (s, 1H), 5.42 (s, 1H), 5.41 (s, 1H),

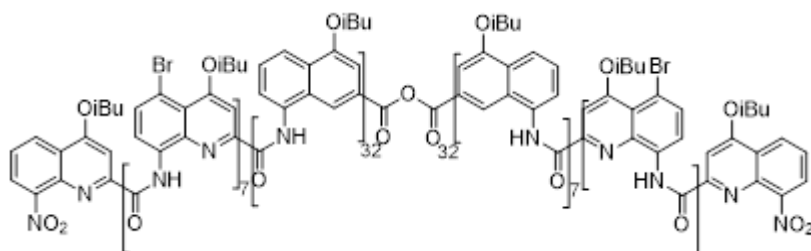
5.40 (s, 2H), 5.38 (s, 2H), 5.37 (s, 2H), 5.35 (m, 10H), 3.95 – 3.17 (m, 80H), 2.37 – 1.98 (m, 40H), 1.25 – 0.90 (m, 240H). MS (ES⁺): *m/z* calcd for C₅₆₀H₅₅₇Br₇N₈₀O₈₃ [M+4H]⁴⁺ 2573.65 found 2573.66.



Synthesis of 40-mer acid chloride (⁷BrQ₄₀-COCl) **16c**.

Oxalyl chloride (4 μL, 48.6 μmol) was added dropwise into a solution of compound **16b** (50 mg, 4.86 μmol) in 1 mL CHCl₃. The reaction was stirred at room temperature overnight and monitored by ¹H NMR. After

removal of solvents with pump, the product was obtained as yellowish solid quantitatively. ¹H NMR (300 MHz, CDCl₃): δ 10.92 (s, 1H), 10.79 (s, 1H), 10.57 (s, 1H), 10.55 (s, 1H), 10.42 (s, 1H), 10.22 (s, 1H), 10.20 (s, 1H), 10.10 (s, 1H), 10.03 (s, 1H), 9.92 (s, 1H), 9.88 (s, 1H), 9.85 (s, 1H), 9.79 (s, 3H), 9.74 (s, 1H), 9.69 (s, 1H), 9.62 (s, 1H), 9.54 (m, 4H), 9.51 (m, 2H), 9.48 (m, 2H), 9.45 (m, 2H), 9.40 (m, 11H), 8.13 – 8.10 (m, 1H), 7.94 (d, *J* = 3.73 Hz, 1H), 7.88 (d, *J* = 3.96 Hz, 1H), 7.71 – 6.42 (m, 112H), 6.37 (s, 1H), 6.07 (s, 1H), 6.01 (s, 1H), 5.99 (s, 1H), 5.87 (s, 1H), 5.80 (s, 1H), 5.76 (s, 1H), 5.69 (s, 1H), 5.66 (s, 1H), 5.62 (s, 1H), 5.60 (s, 1H), 5.56 (s, 1H), 5.54 (s, 1H), 5.52 (s, 1H), 5.50 (s, 1H), 5.49 (s, 1H), 5.47 (m, 2H), 5.44 (s, 1H), 5.43 (s, 1H), 5.42 (s, 1H), 5.40 (s, 3H), 5.38 (m, 4H), 5.35 (m, 10H), 3.95 – 3.22 (m, 80H), 2.31 – 2.01 (m, 40H), 1.33 – 0.91 (m, 240H).



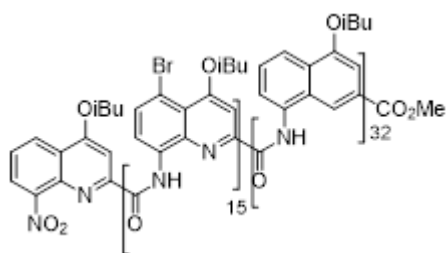
Synthesis of 80-mer

18. To a solution of compound **16c** in 0.7 mL CHCl₃ was added DIPEA (1.7 μL, 9.72

μmol) at 0°C under argon. The reaction was warmed up to room temperature, allowing water in the reaction atmosphere to react with **16c** to form **16b** with which **16c** coupled to generate **18**, and stirred overnight and controlled by ¹H NMR. After completed, the reaction was washed by H₂O, 0.1 M HCl, dried by Na₂SO₄, filtered, concentrated and purified by recycling GPC to give the product **18** as a yellowish solid. ¹H NMR (300 MHz, CDCl₃): δ 10.56 (m, 3H), 10.22 (s, 2H), 10.10 (s, 2H), 9.91 (s, 2H), 9.83 (s, 2H), 9.78 (m, 4H), 9.72 (m, 2H), 9.68 (m, 3H), 9.58

– 9.35 (m, 58H), 8.12 – 8.10 (m, 2H), 7.72 – 7.69 (m, 2H), 7.55 – 6.17 (m, 226H), 5.86 (m, 2H), 5.79 – 5.75 (m, 5H), 5.68 (m, 2H), 5.61 (m, 3H), 5.55 – 5.51 (m, 6H), 5.44 (m, 10H), 5.40 (m, 3H), 5.38 – 5.29 (m, 45H), 3.97 – 3.07 (m, 160H), 2.37 – 1.88 (m, 80H), 1.32 – 0.87 (m, 480H). MS (MALDI): m/z calcd for $C_{1120}H_{1104}Br_{14}N_{160}O_{165}$ $[M]^+$ 20564.2 found 20458.8.

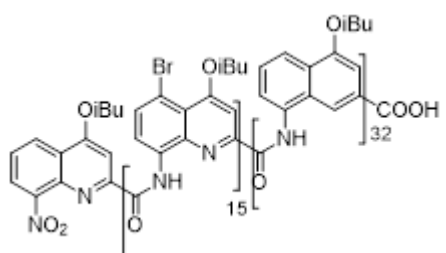
5.4.9 Synthesis of 48-mer 17a



To a mixture of compound **8d** ($Q_{32}\text{-NH}_2$) (83.1 mg, 10.6 μmol) and DIPEA (9 μL , 53.4 μmol) in 1.1 mL CHCl_3 was added dropwise the solution of compound **12c** ($^{15}\text{Br}Q_{16}\text{-COCl}$) (109 mg, 21.3 μmol) at 0°C under argon. The reaction was warmed up to room

temperature, stirred overnight and controlled by ^1H NMR. After completed, the reaction was washed by H_2O , 0.1 M HCl, dried by Na_2SO_4 , filtered, concentrated and purified by recycling GPC to give the product **17a** as a yellowish solid (40 mg, 30% yield). ^1H NMR (300 MHz, CDCl_3): δ 11.01 (s, 1H), 10.98 (s, 1H), 10.67 (s, 2H), 10.38 (s, 1H), 10.37 (s, 1H), 10.21 (s, 1H), 10.16 (s, 1H), 10.01 (s, 1H), 9.99 (s, 1H), 9.96 (s, 1H), 9.91 (s, 1H), 9.87 (s, 2H), 9.83 (s, 1H), 9.78 (s, 1H), 9.74 (s, 1H), 9.70 (s, 1H), 9.67 (s, 1H), 9.62 – 9.60 (m, 7H), 9.54 (s, 1H), 9.49 (s, 1H), 9.46 – 9.38 (m, 19H), 8.15 – 8.12 (m, 1H), 7.87 – 7.85 (m, 1H), 7.81 – 7.79 (m, 1H), 7.69 – 6.30 (m, 127H), 6.14 (s, 1H), 6.06 (s, 1H), 6.03 (s, 1H), 5.94 (s, 1H), 5.85 (s, 2H), 5.79 (s, 1H), 5.74 (s, 1H), 5.64 (m, 3H), 5.59 (m, 3H), 5.55 (s, 1H), 5.53 (s, 1H), 5.49 (s, 2H), 5.48 (s, 2H), 5.45 (m, 2H), 5.43 (s, 2H), 5.41 – 5.33 (m, 23H), 3.97 – 3.20 (m, 96H), 2.76 (s, 3H), 2.36 – 1.96 (m, 48H), 1.30 – 0.88 (m, 288H). MS (ES^+): m/z calcd for $C_{673}H_{663}Br_{15}N_{96}O_{99}$ $[M+4H]^{4+}$ 3219.7 found 3219.7.

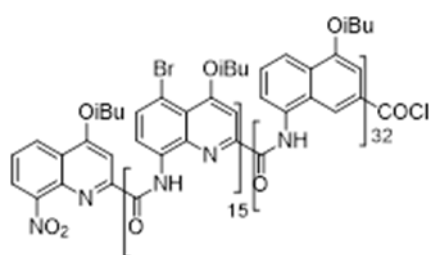
5.4.10 Synthesis of 96-mer 19



Synthesis of 48-mer acid ($^{15}\text{Br}Q_{48}\text{-COOH}$) 17b. To a solution of compound **17a** (40 mg, 3.11 μmol) in 1 mL THF/MeOH (9/1, v/v) was added ground NaOH (2.5 mg, 62.2 μmol). The reaction was stirred at room temperature overnight and monitored by TLC (CHCl_3)

until complete (if not, more time and/or NaOH could be needed). 0.1 M HCl was used to

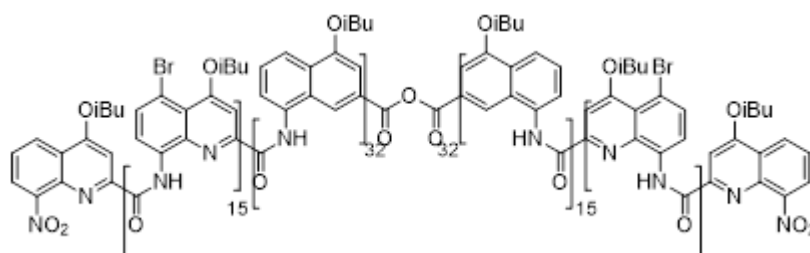
protonate the product until pH value of reaction went to approx. 5. The reaction was evaporated to remove organic solvents and the resulting residue was dissolved into CHCl₃, washed by H₂O and brine, dried by Na₂SO₄, filtered and concentrated to provide the product **17b** as a yellowish solid quantitatively. ¹H NMR (300 MHz, CDCl₃): δ 10.79 (s, 1H), 10.66 (s, 1H), 10.42 (s, 1H), 10.36 (s, 2H), 10.21 (s, 1H), 10.18 (s, 1H), 10.01 (s, 2H), 9.91 (s, 1H), 9.87 (s, 2H), 9.82 (s, 1H), 9.77 (s, 1H), 9.74 (s, 1H), 9.70 (s, 1H), 9.67 (s, 1H), 9.63 – 9.60 (m, 7H), 9.54 (s, 2H), 9.50 (s, 1H), 9.46 – 9.38 (m, 20H), 7.92 – 7.85 (m, 2H), 7.69 – 6.34 (m, 130H), 6.24 (s, 1H), 5.99 (s, 1H), 5.98 (s, 1H), 5.93 (s, 1H), 5.85 (s, 2H), 5.79 (s, 1H), 5.74 (s, 1H), 5.64 (s, 3H), 5.59 (s, 3H), 5.54 (m, 2H), 5.48 (m, 4H), 5.46 (m, 2H), 5.43 – 5.39 (m, 7H), 5.37 – 5.33 (m, 16H), 3.96 – 3.20 (m, 96H), 2.34 – 1.91 (m, 48H), 1.25 – 0.88 (m, 288H). MS (ES⁺): *m/z* calcd for C₆₇₂H₆₅₇Br₁₅N₉₆O₉₉ [M+4H]⁴⁺ 3216.2 found 3215.6.



Synthesis of 48-mer acid chloride (¹⁵BrQ₄₈-COCl) **17c**.

Oxalyl chloride (2.7 μL, 31.1 μmol) was added dropwise into a solution of compound **17b** (40 mg, 3.11 μmol) in 1.1 mL CHCl₃. The reaction was stirred at room temperature overnight and monitored by ¹H NMR. After

removal of solvents with pump, the product **17c** was obtained as yellowish solid quantitatively. ¹H NMR (300 MHz, CDCl₃): δ 10.92 (s, 1H), 10.79 (s, 1H), 10.67 (s, 1H), 10.41 (s, 1H), 10.36 (s, 1H), 10.19 (s, 2H), 10.02 (s, 2H), 9.92 (s, 1H), 9.87 (s, 2H), 9.84 (s, 1H), 9.79 (s, 1H), 9.75 (s, 1H), 9.71 – 9.61 (m, 10H), 9.55 (s, 1H), 9.50 – 9.39 (m, 21H), 7.94 – 7.86 (m, 2H), 7.70 – 6.37 (m, 129H), 6.06 (s, 1H), 6.01 (s, 1H), 5.98 (s, 1H), 5.93 (s, 1H), 5.85 (s, 1H), 5.79 (s, 1H), 5.74 (s, 1H), 5.64 (m, 3H), 5.59 (s, 3H), 5.55 (m, 2H), 5.49 – 5.48 (m, 4H), 5.46 (m, 2H), 5.43 (s, 1H), 5.40 (m, 6H), 5.37 – 5.33 (m, 18H), 3.97 – 3.20 (m, 96H), 2.35 – 1.97 (m, 48H), 1.19 – 0.83 (m, 288H).



Synthesis of 96-mer

19. To a solution of compound **17c** in 0.7 mL toluene was added DIPEA (2.7 μL, 15.55

μmol) at 0°C under argon. The reaction was warmed up to room temperature, allowing water in the reaction atmosphere to react with **17c** to form **17b** with which **17c** coupled to generate **19**, and stirred overnight and controlled by ^1H NMR. After completed, the reaction was washed by H_2O , 0.1 M HCl, dried by Na_2SO_4 , filtered, concentrated and purified by recycling GPC to give the product **19** as a yellowish solid. ^1H NMR (300 MHz, CDCl_3): δ 10.67 (s, 2H), 10.36 (s, 2H), 10.20 (s, 2H), 10.06 – 9.33 (m, 88H), 7.67 – 5.28 (m, 177H), 3.97 – 3.06 (m, 192H), 2.37 – 1.88 (m, 96H), 1.22 – 0.83 (m, 576H). MS (MALDI): m/z calcd for $\text{C}_{1344}\text{H}_{1312}\text{Br}_{30}\text{N}_{192}\text{O}_{197}$ $[\text{M}]^+$ 25702.4 found 25380.8.

6 References

- 1 (a) Gellman, S. H., Foldamers: A Manifesto. *Accounts of Chemical Research* **1998**, *31* (4), 173-180, and references therein; (b) Guichard, G.; Huc, I., Synthetic foldamers. *Chem Commun (Camb)* **2011**, *47* (21), 5933-41, and references therein.
- 2 (a) Sanford, R.; Bing Gong, A., Evolution of Helical Foldamers. *Current Organic Chemistry* **2003**, *7* (16), and references therein; (b) Zhang, D.-W.; Zhao, X.; Hou, J.-L.; Li, Z.-T., Aromatic Amide Foldamers: Structures, Properties, and Functions. *Chemical Reviews* **2012**, *112* (10), 5271-5316, and references therein.
- 3 (a) Hill, D. J.; Mio, M. J.; Prince, R. B.; Hughes, T. S.; Moore, J. S., A Field Guide to Foldamers. *Chemical Reviews* **2001**, *101* (12), 3893-4012, and references therein; (b) Hecht, S.; Huc, I., *Foldamers: structure, properties and applications*. John Wiley & Sons: 2007, and references therein.
- 4 (a) Sharma, G. V. M.; Subash, V.; Narsimulu, K.; Sankar, A. R.; Kunwar, A. C., De Novo Design and Synthesis of Helix–Turn–Helix Structure from Short and Robust Mixed Helices Derived from C-Linked Carbo- β -Amino Acids. *Angewandte Chemie International Edition* **2006**, *45* (48), 8207-8210; (b) Goodman, J. L.; Petersson, E. J.; Daniels, D. S.; Qiu, J. X.; Schepartz, A., Biophysical and Structural Characterization of a Robust Octameric β -Peptide Bundle. *Journal of the American Chemical Society* **2007**, *129* (47), 14746-14751; (c) Price, J. L.; Horne, W. S.; Gellman, S. H., Discrete Heterogeneous Quaternary Structure Formed by α/β -Peptide Foldamers and α -Peptides. *Journal of the American Chemical Society* **2007**, *129* (20), 6376-6377; (d) Sánchez-García, D.; Kauffmann, B.; Kawanami, T.; Ihara, H.; Takafuji, M.; Delville, M.-H.; Huc, I., Nanosized Hybrid Oligoamide Foldamers: Aromatic Templates for the Folding of Multiple Aliphatic Units. *Journal of the American Chemical Society* **2009**, *131* (24), 8642-8648; (e) Solà, J.; Fletcher, S. P.; Castellanos, A.; Clayden, J., Nanometer-Range Communication of Stereochemical Information by Reversible Switching of Molecular Helicity. *Angewandte Chemie International Edition* **2010**, *49* (38), 6836-6839; (f) Delsuc, N.; Massip, S.; Léger, J.-M.; Kauffmann, B.; Huc, I., Relative Helix–Helix Conformations in Branched Aromatic Oligoamide Foldamers. *Journal of the American Chemical Society* **2011**, *133* (9), 3165-3172; (g) Fremaux, J.;

-
- Fischer, L.; Arbogast, T.; Kauffmann, B.; Guichard, G., Condensation approach to aliphatic oligourea foldamers: helices with N-(pyrrolidin-2-ylmethyl)ureido junctions. *Angewandte Chemie* **2011**, *50* (48), 11382-5; (h) Fremaux, J.; Fischer, L.; Arbogast, T.; Kauffmann, B.; Guichard, G., Condensation Approach to Aliphatic Oligourea Foldamers: Helices with N-(Pyrrolidin-2-ylmethyl)ureido Junctions. *Angewandte Chemie International Edition* **2011**, *50* (48), 11382-11385; (i) Byrne, L.; Solà J.; Boddaert, T.; Marcelli, T.; Adams, R. W.; Morris, G. A.; Clayden, J., Foldamer-Mediated Remote Stereocontrol: >1,60 Asymmetric Induction. *Angewandte Chemie International Edition* **2014**, *53* (1), 151-155.
- 5 Horne, W. S.; Johnson, L. M.; Ketas, T. J.; Klasse, P. J.; Lu, M.; Moore, J. P.; Gellman, S. H., Structural and biological mimicry of protein surface recognition by α/β -peptide foldamers. *Proceedings of the National Academy of Sciences* **2009**, *106* (35), 14751-14756.
- 6 Horne, W. S.; Price, J. L.; Keck, J. L.; Gellman, S. H., Helix Bundle Quaternary Structure from α/β -Peptide Foldamers. *Journal of the American Chemical Society* **2007**, *129* (14), 4178-4180.
- 7 Checco, J. W.; Kreitler, D. F.; Thomas, N. C.; Belair, D. G.; Rettko, N. J.; Murphy, W. L.; Forest, K. T.; Gellman, S. H., Targeting diverse protein-protein interaction interfaces with α/β -peptides derived from the Z-domain scaffold. *Proceedings of the National Academy of Sciences* **2015**, *112* (15), 4552-4557.
- 8 (a) Obayashi, T.; Masud, M. M.; Ozaki, A. N.; Ozaki, H.; Kuwahara, M.; Sawai, H., Enzymatic synthesis of labeled DNA by PCR using new fluorescent thymidine nucleotide analogue and superthermophilic KOD dash DNA polymerase. *Bioorganic & medicinal chemistry letters* **2002**, *12* (8), 1167-1170; (b) Petsko, G. A.; Ringe, D., Protein structure and function. New Science Press: 2004.
- 9 Hartman, M. C.; Josephson, K.; Lin, C.-W.; Szostak, J. W., An expanded set of amino acid analogs for the ribosomal translation of unnatural peptides. *PLoS One* **2007**, *2* (10), e972.
- 10 Kumar, K. S. A.; Bavikar, S. N.; Spasser, L.; Moyal, T.; Ohayon, S.; Brik, A., Total Chemical Synthesis of a 304 Amino Acid K48-Linked Tetraubiquitin Protein. *Angewandte Chemie International Edition* **2011**, *50* (27), 6137-6141.
- 11 (a) Kent, S. B. H., Total chemical synthesis of proteins. *Chemical Society Reviews* **2009**, *38* (2), 338-351; (b) Pattabiraman, V. R.; Bode, J. W., Rethinking amide bond synthesis. *Nature* **2011**,

480 (7378), 471-479.

- 12 Qiu, J.; El-Sagheer, A. H.; Brown, T., Solid phase click ligation for the synthesis of very long oligonucleotides. *Chemical Communications* **2013**, *49* (62), 6959-6961.
- 13 (a) Hawker, C. J.; Fréchet, J. M. J., Preparation of polymers with controlled molecular architecture. A new convergent approach to dendritic macromolecules. *Journal of the American Chemical Society* **1990**, *112* (21), 7638-7647; (b) Grayson, S. M.; Fréchet, J. M. J., Convergent Dendrons and Dendrimers: from Synthesis to Applications. *Chemical Reviews* **2001**, *101* (12), 3819-3868, and references therein; (c) Walter, M. V.; Malkoch, M., Simplifying the synthesis of dendrimers: accelerated approaches. *Chemical Society Reviews* **2012**, *41* (13), 4593-4609, and references therein; (d) Roy, R.; Shiao, T. C., Glyconanosynthons as powerful scaffolds and building blocks for the rapid construction of multifaceted, dense and chiral dendrimers. *Chemical Society Reviews* **2015**, , and references therein.
- 14 Huc, I., Aromatic Oligoamide Foldamers. *European Journal of Organic Chemistry* **2004**, *2004* (1), 17-29, and references therein.
- 15 Qi, T.; Maurizot, V.; Noguchi, H.; Charoenraks, T.; Kauffmann, B.; Takafuji, M.; Ihara, H.; Huc, I., Solvent dependence of helix stability in aromatic oligoamide foldamers. *Chemical Communications* **2012**, *48* (51), 6337-6339.
- 16 Zhang, A.; Ferguson, J. S.; Yamato, K.; Zheng, C.; Gong, B., Improving Foldamer Synthesis through Protecting Group Induced Unfolding of Aromatic Oligoamides. *Organic Letters* **2006**, *8* (22), 5117-5120.
- 17 (a) Delsuc, N.; Massip, S.; Leger, J. M.; Kauffmann, B.; Huc, I., Relative helix-helix conformations in branched aromatic oligoamide foldamers. *Journal of the American Chemical Society* **2011**, *133* (9), 3165-72; (b) Sanchez-Garcia, D.; Kauffmann, B.; Kawanami, T.; Ihara, H.; Takafuji, M.; Delville, M.-H.; Huc, I., Nanosized hybrid oligoamide foldamers: aromatic templates for the folding of multiple aliphatic units. *Journal of the American Chemical Society* **2009**, *131* (24), 8642-8648; (c) Kudo, M.; Maurizot, V.; Kauffmann, B.; Tanatani, A.; Huc, I., Folding of a Linear Array of α -Amino Acids within a Helical Aromatic Oligoamide Frame. *Journal of the American Chemical Society* **2013**, *135* (26), 9628-9631.
- 18 Qi, T.; Deschrijver, T.; Huc, I., Large-scale and chromatography-free synthesis of an octameric

-
- quinoline-based aromatic amide helical foldamer. *Nat. Protocols* **2013**, 8 (4), 693-708.
- 19 (a) Jiang, H.; L  ger, J.-M.; Huc, I., Aromatic δ -Peptides. *Journal of the American Chemical Society* **2003**, 125 (12), 3448-3449; (b) Dolain, C.; Gr  ard, A.; Laguerre, M.; Jiang, H.; Maurizot, V.; Huc, I., Solution Structure of Quinoline- and Pyridine-Derived Oligoamide Foldamers. *Chemistry – A European Journal* **2005**, 11 (21), 6135-6144.
- 20 Wolffs, M.; Delsuc, N.; Veldman, D.; Anh, N. V.; Williams, R. M.; Meskers, S. C. J.; Janssen, R. A. J.; Huc, I.; Schenning, A. P. H. J., Helical Aromatic Oligoamide Foldamers as Organizational Scaffolds for Photoinduced Charge Transfer. *Journal of the American Chemical Society* **2009**, 131 (13), 4819-4829.
- 21 Srinivas, K.; Kauffmann, B.; Dolain, C.; L  ger, J.-M.; Ghosez, L.; Huc, I., Remote Substituent Effects and Regioselective Enhancement of Electrophilic Substitutions in Helical Aromatic Oligoamides. *Journal of the American Chemical Society* **2008**, 130 (40), 13210-13211.

III Assessment of helix rigidity in solution and in gas phase

1 Introduction

Intensive efforts have been dedicated to the design, synthesis and structural investigation of these folded molecules.¹ Since developed around two decades ago, foldamers has been developed from peptide and nuclear acid analogues in early age, e.g., β -, γ - and δ - amino acid, to totally non-natural congeners, such as aromatic amide oligomers² (Figure 1). With the development of understanding of chemical structures, the design and synthesis of foldameric building blocks have been becoming more and more mature.^{1d, 2} But understanding the structural dynamics of these foldamers has been challenging the researchers, especially for the abiotic families of foldamer. Many techniques/tools, which are generally used in chemistry, biology and even materials science, have been successfully employed to characterize the supramolecular structures of foldamers. For the biotic analogues of biopolymers and some well-folded abiotic oligomers, nuclear magnetic resonance (NMR) is mostly common used to elucidate their structures in solution, and to show the accuracy of the design. Using similar NMR experiment that has been used to determine the natural α -peptide structures, ¹H NMR has been applied for the characterization of aliphatic β -, γ - and δ -peptides and of their hybrids. In particular, two dimensional NMR spectra allowed to assign the ¹H NMR spectra of β -peptides

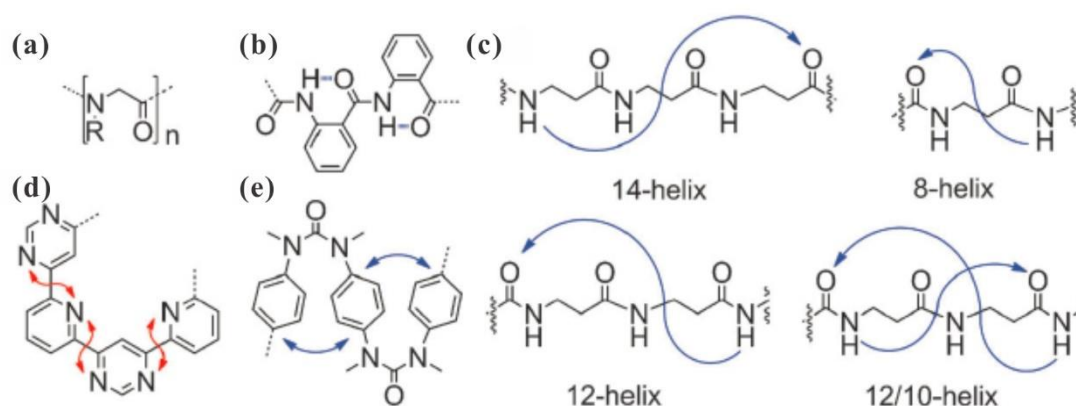


Figure 1 Some examples of building blocks of foldamers: peptoids (a), aromatic oligoamides (b), b-peptides (c), aza-aromatic oligomers (d) and tertiary aromatic ureas (e).^{1d}

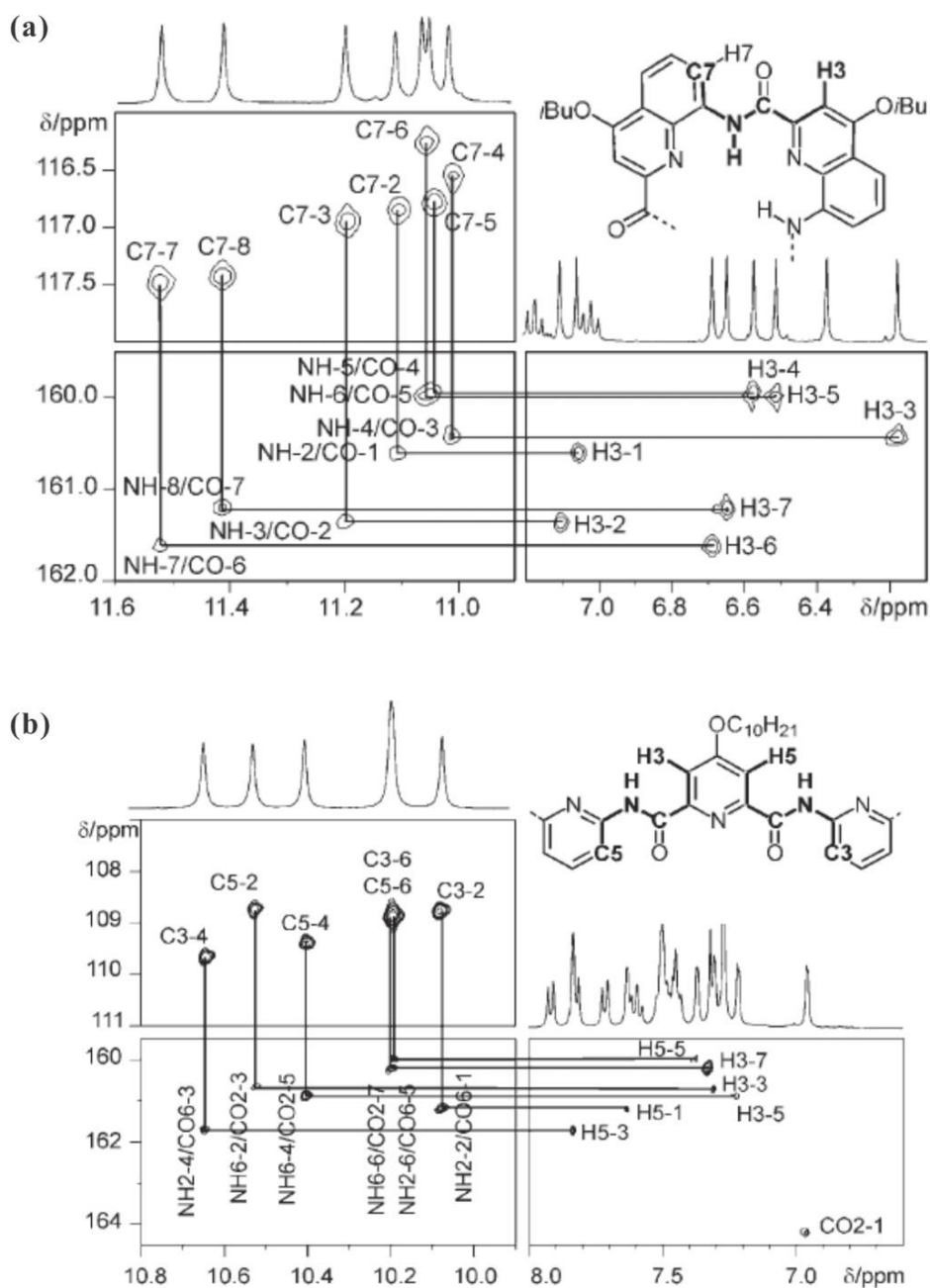


Figure 2 The partial HMBC spectra of quinoline-based (a) and pyridine-based foldamers. The horizontal scale is the proton resonances and the vertical one the carbon resonances. For quinoline-based foldamer, (a) shows the cross-peaks between carbons C7 and amide protons (a, top right), between amide protons and carbonyl carbons (a, bottom left), and between carbonyl and H3 protons (a, bottom right) used for sequence assignment to go from residue i to residue $i+1$. For pyridine-based foldamer, (b) displays the cross-peaks between carbons C5 and C3 and amide protons (b, top right), between amide protons and carbonyl carbons (b, bottom left), and between carbonyl and protons H3 and H5 (b, bottom right) used for sequence assignment to go from residue i to residue $i+2$.³

comprised of enantiomerically pure trans-2-aminocyclohexane-carboxylic acid or trans-2-aminocyclopentane-carboxylic acid units and confirm that their solution structures were similar to their well-defined helical conformations observed in the solid state.⁴ This technique has been successfully extended to study the aromatic foldamers (Figure 2) and the results have shown, as for their aliphatic analogues, that these quinoline- and pyridine-based aromatic amide oligomers have similar architecture that those observed in the solid state.³ For some foldamer molecules, for example, oligo(m-phenylene ethynylene)s, they prefer to aggregate with each other, which causes NMR to become unable to afford high enough resolution for the conformational order owing to the overlap of characteristic signals. The corresponding assignment of signals and the determination of folding come out to be difficult if not impossible.⁵ Therefore, other spectroscopic techniques were introduced to characterize the architectures of foldameric sequences, such as UV/vis⁵⁻⁶, fluorescence⁷, circular dichroism⁸ and even electron spin resonance⁹. The spectral changes of curves (e.g. intensity of Uv/Vis, fluorescence and CD spectra) revealed either the alteration of the number of monomer in the foldamer sequence⁵, or cooperative conformational transition between helix and coil⁷, or self-assembly of foldamers into helical columns⁸ or helical pitch of foldameric molecule⁹. MALDI mass spectroscopy was also applied to demonstrate the formation of molecular ladders after covalently combining two different m-phenylene ethynylene-based foldamer molecules with dynamic covalent chemistry.¹⁰ Microscopies, for example Scanning tunneling microscopy¹¹, atom force microscopy and polarized light microscopy¹², have also been employed to delineate the structural properties of foldamers.

Using these techniques towards foldamers has given access to understanding foldamers in detail, especially their physicochemical properties in solution.^{3-10, 13} But, when the atmosphere of foldamers is unrestricted enough, i.e. in gas phase where steric hindrance of surroundings toward foldamer molecules reduces significantly, allowing these molecules to ‘deform’, there still is a blank about how the foldameric molecules would act and the related physicochemical properties of foldamers would be. Understanding of these questions happening in gas phase undoubtedly enables us to disclose whether the conformation of foldameric molecules is stable and rigid in such surroundings or not. On the other hand, even though physicochemical

properties of foldamer in solution has been revealed a lot³, the motion properties of foldamers in solution are still kept unknown. When the foldameric molecules diffuse in solution, what is (are) the style(s) of movement for these molecules? Translational diffusion or rotational one? Or both ways? Given that each technique has its own capability and limitation and according to these questions, in collaboration with other groups, we have attempted to investigate 1) the conformation of foldamer molecules in gas phase, further the stability and rigidity of structural conformation of foldamers using ion mobility mass spectrometry with Dr. Frédéric Rosu and Dr. Valérie Gabelica at IECB, Bordeaux, France, 2) the translational diffusion of foldamer in solution using diffusion ordered spectroscopy (DOSY) with Prof. Aldrik H. Velders at Wageningen University, Netherlands, and 3) the rotational diffusion property by using fluorescence anisotropy with Prof. Jean Duhamel at University of Waterloo, Canada. Therefore, three techniques (ion mobility spectrometry-mass spectrometry, diffusion ordered spectroscopy and fluorescence anisotropy spectroscopy) have been employed to understand quinoline-based foldamers that are synthesized during my thesis. With these techniques, we determined these physicochemical properties of these quinoline-based foldamers and the relationship between these physicochemical parameters and the sizes of foldamer molecules, further, the rigidity of foldamer molecules.

2 Ion mobility spectrometry-Mass spectrometry (IMS-MS)

2.1 Introduction

Ion mobility spectrometry (IMS) is an analytic technique by which various molecules extracted to the gas phase can be separated and analyzed according to their size and shape.¹⁴ Whereas, mass spectrometry (MS) could provide structure information of samples in gas phase according to the mass-charge-ratio (m/z).¹⁵ Therefore, the hyphenation between IMS and MS technique enables the separation of ions as a function of their shape in the IMS dimension and as a function of their mass-to-charge ratio in MS dimension. This becomes a crucial advantage for analysis of the isomers of the same chemical structures (isobaric ions). Basically, the most important parameter to describe IMS-MS is the collision cross section (CCS, Ω), rotationally averaged cross-sectional area that is covered by the ion and a function of drift time of ion. Even though this IMS-MS technique has been developed since more than half a century,¹⁶ its bloom worldwide just happened around 15 years with the coupling with electrospray source.¹⁷ According to the development and the commercial availability, several kinds of IMS spectrometers have been invented, such as drift tube IMS (DTIMS), traveling wave IMS (TWIMS), field-asymmetric IMS (FAIMS).^{14b} For structural purpose, one obvious advantage of DTIMS over the other IMS spectrometers is that it uses the low electric field that avoids the perturbation of ions. Meanwhile, it allows the direct determination of structural parameters and if the drift tube is long enough (>50cm), and possesses high separation resolution (so-called resolving powerⁱⁱ R , >100). We have used a DTIMS operated in helium for the experiments (Figure 3).

Herein, a brief introduction of DTIMS is presented as follows. In DTIMS, Ion is pulsed into the tube filled with inert gas (also called as buffer gas, typically, nitrogen or helium) under a static uniform electric field E , and then propelled along the direction of E . When Voltage V is

ⁱⁱ Resolving power is defined as: $R = \frac{\Omega}{\Delta\Omega}$, where Ω is collision cross section (\AA) of target ion, $\Delta\Omega$ is the collision cross section difference between target ion and distinct ion. For example, if one IMS spectrometer has resolving power with 100, that is to say, it could discriminate an ion with collision cross section, like 500 \AA , from another ion with collision cross section $500 \pm 5 \text{ \AA}$.

Agilent ESI-IMS-Q-TOF instrument. 80 cm drift cell, 3.9 torr He. All Ions are gated and separated in drift time and transmitted to the Q-TOF. Agilent ESI-IMS-Q-TOF was used. Collision cross sections (CCS) were determined in He from ramping the voltage on the drift tube (5 voltages, 1 min data acquisition per voltage). T = 296 K

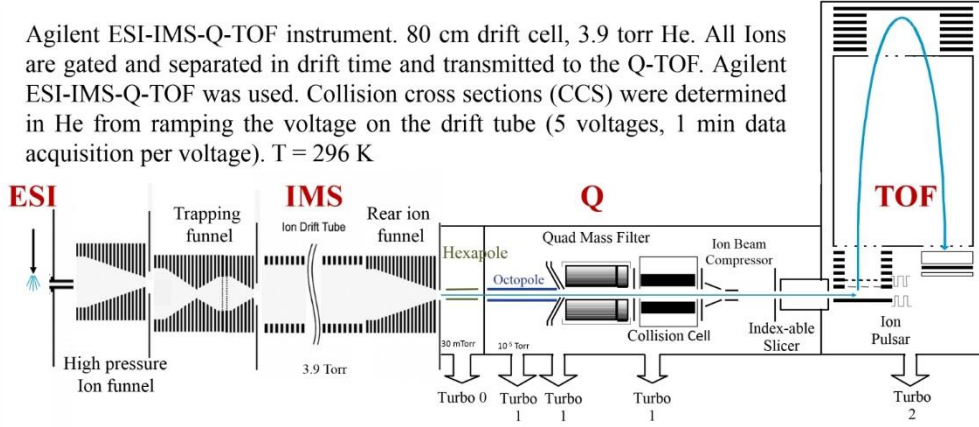


Figure 3 The IMS-MS instrument used in our study and some corresponding parameters as it works.

applied to the tube (L , cm), E can be expressed as:

$$E = \frac{V}{L} \quad (2.1)$$

Once the driving force originated from E equals to the friction force caused by the collisions between ion and inert gas molecule, the drift velocity of ion V_d is linearly proportional to E and given as

$$V_d = K \cdot E \quad (2.2)$$

where K is a parameter of mobility. Generally, the reduced mobility K_0 is used practically instead of K . Under standard pressure and temperature ($P_0 = 760$ Torr and $T_0 = 273$ K), K_0 can be expressed as:

$$K_0 = K \cdot \frac{P}{P_0} \cdot \frac{T_0}{T} \quad (2.3)$$

In weak electric field, K_0 is independent on electric field (low field limit ($E/N \leq 2 \times 10^{-21}$ V.m²), N is the number density of the inert gas in the tube), and can be calculated by Mason-Schamp equation¹⁸:

$$K_0 = \frac{3ze}{16N_0} \left(\frac{2\pi}{\mu k_B T} \right)^{\frac{1}{2}} \frac{1}{\Omega} \quad (2.4)$$

where z is the charge state of ion, e is the elementary charge, N_0 is the number density of the inert gas under pressure P_0 and temperature T_0 , k_B is Boltzmann constant, T is the temperature of inert gas, Ω is the collision cross section of ion and μ is the reduced mass and given as:

$$\mu = \frac{Mm}{M+m} \quad (2.5)$$

where M and m are the masses of ion and inert gas molecule, respectively. In a tube (L , cm) and

under known pressure and temperature, the time for an ion (t_d) to drift through the tube can be termed as:

$$t_d = \frac{L}{V_d} \quad (2.6)$$

The arrival time of the ion to be detected is the summation of the time in the tube t_d and the time outside of drift cell and before detection t_0 , namely,

$$t_A = t_d + t_0 \quad (2.7)$$

Combining equation (2.1), (2.2), (2.3), (2.4), (2.6) and (2.7) yields:

$$t_A = \frac{L^2}{K_0} \cdot \frac{T_0}{P_0 T} \cdot \frac{P}{V} + t_0 \quad (2.8)$$

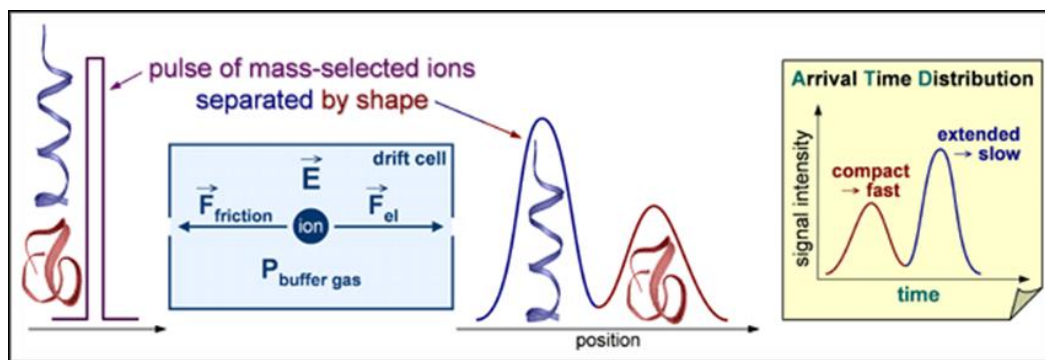


Figure 4 The scheme of ion separation under a static uniform electric field E.ⁱⁱⁱ

Based on equation (2.8), as P and T are constant and known, t_A has a linear relationship with $1/V$, the slope of which is proportional to K_0 , and the intercept at axis t_A of which is t_0 .

After obtaining K_0 , the experimental CCS Ω can be generated with equation (2.4).

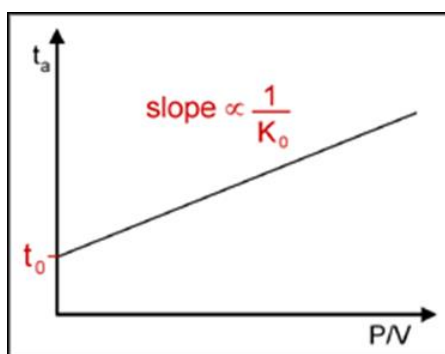


Figure 5 The slope from equation (2.8) is proportional to $1/K_0$.ⁱⁱ

ⁱⁱⁱ These two pictures are from Prof. Michael T. Bowers' homepage at UCSB: https://labs.chem.ucsb.edu/bowers/michael/theory_analysis/ion-mobility/index.shtml

To determine the precise structural information generated by experimental CCS Ω , molecular dynamics simulation is always co-employed to support and complement the experimental CCS results. Different approximate approaches of calculation of theoretical CCS have been applied to fit the practical results, such as trajectory model (TM) and projection superposition approximation (PSA).^{14a} PSA model takes into account a modified projection model that considers atoms as soft spheres which combined effect can then superimpose, and the whole Projection Approximation (PA) is corrected by a shape factor. The trajectory method is more ancient: it takes into account Lenard-Jones interaction potentials to model the way the gas slows down the ion by interacting with it during a collision event. TM is more computationally expensive because it is time consuming and the Lenard-Jones interactions potentials are unknown for foldamers.

The hyphenation of the two analytic techniques ion mobility and mass spectrometry (IMS-MS) allows additional separation dimension: separate and analyze samples not only by size and shape, but also as a function of their mass-charge-ratio.^{17, 19} This advantage has offered exceptional advantages for investigation of the configuration and the structure of biomolecules^{14a, 20} and supramolecules²¹, like isomerization and chirality. Metallosupramolecular isobaric self-assembled trigonal prismatic cage isomers have been distinguished by using IMS-MS with which the stability of these isomers affected by the tiny structural difference, the relative orientation (*cis* and *trans*) of bidentate cyclometallated ligand, was revealed.²² Cd²⁺ contained hexagonal macrocycles and linear polymers were also examined with use of traveling wave IMS-MS.²³ Mechanically interlocked polymers was given a new structural insight by IMS-MS, and the results of IMS-MS revealed that the dibenzo-24-crown-8 macrocycle preferentially remains associated with the ammonium moiety of the rod and is hindered from moving along the rod.²⁴

Herein, in cooperation with Dr. Frédéric Rosu and Dr. Valérie Gabelica at IECB, Bordeaux, France, a study of foldamer with IMS-MS is presented. Three series of quinoline-based foldamers (bromine-free foldamers, brominated foldamers and brominated anhydride foldamers) have been injected into ion mobility spectrometer to determine their configurations, further to assess the tubular structure and rigidity of these helical structures in gaseous phase.

Two approximate molecular modellings were also applied to investigate the CCS theoretically.

2.2 Results and discussion

Bromine-free quinoline-based foldamers have been synthesized. Polybromination of these foldamers in the presence of NBS allowed us to obtain unique products, brominated quinoline-based foldamers. Based on these brominated foldamers, the anhydride oligomers were formed by coupling brominated foldamers acids with their corresponding acid chloride^{iv} (Figure 5). With IMS-MS, bromine-free foldamers of 8, 16 and 32 units (8mer, 16mer and 32mer), brominated foldamers of 8, 16 and 32 units (brominated 8mer, brominated 16mer and brominated 32mer), and anhydride foldamers of 16 (anhydride 16mer) – coupling 8-unit brominated foldamer acid with its acid chloride – and 32 units (anhydride 32mer) – coupling 16-unit brominated foldamer acid with its corresponding acid chloride – were investigated.

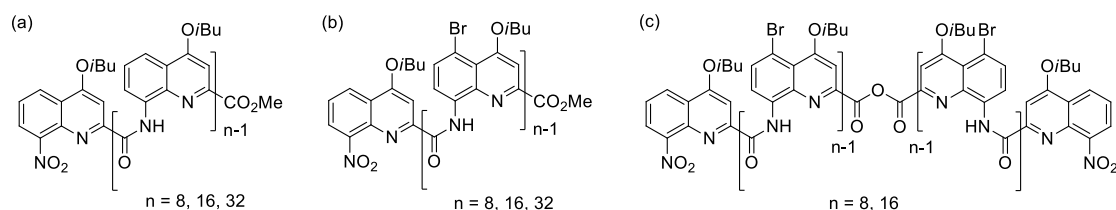


Figure 5 The chemical structures of foldamers (a) bromine-free foldamers, (b) brominated foldamers and (c) anhydride foldamers.

As mentioned above, the CCS of an ion can be gained by using the equation (2.4) with K_0 that is proportional to the slope of a plot of t_A and I/V , that is, building up a plot of t_A and I/V is pre-conditional and essential to gain the CCS of an ion. As shown in Figure 6, the result of IMS-MS tells us the exact mass of 8mer and its arrival time distribution. A plot of t_A and I/V is obtained as well, exhibiting a linear correlation between t_A and I/V . The slope of this plot gave the value of K_0 that further yielded the CCS of $(8\text{mer})^{1+} = 351.6 \pm 1 \text{ \AA}^2$ and $(8\text{mer})^{2+} = 370.1 \pm 1 \text{ \AA}^2$. The experimental values are obtained after 3 independent experiments (different days). Two approximate methods of molecular modelling (TM and PSA) were employed to calculate

^{iv} The syntheses of these foldamers have been presented in Chapter II.

the theoretical CCS of 8mer. These experimental and theoretical results of CCS of 8mer are shown in Figure 6. The experimental results of CCS are in good agreement with the theoretical ones, especially with the one based on PSA modeling in helium, revealing that theoretical treatments can be applied to foldamers. Since the parameterization of the theoretical models to determine CCS of large organic molecule has never been done, the initial test shows that the actual models are good but further improvement will be done. Measurements of 16mer show similar narrow arrival time distribution of the ion by IMS-MS (Figure 9a) which demonstrates a narrow distribution of conformation of 16mer, no other unexpected conformation appeared and the helical structures of 16mer in gas phase is rigid enough to keep itself in a stable conformation. For 8mer and 32mer, similar results – only one CCS – were obtained as well.

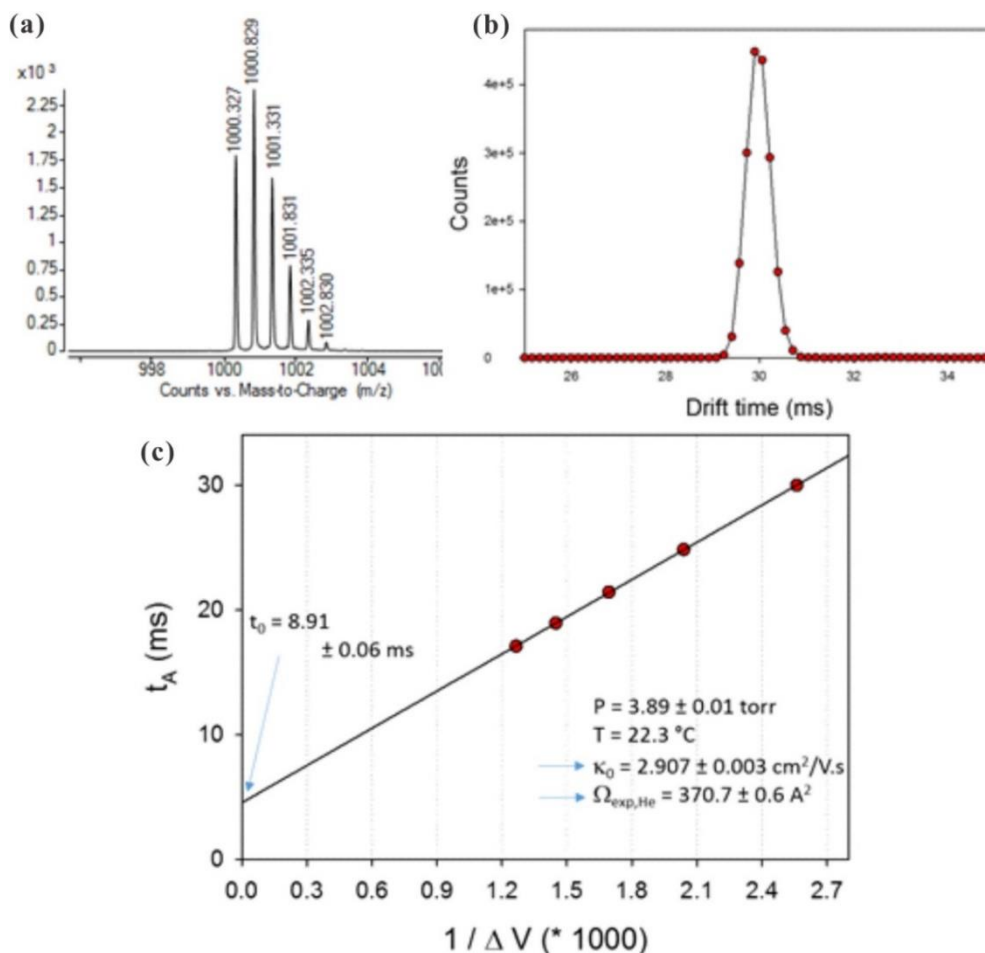


Figure 6 The electrospray ionization mass spectrum of 8mer (a), its arrival time distribution (b) and a plot of t_A and $1/V$ (c).

These data solidly confirm that the tubular structure of quinoline-based helical foldamers are conserved in gas phase. As known from the X-ray crystallography and NMR studies^{3, 25}, this only one conformation is a rigid helical structure.

Good agreement between the experimental values and calculated one indicates that the proposed tubular structural model is good and also the theoretical model is correctly parameterized. As comparison, the CCS of a partially unfolded 8mer which form partially a stable ribbon-like structure was calculated (Figure 7). The resulting CCS values are much higher than the experimental one (490.4 Å², for helical structure: 351.6 Å²). This structure can then be ruled out, that is to say, the helical structure is conserved.

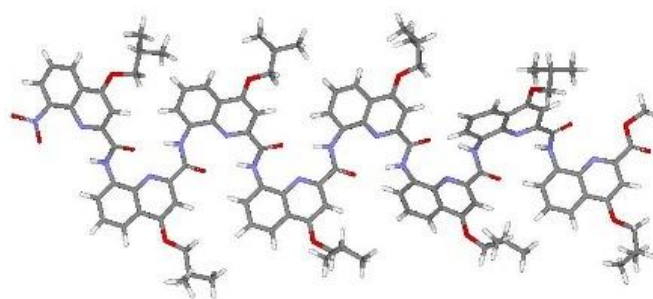


Figure 7 Ribbon structure of 8mer used for the referring calculation.

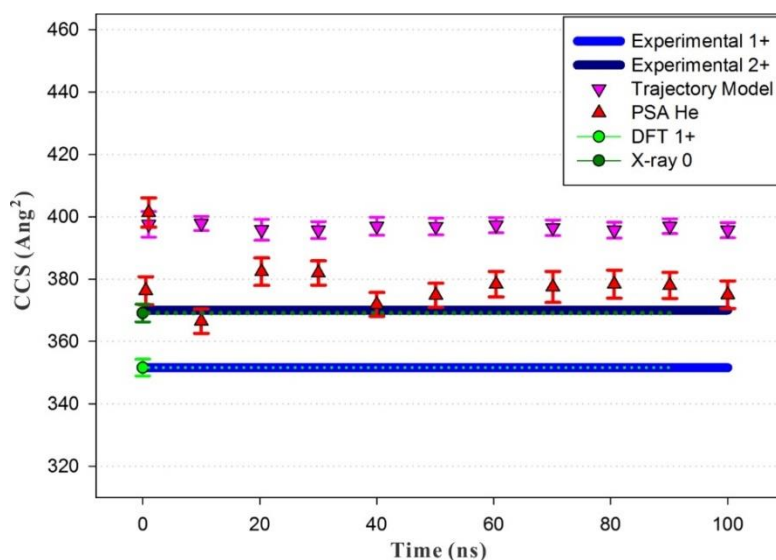


Figure 8 The CCS results of 8mer based on experiments and molecular modelling. Green dot: CCS calculated using the X-ray structure. X-ray structure: packing effect on the isobutyl side chain and also presence of CH₂Cl₂ that has been removed for the calculation. Side chains of the molecule are relaxed and CCS increase a little bit.

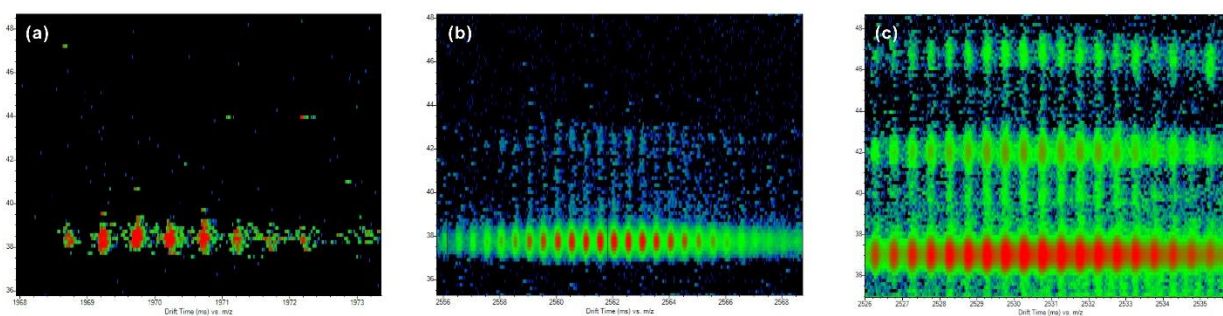


Figure 9 The CCS of 16mer (a) (572\AA^2), brominated 16mer (b) (567\AA^2) and anhydride 16mers (from top to bottom: 720\AA^2 , 643\AA^2 and 567\AA^2) shows three different results, revealing three conformations for this molecule.

For the brominated foldamers, CCS measurements presented only one distinct arrival time distribution in IMS-MS curves (Figure 9b), revealing that the conformation of these brominated foldamers is just one as well, alike to those bromine-free foldamers, and that the helical structures of these brominated foldamers are also conserved during the time scale of the experiment. It must be noted that the CCS results of the brominated foldamers are similar to these of the corresponding bromine-free foldamers (Table 1 and Figure 10), meanwhile, the charge states (even high or low) of these two series of foldamer ions do not change the CCS values obviously (Figure 10), which confirm that bromination of backbones of foldamers has no influence upon the structure of the foldamers,. The rigidity of the helices can be inferred from the width of the experimental CCS distribution. A narrow distribution indicates a narrow distribution of conformation. It is important to note that compared to proteins and peptides, all the arrival time distribution are much smaller (30% or more). Ion mobility of a very rigid system, namely a molecule that will not explore a large conformation space, only results in a narrow CCS distribution.^{14a}

Table 1 the CCS_{He} results of brominated foldamers and bromine-free foldamers. Values obtained from 3 independent measurements.

Foldamers	8mer ¹⁺	16mer ²⁺	32mer
CCS (brominated, \AA^2)	353.8	575.4	1013.3
CCS (bromine-free, \AA^2)	351.6	573.2	1007.7

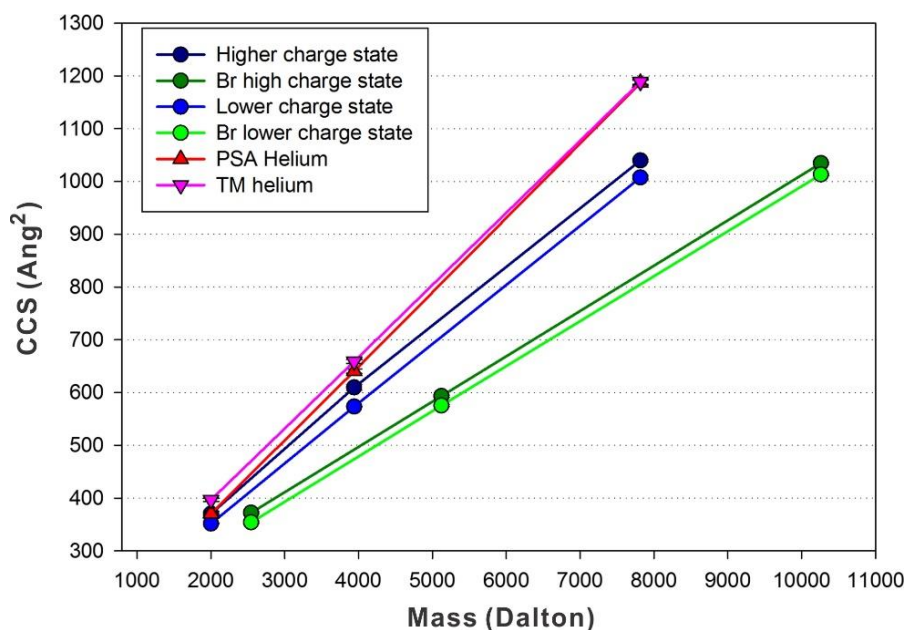


Figure 10 The theoretical and experimental CCS results of bromine-free foldamers (8mer, 16mer and 32mer) and the experimental CCS results of brominated foldamers.

The theoretical approximate modelling for bromine-free foldamers exhibits a comparable match with the experimental results (Figure 10), even though there is the divergence between theoretical and experimental results increases with the incremental size of foldamer. The theoretical model must be better parameterized for large organic molecules. We present here the first experiments of foldamers and the agreement between accurate experimental values and theoretical values are promising.

For the anhydride foldamers, three CCS results were obtained for each molecule (Figure 9c). This phenomenon directly reveals that three conformations appeared in gas phase for each anhydride foldamer, unlike those for two series of foldamers mentioned above. These results are surprising since in the solid state and in solution, no other conformation could be observed. The anhydride function in the middle of the oligomeric sequence probably act as a destabilizing flexible bond that is able to change its direction easily in space when the stereo-hindrance for the direction change decreases enough in gas phase. Further investigation into this interesting phenomenon is needed and now underway.

2.3 Conclusion

IMS-MS has been successfully applied to investigate quinoline-based foldamers. For bromine-free and brominated foldamers, the CCS results reveal that their helical structures in gas phase are conserved and the molecules are rigid. The narrow width of the arrival time distribution shows very low structural heterogeneity. The similar CCS values between bromine-free and brominated foldamers show that bromination does not affect the structure and rigidity of foldamers themselves. The theoretical calculation for bromine-free foldamers give comparable CCS result as experiments does. Additional effort to better parameterize the theoretical model will be done. For anhydride foldamers, three CCS values for one foldamer were observed which indicate the presence of three conformations, which is probably caused by the flexible anhydride bond. This interesting phenomenon is now studied in more details.

2.4 Experimental section

All the foldamers have been synthesized (in 2nd chapter) and used them directly.

IMS-MS Experiments were performed on an Agilent 6560 DTIMS-Q-TOF instrument (Agilent Technologies, Santa Clara, CA) with the dual-ESI source in the positive ion mode. The drift tube length is 78.1 cm. The syringe pump flow rate was set as 180 $\mu\text{l/h}$. The source and Q-TOF parts were optimized to have soft conditions (to avoid energy activation of the ions by collision). The drying gas was 200 $^{\circ}\text{C}$. The instrument was operated at a low field (~ 17 V/cm). The trap funnel exit and the drift tube entrance are bias of 10 V to allow ion injection to travel to the drift tube. The RF amplitude in the trap funnel is optimized for the foldamers (200 V) and also to avoid RF heating of the ions.

For nitrogen experiments, the collision gas pressure was around 4.2 Torr and monitored throughout the experiment with the pirani gauge. The drift tube pressure was 0.14 Torr higher than the trapping funnel pressure. The drift cell exit voltage was 210 V, and the drift cell entrance voltage was ramped from 1000 to 1700 V. For helium experiments, the pumping system was modified by connecting an E2M80 oil pump (Edwards SAS, Gennevilliers, France) to the source region, whereas the original pump was connected to the Q-TOF region. Helium

(Alphagaz 1 grade from Air Liquide, H₂O <3 ppm, C_nH_m <0.5 ppm, O₂ <2 ppm) was introduced in the drift tube through the same tubings as in the standard configuration. The pressures in the drift tube and in the front funnel were monitored using capacitance diaphragm gauges (CDG-500, Agilent Technologies). The drift tube pressure was set around 3.70 Torr (measured accurately by the CDG), and 0.23 Torr higher than the trapping funnel pressure, to ensure no nitrogen enters the drift tube. Lower pressure differential resulted in higher collision cross sections, indicating helium contamination with nitrogen coming from the electrospray source. Experiments were also repeated with the ‘Alternate Gas Option’ added to the standard configuration. Here, CDGs are connected to the trapping funnel and to the drift tube for all measurements. An additional flow controller admits gas in the trapping funnel, and the flow controller is regulated by a feedback reading of the pressure in the drift tube. We connected a second Tri-scroll 800 pump (Agilent Technologies) to the source region (with an Edwards SP16K connected to the front pumping line), while the original Tri-scroll 800 pump is connected to the Q-TOF region. This configuration stabilizes the drift tube pressure. For nitrogen and helium measurements, the pressure in the drift tube was 3.89 ± 0.01 Torr for helium and 3.65 ± 0.01 Torr for nitrogen. The actual pressure can vary and the results would not change, but the pressure differential between the drift tube and the trapping funnel must always be at least 0.19 Torr.

All the data obtained were analyzed by using the IM-MS Browser software version B.06.01 (Agilent Technologies) that measures the centroid arrival time of a selected peak as a function of the drift voltage and then performs all calculations with the equations mentioned above. The automatic calculations were checked by manually integrating the peaks using PeakFit v4.11 (Systat Softwares, San Jose, CA).

3 Diffusion-ordered spectroscopy (DOSY)

3.1 Introduction

Given that most of chemical reactions take place in solution, to understand how these solutes, e.g., foldamer molecules, move in solution and to know the hydrodynamic parameters of solutes apparently become significant, according to which, one could obtain insight not only into the interpretation of the relative chemical reactions, but also into the acquirement of more pictures about physicochemical properties of these solutes themselves. Translational diffusion is one of the most frequent and momentous modes of molecular motions in solution. The information related to translational diffusion can provide us the detail of how the solutes move in solution. The corresponding translational diffusion coefficient D and the hydrodynamic radius of solute molecule R_h – which is calculated according to D value, give access to affording information about the detailed behavior of solutes in solution. To understand the translational diffusion and obtain values of D and R_h , diffusion ordered spectroscopy (DOSY) affords us a convenient approach.²⁶ Herein, in collaboration with Prof. Aldrik H. Velders at Wageningen University, Netherlands, DOSY was employed to determine the translational diffusion behavior of nanosized quinoline-based foldamers in solution, and further to explore the rigidity of these foldamers in solution.

In general, as solutes move in a homogenous solution without any chemical potential gradient, that is to say, the solution system stays in a dynamic equilibrium state, the movement of solutes is called as self-diffusion, a random translational diffusion. For solutes, such as ion, molecule or molecular cluster, when its initial position is at r_0 and after time t it moves to position r_t with self-diffusion, the probability $P(r_0, r_t, t)$ at position r_t could be expressed as:

$$P(r_0, r_t, t) = (4\pi Dt)^{-\frac{3}{2}} \exp\left(-\frac{(r_t - r_0)^2}{4Dt}\right) \quad (3.1)$$

where D is the self-diffusion coefficient.

Two main theories (known as Einstein-Smoluchowski theory and Kirkwood-Riseman theory) have been utilized for the calculation of the diffusion coefficient D . For macromolecules, based on the theoretical calculations, the former one could provide better results²⁷, and is presented

as:

$$D = \frac{k_b T}{f} = \frac{RT}{N_A f} \quad (3.2)$$

Where k_b is the Boltzmann constant, T is the absolute temperature, f is the hydrodynamic friction coefficient, R is the ideal gas constant: $R = k_b N_A$ and N_A is the Avogadro's number ($6.02 \times 10^{23} \text{ mol}^{-1}$). As the solute is in an isotropic homogenous medium of viscosity η with uniform velocity, f is given by Stokes as:

$$f = 6\pi\eta R_h \quad (3.3)$$

Where R_h is the hydrodynamic radius of the solute. Combination of equations (3.2) and (3.3) yields the well-known Stokes-Einstein equation:

$$D = \frac{k_b T}{6\pi\eta R_h} \quad (3.4)$$

It must be noted that the shape of the solute fitting for this equation is just sphere, and the size of this spherical solute must be much larger than that of solvent. For the solute that is not spherical and the size of which is comparable or a little larger than that of solvent, the correction factors should be introduced to make sure the diffusion coefficient is adequately close to the real one. The corrected Stokes-Einstein equation is presented as^{26c}:

$$D = \frac{k_b T}{c(R_{sov}, R_h) f(a, b) 6\pi\eta R_h} \quad (3.5)$$

Where $c(R_{sov}, R_h)$ is a function of R_{sov}/R_h , and $f(a, b)$ is related to the semimajor and semiminor for the prolate (American football-like, semimajor: a ; semiminor: b) or oblate (pumpkin-like, semimajor: b ; semiminor: a) ellipsoid molecules. $c(r_{sov}, r_h)$ is expressed by Chen as²⁸:

$$c(R_{sov}, R_h) = 6 \left(1 + 0.695 \left(\frac{R_{sov}}{R_h}\right)^{2.234}\right)^{-1} \quad (3.6)$$

Depending on the geometries (i.e. prolate or oblate), $f(a, b)$ could be expressed as different equations. For the prolate ellipse, it is given as^{26c, 29}:

$$f(a, b) = \frac{\sqrt{1 - \left(\frac{b}{a}\right)^2}}{\left(\frac{b}{a}\right)^{\frac{2}{3}} \ln \frac{1 + \sqrt{1 - \left(\frac{b}{a}\right)^2}}{\frac{b}{a}}} \quad (3.7)$$

For the oblate ellipsoid, it is expressed as^{26c, 29}:

$$f(a, b) = \frac{\sqrt{\left(\frac{b}{a}\right)^2 - 1}}{\left(\frac{b}{a}\right)^{\frac{2}{3}} \arctan \sqrt{\left(\frac{b}{a}\right)^2 - 1}} \quad (3.8)$$

When the magnetic field gradients are applied to a solution containing the solute(s) that need(s) to be measured, the positions of NMR-active nuclei contained by solute(s) can be labelled by

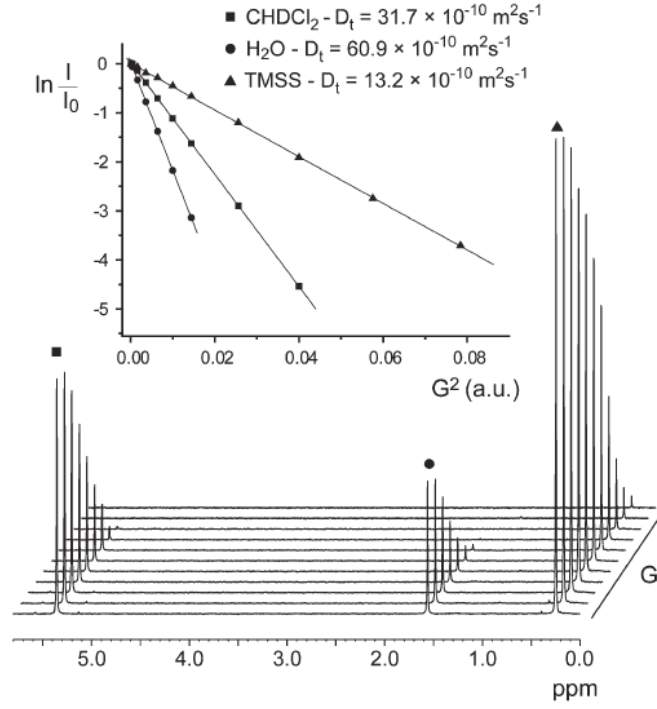


Figure 11 The signal decays that depend on G and trends of $\ln I_{(2\tau, G)}/I_{(2\tau, 0)}$ versus x (here the variable parameter is G) for a solution tetrakis(trimethylsilyl)silane (TMSS) and water in CD_2Cl_2 .

Larmor frequency. By recording the shift of position, D can be obtained. The most common and convenient method to acquire D is the pulsed gradient spin echo NMR technology. As this external gradient of magnetic field is applied, the signal intensity of an individual self-diffusion solute can be given as:

$$\begin{aligned} I_{(2\tau, G)} &= I_{(0,0)} \exp\left(\frac{-2\tau}{T_2}\right) \exp\left(-\gamma^2 G^2 \delta^2 \left(\Delta - \frac{\delta}{3}\right) D\right) \\ &= I_{(2\tau,0)} \exp\left(-\gamma^2 G^2 \delta^2 \left(\Delta - \frac{\delta}{3}\right) D\right) \end{aligned} \quad (3.9)$$

where $I_{(0,0)}$ and $I_{(2\tau,0)}$ are the signal and echo intensity which is observed immediately after the first pulse and at time 2τ , respectively; γ is gyromagnetic ratio, G is magnetic field gradient, δ is the duration of a pulse and Δ is the time interval between two pulsed gradients. In general,

$(\Delta - \delta/3)$ is referred as the diffusion time. Equation (9) also can be described as:

$$\ln \frac{I_{(2\tau, G)}}{I_{(2\tau, 0)}} = -\gamma^2 G^2 \delta^2 \left(\Delta - \frac{\delta}{3} \right) D = -x D \quad (3.10)$$

Here, the term $\gamma^2 G^2 \delta^2 (\Delta - \delta/3)$ is shortened as x . So diffusion coefficient D could be obtained by ratio of $\ln I_{(2\tau, G)}/I_{(2\tau, 0)}$ and x . The absolute value of the slope of the diagram between $\ln I_{(2\tau, G)}/I_{(2\tau, 0)}$ and x is equal to D . Examples are shown in Figure 11, the value of D of a solute is easily obtained by calculating the corresponding slope. As also shown in Figure 11, the smaller the solute molecule is, the larger the related D value would be.

As known from equation (3.5), the diffusion coefficient D depends on the effective size, shape and molecular weight of the target solute. Once the D is obtained from DOSY, it can be used to probe the intermolecular interactions, molecular size and aggregation of solute(s).^{26b, 26c} The dimensions of a series of helical, metal-coordinated compounds in solution, has already been provided by using DOSY, and the spectral separation of five components from a mixture of helical compounds was also reached by discriminating their diffusion coefficients (Figure 12).³⁰ The folding and aggregation behaviors of protein p53 has also been successfully analyzed with DOSY.³¹

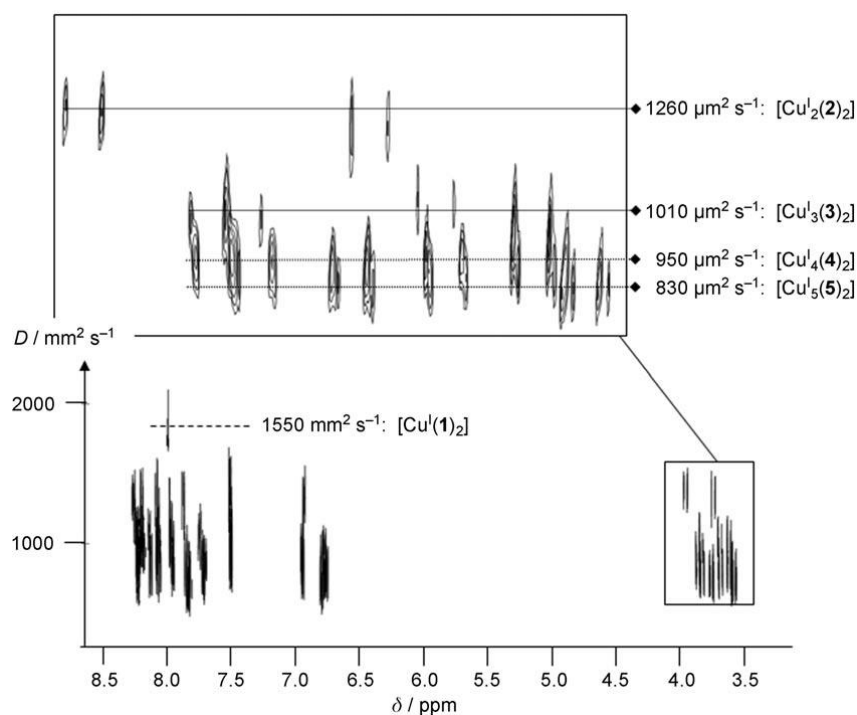


Figure 12 Spectral separation of five components from a mixture of helical compounds using DOSY technique.³⁰

3.2 Results and discussion

Aromatic amide foldamers containing 2, 4, 8, 16, 32 and 64 quinoline units^v have been studied by DOSY to explore their translational diffusion property in solution. A DOSY experiment of an equimolar mixture of the different foldamers has been carried out in CDCl₃ in order to visualize the spectral separation of these foldamers on the NMR spectra. The 1D ¹H NMR spectrum shows peaks that are difficult to identify, due to the overlapping of quinoline signals coming from different foldamers. Once the pulsed gradient spin echo NMR sequence is applied, this complex 1D-¹H NMR disintegrated into a 2D spectrum which shows a series of readable vertical stacking of spectra, due to the different diffusion coefficients *D*, stemming from the actual differences in the size of foldamers. The proton signals in the amide region, 9.3 ~ 12.4 ppm, are well separated, clearly discriminating the signals of all these 6 foldamers, thus allowing us to ‘spectrally’ distinguish the structure-analogous foldamers present in the mixture. It is noteworthy, that this separation has been carried out just by using diffusion coefficients *D* stemming from DOSY experiments (Figure 13).

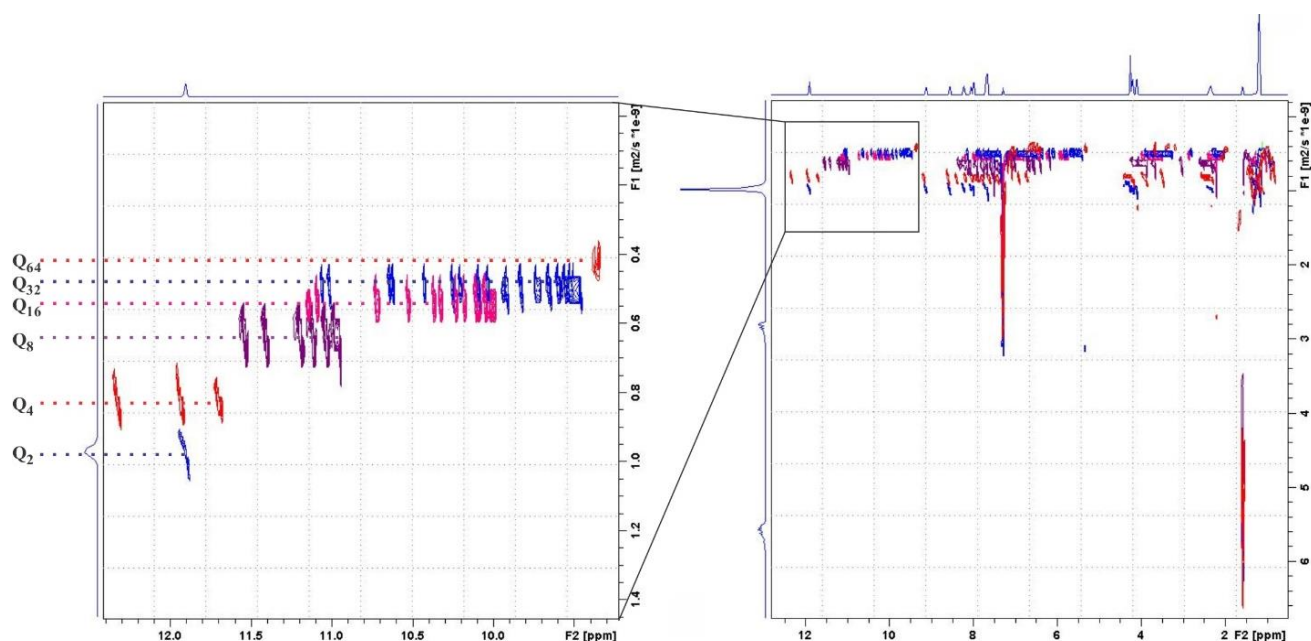


Figure 13 The DOSY spectrum of the mixture of foldamers, containing 2, 4, 8, 16, 32 and 64 units (right) and the corresponding amide region (left).

^v Synthesis of these foldamers is available in Chapter II.

The resulting translational diffusion coefficients D of foldamers have been collected and shown in Table 2. Values of D decrease from 1070 to 339 $\mu\text{m}^2/\text{s}$ with the incremental length of foldamers from 2mer to 64mer (Figure 14a). This experimental results match well with the theoretical prediction.^{26b} Interestingly, by plotting D over the reciprocal cubic root of the molecular weight of foldamer, a linear dependence can be observed (Figure 14b) which shows that there is a linear relationship between D and the reciprocal cubic root of the number of

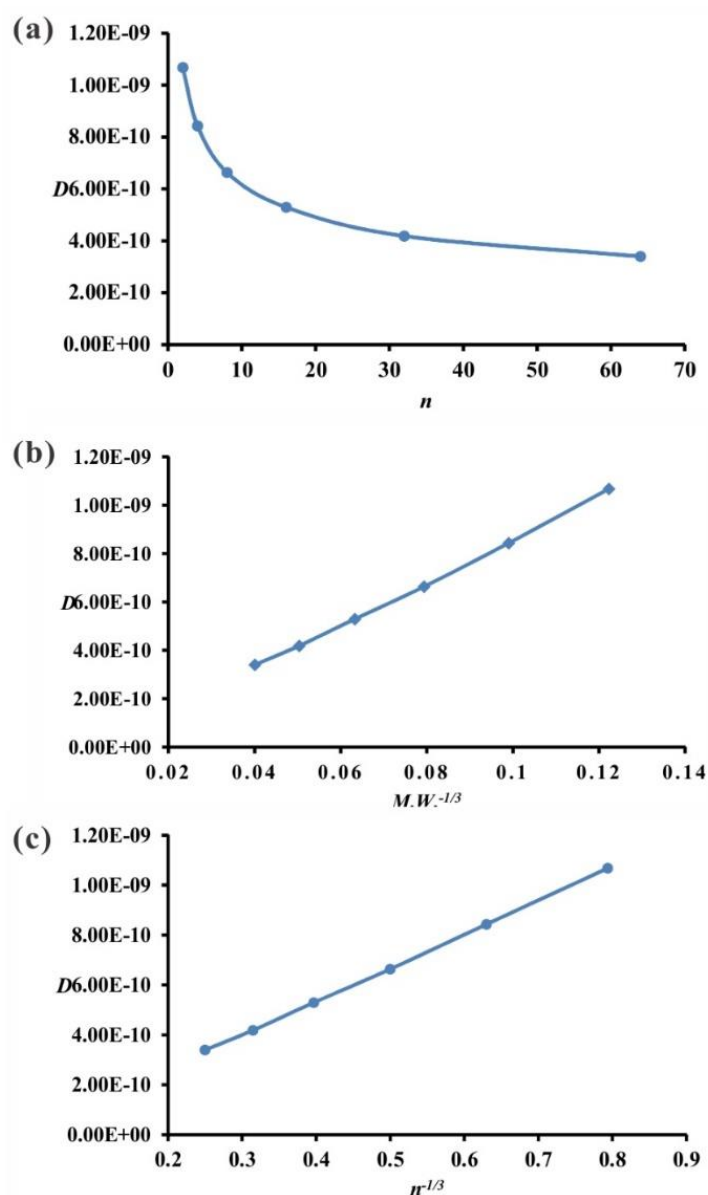


Figure 14 Plots of diffusion coefficients D obtained from DOSY experiments and the number of quinoline units in foldamer sequences (n) (a), and the linear relationships between D and the reciprocal cubic root of molecular weight of foldamer ($M.W.^{-1/3}$) (b), and between D and the reciprocal cubic root of the number of quinoline units in foldamer sequences ($n^{-1/3}$) (c).

quinoline units in foldamer sequences (Figure 14c). These two linear relationships are interesting, and I am going to explain the former one firstly here, and will present the reasons for the later after the discussion of hydrodynamic radius R_h (see the derivation of equation 3.17). Since the partial specific volume (v) of a molecule in solution is given as:

$$v = \frac{4N_A}{3M} \pi R_h^3 \quad (3.11)$$

where N_A is the Avogadro's number, M is the molecular weight of target molecule and R_h is the hydrodynamic radius. Combination of this equation with equation (3.5) can give an equation as:

$$D = \frac{k_b T N_A^{\frac{1}{3}}}{2^{\frac{1}{3}} 3^{\frac{4}{3}} c(R_{sov}, R_h) f(a, b) \eta \pi^{\frac{2}{3}} v^{\frac{1}{3}}} \times M^{-\frac{1}{3}} \quad (3.12)$$

For the certain molecules, foldamer molecules, all of them are much larger in size than solvent molecule, CDCl_3 . So $c(R_{sov}, R_h) \approx 1$. Meanwhile, as the molecule is certain, the value of $f(a, b)$ is also invariable. So, according to equation (3.12), one can see that D shows a linear relationship with $M^{-\frac{1}{3}}$, which has been revealed by the experimental results (Figure 14b).

Table 2 The related information of quinoline-based foldamers: the number of quinoline unit (n), the cubic root of the number of quinoline unit ($n^{1/3}$), the cubic root of molecule weight ($M.W.^{1/3}$), the translational diffusion coefficients (D) from DOSY experiments, parameters a and b , the related correction factor $f(a, b)$ and the resulting hydrodynamic radii (R_h).

Foldamer	2mer	4mer	8mer	16mer	32mer	64mer
n	2	4	8	16	32	64
$n^{1/3}$	1.2599	1.5874	2	2.5198	3.1748	4
$M.W.^{1/3}$	8.176	10.10	12.60	15.79	19.85	24.97
D ($\mu\text{m}^2/\text{s}$)	1070	843	663	529	418	339
a (\AA)*	1.525	3.05	6.10	12.2	24.4	48.8
b (\AA)*	9.65	9.65	9.65	9.65	9.65	9.65
$f(a, b)$	1.293	1.115	1.018	1.005	1.079	1.253
R_h (\AA)	3.02	4.44	6.17	7.84	9.23	9.80

* The values of a and b are based on the crystal parameters of 8mer. The diameter of 8mer crystal structure was set as $2b$, 19.3 \AA , and the height of 8mer was set as $2a$, 12.2 \AA .

The crystalline structure of 8mer and the energy-minimized structures of these quinoline-based foldamers^{vi} (i.e., 2mer, 4mer, 16mer, 32mer and 64mer) are shown in Figure 15. Taking these molecules as ellipsoidal models, their structures can present geometric conformations ranging

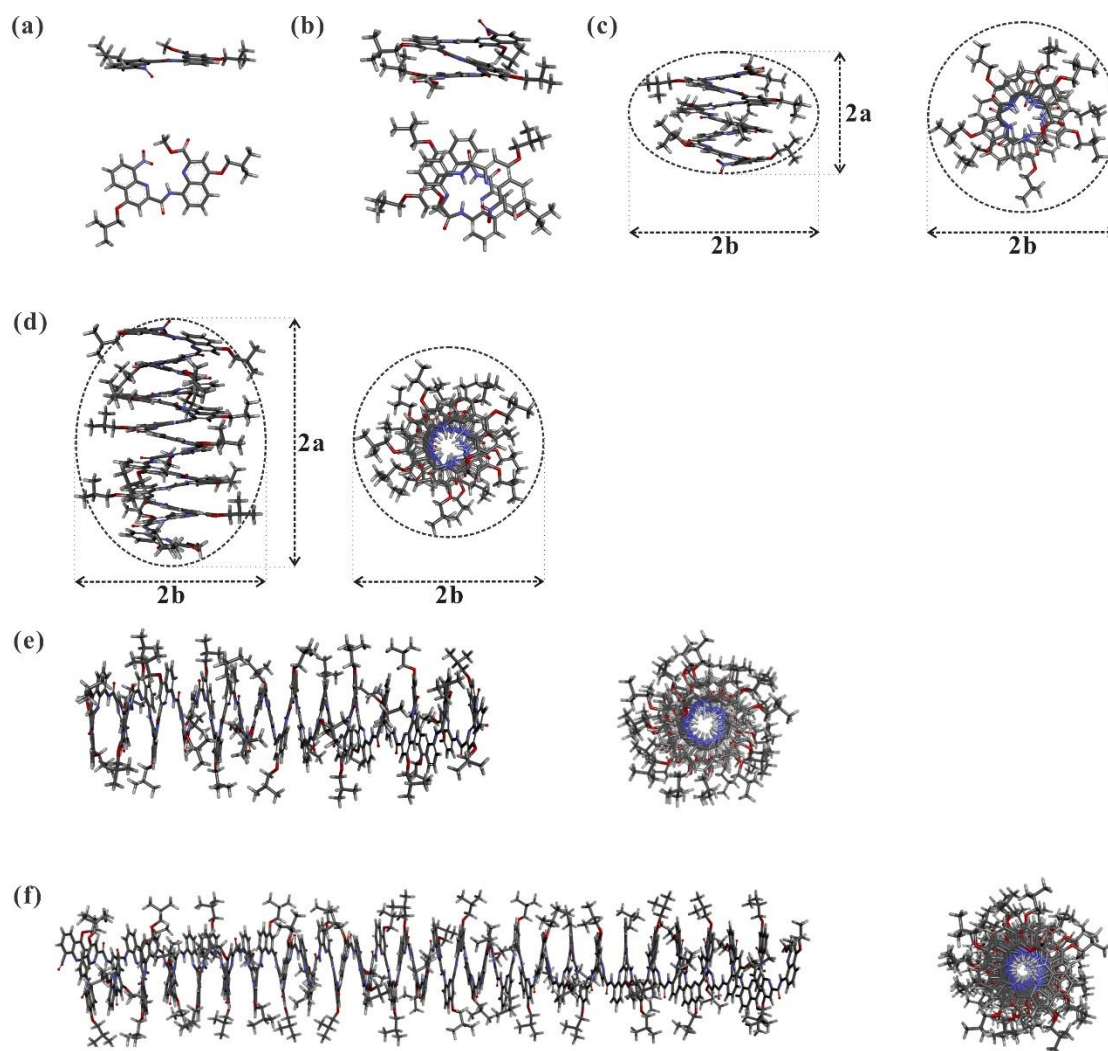


Figure 15 The energy-minimized conformations of quinoline-based foldamers: 2mer (a, top: side view; bottom: top view), 4mer (b, top: side view; bottom: top view), 16mer (d, left: side view; right: top view), 32mer (e, left: side view; right: top view) and 64mer (f, left: side view; right: top view). All the minimizations of these conformations are based on the parameters of crystallin structure of foldamer 8mer (f, left: side view; right: top view). 2mer, 4mer and 8mer were taken as oblate ellipsoids (c); 16mer, 32mer and 64mer as prolate ellipsoids (d).

from the oblate shape (pumpkin-like, 2mer, 4mer and 8mer) to the prolate profile (American

^{vi} These energy-minimized structures are calculated according to the crystalline structures of 8mer.

football-like, 16mer, 32mer and 64mer). Since geometries of molecules can affect the correction factor $f(a, b)$ (equations 3.7 and 3.8), the variable geometric conformation prevents me from using one uniform equation (equations 3.5, 3.7 and 3.8) to calculate the related

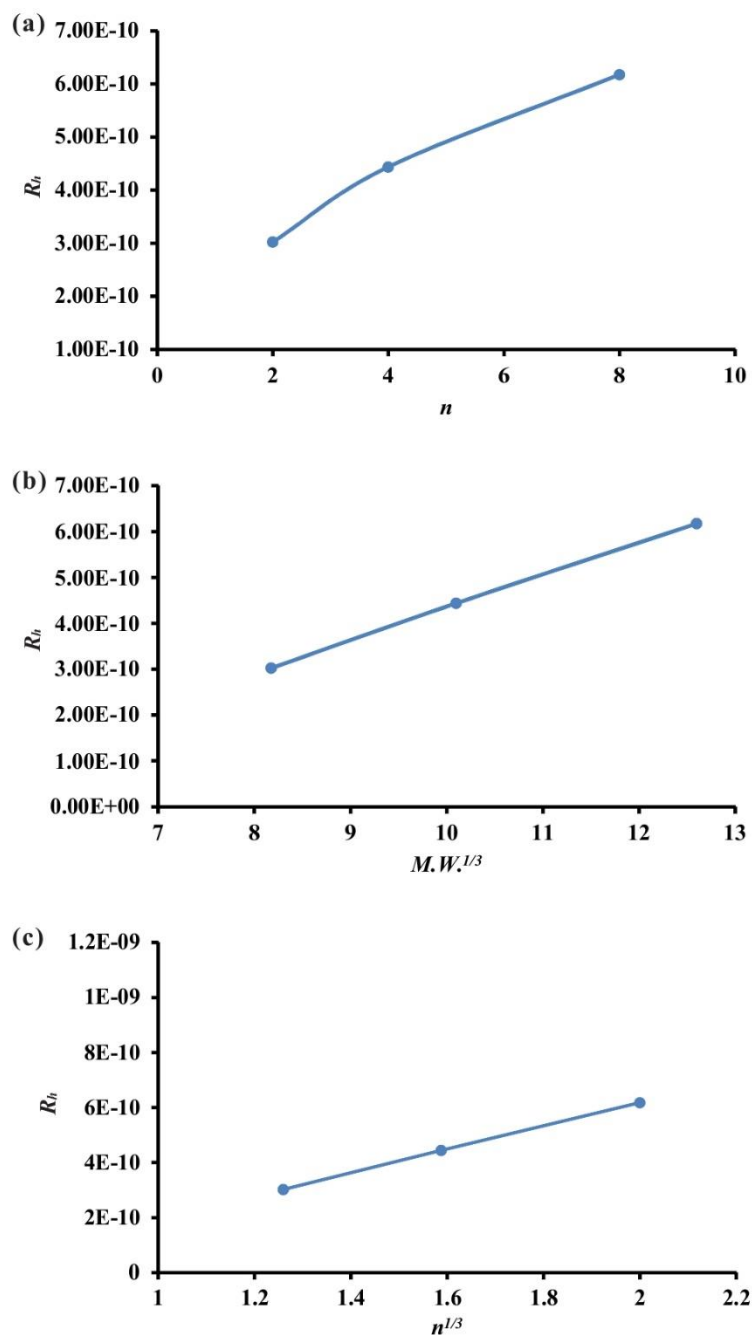


Figure 16 Evolution of hydrodynamic radii R_h of 2mer, 4mer and 8mer, generated from the oblate ellipsoid model, with the number of quinoline units n in foldamer sequences (a), the cubic root of molecular weight $M.W.^{1/3}$ (b) and the cubic root of the number of quinoline units (c) of foldamer molecules $n^{1/3}$.

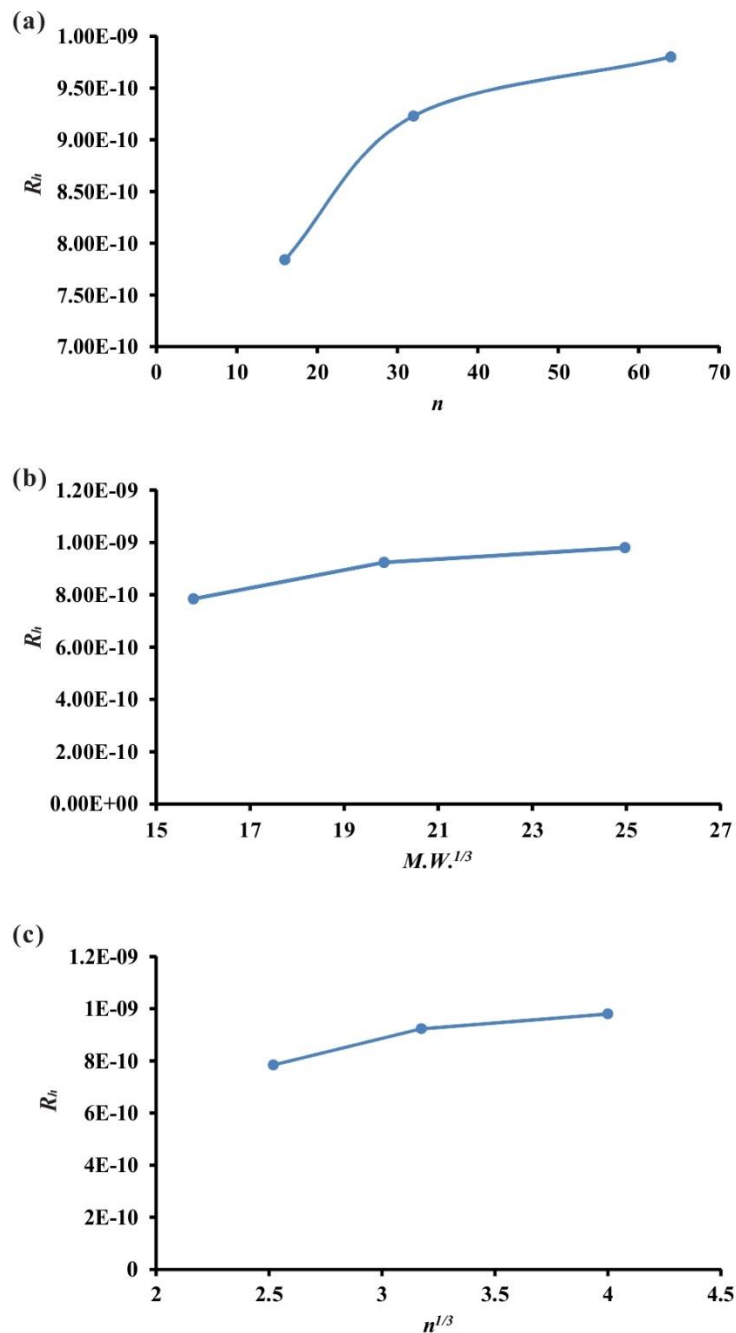


Figure 17 Evolution of hydrodynamic radii R_h of 16mer, 32mer and 64mer, generated from the oblate ellipsoid model, with the number of quinoline units n in foldamer sequences (a), the cubic root of molecular weight $M.W.^{1/3}$ (b) and the cubic root of the number of quinoline units (c) of foldamer molecules $n^{1/3}$.

hydrodynamic radii R_h . To solve this issue, these 6 foldamer molecules are categorized into two types by the geometry: the oblate type, including 2mer, 4mer and 8mer, and the prolate type, involving 16mer, 32mer and 64mer. For the former type, $f(a, b)$ would be calculated by equation (3.8); for the later, $f(a, b)$ would be equation (3.7). The related values of $f(a, b)$ have been

calculated and shown in Table 2. Based on the measured D , substitution of $f(a, b)$ into equation (3.5) permitted the calculation of the relative hydrodynamic radii R_h of foldamers^{vii} (Table 2). Given that the equations used for R_h calculation are two different ones, discussion of R_h would be split into two types in the following contents. For each type of these two calculations, the R_h value always rises up with the incremental length of foldamer molecules: from 3.02 to 6.17 Å with 2mer to 8mer, and from 7.84 to 9.80 Å with 16mer to 64mer (Figure 16a and 17a). The cubic root dependence of hydrodynamic radius (R_h) on molecular weight (M.W.) is found, which can be explained by equation (3.11) (Figure 16b and 17b). Meanwhile, a linear relationship between R_h and the cubic root of the number of quinoline units in foldamer sequence (n) was also established (Figure 16c and 17c). Actually, considering the structure of quinoline-based foldamers (tightly compact with an ignorable inner cavity), the size of foldamer molecules increases with the addition of quinoline unit. Herein, if the average volume of one quinoline unit in the foldameric sequences is set as c , the overall volumes of a foldamer molecule containing n quinoline units can be expressed as nc , namely:

$$v = nc \quad (n = 2, 4, 8, 16, 32, \text{ and } 64) \quad (3.13)$$

According to equation (3.11), substitution of equation (3.13) into equation (3.11) gives:

$$nc = \frac{4N_A}{3M} \pi R_h^3 \quad (3.14)$$

which can be derived as:

$$R_h = \left(\frac{3Mc}{4\pi N_A} \right)^{\frac{1}{3}} \times n^{\frac{1}{3}}$$

$$R_h \propto n^{\frac{1}{3}} \quad (3.15)$$

Equation (3.15) clearly gives the linear proportion between R_h and the cubic root of n , and demonstrates the experimental results (Figure 16c and 17c).

The relationship between D and R_h in equation (3.5) can be expressed as

$$D \propto \frac{1}{R_h} \quad (3.16)$$

Based on equation (3.15) and (3.16), a relationship between D and n can be derived as:

$$D \propto n^{-\frac{1}{3}} \quad (3.17)$$

^{vii} $k_b = 1.38 \times 10^{-23} \text{ m}^2 \text{ kg s}^{-2} \text{ K}^{-1}$, $T = 300 \text{ K}$, $\pi = 3.1415926$, $\eta = 5.27 \times 10^{-4} \text{ Pa.s}$.

This equation is able to exactly explain the experimental results mentioned before that translational diffusion coefficient D is linearly proportional to the reciprocal cubic root of the number of quinoline units in foldamer sequence n (Figure 14c).

3.3 Conclusion

DOSY NMR has been employed to resolve a mixture of different quinoline-based foldamers based on their diffusion coefficients, depending on their size and shape in solution. The related DOSY results enabled the ‘spectral’ separation of a series of foldamers, the structures of which are similar, offering a potential method to analyze different compounds with analogous structures but diverse diffusion coefficients. As the number of quinoline monomers increases, their diffusion coefficients decrease. The linear dependences of diffusion coefficients on the reciprocal cubic root of molecular weight and on that of the number of quinoline unit in foldamer sequence have been revealed. The resulting hydrodynamic radii of these foldamers generally increase with the incremental number of monomers in foldamer sequences. Even though the correction factors are different due to the geometries of the foldamers, the resulting hydrodynamic radii display a linear relationship with their corresponding cubic root of molecular weight and with that of the number of quinoline unit in foldamer sequence. All these experimental results about diffusion coefficient and hydrodynamic radius have been explained by the theoretical derivation.

3.4 Experimental section

All the foldamers are synthesized as described in Chapter II.

All the NMR experiments are carried out in CDCl_3 and are acquired exponentially in 128 increments, 32 scans, d_2 0.05 s and p_3 1700.0 μs , 300K on a Bruker NMR spectrometer.

4 Fluorescence anisotropy spectroscopy

4.1 Introduction

DOSY NMR experiment of quinoline-based foldamers has given access to the insight of the translational diffusion of foldamers in solution. However, whether these foldamers can diffuse rotationally in solution or not still keeps unknown.

If a molecule is able to emit fluorescence, its rotational motion in solution can be measured by the depolarization of fluorescence emission, which is the most common investigation of fluorescence anisotropy. Herein, another technique, fluorescence anisotropy spectroscopy, would be employed to attempt to explore the rotational diffusion of quinoline-based foldamers in solution, in cooperation with Prof. Jean Duhamel at University of Waterloo, Canada.

As light emitted by a fluorophore displays different intensities along diverse axes of polarization, this fluorophore is stated to own a property of fluorescence anisotropy. Fluorescence of a molecule possesses two vector components: absorption transition moment that is parallel to the electric field of the incident excitation light, and emission transition moment which may, or may not be aligned parallel to the absorption transition moment, both of which depend on how the electrons are excited, namely the structure of fluorescent molecule itself. Anisotropy can be defined as:³²

$$R = \frac{(I_{\parallel} - GI_{\perp})}{I_{\parallel} + 2GI_{\perp}} \quad (4.1)$$

where I_{\parallel} and I_{\perp} are the emission intensities of fluorescent molecules parallel and perpendicular to the electric field of the excitation light, respectively, G is the correction factor for any intensity bias from the instrument, such as the lenses and the monochromator grating. Measuring R along time provides a direct information of dynamics of fluorescence decay process that reveals the time-dependent depolarization of fluorescent molecules. Anisotropy of this time-resolved fluorescence measurement could be expressed as:³²

$$R(t) = \frac{(I_{\parallel}(t) - GI_{\perp}(t))}{I_{\parallel}(t) + 2GI_{\perp}(t)} \quad (4.2)$$

According to this equation, anisotropy is a function of time, and at a certain time t , the corresponding anisotropy $R(t)$ can be obtained by measuring the related emission intensities at

this certain time. For the time-resolved fluorescence measurement, the duration of depolarization process of molecule should be similar to the lifetime of emission of fluorophore. Otherwise, if the duration of depolarization process is significantly larger than that of emission of fluorophore, the depolarization process would fail to be recorded after the emission of fluorophore is done.

For the rotational diffusion of fluorescent molecules, as the molecules exhibits as the spherical shape, $R(t)$ decays exponentially with time and is given as:³³

$$R(t) = r_0 \exp\left(-\frac{t}{\tau_{rot}}\right) = r_0 \exp(-6Dt) \quad (4.3)$$

where r_0 is intrinsic anisotropy, τ_{rot} is the rotational correlation time that is the time the anisotropy decreases to 1/e of its initial value because of the molecular rotation, D is the rotational diffusion coefficient, and r_0 is the fundamental anisotropy, related to the angle β between absorption transition moment and emission transition moment:³²

$$r_0 = 0.4 \times \frac{3\cos^2\beta - 1}{2} \quad (4.4)$$

So, the range of anisotropy of a fluorophore can be generally calculated as: -0.2 ~ 0.4, based on equation (4.4). If a measured anisotropy data is beyond this range, it must be wrong or influenced significantly by the instrument. Equation (4.3) can be expressed alternatively as:

$$\ln \frac{R(t)}{r_0} = -\frac{1}{\tau_{rot}} \cdot t \quad (4.5)$$

Plot of $\ln \frac{R(t)}{r_0}$ is linearly proportional to t , and the absolute value of reciprocal of the slope gives the rotational correlation time τ_{rot} . According to τ_{rot} , one can estimate the rotational motion of a fluorescent molecule.

Generally, the anisotropy decay of fluorescent molecule is influenced by its local surroundings, such as viscosity, PH value, ion concentration and so forth. Meanwhile, in most cases, the fluorophores that undergo anisotropic rotations in solution are asymmetrical. If the asymmetrical fluorophore is influenced by more than one situation of its local surroundings, the anisotropy decay would not exhibits as exponential. Instead, the multi-exponential decay of fluorescence would be expected:³⁴

$$r(t) = r_0 \sum_j g_j \exp\left(-\frac{t}{\tau_{rot_j}}\right) = \sum_j r_{0_j} \exp\left(-\frac{t}{\tau_{rot_j}}\right) \quad (4.6)$$

where g_j is the fractional amplitudes of each rotational correlation time in the process of fluorescence anisotropy decay, and $\sum g_j = 1$. r_0 is the intrinsic anisotropy of molecule and $r_0 = \sum r_{0j}$.

In this case, the correlation times are determined by the rates of rotation along the various molecular axes. In particular case of prolate and oblate ellipsoids, the anisotropy decay can be expressed as:³⁵

$$r(t) = a_1 \exp(6D_2t) + a_2 \exp[-(D_1 + 5D_2)t] + a_3 \exp[-(4D_1 + 2D_2)t] \quad (4.7)$$

where D_1 and D_2 are the rotation diffusion coefficients around axis of symmetry plane and equatorial axis, respectively. The pre-exponential factors a_n ($n = 1, 2$ and 3) are given as:

$$a_1 = 0.1(3\cos^2\theta_1 - 1)(3\cos^2\theta_2 - 1) \quad (4.8)$$

$$a_2 = 0.3\sin 2\theta_1 \sin 2\theta_2 \cos \phi \quad (4.9)$$

$$a_3 = 0.3 \sin^2\theta_1 \sin^2\theta_2 (\cos^2\phi - \sin^2\phi) \quad (4.10)$$

where θ_1 and θ_2 are the angles between the absorption transition moment and the emission transition moment, respectively, and the axis of symmetry plane. ϕ is the angle between the projections of these two moments in the plane that is vertical to the axis of symmetry plane.

Herein, a series of quinoline-based foldamers has been functionalized by with a fluorophore group (perylene bisimide) and a rigid aromatic amine was used to link the foldamers and fluorophore group to make sure the orientation of this fluorophore perpendicular to the axes of foldameric helices. These functionalized foldamers were characterized with steady-state and time-resolved nanosecond-scale fluorescence anisotropy spectrometer, attempting to investigate their rotational diffusion in solution, in cooperation with Prof. Jean Duhamel at University of Waterloo, Canada.

4.2 Results and discussion

Quinoline-based foldamers, 2mer, 8mer, 16mer and 32mer were employed in this study. After saponification, the acids of these foldamers were activated into acid chloride that then coupled with a perylene monoamine, forming the desired products (PB-Q_n, $n = 2, 8, 16$ and 32 ; Figure 18). Considering that the nitro group in foldamer sequence could quench partially the

fluorescence, I a compound terminated with Boc protected amino group (PB-Q₈-NH-Boc) was also synthesized as a reference compound of PB-Q₈-NO₂ (abbreviated as PB-Q₈ in the coming context) to see whether we can obtain better results: sensitivity and intensity (Figure 18c). A model molecule, *N,N'* Bis(3-pentyl)perylene bisimide (C₅₂-PB), was also introduced as reference (Figure 18b).

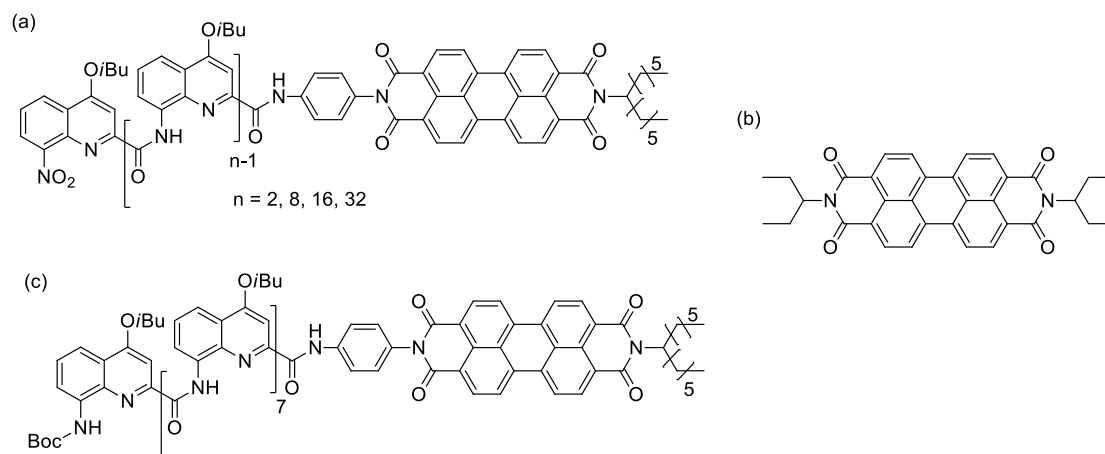


Figure 18 The chemical structures of foldamers functionalized by perylene bisimide (a), the reference compounds Boc-NH-8mer (b) and C₅₂-PB (c), and their corresponding representative HNMR of NH region (CDCl₃, 300 MHz) of functionalized foldamers (d).

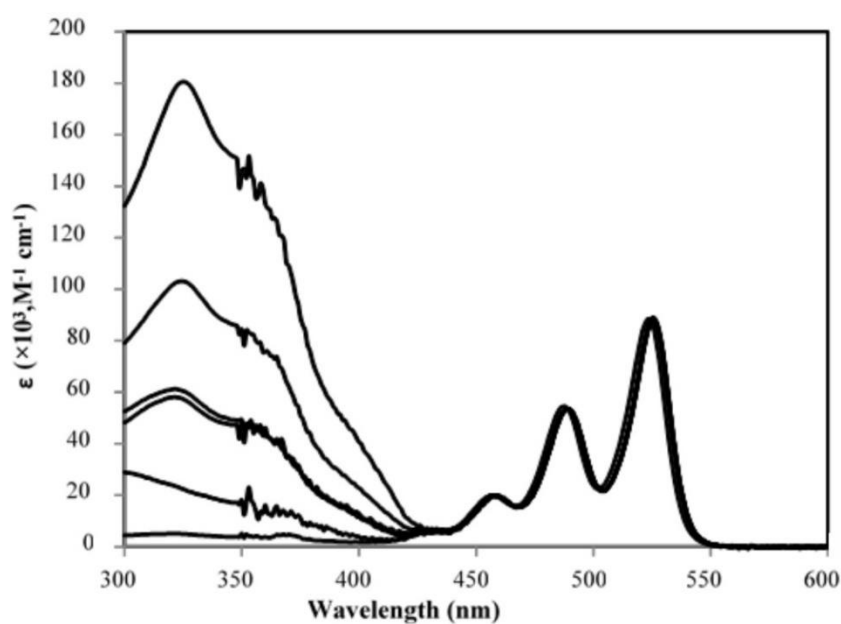


Figure 19 Molar extinction coefficient of perylene-labeled foldamers in DCM normalized by concentration. From bottom to top: C₅₂-PB, PB-Q₂, PB-Q₈ \approx PB-Q₈-NH-Boc, PB-Q₁₆, and PB-Q₃₂.

These molecules were also characterized using UV/Vis absorbance spectroscopy in dichloromethane (DCM). Their spectra were converted into molar extinction coefficient spectra by normalizing the perylene peak at 488 nm to a value of $5.36 \times 10^3 \text{ M}^{-1}\text{cm}^{-1}$ which is obtained from reference compound C5₂-PB in DCM, as shown in Figure 19. A good overlap of the perylene region between the functionalized foldamers and the reference compound C5₂-PB appeared, demonstrating the successful label of foldamers with perylene bisimide. In the quinoline region, all the peaks of all functionalized foldamers presented around 325 nm and their absorbance intensities increased with proportionally to the number of quinoline units in foldamers which indicate the successful labeling of these compounds.

The steady increase in absorbance at 325 nm made it possible to calculate the molar extinction coefficient of quinoline unit in foldamer sequence $\epsilon(\text{PB} - Q_n)$. The molar extinction coefficient at 325 nm of each functionalized foldamer was plotted as a function of the number of quinoline units. Given that perylene and quinoline can absorb light of 325 nm, the ideal molar extinction coefficient of quinoline unit in foldamer sequence $\epsilon(\text{PB} - Q_n)$ can be given as:

$$\epsilon(\text{PB} - Q_n) = \epsilon(\text{C5}_2 - \text{PB}) + n \cdot \epsilon(\text{Q}) \quad (4.6)$$

where $\epsilon(\text{C5}_2 - \text{PB})$ and $\epsilon(\text{Q})$ are the molar extinction coefficients at 325 nm of C5₂-PB and quinoline monomer, respectively.

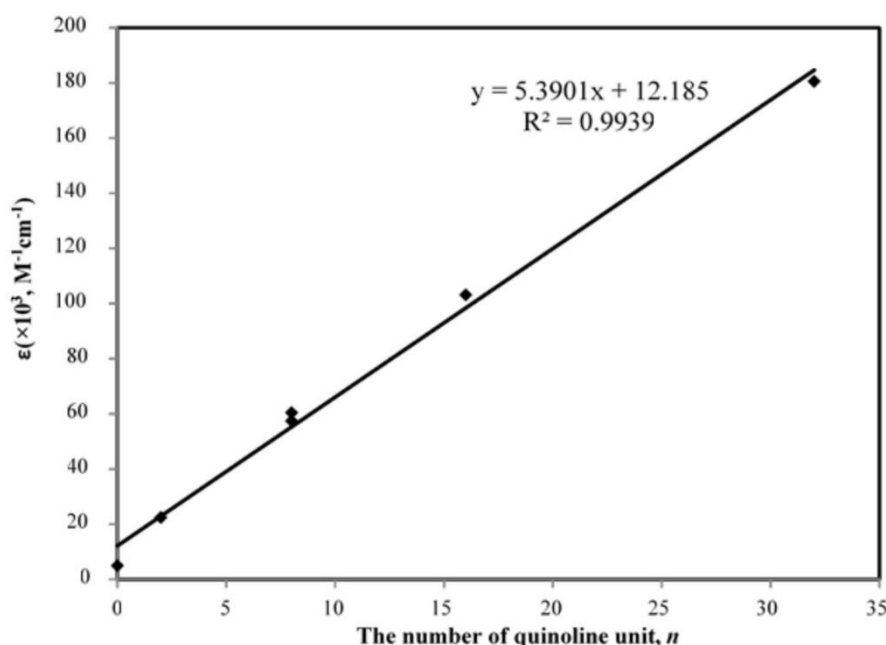


Figure 20 Molar Extinction coefficient determination for polymerized quinoline groups.

Within experimental error, a straight line was obtained in Figure 20. The slope of the line was equal to $5.4 \times 10^3 \text{ M}^{-1}\text{cm}^{-1}$, which was taken as the extinction coefficient of quinoline unit in foldamer sequence. This confirms that the stacked quinoline units absorb light identically regardless of how long the foldamer chain is.

Table 3 Steady-state anisotropy r , lifetimes τ obtained from unpolarized fluorescence decays and the resulting rotation correlation time τ_{rot} of the perylene-functionalized foldamers and the reference compound C5₂-PB.

Sample	r (DCM)	r (BzOH)	r (Toluene)	τ (BzOH, ns)	τ (Toluene, ns)	τ_{rot} (BzOH, ns)	τ_{rot} (Toluene, ns)
PB-Q ₂	0.278	0.335	0.256	0.579	0.312	5.54	0.850
PB-Q ₈	0.313	0.355	0.252	0.319	0.318	7.55	0.818
PB-Q ₁₆	0.286	0.353	0.260	0.273	0.381	5.67	1.10
PB-Q ₃₂	0.299	0.351	0.300	0.272	0.373	5.02	2.24
C5 ₂ -PB		0.085	-0.017	3.52	5.05	1.05	-0.234

The anisotropy behavior of these perylene-functionalized foldamers was firstly determined by acquiring the polarized steady-state emission spectra. This determination was operated in DCM, benzyl alcohol (BzOH) and toluene, and the correction factor G was calculated for each sample

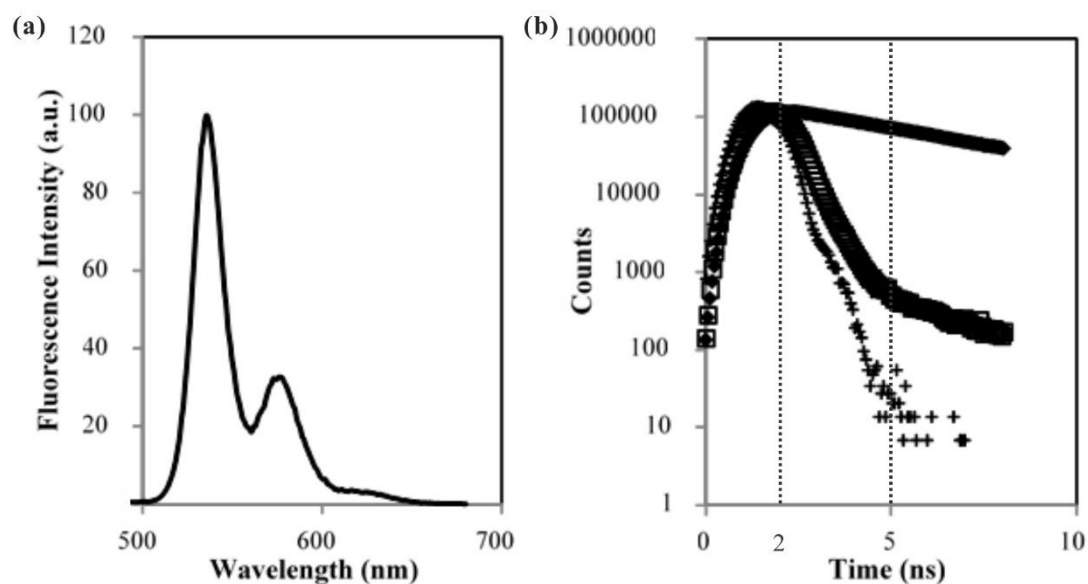


Figure 21 The Steady-state fluorescence spectrum of PB-Q₂ in toluene (a) and the polarized time-resolved fluorescence decays in toluene for C5₂-PB (◆), PB-Q₂ (□), and the instrument response function (IRF) (+) acquired with a light -scattering prompt (b). The dashed lines indicate the workable range for the analysis of the anisotropy decays

and just varied by 1.5% or less for all the sample in a given solvent. The values of steady-state anisotropy were then calculated, as shown in Table 3. Compared to the reference compound C5₂-PB, low steady-state emission intensity was observed (see the example, Figure 21a, the one of PB-Q₂), with relative quenching of the fluorescence intensity amounting to approximately 95%.

As shown in Table 3, only small differences of anisotropy values are observed for all the molecules in these three solvents. In toluene, a slight increase in anisotropy with incremental length of foldamers could be detected. However, the change is very small and in the error margin of the measurements. All samples PB-Q_n presented significantly higher anisotropy than the foldamer-free reference compound C5₂-PB, and partially this is related with the quenching of the fluorophore according to the equation above. Assuming an instant anisotropy, r_0 , around 0.35 in toluene and 0.37 in BzOH (see Figure 22 for anisotropy decays value at time zero) the rotational correlation times can be estimated by rearranging equation above:

$$\tau_{rot} = \frac{\tau r}{r_0 - r}$$

And the values are shown in Table 3. The estimated τ_{rot} values are around 6 ns in BzOH, and around 1 ns in toluene, which produces a ratio slightly lower than the ratio of viscosities (5.474 cP and 0.5867 cP for BZOH and toluene respectively). It means that in the more viscous solvent the molecule is not filling the full effect of viscosity, i.e., the solvent molecules are slow to fill the voids created by molecular movement and in consequence the molecule experience a lower average viscosity. Interestingly, the rotational correlation times do not scale up with the incremental length of the foldamers, which probably suggests that depolarization is achieved through rotation around the long axes of the foldamer. Since perylene is known to have the absorption and emission transition moments collinear (r_0 is around 0.4) and aligned with the long axis of the fluorophore, It is reasonable to assume that the perylene is in a conformation in which the long axis of foldameric helical structure is perpendicular to the long axis of fluorophore, perylene, (if the long axis of perylene was aligned with the foldamer long axis, rotation along this axis would not contribute to depolarization). Similar conclusions can be drawn from time resolved anisotropy.

To obtain better observation of anisotropy of foldamers, time-resolved fluorescence decays were

acquired for these perylene-functionalized foldamers. First, the unpolarised fluorescence decays were acquired. All the perylene-functionalized foldamers and the reference compound C5₂-PB displayed one dominant lifetime with a contribution of 95% or greater, and these lifetimes are listed in Table 3. Strong quenching of these perylene-functionalized foldamer was found by DCM, so fluorescence decays were not acquired in this solvent.

As shown in Table 3, the observed lifetimes of all compounds are in the approx. 300 ps range which approaches the resolution limit of the current instrument. The polarized fluorescence decays of the samples were acquired and the resulting anisotropy decays are shown in Figure 22. All fluorescence decays, like for PB-Q₂ in toluene presented in Figure 21b, showed a long decay which is parallel to that of the reference compound C5₂-PB. This long decay was attributed to a residual contribution (<5%) of unattached dye. Since the fluorescence decay departs from the instrument response function after ~ 2 ns and the long-lived species (the unattached dye) dominates the decay after ~5 ns, the useable range of the decays to determine the fluorescence anisotropy was between 2 and 5 ns (Figure 21b).

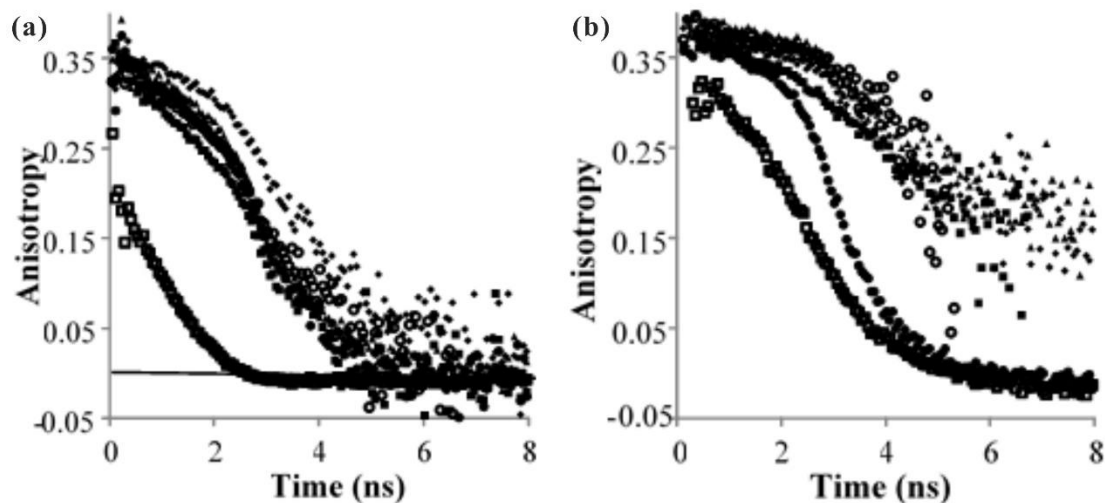


Figure 22 Fluorescence anisotropy decays in toluene (a) and BzOH (b) of (■) PB-Q₂, (●) PB-Q₈, (▲) PB-Q₁₆, (◆) PB-Q₃₂ (○), PB-Q₈-NH-Boc and (□) C5₂-PB.

The fluorescence anisotropy decays were calculated with equations (4.2). In contrast to the reference compound C5₂-PB that exhibited a significantly fast decay in toluene, these PB-Q_n samples showed longer anisotropy decays consistent with the increase in rotational correlation

times upon binding of the fluorophore to the foldamer. However, there is not a clear scaling up of the anisotropy decay times with the molecular size of the foldamer, in line with our previous analysis of the steady state anisotropy. In BzOH for the shortest foldamers, it is observed some dependence of size, but more notorious is that for the longer foldamers the anisotropy decay does not falls to zero at longer times, which could be related with the hindered rotation of a fraction of molecules in the more viscous solvent (Figure 22).

4.3 Conclusion

According to these preliminary results, the linear increase in UV absorbance with the number of unit contained in the foldamers allowed the determination of the molar extinction coefficient of quinoline unit in foldamer sequence, which was found as $5.4 \times 10^3 \text{ M}^{-1} \cdot \text{cm}^{-1}$. All these perylene-labeled foldamers showed measureable anisotropy in BzOH and toluene, revealing that the rotational diffusion of foldamers in solution took place. Further research is underway to attempt to obtain more insight into the rotational diffusion of quinoline-based helical foldamers.

4.4 Experimental section

4.4.1 Synthesis of perylene bisimide-functionalized foldamers (PB-Q_n)

The related reactions were operated under a dry nitrogen environment. Chemicals and reagents were used as commercially supplied without any further purification unless otherwise stated. Tetrahydrofuran (THF) and Toluene were dried over alumina columns under nitrogen. Chloroform and diisopropylethylamine (DIPEA) were distilled over calcium hydride (CaH₂) prior to use. Reactions were monitored by thin layer chromatography (TLC) on Merck silica gel 60-F254 plates and observed under UV light (254 and 365 nm). Column chromatography was carried out on Merck GEDURAN Si60 (40-63 μm). Analytical and semi-preparative GPC was carried out on Shimadzu Recycling GPC system equipped with LC-20 AD pump, SPD-M20A UV detector and a set of 1H, 1.5H, 2.5H and 3H columns (size: 20×600 mm) in chloroform/0.5~1% ethanol as eluent with a flow rate of 3.5 mL/min.

ESI mass spectra were obtained on a Waters LCT Premier and a Bruker Reflex III spectrometers respectively, from the Mass Spectrometry Laboratory at the European Institute of Chemistry and Biology (UMS 3033 - IECB), Pessac, France and a Voyager DE-STR mass spectrometer from AB Sciex, Les Ulis, France. NMR data were recorded at 300 MHz using an Avance II NMR spectrometer (Bruker Biospin) with a vertical 7.05T narrow-bore/ultrashield magnet operating at 300 MHz for ^1H observation and 75 MHz for ^{13}C observation by means of a 5-mm direct BBO H/X probe with Z gradient capabilities. All chemical shifts are quoted in parts per million (ppm, δ) relative to the ^1H residual signal of the deuterated solvent used (CDCl_3 at 7.26 ppm). ^1H NMR splitting patterns with observed first-order coupling are designated as singlet (s), doublet (d), double doublet (dd), triplet (t), or quartet (q). Splitting patterns that could not be interpreted or easily visualized are designated as multiplet (m) or broad (br). Coupling constants (J) are reported in hertz. Samples were not degassed. Data processing was performed with Topspin 2.0 software.

General methods to synthesize PB-Q_n

The perylene bisimide (PB) was synthesized by modifying the methods from literature and all the quinolined foldamers and their acids were prepared and described in Chapter 2.

The quinoline-based foldamers was activated by oxalyl chloride (5 equiv.) in chloroform for approx. 3 h. After removal of solvent and the remaining oxalyl chloride under vacuum, the product, acid chloride, was generated equivalently.

To the PB and DIPEA mixture in chloroform the solution of acid chloride in chloroform was added dropwise at 0 °C. The reaction was allowed to warm up to room temperature and processed overnight. After evaporating solvent, the reaction residue was refluxed in pyridine/water mixture (5:1, vol/vol) overnight. Then toluene was used to azeotrope the pyridine and water with rotary evaporator, and the resulting residue was purified by recycling GPC, yielding the product PB-Q_n.

4.4.2 Measurement with fluorescence anisotropy spectrometry

HPLC grade dichloromethane (DCM), benzyl alcohol (BzOH) and toluene were obtained from Sigma-Aldrich. BzOH and toluene were used as received, DCM was filtered through a basic alumina column before use.

The perylene-labeled PB-Q₂, PB-Q₈, PB-Q₁₆, PB-Q₃₂ and PB-Q₈-NH-Boc were used as received. *N,N'* Bis(3-pentyl)perylene bisimide (C₅₂-PB) was purchased from Sigma-Aldrich and used as received.

Absorbance measurements were obtained for serial dilutions of the model compound in DCM, BzOH, and toluene to determine the molar extinction coefficient of C₅₂-PB in each solvent. The absorbance spectra of the perylene-labeled foldamers were obtained in DCM.

Solutions for the fluorescence measurements were prepared by dissolving each sample in the solvent, diluting to an absorbance of 0.1 at the wavelength of excitation, and then degassing the sample by bubbling with nitrogen for at least 30 minutes. Samples in DCM and toluene were excited at 460 nm, while samples in BzOH were excited at 466 nm.

5 General conclusion

Three techniques, ion mobility spectrometry, diffusion ordered spectroscopy and fluorescence anisotropy spectroscopy, have been introduced to foldamer chemistry, attempting to assess the rigidity of quinoline-based foldamers in gas phase and to determine the translational and rotational diffusions in solution.

With IMS-MS, the only one CCS value of bromine-free, brominated foldamers reveals that there is only one conformation in gas phase for these foldamers, which further demonstrates the rigidity of helical structures of these quinoline-based foldamers. Interestingly, for the anhydride foldamers, we found out three CCS values for each this kind of foldamer in gas phase. This phenomenon is not discovered in solution and solid state and probably results from the existence of the flexible anhydride bond which can change its direction as the ambient steric hindrance decreases enough. More studies are needed for this series of foldamer by using other tools, like DOSY, HMBC and HNMR in varied solvents.

DOSY and fluorescence anisotropy results revealed that the quinoline-based foldamers can travel through solution with translational and rotational diffusions. DOSY also determined translational diffusion slows down with incremental length of foldamers. Fluorescence anisotropy spectroscopy suggests that the rotational diffusion can be affected by the viscosity of solvents: the rotational correlation time would drop down with the increasing viscosity of solvents. Based on these two techniques, some physicochemical parameters of foldamer are obtained as well, including the self-diffusion coefficient, the hydrodynamic radii of foldamers, the molar extinction coefficient of quinoline unit in foldamer sequence and the rotational correlation time.

6 Reference

- 1 (a) Gellman, S. H., Foldamers: a manifesto. *Accounts of Chemical Research* **1998**, *31* (4), 173-180;
(b) Hill, D. J.; Mio, M. J.; Prince, R. B.; Hughes, T. S.; Moore, J. S., A field guide to foldamers. *Chemical reviews* **2001**, *101* (12), 3893-4012; (c) Hecht, S.; Huc, I., *Foldamers: structure, properties and applications*. John Wiley & Sons: 2007; (d) Guichard, G.; Huc, I., Synthetic foldamers. *Chemical Communications* **2011**, *47* (21), 5933-5941.
- 2 Zhang, D.-W.; Zhao, X.; Hou, J.-L.; Li, Z.-T., Aromatic amide foldamers: structures, properties, and functions. *Chemical reviews* **2012**, *112* (10), 5271-5316.
- 3 Dolain, C.; Gr̄ard, A.; Laguerre, M.; Jiang, H.; Maurizot, V.; Huc, I., Solution Structure of Quinoline - and Pyridine - Derived Oligoamide Foldamers. *Chemistry-A European Journal* **2005**, *11* (21), 6135-6144.
- 4 Barchi, J. J.; Huang, X.; Appella, D. H.; Christianson, L. A.; Durell, S. R.; Gellman, S. H., Solution conformations of helix-forming β -amino acid homooligomers. *Journal of the American Chemical Society* **2000**, *122* (12), 2711-2718.
- 5 Nelson, J. C.; Saven, J. G.; Moore, J. S.; Wolynes, P. G., Solvophobic Driven Folding of Nonbiological Oligomers. *Science* **1997**, *277* (5333), 1793-1796.
- 6 Prince, R. B.; Barnes, S. A.; Moore, J. S., Foldamer-Based Molecular Recognition. *Journal of the American Chemical Society* **2000**, *122* (12), 2758-2762.
- 7 Prince, R. B.; Saven, J. G.; Wolynes, P. G.; Moore, J. S., Cooperative Conformational Transitions in Phenylene Ethynylene Oligomers: Chain-Length Dependence. *Journal of the American Chemical Society* **1999**, *121* (13), 3114-3121.
- 8 Brunsveld, L.; Meijer, E.; Prince, R. B.; Moore, J. S., Self-assembly of folded m-phenylene ethynylene oligomers into helical columns. *Journal of the American Chemical Society* **2001**, *123* (33), 7978-7984.
- 9 Matsuda, K.; Stone, M. T.; Moore, J. S., Helical Pitch of m-Phenylene Ethynylene Foldamers by Double Spin Labeling. *Journal of the American Chemical Society* **2002**, *124* (40), 11836-11837.
- 10 Hartley, C. S.; Elliott, E. L.; Moore, J. S., Covalent Assembly of Molecular Ladders. *Journal of the American Chemical Society* **2007**, *129* (15), 4512-4513.

-
- 11 Zhu, J.; Dong, Z.; Lei, S.; Cao, L.; Yang, B.; Li, W.; Zhang, Y.; Liu, J.; Shen, J., Design of Aromatic Helical Polymers for STM Visualization: Imaging of Single and Double Helices with a Pattern of π - π Stacking. *Angewandte Chemie* **2015**, *127* (10), 3140-3144.
- 12 Yashima, E.; Maeda, K.; Iida, H.; Furusho, Y.; Nagai, K., Helical Polymers: Synthesis, Structures, and Functions. *Chemical Reviews* **2009**, *109* (11), 6102-6211.
- 13 Longhi, G.; Abbate, S.; Lebon, F.; Castellucci, N.; Sabatino, P.; Tomasini, C., Conformational Studies of Phe-Rich Foldamers by VCD Spectroscopy and ab Initio Calculations. *The Journal of Organic Chemistry* **2012**, *77* (14), 6033-6042.
- 14 (a) D'Atri, V.; Porrini, M.; Rosu, F.; Gabelica, V., Linking molecular models with ion mobility experiments. Illustration with a rigid nucleic acid structure. *Journal of Mass Spectrometry* **2015**, *50* (5), 711-726; (b) Cumeras, R.; Figueras, E.; Davis, C. E.; Baumbach, J. I.; Gracia, I., Review on Ion Mobility Spectrometry. Part 1: current instrumentation. *Analyst* **2015**, *140* (5), 1376-1390.
- 15 Heck, A. J.; van den Heuvel, R. H., Investigation of intact protein complexes by mass spectrometry. *Mass spectrometry reviews* **2004**, *23* (5), 368-389.
- 16 McDaniel, E.; Martin, D.; Barnes, W., Drift tube - mass spectrometer for studies of low - energy ion - molecule reactions. *Review of Scientific Instruments* **1962**, *33* (1), 2-7.
- 17 Lanucara, F.; Holman, S. W.; Gray, C. J.; Evers, C. E., The power of ion mobility-mass spectrometry for structural characterization and the study of conformational dynamics. *Nat Chem* **2014**, *6* (4), 281-294.
- 18 Mason, E. A.; Schamp Jr, H. W., Mobility of gaseous ions in weak electric fields. *Annals of Physics* **1958**, *4* (3), 233-270.
- 19 Cumeras, R.; Figueras, E.; Davis, C. E.; Baumbach, J. I.; Gracia, I., Review on Ion Mobility Spectrometry. Part 2: hyphenated methods and effects of experimental parameters. *Analyst* **2015**, *140* (5), 1391-1410.
- 20 (a) Ruotolo, B. T.; Benesch, J. L.; Sandercock, A. M.; Hyung, S.-J.; Robinson, C. V., Ion mobility-mass spectrometry analysis of large protein complexes. *Nature Protocols* **2008**, *3* (7), 1139-1152; (b) Jurneczko, E.; Barran, P. E., How useful is ion mobility mass spectrometry for structural biology? The relationship between protein crystal structures and their collision cross sections in the gas phase. *Analyst* **2011**, *136* (1), 20-28.

-
- 21 (a) Li, X.; Chan, Y.-T.; Newkome, G. R.; Wesdemiotis, C., Gradient Tandem Mass Spectrometry Interfaced with Ion Mobility Separation for the Characterization of Supramolecular Architectures. *Analytical Chemistry* **2011**, *83* (4), 1284-1290; (b) Robbins, P. J.; Surman, A. J.; Thiel, J.; Long, D.-L.; Cronin, L., Use of ion-mobility mass spectrometry (IMS-MS) to map polyoxometalate Keplerate clusters and their supramolecular assemblies. *Chemical Communications* **2013**, *49* (19), 1909-1911.
- 22 Ujma, J.; De Cecco, M.; Chepelin, O.; Levene, H.; Moffat, C.; Pike, S. J.; Lusby, P. J.; Barran, P. E., Shapes of supramolecular cages by ion mobility mass spectrometry. *Chemical Communications* **2012**, *48* (37), 4423-4425.
- 23 Chan, Y.-T.; Li, X.; Soler, M.; Wang, J.-L.; Wesdemiotis, C.; Newkome, G. R., Self-Assembly and Traveling Wave Ion Mobility Mass Spectrometry Analysis of Hexacadmium Macrocycles. *Journal of the American Chemical Society* **2009**, *131* (45), 16395-16397.
- 24 Scarff, C. A.; Snelling, J. R.; Knust, M. M.; Wilkins, C. L.; Scrivens, J. H., New Structural Insights into Mechanically Interlocked Polymers Revealed by Ion Mobility Mass Spectrometry. *Journal of the American Chemical Society* **2012**, *134* (22), 9193-9198.
- 25 Jiang, H.; L'éger, J.-M.; Huc, I., Aromatic δ -Peptides. *Journal of the American Chemical Society* **2003**, *125* (12), 3448-3449.
- 26 (a) Johnson Jr, C. S., Diffusion ordered nuclear magnetic resonance spectroscopy: principles and applications. *Progress in Nuclear Magnetic Resonance Spectroscopy* **1999**, *34* (3-4), 203-256; (b) Cohen, Y.; Avram, L.; Frish, L., Diffusion NMR Spectroscopy in Supramolecular and Combinatorial Chemistry: An Old Parameter—New Insights. *Angewandte Chemie International Edition* **2005**, *44* (4), 520-554; (c) Macchioni, A.; Ciancaleoni, G.; Zuccaccia, C.; Zuccaccia, D., Determining accurate molecular sizes in solution through NMR diffusion spectroscopy. *Chemical Society Reviews* **2008**, *37* (3), 479-489.
- 27 Rodríguez Schmidt, R.; Hernández Cifre, J. G.; García de la Torre, J., Translational diffusion coefficients of macromolecules. *Eur. Phys. J. E* **2012**, *35* (12), 1-5.
- 28 Chen, H. C.; Chen, S. H., Diffusion of crown ethers in alcohols. *The Journal of Physical Chemistry* **1984**, *88* (21), 5118-5121.
- 29 Perrin, F., Mouvement Brownien d'un ellipsoïde (II). Rotation libre et dépolarisation des

-
- fluorescences. Translation et diffusion de molécules ellipsoïdales. *J. phys. radium* **1936**, 7 (1), 1-11.
- 30 Allouche, L.; Marquis, A.; Lehn, J.-M., Discrimination of Metallosupramolecular Architectures in Solution by Using Diffusion Ordered Spectroscopy (DOSY) Experiments: Double-Stranded Helicates of Different Lengths. *Chemistry – A European Journal* **2006**, 12 (28), 7520-7525.
- 31 Dehner, A.; Kessler, H., Diffusion NMR Spectroscopy: Folding and Aggregation of Domains in p53. *ChemBioChem* **2005**, 6 (9), 1550-1565.
- 32 Lakowicz, J. R., *Principles of fluorescence spectroscopy*. 3rd ed.; Springer Science & Business Media: 2006.
- 33 Kawski, A., Fluorescence anisotropy: theory and applications of rotational depolarization. *Critical Reviews in Analytical Chemistry* **1993**, 23 (6), 459-529.
- 34 Smith, T. A.; Ghiggino, K. P., A review of the analysis of complex time-resolved fluorescence anisotropy data. *Methods and Applications in Fluorescence* **2015**, 3 (2), 022001.
- 35 Valeur, B.; Berberan-Santos, M. N., *Molecular fluorescence: principles and applications*. John Wiley & Sons: 2012.

IV Mechanochemistry of foldamers

1 Introduction

With the rational designs and inter-/intra-molecular non-covalent bindings, synthetic organic oligomers are able to conform to the structures and functions of biopolymers, sometimes, even beyond.¹ Synthetic foldamers^{1b} are such a series of artificial oligomers adopting folded conformations inspired by natural biopolymers in the presence of non-covalent bindings,² like hydrogen bond^{2a}, π - π stacking^{2d, 2f}, solvophobic effect^{2b}, metal-ligand coordination³, etc. With the help of these non-covalent bindings, a various range of backbones have been designed and programmed to build up biotic and abiotic foldamers.^{1b, 2b, 2e, 2f, 4} Aromatic oligoimides, thanks to the robustness of their own structures and predictability of their folding modes, are becoming a growingly popular and important class of foldamers. In general, hydrogen bonding (H and N, H and O, or H and F), electrostatic attraction/repulsion and solvophobic effect mainly lead to the deformation of backbones of aromatic oligoimides and the formation of folded structures. The π - π stacking forces between aromatic backbones also reinforce the intramolecular attraction, further stabilizing their folded conformations. All these non-covalent forces stabilize the folded conformation of foldamers (Figure 1).⁵

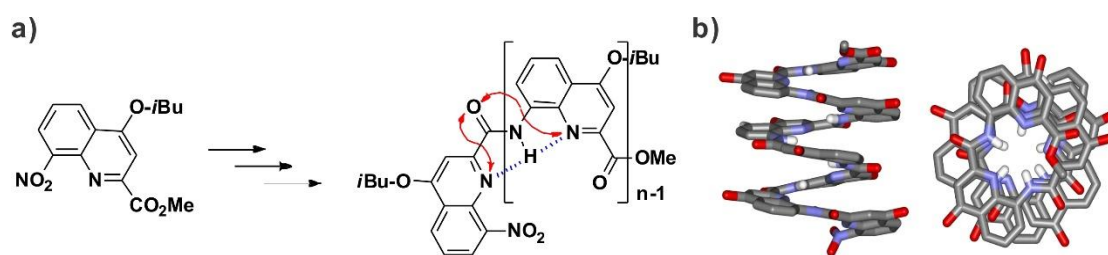


Figure 1 a) The chemical structure of quinoline-based foldamers studied in this chapter and b) an example of crystalline structure of aromatic oligoimide foldamer which includes 8 quinoline units and is stabilized by non-covalent interactions (forces).

The stability of these aromatic foldamers, however, is not unalterable as their internal structures (like the length of molecule⁶) and/or external atmospheres (for instance, solvent⁷ or temperature⁶) are modified. As the length of aromatic foldamers based on 8-amino-2-quinoline

carboxylic acid increased from 6 quinoline units up to 16 units, the foldamers handedness inversion slowed down with five orders of magnitude (half-life from 0.2 h to 1870.0 h at 10 °C). When temperature went up from 0 to 30 °C, the retention times of these foldamers in chiral HPLC extended as well, and the half-time of handedness inversion decreased due to more absorption of external energy.⁶ The change of solvent can also has an apparent effect on the stability of foldamers' handedness. These foldamers showed poor stability of their helical conformation in chloroform and THF, but were able to keep their helical conformation in protic media (alcohol or its mixture with water) for a relatively long time, probably due to the fact that the solvophobic effect caused by these protic solvents surpasses their corresponding competition with intramolecular hydrogen-bonding.⁷ Nevertheless, the change of either internal structures or external atmospheres finally comes to the alteration of the intra-/inter-molecular non-covalent forces which responsively stabilize the conformation of foldamers, even though there are several kinds of non-covalent forces (hydrogen bonding between H of amide group and N atom of quinoline unit, π - π stacking forces between aromatic backbones of quinoline units, electrostatic repulsion between O from amide moiety and the endocyclic quinoline N) influencing the conformation at the same time.

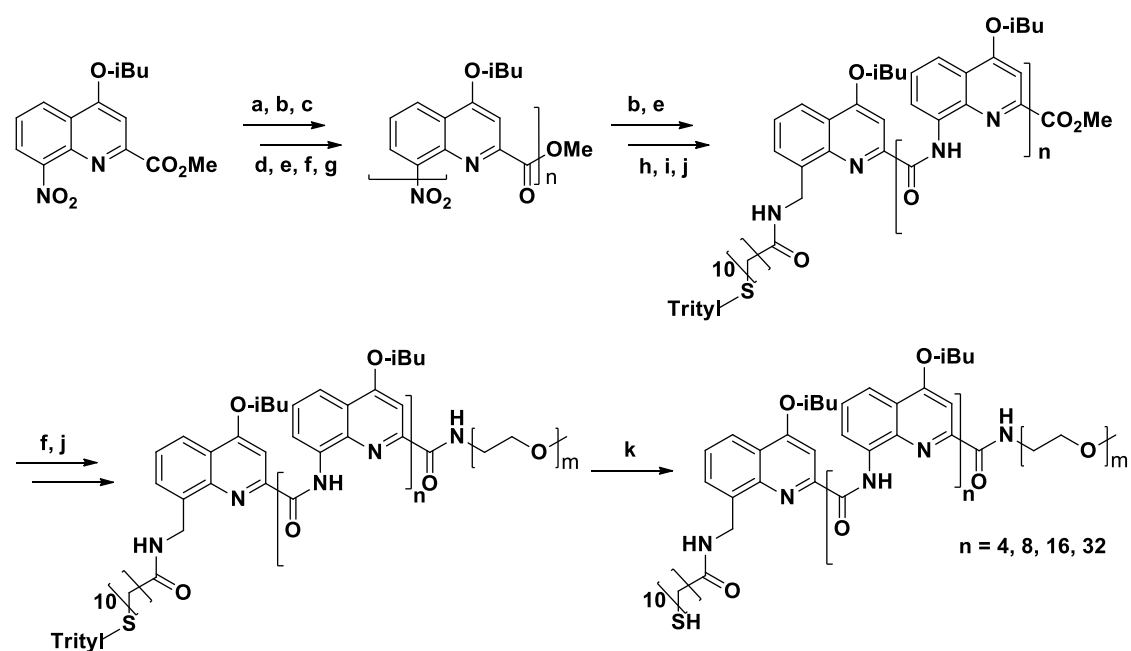
Although investigations of intra-/inter-molecular non-covalent interactions of foldamers have been conducted with ensemble averaging techniques⁶⁻⁸ (for example, as mentioned above, nuclear magnetic resonance and circular dichroism), how these non-covalent forces monitor the conformation of foldamers at the molecular level is still an open question. An efficient approach to explore the answer to that question is the study of a single molecule one at a time. Atomic force microscopy-based single molecule force spectroscopy (AFM-SMFS)⁹ has become an efficient tool to monitor mechanical forces with sub-nanometer resolution, and has been widely used to investigate molecular-level processes in individual biomolecules and synthetic macromolecular systems.⁹⁻¹⁰ For example, non-covalent binding like H-bonding, π - π stacking, metal-ligand, specific host-guest interactions,... have been investigated, revealing details about the strength of inter- and intramolecular interactions.⁹⁻¹¹ However, implementing single-molecule force spectroscopy on small molecules, like our foldamers, remains a major challenge.^{11q, 11t, 11u} The main non-covalent forces that influence the conformation of foldamers

include not only hydrogen binding but also π - π stacking, but how these non-covalent forces keep the conformation of these supramolecular structures in balance and how large they could be are still waiting for exploration. Herein, we employed AFM-SMFS as a tool and synthesized a series of quinoline-based foldamers with different lengths. Based on 8-amino-2-quinoline carboxylic acid, various nanosized aromatic oligoimide foldamers have been prepared. They were functionalized at one end with a thiol group, which can anchor onto an Au surface, and at the other end with poly(ethylene glycol) (PEG) which works as a linker to interact with the AFM tip, allowing the mechanical stretching of the foldamer molecules. We revealed that these quinoline-based foldamer molecules can indeed be stretched by the AFM, showing a plateau-like profile which suggests the unfolding of the foldamer molecules. The preliminary results provide the relative values of unfolding forces and stretched length of foldamers with 17 and 33 quinoline units.

2 Synthesis and basic principle of AFM-SMFS

2.1 Synthesis

By employing segment doublings strategy, varied size foldamers (4mer, 8mer, 16mer and 32mer) have been synthesized based on quinoline monomer. In cooperation with Dr. Markandeya Nagula, these foldamers were elongated with an aminomethyl quinoline monomer, and then functionalized with trityl-protected thiol group which can anchor onto the Au surface after deprotection. These foldamers were further functionalized with one amine terminated polyethylene glycol (PEG) in the presence of PyBOP. This flexible PEG part can interact with the AFM cantilever, allowing to stretch the foldamers. Before anchoring the foldamers onto Au surface, TFA was used to remove the trityl group.



a), Pd/C , H_2 , r.t., overnight; b), KOH , $\text{THF/H}_2\text{O}$, r.t., overnight; c), oxalyl chloride, DCM , r.t., ~ 4 h; d), DIPEA , DCM or CHCl_3 , $0\text{ }^\circ\text{C}$ to r.t., overnight; e), Pd/C , NH_4VO_3 , NH_4HCO_2 , EtOAc/EtOH , $95\text{ }^\circ\text{C}$, overnight; f), NaOH , THF/MeOH , r.t., 0.5 h to overnight; g), $\text{pyridine/H}_2\text{O}$, reflux, overnight; h), Ghosez reagent, CHCl_3 , r.t., approx. 3 h; i), TFA , DCM or CHCl_3 , r.t. 4 to 6 h; j) PyBOP , DIPEA , CHCl_3 , r.t., overnight; k) $\text{CHCl}_3/\text{H}_2\text{O}$, TFA , r.t., approx. 4 h.

2.2 Basic principle of AFM-SMFS

The basic principle consists in approach-retraction cycles between an AFM tip and a surface onto which the molecule of interest is attached. The corresponding force-distance curves are

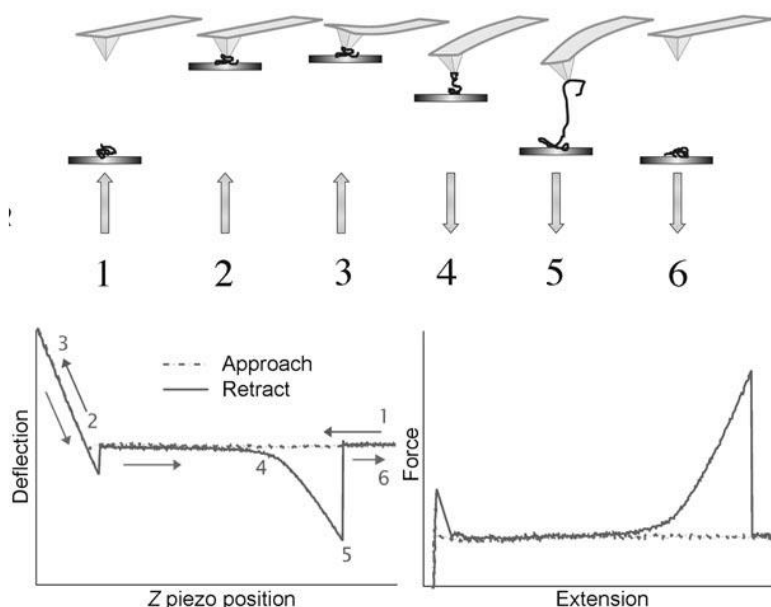


Figure 2 The schematic illustration of the principle of AFM-SMFS¹²

recorded. The equipment consists mainly of a cantilever at the end of which there is a nanosized tip that interacts with the sample molecule, a piezo electric scanner to precisely move the AFM tip, a laser to detect the cantilever deflection, and a photo-sensitive diode to detect the laser. The sample molecule can be anchored on the surface (generally, mica, Au or silica) by covalent binding or physical absorption. A typical SMFS experiment consists in approaching the tip towards the surface (position 1 in Figure 2). In this initial stage, no force is detected. Once the tip and surface get into contact while continuing the approach, an external force is applied to the cantilever, resulting in a deflection of cantilever (upwards, 2 in Figure 2) and meanwhile, allowing the sample molecule to interact with the cantilever by physical absorption or formation of a specific bond (position 3). After this contact, the tip is retracted from the surface (position 4). If sufficient interactions took place between the molecule and the tip during the contact, the molecule will bridge the tip and surface and will be stretched during the separation. The unfolding (and potential deformation) of the molecule induces a restoring force, detected by the

cantilever (downwards, position 5). Once this restoring force exceeds the interaction between the tip and the sample molecule, the sample molecule drops off from the tip, and the cantilever jumps back to its original position (position 6). The characteristic unfolding profiles of the sample molecule depends on the chemical and/or stereo-conformational structures of the sample molecules. They can display, among others, a single peak^{12a, 19f}, or a saw-tooth pattern^{13a}.

14.

3 Results and Discussion

A series of quinoline-based foldamers (4mer, 8mer, 16mer and 32mer) have been successfully synthesized beforehand. Their solid structures (Figure 3) demonstrate that all of these foldamers

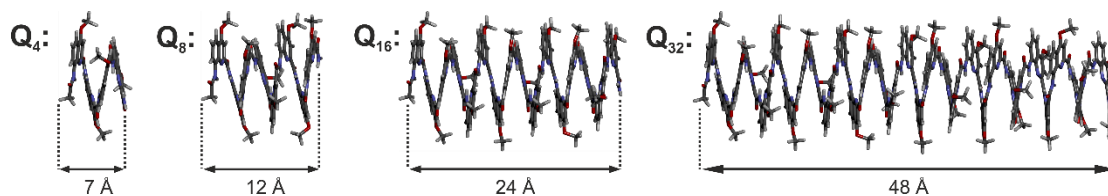


Figure 3 The crystalline structures of quinoline-based foldamers with 4, 8, 16 and 32 units.

exhibit wonderful helical secondary structures due to the rational design and the intramolecular non-covalent interactions.^{5b} In cooperation with Dr. Markandeya Nagula, all these four oligomers were added with an aminomethyl quinoline carboxylic acid monomer, forming as foldamers with 5, 9, 17 and 33 quinoline units, respectively. The addition of aminomethyl terminal group at this quinoline unit not only afford the opportunity that this terminal amino group is able to be parallel in space to the axis of the folded structure of the related molecule (see the energy-minimized structure of foldamer with 9 units, Figure 4), but also rises the reactivity of this amino group. By reacting with this aminomethyl group, an aliphatic chain terminated with a protected thiol group was easily added to these foldamers. Due to the addition of aminomethyl group at foldamer terminal, this design potentially offered these resulting molecules to be placed vertical to the substrate (Au surface) in solution when they are mobilized on the substrate. This vertical standing of foldamer benefits the interaction between these studied foldamers and the AFM tip (explained later).

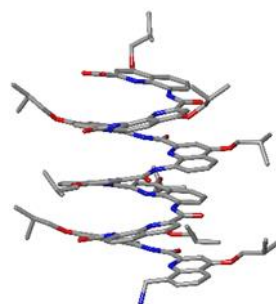


Figure 4 The energy-minimized structure of 9mer with aminomethyl group as terminal (shown at the bottom).

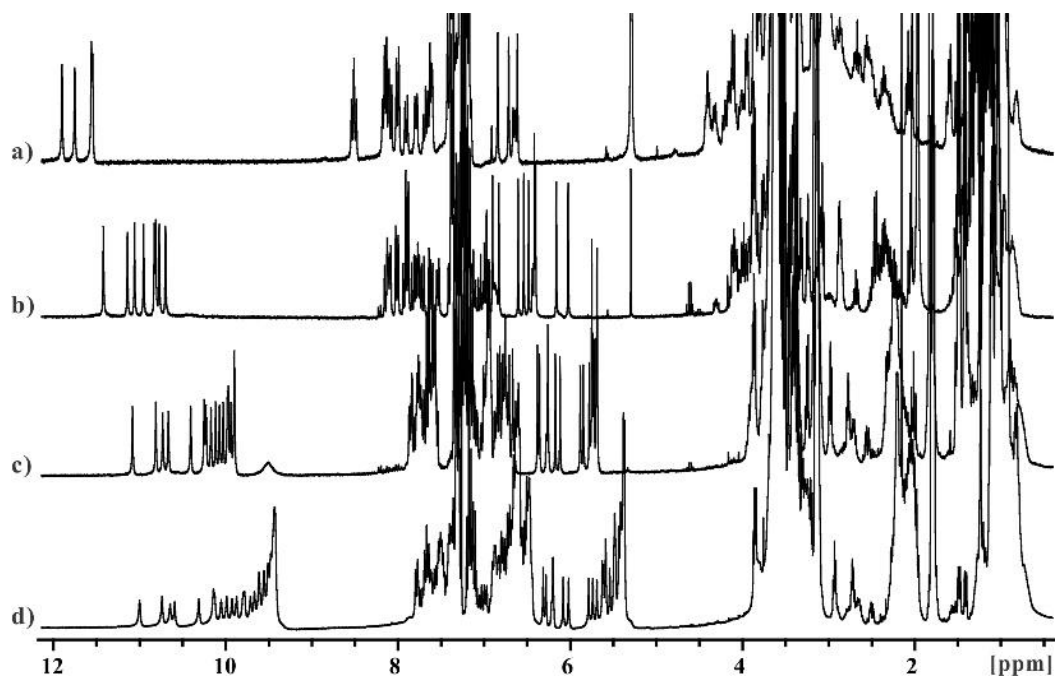


Figure 5 The full ^1H NMR spectra (300 MHz, CDCl_3) of foldamers with 5, 9, 17 and 33 quinoline units (a, b, c and d, respectively, top to bottom) after linking with PEG (around 4 – 2 ppm).

A poly(ethylene glycol) (PEG) segment was linked to other terminal of the foldamer with the PyBOP coupling reagent after saponification of its ester. Recycling GPC allowed us to separate the final product and the starting materials easily with high purity (Figure 5). This PEG part not only enables the AFM cantilever to interact with the sample molecule, permitting the occurrence of stretching the foldamer-included molecule itself, but also avoid the overlap of unspecific adhesion force (if any) between the surface and the tip and the characteristic force extension of foldamer molecule when the cantilever retracts and starts to stretch the sample molecules (position 4, Figure 2). The protected foldamers were deprotected with TAF at room temperature to remove trityl group, giving the free thiol group. The precursor solution for functionalization of Au surface with foldamer molecules was prepared by mixing dodecyl sulfide (DDS) with these deprotected foldamer (DDS : foldamer = 3.9 : 22, mol/mol) in chloroform. Subsequently, the Au surface ($2 \times 2 \text{ cm}^2$) cleaned by UV-ozone beforehand was sunk into these solutions (2 mL) for 1 h to make the deprotected foldamers anchor onto the surface. After removal of the free foldamer molecules on the surface by abundant rinsing, the functionalized Au surfaces can be measured with AFM (Figure 6).

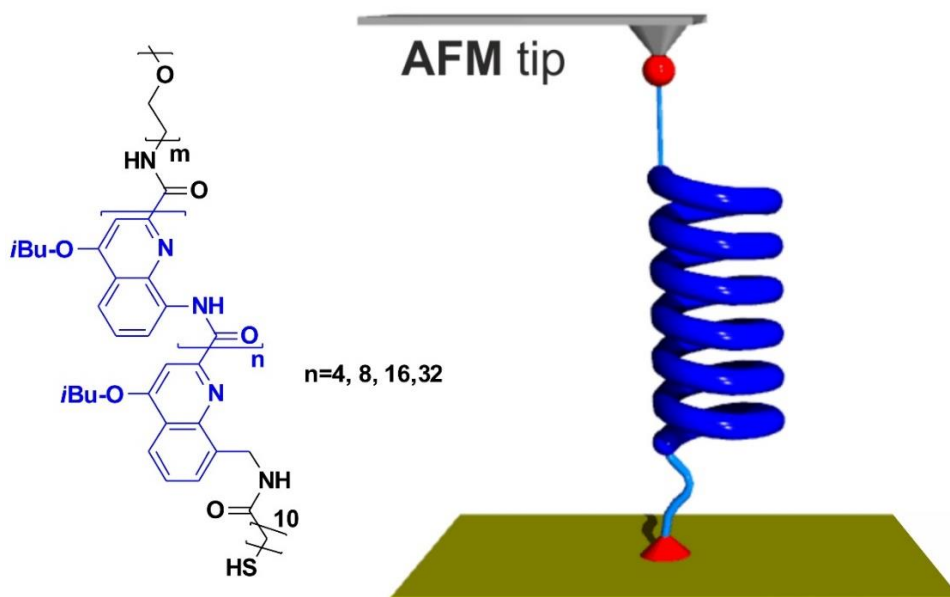


Figure 6 Chemical structure (left) of foldamers functionalized with the thiol group able to anchor onto the Au surface and the PEG segment allowing the AFM tip to interact with the foldamer system and to stretch it, and scheme (right) of the SMFS experiment.

For the experiment of single molecule force spectroscopy on foldamer molecules, the AFM tip was brought toward the foldamer-functionalized Au surface in *N,N*-dimethylformamide (DMF), allowing the flexible PEG spacer to interact with the tip of cantilever. Then, cantilever was gradually separated from Au surface at a constant pulling rate of 250 nm/s and the molecule was stretched progressively, which yielded a deflection-position profile. Using the spring constant of the cantilever and tip displacement, the profile is then converted in a force-extension profile (Figure 7). Several types of profiles were observed. Non-repeatable profiles with multiple peaks of random position and intensity were not considered. They are the signatures of the pulling of multiple molecules at the same time or the presence of contaminations. Only "clean" profiles with a reproducible shape were considered. The characteristic shape of those profiles is a single peak containing a plateau (Figure 7). It must be noted that the cantilevers were not calibrated and that is the constant nominal stiffness was used. The front part **I** and the late peak part **III** were attributed to the extension of the PEG spacer (characteristic signature of the extension of a random coil), and the middle plateau part **II** to the stretching of the foldamer structure. This plateau is indeed not present in the force-extension profile of pure PEG^{12a}. We

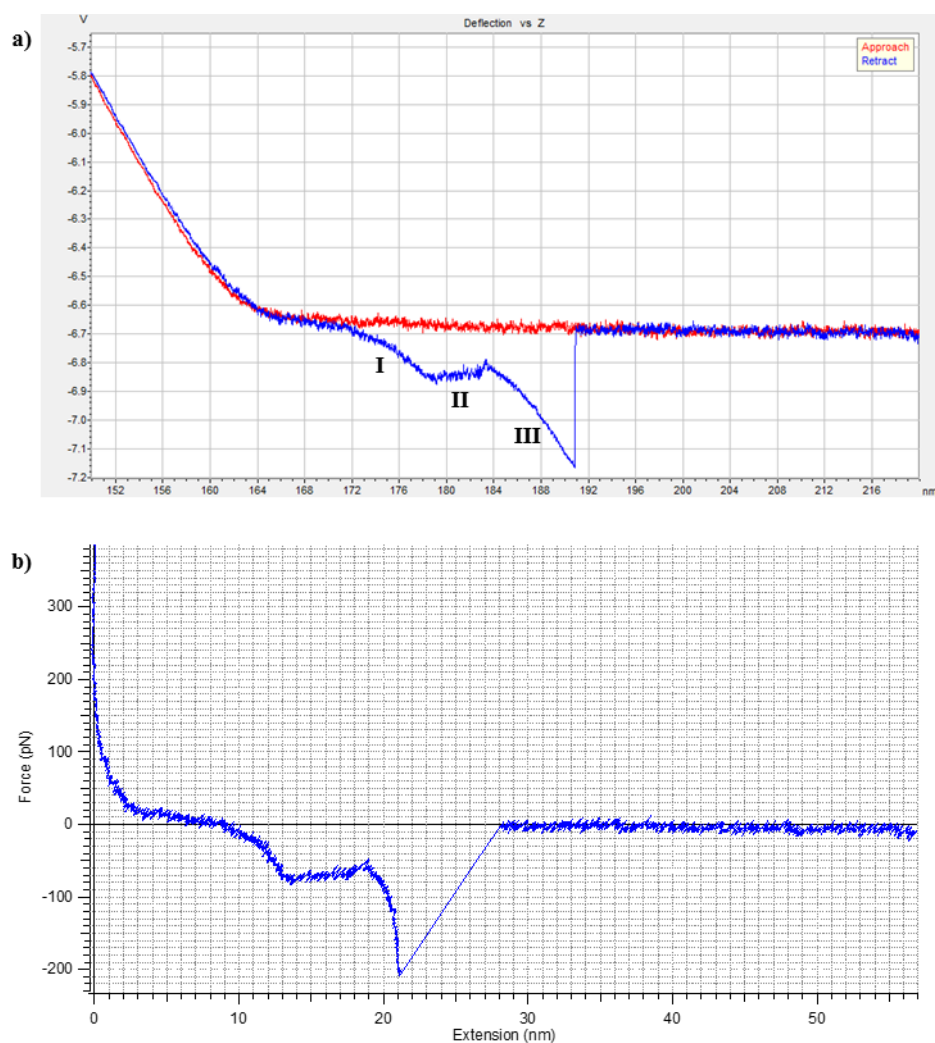


Figure 7 Raw deflection-position profile (a) of foldamer (with 17 units) operated in freshly distilled DMF and its corresponding force-extension profile (retraction track only) (b).

interpret this plateau as the successive breakings of the non-covalent interactions (hydrogen bonding between H of amide group and N of quinoline unit, π - π stacking between quinoline units in vertical direction) within the foldamer molecule. The scheme in Figure 8a illustrates our explanations for the events occurring when stretching the whole foldamer-included molecules and the resulting force-extension profiles (Figure 8b). When the AFM tip starts pulling on the molecule (**II**), the PEG linker uncoils, which gives rise to a characteristic parabolic profile arising from the entropic restoring force generated. This is the typical response of a worm-like chain under extension.^{ref} Once the restoring force exceeds the intramolecular interactions (hydrogen bonding and π - π stacking force) in the foldamer, these non-covalent interactions are broken gradually (in series) and the foldamer is unfolded progressively.

Because the building blocks of foldamers are the same along the molecule and thus the intramolecular hydrogen bonding/ π - π stacking is almost identical, the corresponding exerted force keeps constant. This results in the appearance of a plateau-like profile, as the foldamer is stretched over the time (III). As the stretching continues and the foldamer is unfolded completely, the PEG part is stretched further (IV). PEG detaches from the AFM tip suddenly and the tip jumps back to its original position (V) when the force exceeds the interaction between PEG and the AFM tip which is the weakest link in this system. The covalent bonds in the whole foldamer-included molecule and the Au-S bonds anchoring the molecule onto the Au surface (1-1.5 nN) are indeed much larger than the physical absorption between PEG and the AFM tip.^{11q, 13}

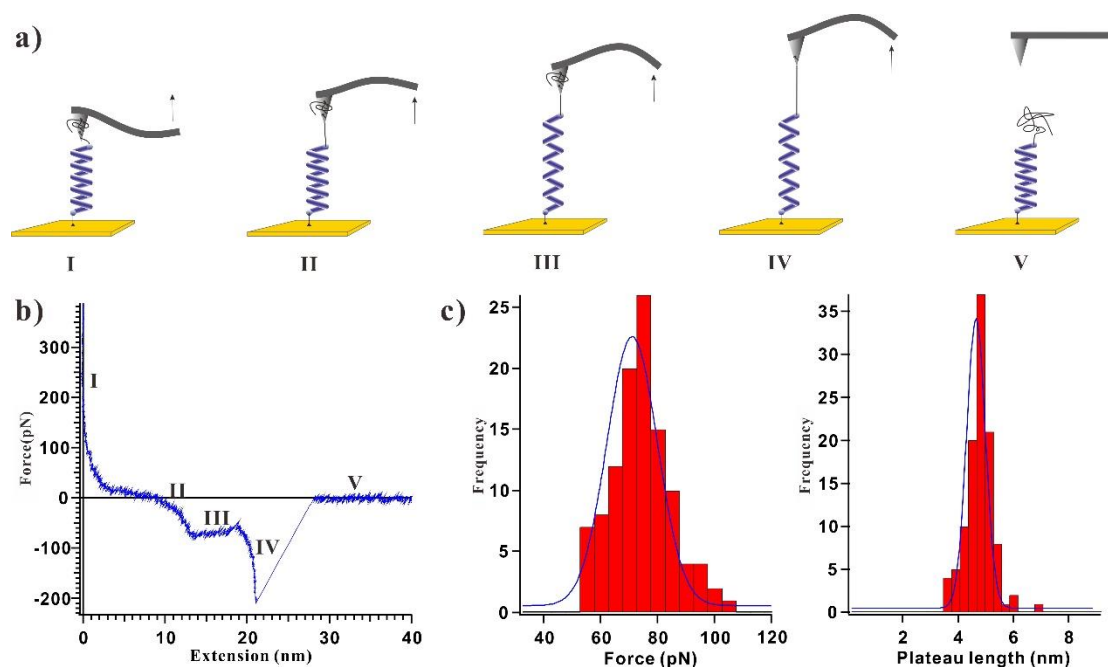


Figure 8 Single molecule force spectroscopy of the foldamer-included molecule with 17 quinoline units in freshly distilled DMF (pulling rate of 250 nm/s). Interpretation of the sequence of events taking place during the pulling (a). Resulting force-extension profile (b) and corresponding histograms (c) of the rupture force and the plateau length ($n = 108$).

The Gaussian fits of the force and extension distributions (based on 108 curves) give a most probable rupture force of 71.1 ± 4.59 pN for the plateau observed for the foldamer with 17 quinoline units in freshly distilled DMF.^{viii} The corresponding plateau length appears at $4.6 \pm$

^{viii} The measured values of 17mer and 33mer are only indicative – they just display an idea of the order

0.3 nm Figure 8c). We then increased the number of quinoline units up to 33 and kept the experimental conditions invariable. The resulting force-extension profile obtained in freshly distilled DMF (Figure 9a) displays similar features— a plateau-like profile – as the one of foldamer with 17 quinoline units. The statistical analyses provided a most probable rupture force of 89.9 ± 5.85 pN (Figure 9b), and an almost double plateau length (9.1 ± 1.5 nm, Figure 9c) compared to the foldamer with 17 units (4.6 ± 0.3 nm). The doubling of the plateau length is consistent with the almost double number of quinoline units. More importantly, these results of plateau lengths, in turn, reveal that the data are reliable and trustworthy to predict the lengths of other foldamers with diverse number of quinoline units^{ix}.

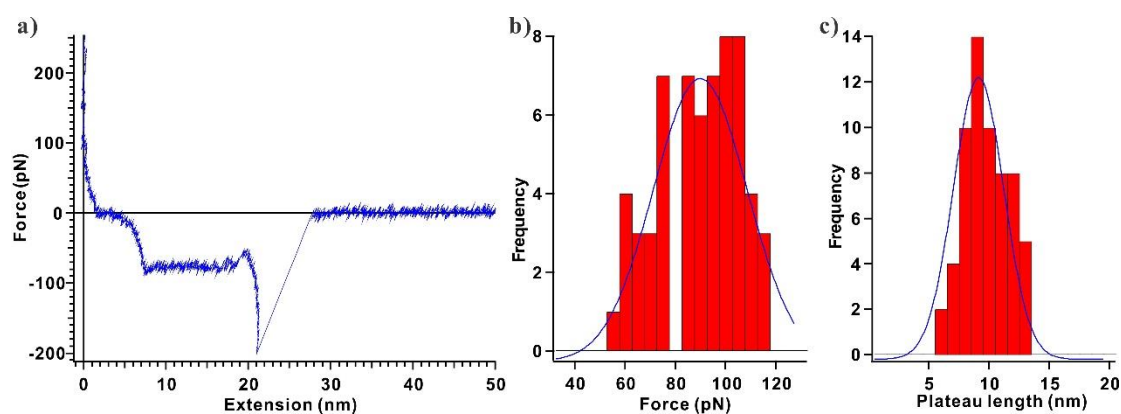


Figure 9 SMFS force-extension profile of foldamer-included molecule of 33 quinoline units at a pulling rate of 250 nm/s in freshly distilled DMF (a) and the corresponding histograms of the rupture force (b) and the plateau length (c) ($n = 60$).

When the measurement was carried out in normal DMF (including H_2O , $> 0.1\%$, from Across), the force-extension profile of foldamer with 33 quinoline units, shown in Figure 10a, was obtained and still shows a plateau-like part in the curve. Compared to the profile obtained in freshly distilled DMF, however, the rupture force decreased dramatically from 89.9 ± 2.85 pN to 20.4 ± 1.59 pN (Figure 10b), and the corresponding plateau length dropped down from 9.1 ± 1.5 nm to 3.1 ± 0.6 nm (Figure 10c). This result is consistent with the relative strengths of intramolecular hydrogen bonding in freshly distilled DMF and water-included DMF: the

of magnitude, and are not discussed further since the cantilevers used for the measurement were not calibrated.

^{ix}The AFM-SMFS experiments about foldamers with 9 and 5 quinoline units are still ongoing, and the corresponding stretched lengths of these two foldamers are waiting to be revealed.

hydrogen bonding in freshly distilled DMF is stronger than in water-included DMF because of the presence of water which is able to break the intramolecular hydrogen bonding of foldamers due to intermolecular bonding with amide groups of the foldamer and consequently weakening inter-component interactions within the foldamer molecules.

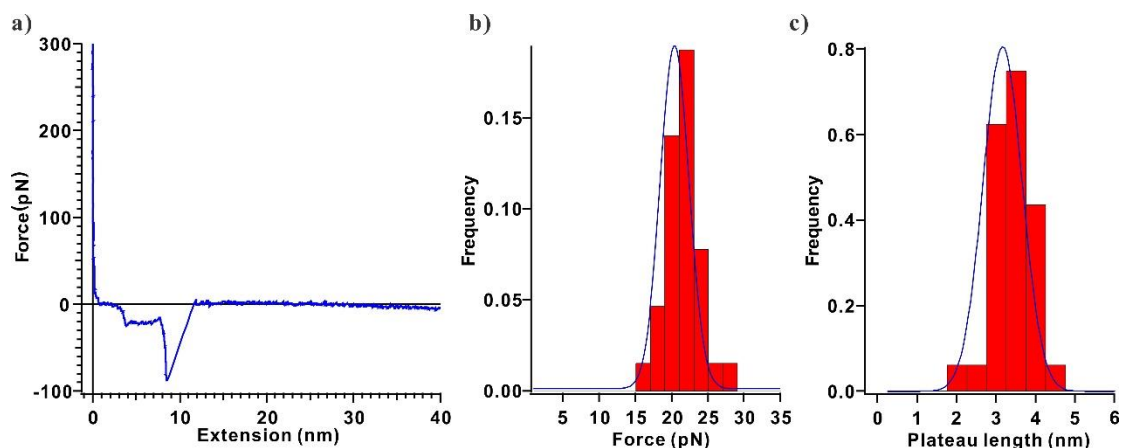


Figure 10 SMFS force-extension profile of foldamer-included molecule of 33 quinoline units at a pulling rate of 250 nm/s in water-included DMF (a) and the corresponding histograms of the rupture force (b) and the plateau length (c) ($n = 31$).

The distribution of the force vs plateau length of the two foldamers is shown in Figure 11a. The foldamer with 17 quinoline units exhibits a highly concentrated distribution (green crosses), revealing that the results are similar to one another, reappear frequently and consequently show high reliability. For the foldamer with 33 units, the distribution of the data in water-included DMF is also relatively compact (blue crosses), even though the number of the corresponding events is not that large ($n = 31$). The distribution obtained in freshly distilled DMF is much more scattered, which is probably due to the presence of some incomplete stretching of foldamer molecules (Figure 11b) and the presence of partially folded structures. Those partially folded structures possibly take place as the right-handed conformation of foldamer molecules inverts into the left-handed one, the related half life time in DMF being 40 min⁷. Further investigations are necessary to understand this in detail.

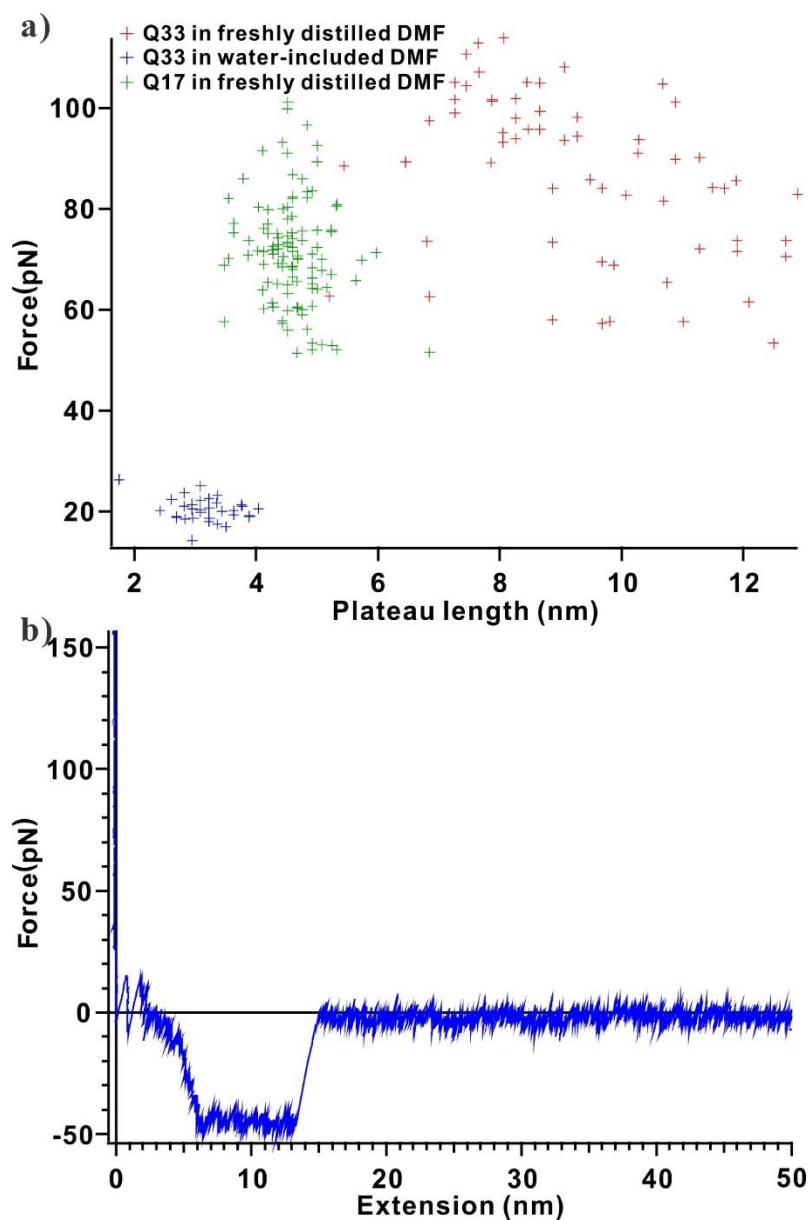


Figure 11 Distribution of force – stretched length profiles of foldamers with 17 and 33 quinoline units in DMF (a) and example of a force curve with an incomplete stretching event happening to foldamer with 33 quinoline units.

4 Conclusion and perspectives

Nanosized quinoline-based foldamers scaffolds were successfully synthesized and functionalized at opposite ends with a thiol group which is able to anchor onto an Au surface and a PEG segment that enables itself to interact with the AFM tip, allowing the foldamer-included molecules to be stretched by the AFM cantilever. The preliminary results of AFM-based single molecule force spectroscopy show that plateau-like curves took place. We attribute them to the successive breaking of the non-covalent forces holding the helical structure of the foldamer molecule. The length of this plateau is directly related to the size of the foldamer molecules. The results obtained in freshly distilled (anhydrous) DMF differed from that in water-included DMF, which suggests that the solvent has a significant effect on the structure and stability of these folded secondary structures. To obtain more details, further research could be carried out with the following objectives.

1, Collect more data about foldamers with 33 quinoline units in freshly distilled DMF. A more robust analysis based on a statistically relevant data set is required to complete the preliminary results.

2, Measure shorter foldamers (with 5 and 9 units) with AFM-SMFS. The results of foldamer with 5 quinoline units which comprise two turns of foldamers and with 9 quinoline units (approx. four turns) could provide us the opportunity to test the limits of SMFS to detect unfolding processes.

3, Change the ambient atmosphere of AFM-SMFS, for example, solvent and temperature. As studied by CD and NMR before⁶⁻⁸, the ambient atmosphere has an effect on the stability of foldamers. Details about handed inversion and stability of foldamers are potentially approachable.

4, Carry out pulling-relaxing cycles. With this method, a better understanding of the folding/unfolding of foldamer is expected, especially the possibility of refolding against an

external load.

5, Investigate the influence of hydrogen bonding upon the stability of foldamers.

Substitution of the H atom of amide group with other groups, like methyl group, can result in the less stability of foldameric conformation. We could thus reasonably expect a change of the unfolding. This could allow us to explore how large the hydrogen bonding is and how it stabilizes the conformation of the foldamer. The number of substitution of H atom with other groups can be monitored, which increases the flexibility of the investigation on hydrogen bonding.

6, Study the effect of coordination between metal ions and the quinoline units towards the conformation and the stability of foldamers.

Introduce some metal ions, such as Cu^{2+} , into the cavity of foldamer, producing coordination interaction inside the foldamer^{3, 14}. How this coordination interaction – a non-covalent force – affects the foldamer itself is of high interest.

7, Introduce interaction(s) between side chains of quinoline units in each turn.

The interaction(s) between side chains of building block could have the potential to strengthen the stability of foldamer, but how they strengthen it and how strong they could be are valuable to investigate, especially for some particular bindings, like disulfides.

8, Put it into application, for example as artificial muscles.

The folding/unfolding process of foldamer molecules is an appropriate approach to simulate the contraction/stretching of muscle fibers. The strands of foldamer molecules with different lengths which are connected to one another in parallel and (or) series way could be remarkable artificial architectures to mimic and explore.

9, Explore the influence of non-covalent forces with computational chemistry.

It is always favorable to bring molecular modeling into practical experiment. Based on the experimental results, molecular modeling can help us to understand the data themselves better, pave the way for the further experiments and sometimes uncover something important which can be received from experiments.

5 Experimental Section

5.1 Methods of NMR

NMR data were recorded at 300 MHz using an Avance II NMR spectrometer (Bruker Biospin) with a vertical 7.05T narrow-bore/ultrashield magnet operating at 300 MHz for ^1H observation and 75 MHz for ^{13}C observation by means of a 5-mm direct BBO H/X probe with Z gradient capabilities. All chemical shifts are quoted in parts per million (ppm, δ) relative to the ^1H residual signal of the deuterated solvent used (CDCl_3 at 7.26 ppm). ^1H NMR splitting patterns with observed first-order coupling are designated as singlet (s), doublet (d), double doublet (dd), triplet (t), or quartet (q). Splitting patterns that could not be interpreted or easily visualized are designated as multiplet (m) or broad (br). Coupling constants (J) are reported in hertz. Samples were not degassed. Data processing was performed with Topspin 2.0 software.

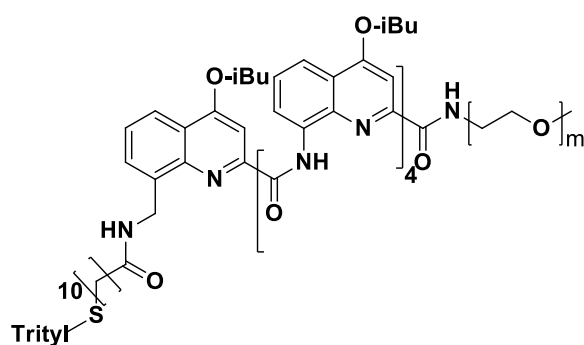
5.2 Methods of Chemical Synthesis

All reactions were carried out under a dry nitrogen environment. Chemicals and reagents were used as commercially supplied without any further purification unless otherwise stated. Dichloromethane (DCM), Tetrahydrofuran (THF) and Toluene were dried over alumina columns under nitrogen. Chloroform, triethylamine (Et_3N) and diisopropylethylamine (DIPEA) were distilled over calcium hydride (CaH_2) prior to use. Reactions were monitored by thin layer chromatography (TLC) on Merck silica gel 60-F254 plates and observed under UV light (254 and 365 nm). Column chromatography was carried out on Merck GEDURAN Si60 (40-63 μm). Circular chromatography purifications were carried out on Chromatotron® with silica gel, Merck grade 7749, TLC grade with binder and fluorescent indicator. Analytical and semi-preparative GPC was carried out on Shimadzu Recycling GPC system equipped with LC-20 AD pump, SPD-M20A UV detector and a set of 1H, 1.5H, 2.5H and 3H columns (size: 20 \times 600 mm) in chloroform/0.5~1% ethanol as eluent with a flow rate of 3.5 mL/min. ESI and MALDI mass spectra were obtained on a Waters LCT Premier and a Bruker Reflex III spectrometers respectively, from the Mass Spectrometry Laboratory at the European Institute of Chemistry

and Biology (UMS 3033 - IECB), Pessac, France and a Voyager DE-STR mass spectrometer from AB Sciex, Les Ulis, France.

General Methods to synthesize trityl-S-mQQ_n-PEG (n = 4, 8, 16, 32)

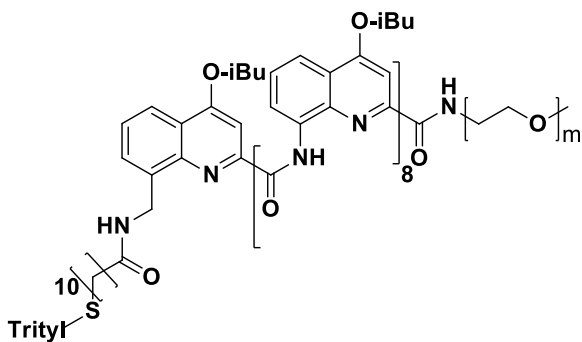
Different size foldamers have been synthesized, and with cooperation with Dr. Markandeya Nagula, were further combined with aminomethyl quinoline monomer and functionalized with trityl-protected thiol group as well. The acid of trityl-S-mQQ_n (trityl-S-mQQ_n-COOH) was mixed with 1.2 equiv amine-terminated poly(ethylene glycol) (average FM: 5056) and 2 equiv PyBOP. After dried under vacuum, freshly distilled chloroform was added at room temperature and then DIPEA at 0 °C. The reaction was allowed to warm up to room temperature and proceed until disappearance of trityl-S-mQQ_n-COOH with a control of ¹H NMR. The crude was washed by water and brine, dried by Na₂SO₄, filtered, evaporated and then purified by recycling GPC to give a pale yellowish solid.



Trityl-S-mQQ₄-PEG

130 mg Trityl-S-mQQ₄-COOH (113.3 μmol), 687.2 mg PEG (135.9 μmol) and 118 mg PyBOP (226.5 μmol) were dissolved in chloroform and 0.075 mL DIPEA was added. After purification,

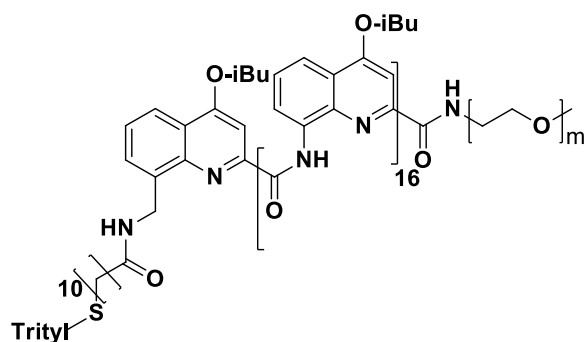
approx. 300 mg pale yellowish solid was obtained (41%). ¹H NMR (300 MHz, CDCl₃): δ 11.90 (s, 1H), 11.75 (s, 1H), 11.56 (s, 1H), 11.54 (s, 1H), 8.51 (t, J = 9.0 Hz, 2H), 8.12 (d, J = 33 Hz, 1H), 8.15 (s, 1H), 8.13 (s, 1H), 8.10 (s, 1H), 8.01 (s, 1H), 7.99 (s, 1H), 8.00 (d, J = 9.0 Hz, 1H), 7.79 (d, J = 6.0 Hz, 1H), 7.70 – 7.60 (m, 4H), 7.42 – 7.15 (m, 18H), 6.84 (s, 1H), 6.71 (s, 1H), 6.65 (d, J = 6.0 Hz, 1H), 6.61 (s, 1H), 4.40 – 2.59 (m, H), 2.57 – 2.26 (m, 5H), 1.63 – 1.52 (m, 4H), 1.45 – 0.81 (d, H).



Trityl-S-mQQ₈-PEG

113 mg Trityl-S-mQQ₈-COOH (42.6 μmol), 258 mg PEG (51.1 μmol) and 44 mg PyBOP (85.2 μmol) were dissolved in chloroform and 0.028 mL DIPEA was added. After purification, approx. 160 mg pale yellowish

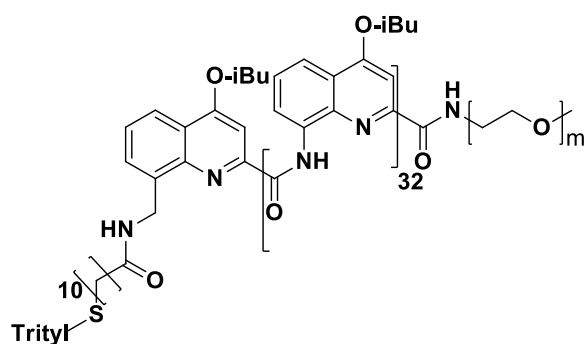
solid was obtained (54%). ¹H NMR (300 MHz, CDCl₃): δ 11.42 (s, 1H), 11.14 (s, 1H), 11.06 (s, 1H), 10.95 (s, 1H), 10.82 (s, 1H), 10.81 (s, 1H), 10.77 (s, 1H), 10.70 (s, 1H), 8.15 – 8.08 (m, 3H), 8.02 (s, 1H), 7.99 (s, 1H), 7.94 – 7.88 (m, 3H), 7.84 – 7.69 (m, 3H), 7.63 (d, J = 6 Hz, 1H), 7.53 (d, J = 6 Hz, 1H), 7.41 – 6.94 (m, 29H), 6.90 (s, 1H), 6.88 – 6.85 (m, 1H), 6.82 (s, 1H), 6.60 (s, 1H), 6.54 (s, 1H), 6.48 (s, 1H), 6.44 – 6.40 (m, 3H), 6.16 (s, 1H), 6.02 (s, 1H), 4.12 – 3.06 (m, H), 2.89 – 2.85 (m, H), 2.54 – 2.15 (m, H), 1.54 – 0.87 (m, H).



Trityl-S-mQQ₁₆-PEG

24 mg trityl-S-mQQ_n-COOH (5 μmol), 36 mg PEG (6 μmol) and 8 mg PyBOP (10 μmol) were dissolved in 1 mL chloroform and 0.07 mL DIPEA was added. After purification, approx. 18 mg pale yellowish

solid was obtained (38%). ¹H NMR (300 MHz, CDCl₃): δ 11.08 (s, 1H), 10.80 (s, 1H), 10.73 (s, 1H), 10.66 (s, 1H), 10.40 (s, 1H), 10.25 (s, 1H), 10.22 (s, 1H), 10.17 (s, 1H), 10.11 (s, 1H), 10.07 (s, 1H), 10.03 (s, 1H), 9.98 (s, 1H), 9.97 (s, 1H), 9.94 (s, 1H), 9.90 (s, 2H), 7.87 – 7.81 (m, 4H), 7.78 – 6.91 (m, 54H), 6.87 (d, J = 3 Hz, 1H), 6.84 – 6.81 (m, 4H), 6.79 – 6.70 (m, 9H), 6.67 – 6.64 (m, 2H), 6.34 (s, 1H), 6.35 (s, 1H), 6.27 – 6.26 (m, 2H), 6.17 (s, 1H), 6.12 (s, 1H), 5.88 (s, 1H), 5.85 (s, 1H), 5.78 (s, 1H), 5.75 (s, 2H), 5.74 (s, 1H), 5.72 (s, 1H), 5.70 (s, 1H), 5.68 (s, 2H), 3.92 – 2.68 (m, H), 2.35 – 2.06 (m, 35H), 1.52 – 0.84 (m, H).



Trityl-S-mQQ₃₂-PEG

85 mg Trityl-S-mQQ₃₂-COOH (10.5 μ mol), 85 mg PEG (15.8 μ mol) and 11 mg PyBOP (21.0 μ mol) were dissolved in 1.5 mL chloroform and 0.1 mL DIPEA was added. After purification, approx. 60 mg pale yellowish solid was obtained (42%).

¹H NMR (300 MHz, CDCl₃): δ 11.00 (s, 1H), 10.74 (s, 1H), 10.64 (s, 1H), 10.59 (s, 1H), 10.31 (s, 1H), 10.14 (s, 1H), 10.13 (s, 1H), 10.05 (s, 1H), 9.99 (s, 1H), 9.92 (s, 1H), 9.87 (s, 1H), 9.80 (s, 1H), 9.78 (s, 1H), 9.71 (s, 1H), 9.66 (s, 1H), 9.61 (s, 2H), 9.55 – 9.43 (m, 15H), 7.79 – 6.44 (m, 117H), 6.31 (s, 1H), 6.28 (s, 1H), 6.21 – 6.20 (m, 2H), 6.08 (s, 1H), 6.02 (s, 1H), 5.78 (s, 1H), 5.73 (s, 1H), 5.69 (s, 1H), 5.62 (s, 1H), 5.61 (s, 1H), 5.59 (s, 2H), 5.54 (s, 1H), 5.49 – 5.37 (m, 18H), 3.87 – 1.95 (m, H), 1.27 – 0.81 (m, H).

Deprotection of thiol group

1 mg foldamer-included molecule (trityl-S-mQQ_n-PEG (n = 4, 8, 16, 32)) was added into round-bottomed flask with 0.9 mL TFA and 0.1 mL chloroform. This reaction was allowed to stir for around 3 h at room temperature and then azeotroped with toluene to remove TFA. After dried under vacuum, the deprotected molecule can be used to functionalize the Au surface immediately.

5.3 Measurement of AFM-SMFS

Before the pulling experiments, the foldamer-included molecules should be anchored onto an Au surface. The precursor solution of deprotected foldamers with a concentration of 13.0 nmol/mL was prepared with mixing dodecyl sulfide (73.3 nmol/mL) in chloroform. The Au surface was cleaned by UV (UV-zone cleaner, Model 42, Jelight Company Inc.) for 30 min, then rinsed by pure EtOH and dried by Argon. The Au surface was then dipped into the precursor solution (2 mL) for around 1 h, allowing the thiol group of foldamer-included molecules to bind to Au, anchoring the molecule onto the surface. After washing with chloroform and ethanol to remove the free foldamer-included molecules, this foldamer-

functionalized Au surface is ready for AFM-SMFS measurement. The AFM cantilever was cleaned by UV-ozone, following the same procedure.

The AFM-SMFS experiments on the foldamer was performed with a PicoLE microscope (Agilent Technologies, Inc.). All the pulling experiments were realized by using silicon nitride cantilevers (MLCT and Biolevers) with a nominal spring constant of 30 pN/nm and a pulling rate of 250 nm/s.

The extension (x) of the molecule depends on the separation distance between the AFM cantilever and the Au surface. This separation distance is obtained from the result of subtraction of the deflection of the cantilever (d) from the travel of the piezo scanner from the reference position (Z), namely, $x = Z - d$. The force (F) experienced by the molecule can be calculated by the deflection of the cantilever (d) and the Hooke's law: $F = d \cdot k_s$, where k_s is the spring constant of the AFM cantilever.

6 Reference

- 1 (a) Huc, I., Aromatic Oligoamide Foldamers. *European Journal of Organic Chemistry* **2004**, 2004 (1), 17-29; (b) Guichard, G.; Huc, I., Synthetic foldamers. *Chemical Communications* **2011**, 47 (21), 5933-5941.
- 2 (a) Gellman, S. H., Foldamers: A Manifesto. *Accounts of Chemical Research* **1998**, 31 (4), 173-180; (b) Hill, D. J.; Mio, M. J.; Prince, R. B.; Hughes, T. S.; Moore, J. S., A Field Guide to Foldamers. *Chemical Reviews* **2001**, 101 (12), 3893-4012; (c) Sanford, R.; Bing Gong, A., Evolution of Helical Foldamers. *Current Organic Chemistry* **2003**, 7 (16); (d) Hecht, S.; Huc, I., *Foldamers: structure, properties and applications*. John Wiley & Sons: 2007; (e) Goodman, C. M.; Choi, S.; Shandler, S.; DeGrado, W. F., Foldamers as versatile frameworks for the design and evolution of function. *Nat Chem Biol* **2007**, 3 (5), 252-262; (f) Zhang, D.-W.; Zhao, X.; Hou, J.-L.; Li, Z.-T., Aromatic Amide Foldamers: Structures, Properties, and Functions. *Chemical Reviews* **2012**, 112 (10), 5271-5316.
- 3 Campbell, V. E.; de Hatten, X.; Delsuc, N.; Kauffmann, B.; Huc, I.; Nitschke, J. R., Cascading transformations within a dynamic self-assembled system. *Nat Chem* **2010**, 2 (8), 684-687.
- 4 (a) Cheng, R. P., Beyond de novo protein design — de novo design of non-natural folded oligomers. *Current Opinion in Structural Biology* **2004**, 14 (4), 512-520; (b) Saraogi, I.; Hamilton, A. D., Recent advances in the development of aryl-based foldamers. *Chemical Society Reviews* **2009**, 38 (6), 1726-1743; (c) Martinek, T. A.; Fulop, F., Peptidic foldamers: ramping up diversity. *Chemical Society Reviews* **2012**, 41 (2), 687-702.
- 5 (a) Dolain, C.; Gr̄ard, A.; Laguerre, M.; Jiang, H.; Maurizot, V.; Huc, I., Solution Structure of Quinoline- and Pyridine-Derived Oligoamide Foldamers. *Chemistry – A European Journal* **2005**, 11 (21), 6135-6144; (b) Jiang, H.; L̄ger, J.-M.; Huc, I., Aromatic δ -Peptides. *Journal of the American Chemical Society* **2003**, 125 (12), 3448-3449.
- 6 Delsuc, N.; Kawanami, T.; Lefeuvre, J.; Shundo, A.; Ihara, H.; Takafuji, M.; Huc, I., Kinetics of Helix-Handedness Inversion: Folding and Unfolding in Aromatic Amide Oligomers. *ChemPhysChem* **2008**, 9 (13), 1882-1890.
- 7 Qi, T.; Maurizot, V.; Noguchi, H.; Charoenraks, T.; Kauffmann, B.; Takafuji, M.; Ihara, H.; Huc,

-
- I., Solvent dependence of helix stability in aromatic oligoamide foldamers. *Chemical Communications* **2012**, 48 (51), 6337-6339.
- 8 Dawson, S. J.; Mészáros, Á.; Pethő, L.; Colombo, C.; Csékei, M.; Kotschy, A.; Huc, I., Controlling Helix Handedness in Water-Soluble Quinoline Oligoamide Foldamers. *European Journal of Organic Chemistry* **2014**, 2014 (20), 4265-4275.
- 9 Duwez, A.-S.; Willet, N., *Molecular manipulation with atomic force microscopy*. CRC Press: 2011.
- 10 (a) Samori, P., Exploring supramolecular interactions and architectures by scanning force microscopies. *Chemical Society Reviews* **2005**, 34 (7), 551-561; (b) Butt, H.-J.; Cappella, B.; Kappl, M., Force measurements with the atomic force microscope: Technique, interpretation and applications. *Surface science reports* **2005**, 59 (1), 1-152; (c) Neuman, K. C.; Nagy, A., Single-molecule force spectroscopy: optical tweezers, magnetic tweezers and atomic force microscopy. *Nature methods* **2008**, 5 (6), 491-505; (d) Liang, J.; Fernández, J. M., Mechanochemistry: One Bond at a Time. *ACS Nano* **2009**, 3 (7), 1628-1645.
- 11 (a) Schneider, H.-J., Binding Mechanisms in Supramolecular Complexes. *Angewandte Chemie International Edition* **2009**, 48 (22), 3924-3977; (b) Custance, O.; Perez, R.; Morita, S., Atomic force microscopy as a tool for atom manipulation. *Nat Nano* **2009**, 4 (12), 803-810; (c) Yount, W. C.; Juwarker, H.; Craig, S. L., Orthogonal Control of Dissociation Dynamics Relative to Thermodynamics in a Main-Chain Reversible Polymer. *Journal of the American Chemical Society* **2003**, 125 (50), 15302-15303; (d) Kudera, M.; Eschbaumer, C.; Gaub, H. E.; Schubert, U. S., Analysis of Metallo-Supramolecular Systems Using Single-Molecule Force Spectroscopy. *Advanced Functional Materials* **2003**, 13 (8), 615-620; (e) Guan, Z.; Roland, J. T.; Bai, J. Z.; Ma, S. X.; McIntire, T. M.; Nguyen, M., Modular Domain Structure: A Biomimetic Strategy for Advanced Polymeric Materials. *Journal of the American Chemical Society* **2004**, 126 (7), 2058-2065; (f) Zou, S.; Schönherr, H.; Vancso, G. J., Force Spectroscopy of Quadruple H-Bonded Dimers by AFM: Dynamic Bond Rupture and Molecular Time-Temperature Superposition. *Journal of the American Chemical Society* **2005**, 127 (32), 11230-11231; (g) Kersey, F. R.; Yount, W. C.; Craig, S. L., Single-Molecule Force Spectroscopy of Bimolecular Reactions: System Homology in the Mechanical Activation of Ligand Substitution Reactions. *Journal of the American Chemical Society* **2006**, 128 (12), 3886-3887; (h) Schäfer, C.; Eckel, R.; Ros, R.;

Mattay, J.; Anselmetti, D., Photochemical Single-Molecule Affinity Switch. *Journal of the American Chemical Society* **2007**, *129* (6), 1488-1489; (i) Zhang, Y.; Liu, C.; Shi, W.; Wang, Z.; Dai, L.; Zhang, X., Direct Measurements of the Interaction between Pyrene and Graphite in Aqueous Media by Single Molecule Force Spectroscopy: Understanding the π - π Interactions. *Langmuir* **2007**, *23* (15), 7911-7915; (j) Vancso, G. J., Feeling the Force of Supramolecular Bonds in Polymers. *Angewandte Chemie International Edition* **2007**, *46* (21), 3794-3796; (k) Gil, R.; Guillerez, M.-G.; Poulin, J.-C.; Schulz, E., Charge-Transfer Complex Study by Chemical Force Spectroscopy: A Dynamic Force Spectroscopic Approach. *Langmuir* **2007**, *23* (2), 542-548; (l) Embrechts, A.; Schönherr, H.; Vancso, G. J., Rupture Force of Single Supramolecular Bonds in Associative Polymers by AFM at Fixed Loading Rates. *The Journal of Physical Chemistry B* **2008**, *112* (25), 7359-7362; (m) Shi, W.; Zhang, Y.; Liu, C.; Wang, Z.; Zhang, X., Interaction between Dendrons Directly Studied by Single-Molecule Force Spectroscopy†. *Langmuir* **2008**, *24* (4), 1318-1323; (n) Zhang, Y.; Yu, Y.; Jiang, Z.; Xu, H.; Wang, Z.; Zhang, X.; Oda, M.; Ishizuka, T.; Jiang, D.; Chi, L.; Fuchs, H., Single-Molecule Study on Intermolecular Interaction between C60 and Porphyrin Derivatives: Toward Understanding the Strength of the Multivalency. *Langmuir* **2009**, *25* (12), 6627-6632; (o) Janke, M.; Rudzevich, Y.; Molokanova, O.; Metzroth, T.; Mey, I.; Diezemann, G.; Marszalek, P. E.; Gauss, J.; Bohmer, V.; Janshoff, A., Mechanically interlocked calix[4]arene dimers display reversible bond breakage under force. *Nat Nano* **2009**, *4* (4), 225-229; (p) Yu, Y.; Yao, Y.; Wang, L.; Li, Z., Charge-Transfer Interaction between Poly(9-vinylcarbazole) and 3,5-Dinitrobenzamido Group or 3-Nitrobenzamido Group. *Langmuir* **2010**, *26* (5), 3275-3279; (q) Lussis, P.; Svaldo-Lanero, T.; Bertocco, A.; Fustin, C.-A.; Leigh, D. A.; Duwez, A.-S., A single synthetic small molecule that generates force against a load. *Nat Nano* **2011**, *6* (9), 553-557; (r) Walhorn, V.; Schafer, C.; Schroder, T.; Mattay, J.; Anselmetti, D., Functional characterization of a supramolecular affinity switch at the single molecule level. *Nanoscale* **2011**, *3* (11), 4859-4865; (s) Gomez-Casado, A.; Dam, H. H.; Yilmaz, M. D.; Florea, D.; Jonkheijm, P.; Huskens, J., Probing Multivalent Interactions in a Synthetic Host-Guest Complex by Dynamic Force Spectroscopy. *Journal of the American Chemical Society* **2011**, *133* (28), 10849-10857; (t) Svaldo-Lanero, T.; Duwez, A.-S., The pulling force of a tiny synthetic molecular machine. *Europhysics News* **2013**, *44* (3), 20-22; (u) Van Quaethem,

-
- A.; Lussis, P.; Leigh, D. A.; Duwez, A.-S.; Fustin, C.-A., Probing the mobility of catenane rings in single molecules. *Chemical Science* **2014**, *5* (4), 1449-1452; (v) Chung, J.; Kushner, A. M.; Weisman, A. C.; Guan, Z., Direct correlation of single-molecule properties with bulk mechanical performance for the biomimetic design of polymers. *Nat Mater* **2014**, *13* (11), 1055-1062; (w) Kuo, T.-Y.; Tseng, W.-H.; Chen, C.-h., Force Spectroscopy of Metal–Crown Ether Multivalency: Effect of Local Environments on Energy Landscape and Sensing Kinetics. *Angewandte Chemie International Edition* **2015**, *54* (32), 9213-9217; (x) Gensler, M.; Eidamshaus, C.; Galstyan, A.; Knapp, E.-W.; Reissig, H.-U.; Rabe, J. P., Mechanical Rupture of Mono- and Bivalent Transition Metal Complexes in Experiment and Theory. *The Journal of Physical Chemistry C* **2015**, *119* (8), 4333-4343; (y) Hosono, N.; Kushner, A. M.; Chung, J.; Palmans, A. R. A.; Guan, Z.; Meijer, E. W., Forced Unfolding of Single-Chain Polymeric Nanoparticles. *Journal of the American Chemical Society* **2015**, *137* (21), 6880-6888.
- 12 Giannotti, M. I.; Vancso, G. J., Interrogation of Single Synthetic Polymer Chains and Polysaccharides by AFM-Based Force Spectroscopy. *ChemPhysChem* **2007**, *8* (16), 2290-2307.
- 13 (a) Duwez, A.-S.; Cuenot, S.; Jerome, C.; Gabriel, S.; Jerome, R.; Rapino, S.; Zerbetto, F., Mechanochemistry: targeted delivery of single molecules. *Nat Nano* **2006**, *1* (2), 122-125; (b) Grandbois, M.; Beyer, M.; Rief, M.; Clausen-Schaumann, H.; Gaub, H. E., How Strong Is a Covalent Bond? *Science* **1999**, *283* (5408), 1727-1730.
- 14 Maurizot, V.; Linti, G.; Huc, I., Solid state characterization of oligopyridine dicarboxamide helicates. *Chemical Communications* **2004**, (8), 924-925.

V Photophysics of Foldamers

1 Introduction

Due to the abuse and shortcoming of fossil fuels and the resultant growing abomination to global environment which have been causing urgent desideratum of clean energy, pollution-free and sustainable energetic stream, such as solar power, is catching more and more attention from all over the world.¹ In Nature, plants and bacterial can make use of photosynthesis to store energy.^{1e, 2} Inspired by Nature, researchers have been exploring the artificial materials that can mimic the functions of those natural plants and that are also able to store the solar energy. A large variety of materials which convert solar energy into a preservable form have been explored.^{1a, 1c, 1e, 3} Around these materials, a significant branch is the supramolecular-structure-based material that is able to absorb solar energy which induces the electron transfer in supramolecular structures, and to store this energy into its supramolecular architectures as electricity.¹ Being explored for application in photo-induced electron transfer (PET) through typical donor-bridge-acceptor (D-B-A) systems, supramolecular materials have been extensively investigated with different donor moieties⁴, bridge molecular components⁵ and acceptor subunits^{3c, 6}. In these D-B-A systems, generally, irradiating these molecules by light could initialize transfer of electron from donor to acceptor in a single-step, i.e. superexchange mechanism or by a multistep hopping from donor to bridge and then finally to acceptor.^{3b, 7} In other words, a key role in electron transfer is performed by the electronic structure (determined by chemical structure⁸) of the molecular bridge units.⁹ The related characteristic properties of PET have been already studied theoretically¹⁰ and experimentally.¹¹ From Fermi Golden Rule¹² and Marcus theory¹³, PET can be influenced not only by the free energy change ΔG and the energy difference ΔE between the bridge-localized intermediate state and the initial/final states of this system, but also by number of modular repeat units of the bridge.⁷ No matter how the repeat units link with one another: cofacially or colinearly, the number of them undoubtedly alters the length of resulting bridge. In turn manipulation towards the length of bridge would affect the properties of PET, for example, the rates of charge

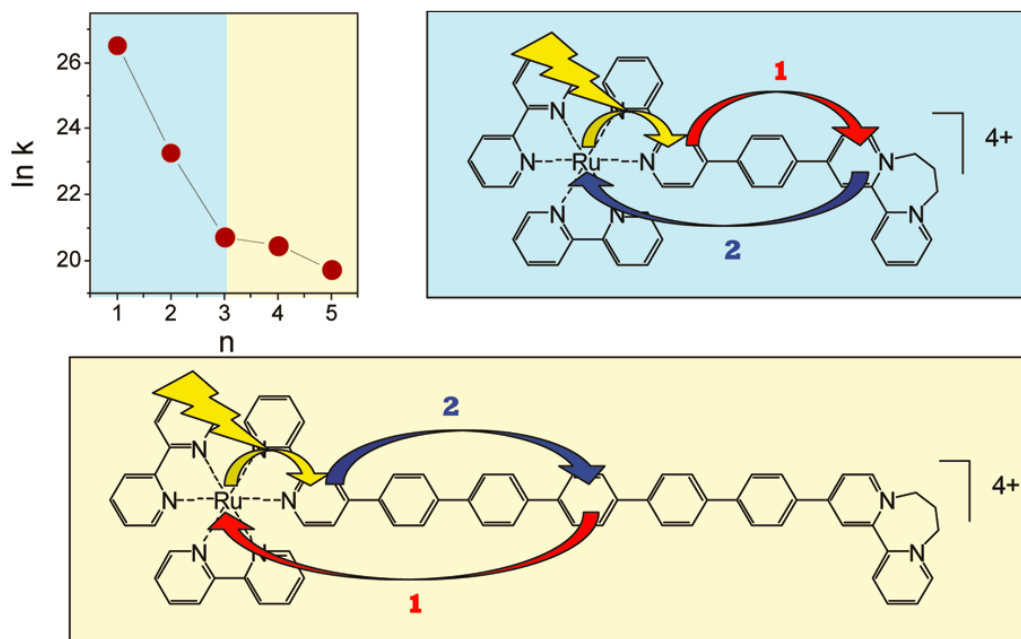


Figure 1 Scheme of oligo-*p*-phenylene-bridged D-B-A electron transfer system: a Ru(II) polypyridine unit working as electron donor (D), oligo-*p*-phenylene (1-5 units) as bridge (B) and a cyclodiquaternarized 2,2'-bipyridine (DQ²⁺) as electron acceptor (A).¹⁴

separation (CS) and charge recombination (CR).⁷ Increment of bridge length, sometimes, caused the drop of rate of CS, but randomly affected the rate of CR (Figure 1).^{8b, 14} When increasing the length of conjugated bridge, the electronic coupling among the repeat units of bridge can be strengthened, lead to decreasing LUMO of bridge and increasing HOMO of bridge, and further cause the crossover of electron transfer mechanism (from single-step superexchange to multiple-steps hopping).^{7, 9, 15}

Short quinoline-based foldamers (with 2, 4, 5 and 9 quinoline units) have been demonstrated to have the ability to work as bridge to transport the electron, after functionalized with oligo *p*-phenylene vinylene (OPV) as electron donor and perylene bisimide (PB) as electron acceptor.¹⁶ Owing to the rigidity and the predictability of backbone structure, quinoline-based foldamers have enabled the electron donor OPV and acceptor PB to separate in a predesigned distance. Its helical property has also allowed to handle the spatial orientations of OPV and PB. There, the robust structure of foldamer was found to have a handle on the distance between OPV and PB. Meanwhile, the relative orientation in space between OPV and PB was also found to be able to influence the performance of electron transfer through those foldamer-bridged D-B-A systems.

Electron transfer was established that a low attenuation factor ($\beta=0.05$) could be ascribed, even in the longer homologues. The ensemble of the findings are commensurate with charge separation occurring via a superexchange mechanism, where electron transfer from donor to acceptor proceeds *via* “virtual” orbitals localized on the bridge, even though the bridge does not figure as a real intermediate in the electron-transfer process.¹⁶ It is worthy to note here that both the rates of CS and CR were found to be very fast and that the rate of CR is lower than that of CS, which unveils the excited states of foldamer-bridge D-B-A systems tend to be more and more stable as length of foldamer increases. Therein, if negligence of the performance of the shortest system (foldamer bridge with 2 quinoline units, OPV-Q₂-PB) firstly, wherever in chloroform or toluene and how ever though space or foldamer bridge, both the rates of CS and CR decreased from OPV-Q₄-PB to OPV-Q₅-PB, but increased for OPV-Q₉-PB. But, if exclusion of the performance of the longest system OPV-Q₉-PB, the rate of CS seems to reveal that these foldamer-bridge systems follow the single-step superexchange mechanism. When all these four systems are discussed together, chaos comes out and no uniform interpretation could be reached.¹⁶

Attempting to find out what the relationship is between the length of foldamer-bridge and the corresponding mechanism of electron transfer and how the electron transports through the long foldamer birdges, further investigations have been carried out here. By employing longer quinoline-based foldamers as bridge, a variety of D-B-A systems of foldamer-bridges functionalized with electron donor OPV and electron acceptor PB have been synthesized. In order to avoid the orientation issue between electron donor and electron acceptor, special design of foldamer-bridges has been made – increment of 5 quinoline units for each foldamer molecule. The robust and steady backbone of quinoline-based foldamers permit the distance between donor OPV and acceptor PB to be stable during PET characteristics.¹⁶⁻¹⁷ In cooperation with Dr. Sergey Denisov and Dr. Nathan D. McClenaghan from Institut des Sciences Mol éculaires, Bordeaux, France, results from fluorescence quenching and transient absorption spectroscopy revealed the fast charge separation and extremely slow charge recombination in this series of compounds, and meanwhile indicated the mechanism of electron transfer in these OPV-Q_n-PB compounds is multiple-step hopping mechanism.

2 Synthesis and Measurements

2.1 Synthesis

In cooperation with Dr. Markandeya Nagula, the foldamer-bridged electron transfer systems were designed as OPV- Q_n -PB, where OPV is electron donor oligo(*p*-phenylene vinylene), Q_n stands for quinolone-based foldamer bridge and n is the number of quinoline units and PB means electron acceptor perylene bisimide (Figure 3). They have been prepared following the approaches mentioned below.

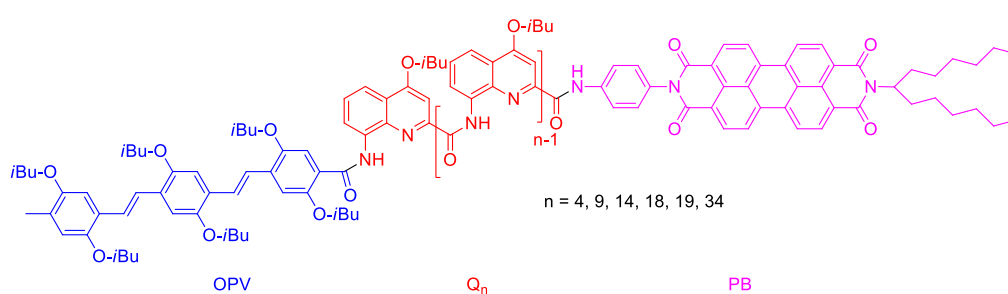


Figure 3 The quinolined-based foldamer-bridged electron transfer systems, OPV- Q_n -PB.

First of all, the electron acceptor, perylene bisimide, was synthesized by combining the methods in literatures.¹⁸ By oxidation with $LiAlH_4$, dihexyl ketone was transformed into tridecan-7-amine¹⁸ⁱ with which perylene dianhydride reacted to form symmetrical perylene bisimide. After hydrolysis and dehydration, one tridecan-amine of this symmetrical perylene bisimide can be removed and from monoamide-perylene monoanhydride, the anhydride group of which reacted with an amino group of *p*-phenylenediamine, generating the target compound, an asymmetrical perylene bisimide (PB) (Figure 4).

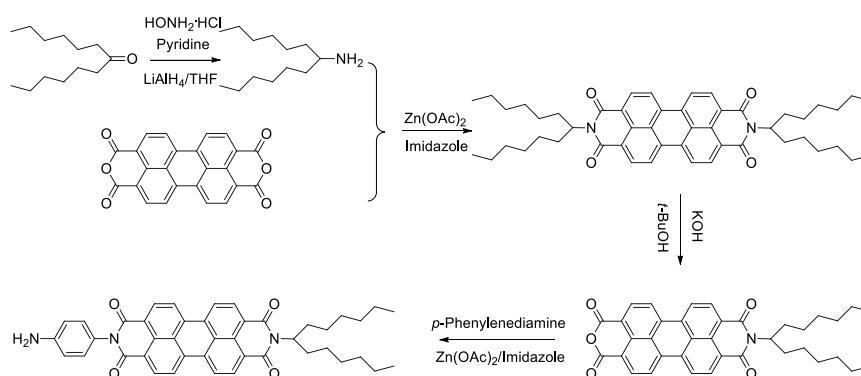


Figure 4 The synthesis of electron acceptor, asymmetrical perylene bisimide.

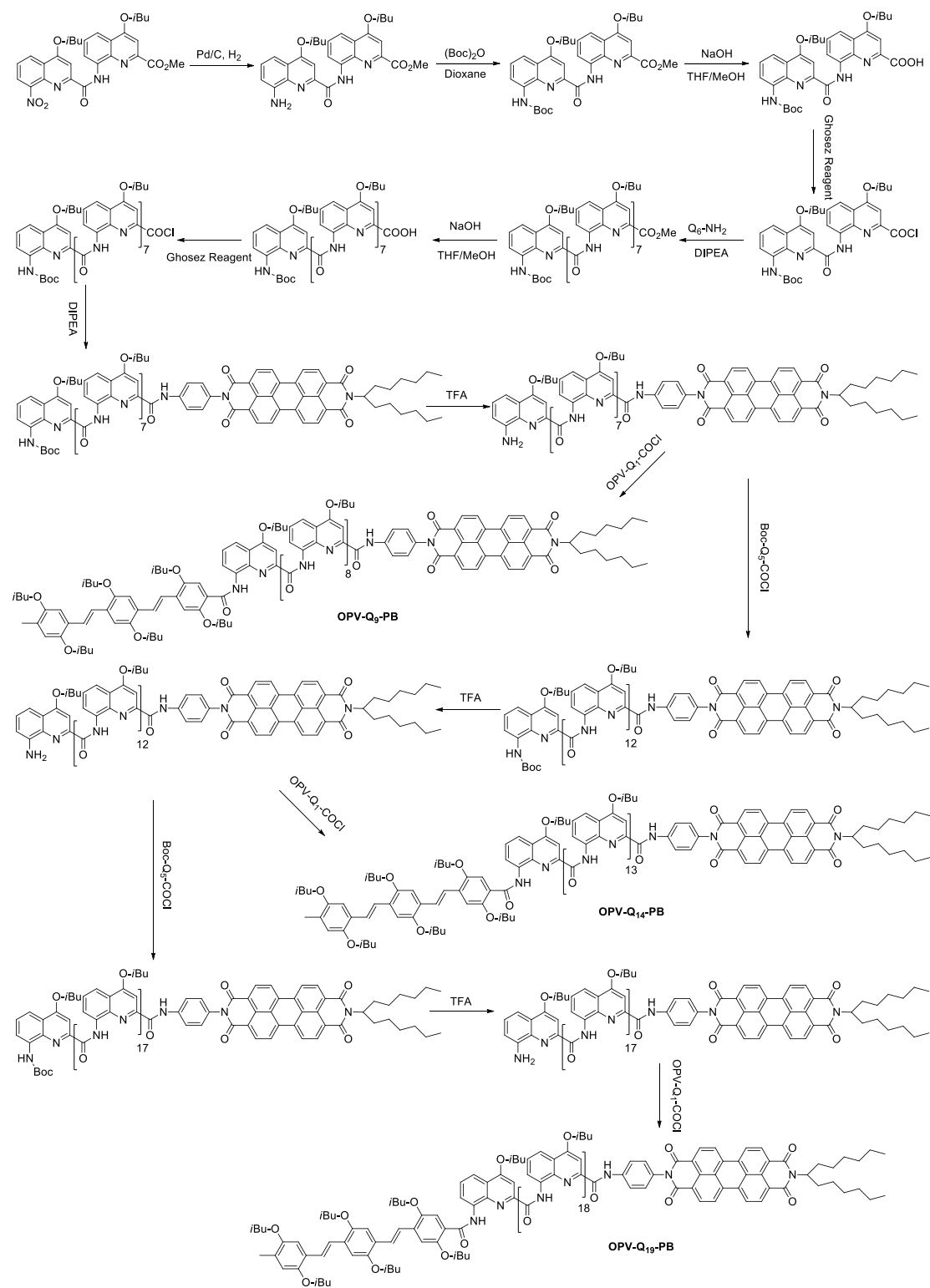


Figure 5 One synthesis procedure of electron transfer molecular systems bridged by quinolone-based foldamers with various lengths.

As shown in Figure 5, Boc-protected octamer, Boc-NH-Q₈-OMe, was synthesized by coupling hexamer amine Q₆-NH₂,^{17d} with Boc-protected dimer acid chloride, Boc-NH-Q₂-COCl, in the

presence of base DIPEA. Combination of this resulting Boc-protected octamer acid chloride Boc-NH-Q₈-COCl with PB generated a key intermediate compound Boc-NH-Q₈-PB. With kind assistance from Dr. Markandeya Nagula, this compound was deprotected with TFA and coupled with OPV-Q₁-COCl in the presence of DIPEA, giving rise to the first target product: electron donor-acceptor pair functionalized nonamer, OPV-Q₉-PB. The extension of chain of Boc-NH-Q₈-PB was carried out through adding Boc-protected pentamer acid chloride Boc-Q₅-COCl to H₂N-Q₈-PB, forming Boc-protected and PB-functionalized tridecamer Boc-NH-Q₁₃-PB. It coupled with OPV-Q₁-COCl, yielding the second target product: electron donor-acceptor pair functionalized tetradecamer, OPV-Q₁₄-PB. Similarly, the further elongation can be realized by coupling deprotected Boc-NH-Q₁₃-PB, namely H₂N-Q₁₃-PB, with Boc-protected pentamer acid chloride Boc-Q₅-COCl, yielding Boc-protected PB-functionalized foldamer, Boc-NH-Q₁₈-PB. After adding OPV-Q₁-COCl to this functionalized 18mer, the third target product, electron donor-acceptor pair functionalized nonadecamer, OPV-Q₁₉-PB, was obtained.

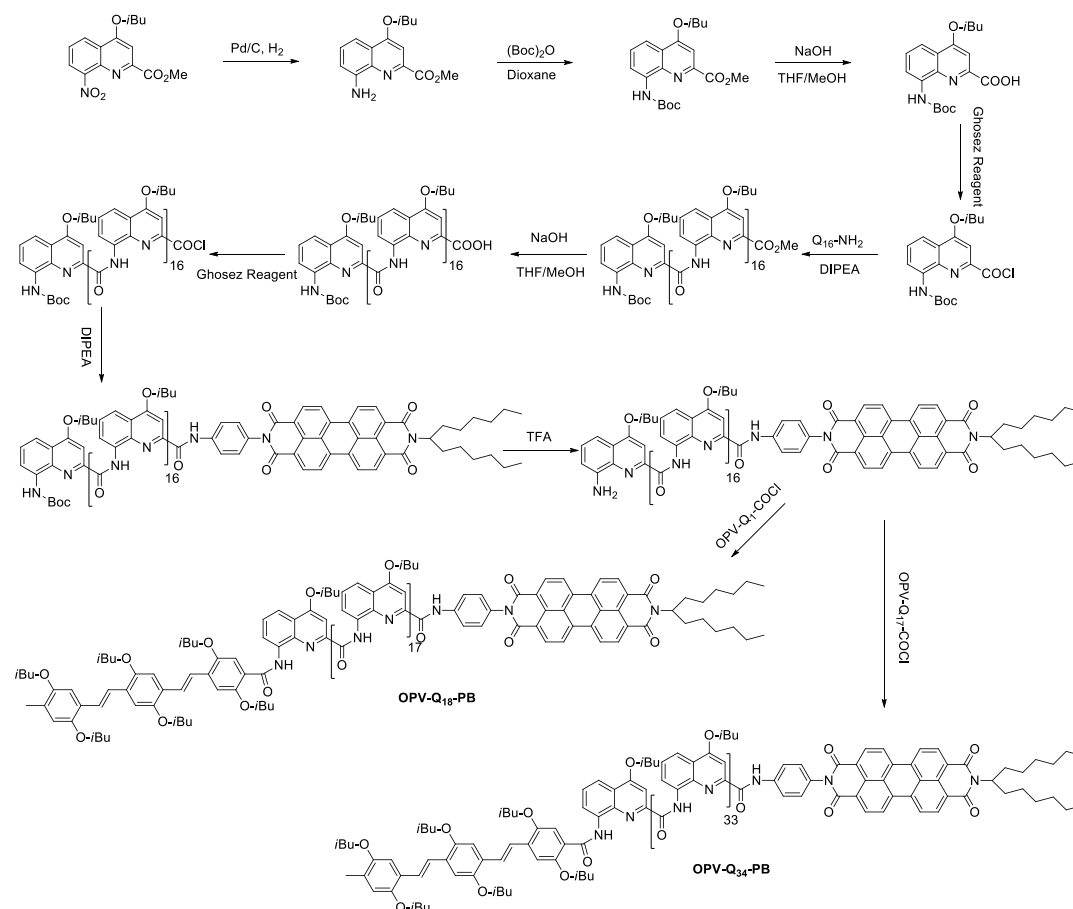


Figure 6 Another synthesis procedure of electron transfer molecular systems bridged by quinolone-based foldamers with various lengths.

Boc-protected quinoline monomer acid chloride Boc-NH-Q₁-COCl reacted with 16mer amine Q₁₆-NH₂, producing Boc-protected 17mer, Boc-NH-Q₁₇-OMe, functionalization of which with PB yielded intermediate Boc-NH-Q₁₇-PB. With help of Dr. Markandeya Nagula, Combination of H₂N-Q₁₇-PB with OPV-Q₁-COCl and OPV-Q₁₇-COCl provided the last two target products, electron donor-acceptor pair functionalized nonadecamer OPV-Q₁₉-PB and tetratriacontamer OPV-Q₃₄-PB, respectively (Figure 6).

2.2 Measurement

In collaboration with Dr. Sergey Denisov in Dr. Nathan D. McClenaghan's group at Institut des Sciences Moléculaires (ISM) in Bordeaux, France, the investigation of photoinduced electron transfer through foldamers has been carried out by employing fluorescence spectroscopy, transient absorption spectroscopy and theoretical simulations. A brief theoretical introduction of these measurements is described as follows.

3 Results and discussion

The five target compounds OPV-Q_n-PB (n = 9, 14, 18, 19 and 34) were prepared with help of Dr. Markandeya Nagula by following the approaches mentioned above (Figure 7). The quinoline-based foldamers form a helical conformation where approx. 2.5 quinoline units can construct a turn in space and the distance between two turns is about 3.5 Å. The electron donor OPV and the electron acceptor PB were covalently combined at the terminals of these foldamers, assembling OPV-Q_n-PB. According to the former research, as the bridge foldamers are short (n ≤ 9), the orientations of OPV and PB in space is crucial for the electron transfer in OPV-Q_n-PB systems, having a serious effect on the rates of CS.¹⁶ In order to avoid changing the orientations of OPV and PB in space, difference of multiple of five quinoline units (2 turns) in foldameric sequences was designed, resulting in foldamers with 9, 14, 19 and 34 quinoline units. In this series of foldamers, the orientations of OPV and PB can almost keep constant. As a reference compound of dissimilar orientations of OPV and PB in space, OPV-Q₁₈-PB was also designed and examined correspondingly. It is worthy to note that the distance between OPV and PB through foldamer bridge (D_{bridge}) is apparently larger than through space (D_{space}) due to the helical structures of foldamers (Table 1). Additionally, analogous molecules Q_n-PB (n = 1, 2, 4, 8 and 17) without electron donor OPV were also investigated to avoid its electronic effects on quinoline units and work as reference compounds.

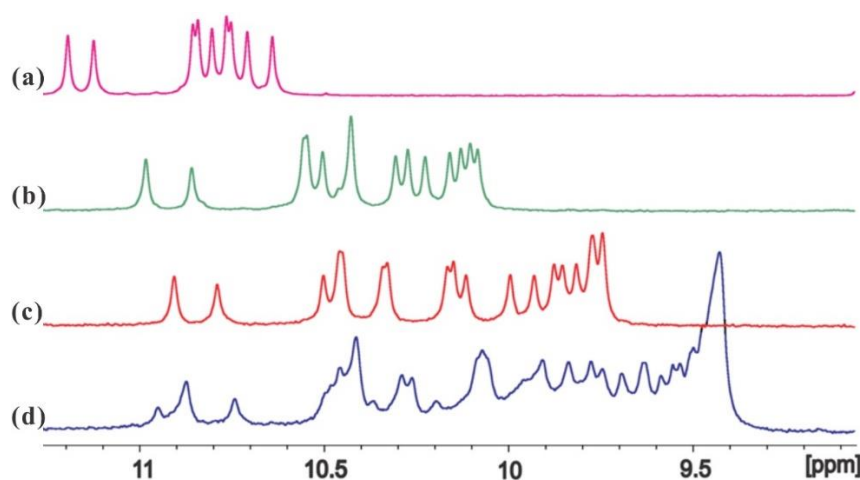


Figure 7 Excerpt of ¹H NMR (300 MHz) spectra showing amide NH region of OPV-Q₉-PB (a), OPV-Q₁₄-PB (b), OPV-Q₁₉-PB (c) and OPV-Q₃₄-PB (d)

Table 1 The distances between donor OPV and acceptor PB through space (D_{space}) and helical foldamer bridge (D_{bridge}), and the dihedral angles between OPV and PB (Φ_{DA}).

Compound	D_{space} (Å)	D_{bridge} (Å)
OPV-Q ₉ -PB	14	69
OPV-Q ₁₄ -PB	21	105
OPV-Q ₁₈ -PB	28	134
OPV-Q ₁₉ -PB	40	142
OPV-Q ₃₄ -PB	52	250

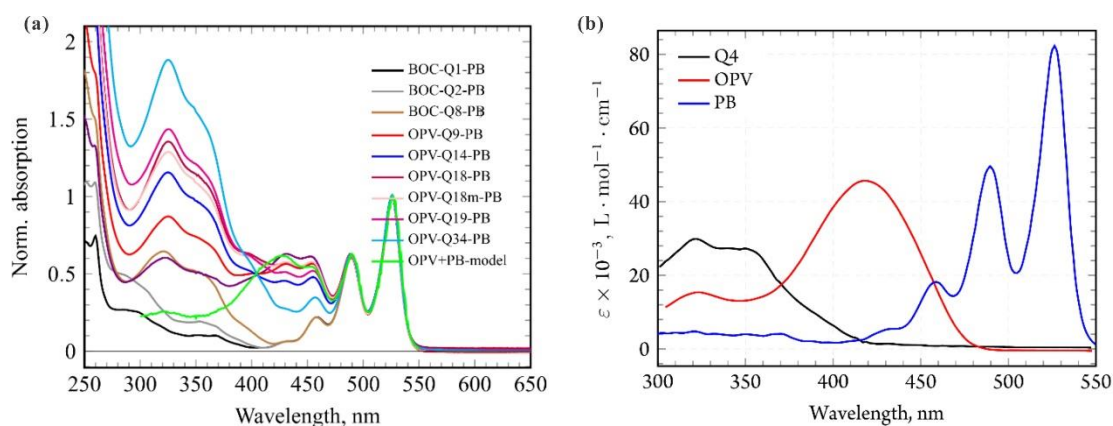


Figure 8 (a) The normalized UV/Vis absorption spectra of OPV-Q_n-PB ($n = 9, 14, 18, 19$ and 34), Boc-Q_n-PB ($n = 1, 2$ and 8) and (b) the reference compounds: OPV, PB and quinoline-based foldamer (4mer) at 525 nm.

The UV/Vis absorption spectra of these five OPV-Q_n-PB compounds have been measured in chloroform and shown in Figure 8, and three obvious absorption regions are displayed: quinoline part ($250 - 400$ nm), OPV part ($350 - 450$ nm), and PB part ($450 - 550$ nm). Quinoline part displays an increase in molar absorption coefficient with the increment of foldamer bridge length. The chromophores parts, namely OPV and PB parts, exhibit relative stable absorption intensity on the whole and only small fluctuations in molar absorption coefficient, which is probably caused by the changes in electronic structure and environment due to the elongation of bridge. Nevertheless, the structure and spectral position of the vibronic bands keep the same for all these compounds, and the intensity and position of PB indicate the invariable quantity of PB in all compounds. The UV/Vis absorption spectra are able to present this characteristic vibronic progression even at high concentration (1.5×10^{-5} M), which ensures the further photophysical analysis not to be hampered by any aggregation of these compounds.

The fluorescence quenching experiments of PB were carried out to test the electron transfer firstly with evaluation of the quantum yield (QY) and the lifetime (τ) of PB. Corresponding fluorescence quenching results with excitation of 532 nm light in CH_2Cl_2 are shown in Figure 9, and the relative QY and τ are collected in Table 2. The fluorescence of PB were diminished dramatically (Figure 9) and the steady-state QY measurements are found to be in a good agreement with time-resolved PB fluorescence lifetime measurements (Table 2), emission lifetimes for PB in CH_2Cl_2 has been reduced to around 60 ps for all studied compounds. This degree of lifetime decrease corresponds well with the level of quenching observed *via* steady-state measurements of fluorescence quantum yield in both CH_2Cl_2 and CHCl_3 solvents, showing a decrease of quantum yield of ca. 150-fold with respect to the parent PB. It must be noted that compound Q₈-PB shows the similar QY and τ to other OPV-Q_n-PB compounds, which reveals that the fluorescence of PB is quenched by the electron not from the OPV group, but from the neighbouring quinoline group of the foldamer-bridge. Based on this result, we could conclude that the initial steps of electron transfer in these OPV-Q_n-PB compounds include 1) the excitation of electron acceptor PB, namely the formation of SOMO state of PB, and subsequently, 2) the transport of electron from quinoline group from bridge to PB (the reduction of PB by quinoline group).

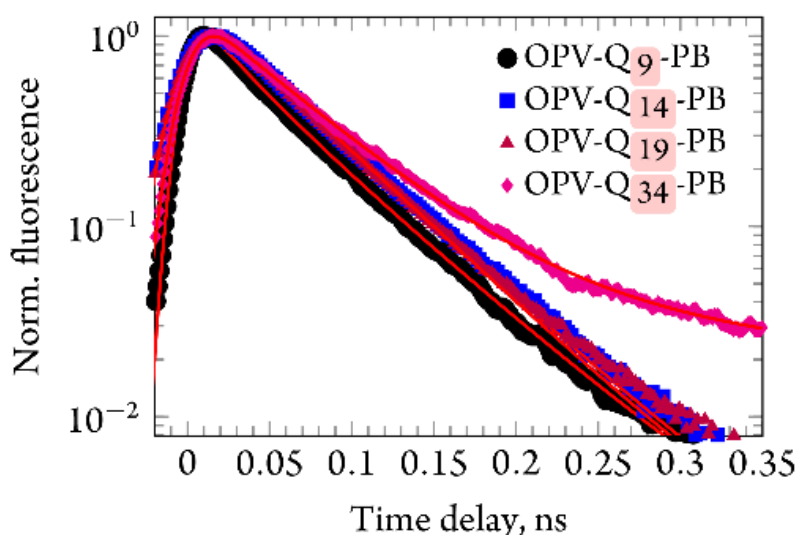


Figure 9 The Time-resolved fluorescence emission of OPV-Q_n-PB (n = 9, 14, 19 and 34) and OPV-excluded Q₈-PB.

Table 2 The quantum yields (QY) and lifetimes (τ) of the studied compounds in CH_2Cl_2 and CHCl_3 (298K), and the ground state bleaching (GSB) of OPV.

Compound	QY (%, CH_2Cl_2)	QY (%, CHCl_3)	τ (ps, CH_2Cl_2)	τ (ps, CHCl_3)	GSB of OPV (ps)
PB	0.88	0.81	4000	3850	--
Q ₈ -PB	0.006	0.006	60	61	--
OPV-Q ₉ -PB	0.006	0.005	55	56	57
OPV-Q ₁₄ -PB	0.006	0.005	60	55	140
OPV-Q ₁₈ -PB	0.007	0.006	60	57	235
OPV-Q ₁₉ -PB	0.006	0.006	55	53	370
OPV-Q ₃₄ -PB	0.006	0.007	60	60	1000

Compared to fluorescence quenching, transient absorption spectroscopy (TRABS) affords a useful approach to access the details of dynamic changes during electron transfer in OPV-Q_n-PB compounds. The TRABS experiments were operated with excitation of 532 nm light in chloroform at room temperature. As shown in Figure 9, Representative TRABS maps of some compounds are presented. For Q₈-PB (Figure 9a), after excitation of PB, the signals of PB anion-radical (absorption at 650 nm) and quinoline cation-radical (absorption at 390 nm) appeared simultaneously with lifetime of approx. 60 ps that was also confirmed with the time-resolved fluorescence quenching results aforesaid. Compound OPV-Q₉-PB also present the signal of PB anion-radical, but no signal of quinoline cation-radical. Instead, the cation-radical and the ground state-bleaching (GSB) of OPV were observed simultaneously. For compounds with longer foldamer-bridges, not only the signals of PB anion-radical, the cation-radical and the GSB of OPV were observed sequentially, but also the signal of cation-radical of quinoline appeared (at 390 nm). It is worthy to note that the appearances of OPV cation-radical and GSB are just after the disappearance of quinoline cation-radical (Figure 9c and 9d). The information given by Figure 9a reveals that once Q₈-PB is activated by external light – formation of PB SOMO, the electron from neighbouring quinoline unit transported to acceptor PB immediately, resulting in the formation of PB anion-radical and quinoline cation-radical at the same time. Compared to other OPV-Q_n-PB compound, lack of OPV group of Q₈-PB ensures the electron transported to PB is from quinoline. This conclusion also confirmed the results of fluorescence quenching of Q₈-PB mention above. As electron donor OPV was linked to foldamer molecules

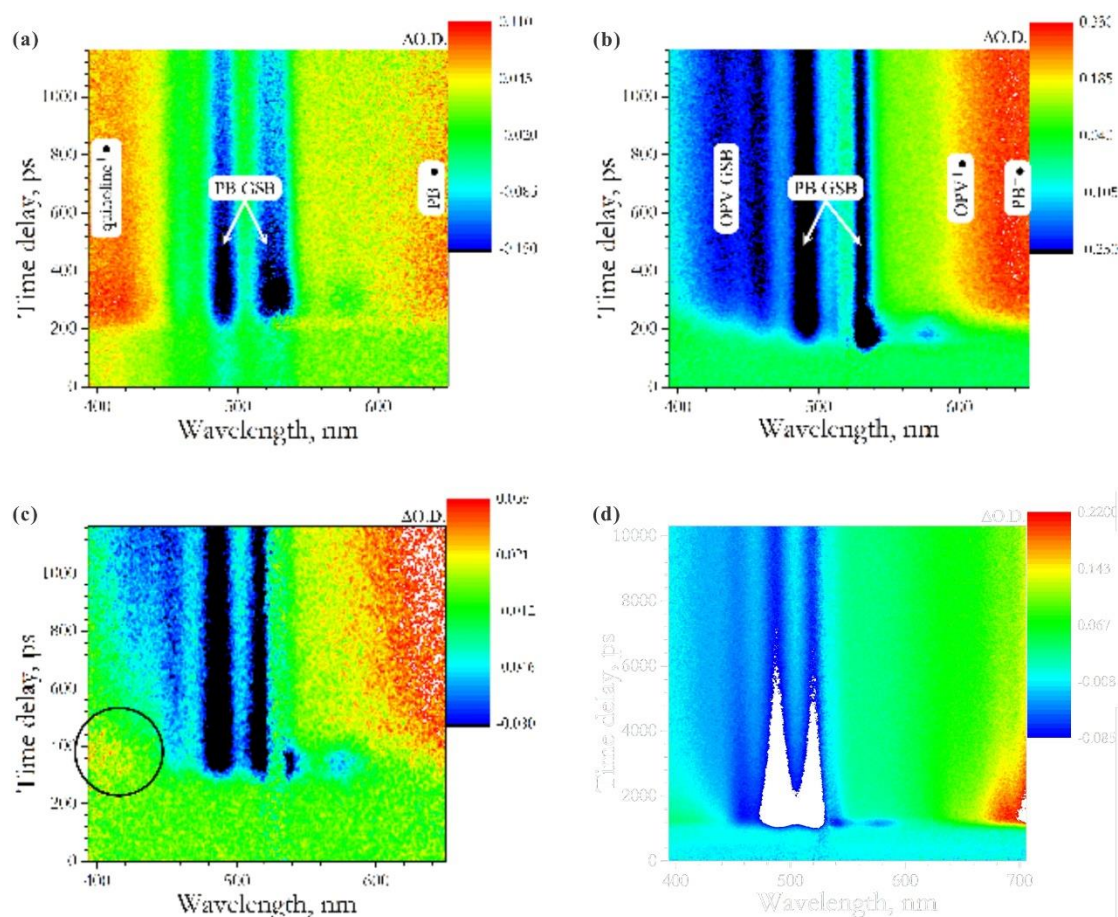


Figure 9 The TRABS maps of Q₈-PB (a), OPV-Q₉-PB (b), OPV-Q₁₉-PB (c), and OPV-Q₃₄-PB (d). Excitation wavelength is 532 nm, the solvent is CHCl₃ and the temperature is room temperature.

and these foldamers are long enough ($n = 14, 19$ and 34 , Figure 9c. For $n = 9$, see explanation below), PB cation-radical (at 650 nm) and quinoline cation-radical (at 390 nm) presented firstly. With a lifetime of approx. 60 ps, quinoline cation-radical disappeared, but immediately, OPV cation-radical (at 610 nm) appeared then. Later, GSB of OPV was detected. All these observations address us to how the electron transfers through these OPV-Q_n-PB compounds, in other words, what the relative mechanism of electron transfer is. According to these results, 4 steps could be included in the mechanism of electron transfer through these foldamer-bridge D-B-A systems: 1) excitation of electron acceptor PB after light activation and formation of SOMO state of PB; 2) electron injection from HOMO of quinoline group of foldamer bridge to SOMO of PB and appearances of PB anion-radical and quinoline cation-radical; 3) hole transfer between modular quinoline units of foldamer bridge with a random, reversible hopping way; 4)

electron transfer from donor OPV to quinoline of foldamer bridge, that is to say, hole trapping by OPV. This multiple-steps mechanism is schemed as a simplified Perrin-Jablonski diagram in Figure 10. Compared to the single-step superexchange mechanism that electron directly transfer from donor to acceptor just by one step, the apparent difference of multiple-steps hopping mechanism is the existence of quinoline cation-radical as soon as PB anion-radical shows up (Figure 9c).

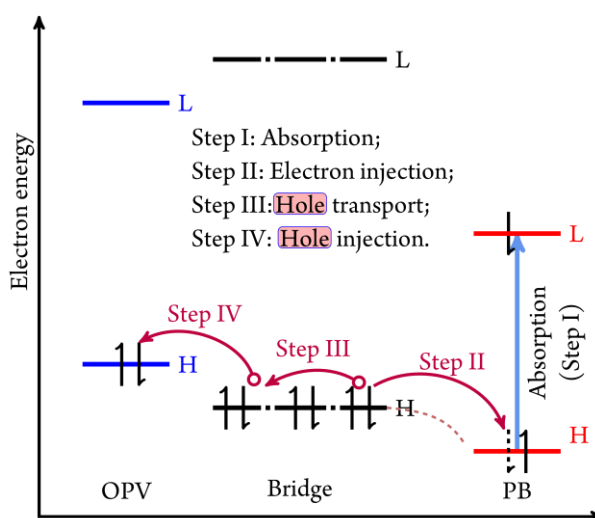


Figure 10 Scheme of multiple-steps mechanism through foldamer-bridge OPV- Q_n -PB systems with simplified Perrin-Jablonski diagram.

In the case of OPV- Q_9 -PB, the rate of electron transfer from the quinoline unit to PB is equal to that of further hole transfer from quinoline unit towards OPV ($17 \times 10^9 \text{ s}^{-1}$), which would be conducive in the case of a 9 quinoline bridge with a concerted, one step electron transfer mechanism, such as superexchange. It could be suggested that increase of foldamer bridge length leads to crossover of electron transport mechanism from single-step to multi-step. Careful study of electron transfer rate temperature dependency (Figure 12 and 13) refutes existence of such a transition (at least in the range of the foldamers that are studied herein). As can be seen for OPV- Q_9 -PB, even at 273 K a difference between rates of PB emission quenching and OPV GSB appearance is observed, showing time constants of 85 and 100 ps, respectively. At lower temperatures this difference becomes greater. Additionally, the temperature dependence of electron transfer between PB and OPV has a positive activation energy, while in

the superexchange mechanism the activation energy should show a negative value. The rate of CS should rise up with temperature decrease, which is explained by an increase of electron coupling between donor and acceptor due to eliminating thermally-induced disorder. However, the lack of activation energy cannot be exclusively indicative of superexchange mechanism absence, yet it is a strong assumption. Previous studies on shorter OPV-Q_n-PB compounds (n = 2, 4, 5) showed that charge transfer between PB and OPV is governed by a superexchange mechanism. The present investigation demonstrates the mechanism crossover from hopping to superexchange occurs at foldamers with quinoline unit ≤ 9 .

To demonstrate the mechanism of electron transfer through foldamer-bridge OPV-Q_n-PB systems is multiple-step hopping, not superexchange, the relationship between the rate of charge (electron) transfer (k_{CT}) and the length of bridge (l) come out as another approach. Generally, as charge (electron) transports through D-B-A system with single-step superexchange mechanism, the relationship between k_{ET} and l is exponential and given as:

$$k_{CT} = Ae^{-\beta l} \quad (1)$$

As charge (electron) transports through D-B-A system with multiple-step hopping mechanism, the relationship between k_{ET} and l becomes hyperbolic and expressed as:

$$k_{CT} = N^{-\eta} \quad (2)$$

For our foldamer-bridge OPV-Q_n-PB systems, the rate of electron transfer between PB and OPV was determined by tracking rate of OPV ground state bleaching appearance; the length of bridge was calculated by the number of quinoline unit multiplied by the average length of one quinoline unit. As shown in Figure 11, absence of exponential dependence of electron transfer rate on length of the bridge illustrates absence of “pure” superexchange in the systems. But the dependence of electron transfer rate on the number of modular quinoline unit shows a hyperbolic performance, especially the existence of OPV-Q₃₄-PB. It is another evidence of occurrence of the hopping mechanism through foldamer-bridge OPV-Q_n-PB systems. Meanwhile, giving the random-walk theory that is frequently applied in DNA hole transfer studies, parameter η in equation (2) varies with direction-bias: a) 2 in the case of unbiased transfer; b) $1 \leq \eta \leq 2$ for acceptor direction-biased random walk; c) $\eta > 2$ for donor direction-biased random walk. As shown in Figure 11, the value of η dropped from 2.25 to 1.1 in DCM

with decrement of temperature from 298 K to 180 K, which indicated qualitative changes in electronic properties of the bridge with temperature and consequently on hole. it is possible to bind cumulative rate of hole transfer and individual hop step: $k_{CT} \approx k_{HOP} N^\eta$, giving the rate of such a hole transfer single step at $2.5 \times 10^{12} \text{ s}^{-1}$ at 298 K or 400 fs in CH_2Cl_2 and $1.8 \times 10^{12} \text{ s}^{-1}$ or 560 fs for CHCl_3 .

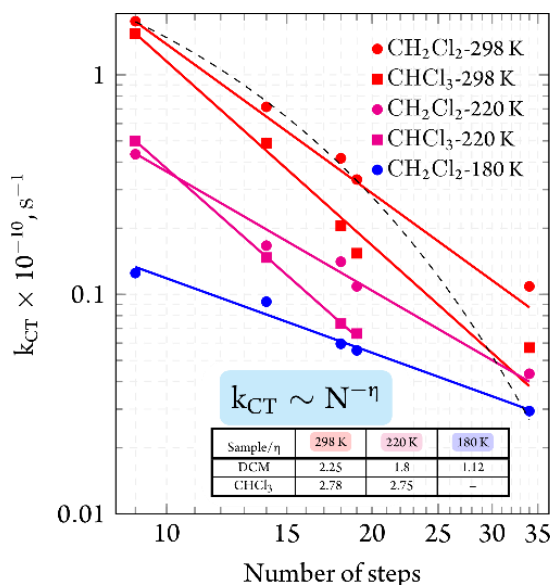


Figure 11 The relationship between electron (charge) transfer rate (OPV-PB) and the number of modular quinoline unit of foldamer-bridge at various temperature and in CH_2Cl_2 and CHCl_3 (dashed line is exponential fit).

Time-resolved fluorescence quenching and TRABS experiments were conducted under diverse temperature in chlorinated solvents (from 180K to 298 K in DCM and from 210 K to 298 K in CHCl_3 , respectively). These conducted experiments permitted determination of the activation energies of electron transfer processes according to Marcus theory of electron transfer in the non-adiabatic regime, because quinoline-quinoline and quinoline-PB electron coupling is weak:

$$k_{CT} = \frac{2\pi}{\hbar} V_{eff}^2 \sqrt{\frac{1}{4\pi\lambda k_B T}} \exp\left(\frac{-\Delta G^\ddagger}{k_B T}\right) \quad (3)$$

where $\Delta G^\ddagger = (\lambda + \Delta G^{RP})/4\lambda$, ΔG^{RP} is the free energy change of radical ion pair formation, λ is the reorganization energy. Experiments were performed in low polarity solvents, and due to the large size of the chromophore, λ is assumed to be dominated by inner-sphere reorganization. Post-treated experimental results, temperature dependence of charge separation and

fluorescence quenching rates, are presented in Figures 12 and 13, respectively, plotted $1/T$ versus logarithmic plot $k_{CT}\sqrt{T}$.

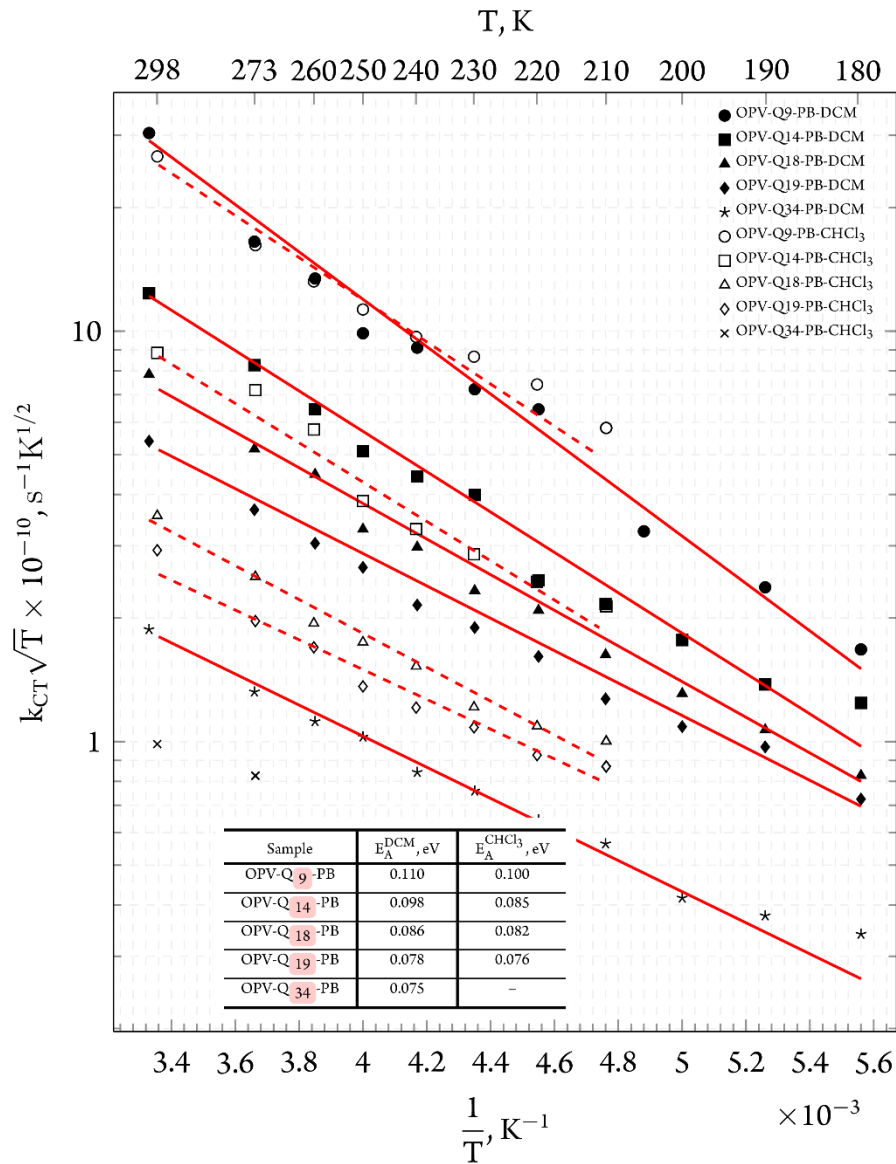


Figure 12 Temperature dependence of charge separation rates between OPV and PB in CH_2Cl_2 and $CHCl_3$, calculated from the rate of OPV GSB appearance ($\lambda_{exc}=532$ nm).

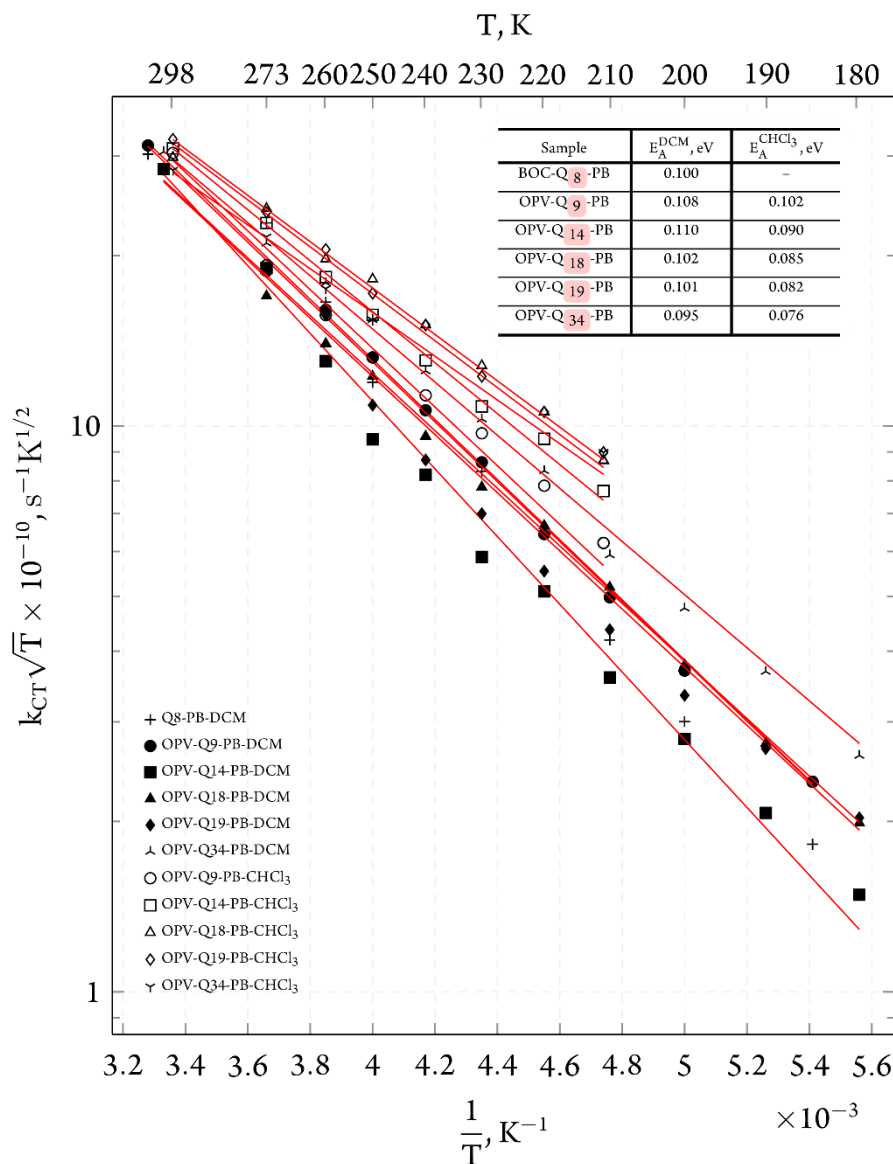


Figure 13 Temperature dependence of the charge injection rate from the quinoline bridge into excited PB low-lying SUMO, calculated from emission rates ($\lambda_{\text{exc}}=532 \text{ nm}$, $\lambda_{\text{obs}}=575 \text{ nm}$) of PB.

The charge separation (CS) of these studied OPV-Q_n-PB is formed in the sub-nanosecond and nanosecond ranges, while charge recombination (CR) occurs much more slowly. The TRABS map (Figure 14) for OPV-Q₉-PB in CHCl₃ shows that the absorption bands corresponding to PB anion-radical (centered at 720 nm) and OPV cation-radical (centered at 625 nm) are relaxing with the same time constants, $\tau = 180 \text{ ns}$. In more polar CH₂Cl₂ solvent, this relaxation time constant equals to 450 ns. PB anion-radical relaxation is accompanied by the formation of the PB triplet state, which is characterized by intense absorption, centered at 500 nm. The absorption band of OPV cation-radical and PB anion-radical for OPV-Q₁₄-PB and OPV-Q₁₉-

PB⁻, are observed even at >80 μ s after excitation pulse, which is equally valid for the OPV-Q₃₄-PB sample. This demonstrates an extremely long time of charge separation in the case of samples longer than 9 quinoline units. The relaxation of the PB triplet state occurs on a much longer timescale – hundreds of microseconds with a time constant >340 μ s for OPV-Q₉-PB and >420 μ s for the rest OPV-Q_n-PB triads (n=14, 18, 19, 34).

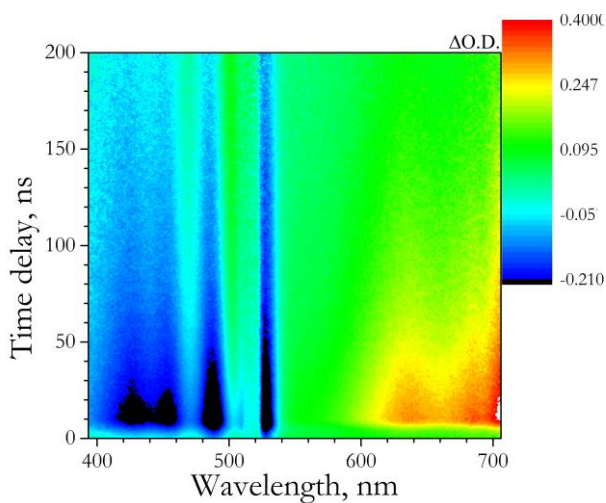


Figure 14 TRABS maps of charge recombination in OPV-Q₉-PB (CHCl₃, λ_{exc} =532 nm)

4 Conclusion

Supramolecular systems based on nanosized foldamers bearing electron donor OPV and electron acceptor PB have been synthesized successfully with 9, 14, 18, 19 and 34 quinoline units, respectively. The time-resolved characterization of charge separation between electron donor OPV and acceptor PB in the sub-nanosecond timescale through these foldamer-bridges was further carried out in solvents with different polarity (CHCl_3 and CH_2Cl_2) at different temperatures. The analysis of experimental data from fluorescence quenching demonstrated that the rates of charge separation in these OPV- Q_n -PB systems are still fast (nanosecond scale) and the rate of charge recombination take place with an extremely slow speed (microsecond scale). Meanwhile, the data of fluorescence quenching and TRABS revealed that the general mechanism of electron transfer leading to a charge separated state in these OPV- Q_n -PB systems could be described by a multiple-step principle, namely hopping mechanism.

5 Experiments

5.1 Methods of NMR

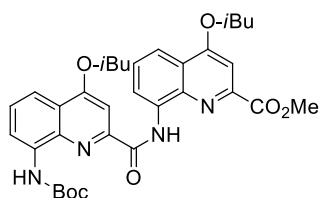
NMR data were recorded at 300 MHz using an Avance II NMR spectrometer (Bruker Biospin) with a vertical 7.05T narrow-bore/ultrashield magnet operating at 300 MHz for ^1H observation and 75 MHz for ^{13}C observation by means of a 5-mm direct BBO H/X probe with Z gradient capabilities. All chemical shifts are quoted in parts per million (ppm, δ) relative to the ^1H residual signal of the deuterated solvent used (CDCl_3 at 7.26 ppm). ^1H NMR splitting patterns with observed first-order coupling are designated as singlet (s), doublet (d), double doublet (dd), triplet (t), or quartet (q). Splitting patterns that could not be interpreted or easily visualized are designated as multiplet (m) or broad (br). Coupling constants (J) are reported in hertz. Samples were not degassed. Data processing was performed with Topspin 2.0 software.

5.2 Methods of Chemical Synthesis

All reactions were carried out under a dry nitrogen environment. Chemicals and reagents were used as commercially supplied without any further purification unless otherwise stated. Dichloromethane (DCM), Tetrahydrofuran (THF) and Toluene were dried over alumina columns under nitrogen. Chloroform, triethylamine (Et_3N) and diisopropylethylamine (DIPEA) were distilled over calcium hydride (CaH_2) prior to use. Reactions were monitored by thin layer chromatography (TLC) on Merck silica gel 60-F254 plates and observed under UV light (254 and 365 nm). Column chromatography was carried out on Merck GEDURAN Si60 (40-63 μm). Circular chromatography purifications were carried out on Chromatotron® with silica gel, Merck grade 7749, TLC grade with binder and fluorescent indicator. Analytical and semi-preparative GPC was carried out on Shimadzu Recycling GPC system equipped with LC-20 AD pump, SPD-M20A UV detector and a set of 1H, 1.5H, 2.5H and 3H columns (size: 20 \times 600 mm) in chloroform/0.5~1% ethanol as eluent with a flow rate of 3.5 mL/min. ESI and MALDI mass spectra were obtained on a Waters LCT Premier and a Bruker Reflex III spectrometers respectively, from the Mass Spectrometry Laboratory at the European Institute of Chemistry

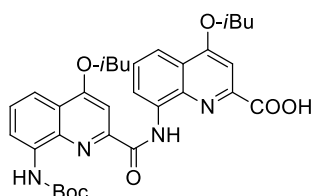
and Biology (UMS 3033 - IECB), Pessac, France and a Voyager DE-STR mass spectrometer from AB Sciex, Les Ulis, France.

5.2.1 Synthesis of Boc-protected octamer, Boc-NH-Q₈-OMe



Boc-NH-Q₂-OMe. Dimer amine (Q₂-NH₂, 1.79 g, 3.46 mmol)[] was mixed with di-tert-butyl carbonate ((Boc)₂O, 2.26 g, 10.4 mmol) and di-isopropal-ethylamine (DIPEA, 1.71 mL, 10.4 mmol) in 40 mL dioxane. The reaction was allowed to process

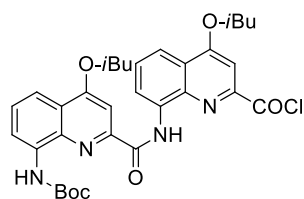
under refluxing until complete. More (Boc)₂O could be added to accelerate the protection. After purifying with silica gel column (eluent: cyclohexane/ethylacetate = 20/1 to 5/1), a pale yellowish solid was obtained as the product (1.89 g, 88.9% yield). ¹H NMR (300 MHz, CDCl₃): δ 12.42 (s, 1H), 9.02 (s, 1H), 8.89 (dd, *J* = 3.27, 4.39 Hz, 1H), 8.48 (dd, *J* = 3.33, 4.44 Hz, 1H), 7.99 (dd, *J* = 3.63, 4.82 Hz, 1H), 7.91 (dd, *J* = 3.60, 4.80 Hz, 1H), 7.77 (s, 1H), 7.68 (t, *J* = 8.05 Hz, 1H), 7.65 (s, 1H), 7.58 (t, *J* = 8.12 Hz, 1H), 4.14 (s, 1H), 4.12 (s, 1H), 4.11 (s, 1H), 4.08 (s, 1H), 4.03 (s, 3H), 2.39 – 2.25 (m, 2H), 1.47 (s, 9H), 1.18 (s, 3H), 1.17 (s, 3H), 1.16 (s, 3H), 1.15 (s, 3H). ¹³C NMR (CDCl₃, 75 MHz): δ 166.13, 163.70, 163.13, 162.74, 153.21, 150.11, 147.17, 139.56, 138.11, 135.39, 134.86, 128.38, 127.66, 122.34, 122.29, 117.42, 116.82, 116.02, 114.97, 101.21, 98.86, 80.67, 75.33, 75.29, 52.99, 46.25, 28.24, 28.19, 19.26, 11.50.



Boc-NH-Q₂-COOH. 155 To the solution of ester **Boc-NH-Q₂-OMe** (1.89 g, 3.07 mmol) in 80 mL THF/MeOH (3/1, v/v) was added base NaOH (0.430 g, 7.68 mmol). This reaction was monitored by ¹H NMR until it came to complete, and then

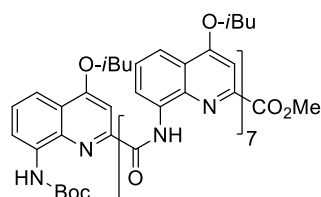
quenched by citric acid. Subsequent removal of organic solvent with rotary evaporator and washing with water and brine were followed by drying with anhydrous Na₂SO₄, yielding a pale yellowish solid as product (1.69 g, 99% yield). ¹H NMR (300 MHz, CDCl₃): δ 11.70 (s, 1H), 8.87 (d, *J* = 3.8 Hz, 1H), 8.82 (s, 1H), 8.41 (d, *J* = 3.66 Hz, 1H), 7.93 (d, *J* = 4.08 Hz, 1H), 7.83 (dd, *J* = 3.71, 4.64 Hz, 1H), 7.65 – 7.58 (m, 3H), 7.51 (t, *J* = 8.06 Hz, 1H), 4.10 (s, 1H), 4.08 (s, 1H), 4.04 (s, 1H), 4.02 (s, 1H), 2.39 – 2.23 (m, 2H), 1.55 (s, 9H), 1.18 (s, 3H), 1.16 (s, 6H), 1.14 (s, 3H). ¹³C NMR (CDCl₃, 75 MHz): δ 164.89, 163.80, 163.39, 162.61, 153.13, 149.49, 146.28, 138.39, 137.62, 135.12, 133.98, 128.33, 127.67, 122.37, 122.21, 118.75, 116.32,

114.69, 99.79, 98.78, 81.31, 77.25, 75.58, 75.16, 28.22, 19.26. HRMS (ES⁺): *m/z* calcd for C₃₃H₃₉N₄O₇ [M+H]⁺ 603.282 found 603.282.



Boc-NH-Q₂-COCl. Ghosez Reagent (1-Chloro-N,N,2-trimethyl-1-propenylamine, 0.448 mL, 3.37 mmol) was added dropwise into a solution of **Boc-NH-Q₂-COOH** (1.69 g, 2.81 mmol) in 12 mL anhydrous chloroform at 0 °C. The reaction was monitored by ¹H

NMR. After completed, the reaction is left under vacuum, removing the solvent and remaining Ghosez Reagent, producing quite pale yellowish solid as product quantitatively. ¹H NMR (300 MHz, CDCl₃): δ 11.97 (s, 1H), 9.05 (d, *J* = 3.85 Hz, 1H), 8.97 (s, 1H), 8.58 (d, *J* = 3.85 Hz, 1H), 8.00 (d, *J* = 4.18 Hz, 1H), 7.88 (d, *J* = 4.10 Hz, 1H), 7.77 – 7.73 (m, 2H), 7.56 (t, *J* = 8.06 Hz, 1H), 7.51 (s, 1H), 4.13 (s, 1H), 4.12 (s, 1H), 4.10 (s, 1H), 4.07 (s, 1H), 2.37 – 2.27 (m, 2H), 1.52 (s, 9H), 1.17 – 1.14 (m, 12H).

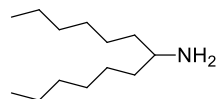


Boc-NH-Q₈-OMe. To a mixture of hexamer amine (Q₆-NH₂) (3.79 g, 2.55 mmol) and DIPEA (2.05 mL, 12.8 mmol) in 10 mL anhydrous chloroform was added the solution of **Boc-NH-Q₂-COCl** in 5 mL chloroform in 0 °C. This reaction was stirred at

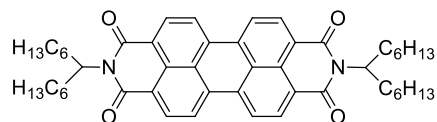
room temperature overnight and monitored by ¹H NMR. After workup with water, 0.1 M HCl, water, sat. NaHCO₃ and brine, the resulting crude was purified by silica gel column, yielding a yellowish solid (5.11 g, 97.6%). ¹H NMR (300 MHz, CDCl₃): δ 11.54 (s, 1H), 11.40 (s, 1H), 11.32 (s, 1H), 11.28 (s, 1H), 11.01 (s, 1H), 10.96 (s, 1H), 10.85 (s, 1H), 8.22 (dd, *J* = 3.32, 4.28 Hz, 1H), 8.16 (dd, *J* = 0.94, 2.11 Hz, 1H), 8.14 (dd, *J* = 0.92, 2.09 Hz, 1H), 8.12 (d, *J* = 0.46 Hz, 1H), 8.09 (d, *J* = 0.44 Hz, 1H), 7.89 (dd, *J* = 3.67, 4.72 Hz, 1H), 7.87 – 7.83 (m, 3H), 7.78 – 6.91 (m, 16H), 6.89 (s, 1H), 6.68 (s, 1H), 6.64 (s, 1H), 6.53 (s, 2H), 6.37 (s, 1H), 6.05 (s, 1H), 4.18 – 3.59 (m, 16H), 3.01 (s, 3H), 2.56 – 2.15 (m, 8H), 1.38 – 1.09 (m, 48H), 0.94 (s, 9H). ¹³C NMR (CDCl₃, 75 MHz): δ 163.72, 163.17, 162.99, 162.86, 162.79, 162.70, 162.63, 162.30, 161.93, 161.16, 160.95, 160.59, 159.45, 159.21, 159.07, 151.34, 149.83, 149.12, 149.06, 148.95, 148.76, 148.30, 145.05, 138.70, 138.04, 137.63, 137.60, 137.56, 137.49, 137.38, 136.44, 133.80, 133.62, 133.35, 133.32, 133.23, 133.01, 132.96, 132.55, 127.46, 126.82, 126.62, 126.27, 125.94, 125.90, 125.71, 122.47, 122.32, 122.29, 121.88, 121.77, 121.60,

121.42, 121.36, 116.96, 116.91, 116.82, 116.75, 116.61, 116.57, 116.10, 116.05, 116.00, 115.60, 115.29, 114.40, 114.30, 100.02, 99.22, 98.97, 98.82, 98.73, 98.07, 97.65, 97.46, 80.05, 77.25, 75.36, 75.33, 75.19, 75.02, 74.72, 53.44, 51.95, 28.29, 28.21, 28.19, 28.16, 28.11, 28.08, 28.05, 27.99, 27.62, 19.63, 19.59, 19.51, 19.47, 19.42, 19.37, 19.28, 19.24, 19.22, 19.17. HRMS (ES⁺): m/z calcd for C₁₁₈H₁₂₄N₁₆O₁₉ [M]⁺ 2070.930 found 2070.934.

5.2.2 Synthesis of asymmetric perylene bisimide.



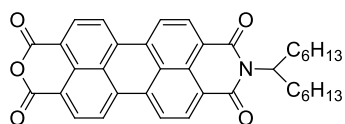
Tridecan-7-amine. To the mixture of dihexyl ketone (3.96 g, 20.0 mmol) and pyridine (10 mL) was added hydroxylamine hydrochloride (1.39 g, 20.0 mmol). After stirred at room temperature for 2 h, the reaction crude was azeotroped by toluene to remove pyridine. A subsequent dissolution of the resulting solid in cyclohexane and filtration was followed by drying under vacuum, giving the intermediate oxime, the solution of which in 8 mL THF was added dropwise into the solution of lithium aluminium hydride (LiAlH₄) in 12 mL THF at 0 °C. The reaction was allowed to warm up to room temperature and then refluxed under argon at 80 °C overnight. After cooled down, the reaction was quenched by H₂O (4 mL), 15% NaOH (4 mL) and H₂O (17 mL) again in ice-bath, filtered and evaporated to remove organic solvents and H₂O (by toluene to form azeotrope). The purification with silica gel column eluted with cyclohexane/ethylacetate (9/1 ~ 0/1) and subsequent ethylacetate including 4% methanol and 10% triethylamine provided colourless gel-like product (3.79 g, 95.3% yield). ¹H NMR (300 MHz, CDCl₃): δ 2.66 (m, 1H), 1.57 (s, 2H), 1.40 – 1.26 (m, 20H), 0.86 (t, $J = 6.90$ Hz, 6H). ¹³C NMR (CDCl₃, 75 MHz): δ 51.23, 38.06, 31.90, 29.51, 26.15, 22.66, 14.10. HRMS (ES⁺): m/z calcd for C₁₃H₂₉N [M+H]⁺ 200.4 found 200.23726.



Symmetrical perylene bisimide: *N,N'*-Bis(1-hexylheptyl)-perylene-3,4:9,10-bis(dicarboximide). The reaction mixture of perylene-

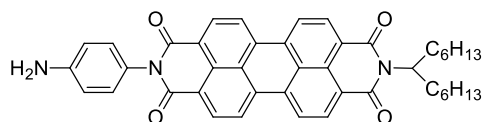
3,4,9,10-tetracarboxylic dianhydride (1.31 g, 3.30 mmol), tridecan-7-amine (2.00 g, 10.0 mmol), zinc acetate (0.458 g, 2.50 mmol) and imidazole (12 g) was reacted at 160 °C for approx. 2.5 h, cooled down to room temperature, poured into an acidic solution of 600 mL 2M HCl and 300 MeOH and then stirred for approx. 1 h. Filtering the reaction crude through funnel, the resulting solid was washed with distilled H₂O until the pH value of filtrate went up to neutral,

dried by pump and purified by flash column, giving a deep red solid quantitatively. ^1H NMR (300 MHz, CDCl_3): δ 8.66 – 8.63 (m, 8H), 5.24 – 5.14 (m, 2H), 2.31 – 2.19 (m, 4H), 1.92 – 1.80 (m, 4H), 1.36 – 1.23 (m, 32H), 0.85 – 0.80 (t, $J = 6.76$ Hz, 12H). ^{13}C NMR (CDCl_3 , 75 MHz): δ . HRMS (ES^+): m/z calcd for $\text{C}_{50}\text{H}_{62}\text{N}_2\text{O}_4$ $[\text{M}+\text{Na}]^+$ 777.0 found 777.46013.



9-(tridecan-7-yl)-1H-isochromeno [6',5',4':10,5,6]anthrax [2,1,9-def]isoquinoline-1,3,8,10(9H)-tetraone. The mixture of reagents symmetrical perylene bisimide (2.39 g, 3.17 mmol),

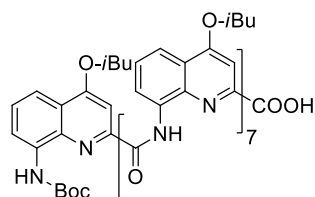
85% KOH (8.86 g, 158 mmol) and *t*-BuOH/ H_2O (104 mL/13 mL, 8/1, v/v) was refluxed at 90 °C for approx. 70 min, cooled down and slowly added 14 mL concentrated HCl at 0 °C. After removal of organic solvent, the crude was dissolved in chloroform, poured into a mixture of 100mL 2 M HCl and 300 mL MeOH and stirred for approx. 1 h. Evaporating CHCl_3 , the crude was filtered and washed with H_2O until neutral. The pure product was obtained by using silica gel column eluted with CHCl_3 (1.65 g, 90.4% yield). ^1H NMR (300 MHz, CDCl_3): δ 8.73 – 8.65 (m, 8H), 5.23 – 5.13 (m, 1H), 2.29 – 2.18 (m, 2H), 1.90 – 1.81 (m, 2H), 1.31 – 1.23 (m, 16H), 0.83 (t, $J = 6.83$ Hz, 6H). ^{13}C NMR (CDCl_3 , 75 MHz): δ . HRMS (ES^+): m/z calcd for $\text{C}_{37}\text{H}_{35}\text{NO}_5$ $[\text{M}+\text{Na}]^+$ 595.7 found 595.47055.



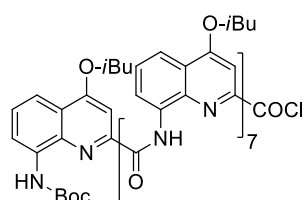
Asymmetrical perylene bisimide: 2-(4-aminophenyl)-9-(tridecan-7-yl)anthra[2,1,9-def:6,5,10-d'e'f']diisoquinoline-1,3,8,10(2H,9H)-tetraone.

After dried under vacuum, the mixture of L3-3 (1.65 g, 2.86 mmol), *p*-phenylenediamine (3.09 g, 28.6 mmol), zinc acetate (0.393 g, 2.15 mmol) and imidazole (17 g) was reacted at 160 °C for 3 h. Cooling down to room temperature, the crude was poured into 200 mL MeOH and stirred for approx. 2 h. After filtration and washing, the crude yielded a red solid as product (1.75 g, 92 % yield). ^1H NMR (300 MHz, CDCl_3): δ 8.76 – 8.66 (m, 8H), 7.13 – 7.10 (m, 2H), 6.86 – 6.83 (m, 2H), 5.22 – 5.16 (m, 1H), 2.30 – 2.19 (m, 2H), 1.89 – 1.83 (m, 3H), 1.31 – 1.23 (m, 16H), 0.83 (t, $J = 6.95$ Hz, 6H). ^{13}C NMR (CDCl_3 , 75 MHz): δ . HRMS (ES^+): m/z calcd for $\text{C}_{43}\text{H}_{42}\text{N}_3\text{O}_4$ $[\text{M}+\text{H}]^+$ 664.8 found 664.45800.

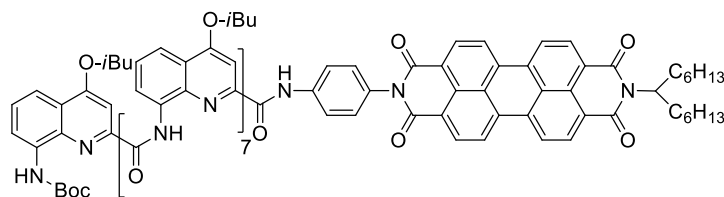
5.2.3 Synthesis of Boc-NH-Q₈-peryene.



Boc-NH-Q₈-COOH. To a solution of Boc-NH-Q₈ (2.00 g, 0.967 mmol) in 100 mL THF/MeOH (9/1, v/v) was added ground NaOH (0.777 g, 19.3 mmol). The reaction was stirred at room temperature and monitored with ¹H NMR. 5% citric acid was used to quench the reaction and protonate the resulting carboxyl group. After removal of organic solvents, the solid was dissolved into DCM, washed by H₂O and brine, dried by anhydrous Na₂SO₄ and evaporated to produce the product quantitatively. ¹H NMR (300 MHz, CDCl₃): δ 11.33 (s, 1H), 11.33 (s, 1H), 11.27 (s, 1H), 11.00 (s, 1H), 10.98 (s, 1H), 10.88 (s, 1H), 10.85 (s, 1H), 8.23 (dd, *J* = 0.77, 1.92 Hz, 1H), 8.21 (dd, *J* = 0.80, 1.97 Hz, 1H), 8.16 (dd, *J* = 1.76, 2.97 Hz, 1H), 8.13 (dd, *J* = 1.74, 2.97 Hz, 1H), 8.10 (dd, *J* = 3.25, 4.39 Hz, 1H), 7.90 (dd, *J* = 3.58, 4.77 Hz, 1H), 7.87 – 6.92 (m, 19H), 6.89 (s, 1H), 6.81 (s, 1H), 6.68 (s, 1H), 6.50 (s, 1H), 6.48 (s, 1H), 6.46 (s, 1H), 6.06 (s, 1H), 4.18 – 3.73 (m, 16H), 2.54 – 2.17 (m, 8H), 1.38 – 1.09 (m, 48H), 0.94 (s, 9H). HRMS (ES⁺): *m/z* calcd for C₁₁₇H₁₂₂N₁₆O₁₉ [M+H]⁺ 2056.918 found 2056.919.



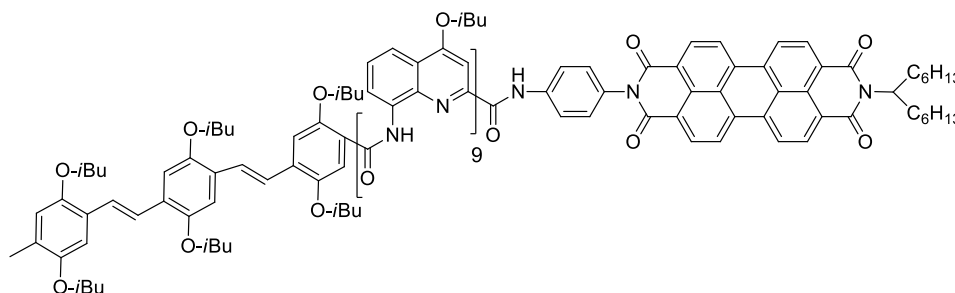
Boc-NH-Q₈-COCl. Ghosez Reagent (0.256 mL, 1.93 mmol) was added dropwise into a solution of **Boc-NH-Q₈-COOH** (2.00 g, 0.967 mmol) in 10 mL CHCl₃. The reaction was allowed to process at room temperature for approx. 4 h and monitored with ¹H NMR. Removing solvent and remaining Ghosez Reagent, the product was obtained quantitatively as a yellowish solid. ¹H NMR (300 MHz, CDCl₃): δ 11.44 (s, 1H), 11.32 (s, 1H), 11.27 (s, 1H), 11.20 (s, 1H), 11.03 (s, 1H), 10.98 (s, 1H), 10.89 (s, 1H), 8.24 – 8.09 (m, 5H), 7.91 – 7.72 (m, 8H), 7.61 – 7.57 (m, 2H), 7.46 – 7.41 (m, 2H), 7.33 – 6.90 (m, 11H), 6.77 (s, 1H), 6.69 (s, 1H), 6.51 (s, 1H), 6.46 (s, 1H), 6.29 (s, 1H), 6.06 (s, 1H), 4.16 – 3.63 (m, 16H), 2.52 – 2.32 (m, 8H), 1.37 – 1.13 (m, 48H), 0.94 (s, 9H).



Boc-NH-Q₈-perylene. To a mixture of asymmetric perylene bisimide (0.350 g, 0.528 mmol) and DIPEA (0.422 mL, 2.64 mmol) in 7.5 mL anhydrous CHCl₃ was added the solution of **Boc-NH-Q₈-**

COCl in 12.5 mL CHCl_3 at ice-bath. The reaction was allowed to stir at room temperature overnight and monitored with ^1H NMR. The resulting crude was washed with H_2O , 0.1 M HCl , saturated NaHCO_3 and brine, dried with Na_2SO_4 , refluxed in pyridine/ H_2O and purified with silica gel column eluting $\text{CHCl}_3/\text{EtOAc}$ (100/1 to 100/14), providing a red solid as product. ^1H NMR (300 MHz, CDCl_3): δ 11.40 (s, 1H), 11.34 (s, 1H), 11.26 (s, 1H), 11.03 (s, 1H), 11.02 (s, 1H), 10.90 (s, 1H), 10.82 (s, 1H), 8.74 – 8.65 (m, 9H), 8.24 – 8.16 (m, 3H), 8.13 – 8.08 (m, 2H), 7.92 – 6.88 (m, 22H), 6.84 (s, 1H), 6.81 (s, 2H), 6.47 (s, 1H), 6.42 (s, 1H), 6.41 (s, 1H), 6.05 (s, 1H), 5.26 – 5.18 (m, 1H), 4.18 – 3.77 (m, 16H), 2.56 – 2.22 (m, 10H), 1.91 – 1.85 (m, 2H), 1.37 – 1.11 (m, 64H), 0.95 (s, 9H), 0.84 (t, $J = 6.96$ Hz, 6H). HRMS (ES^+): m/z calcd for $\text{C}_{160}\text{H}_{162}\text{N}_{19}\text{O}_{22}$ $[\text{M}+\text{H}]^+$ 2703.221 found 2703.224.

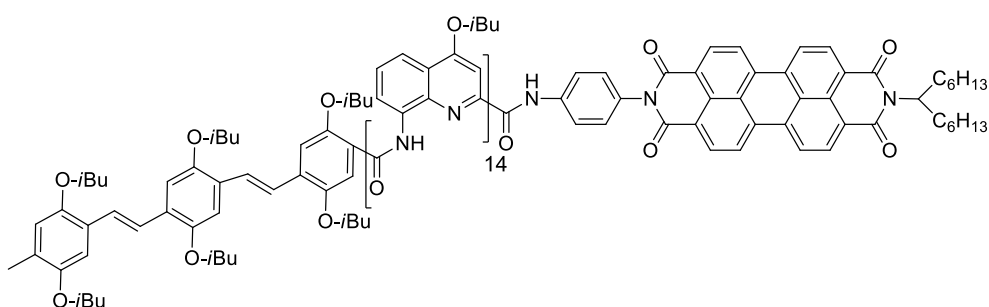
5.2.4 Synthesis of OPV-Q₉-PB.



OPV-Q-CO₂H (22 mg, 0.021 mmol) was dissolved in anhydrous CHCl_3 (0.5 mL) under nitrogen. 1-Chloro-*N,N*,2-trimethyl-1-propenylamine (0.0085 mL, 0.065 mmol) was added and the reaction mixture was stirred at room temperature for 2 hours and dried under vacuum then dissolved in dry CHCl_3 (1 mL) under nitrogen. In another round bottom flask the $\text{H}_2\text{N-Q}_8\text{-PB}$ (48 mg, 0.018 mmol) was dissolved in dry CHCl_3 (2 mL) under nitrogen then both DIPEA (0.016 mL, 0.092 mmol) and acid chloride was added drop wise to the amine consequently and stirred at room temperature overnight. Crude reaction mixture was washed with saturated NaHCO_3 , NH_4Cl , brine solution and extracted with chloroform. Dried with anhydrous Na_2SO_4 , firstly precipitated in MeOH and purified by GPC to get pure red color solid (36 mg, 54%). ^1H NMR (CDCl_3 , 300 MHz) δ ppm = 11.19 (1H, s), 11.12 (1H, s), 10.85 (1H, s), 10.84 (1H, s), 10.80 (1H, s), 10.76 (1H, s), 10.75 (1H, s), 10.71 (1H, s), 10.64 (1H, s), 8.70 (1H, bs), 8.65 (8H, d, $J = 7.75$ Hz), 8.15 (2H, d, $J = 7.67$ Hz), 7.87-8.05 (5H, m), 7.74-7.85 (5H, m), 7.71 (1H, d, $J = 7.85$ Hz), 7.65 (1H, d, $J = 8.17$ Hz), 7.59 (1H, d, $J = 7.19$ Hz), 7.48 (2H, s), 7.45 (1H, d, $J =$

6.70 Hz), 7.28-7.37 (5H, m), 7.23 (2H, s), 7.02-7.20 (8H, m), 7.00 (1H, d, $J = 7.48$ Hz), 6.91 (2H, d, $J = 8.47$ Hz), 6.81 (1H, s), 6.70-6.79 (7H, m), 6.34 (1H, s), 6.28 (2H, s), 6.19 (1H, s), 6.14 (1H, s), 5.79 (1H, s), 5.13-5.26 (1H, m), 3.47-4.12 (30H, m), 2.04-2.53 (20H, m), 1.82-1.91 (2H, m), 1.03-1.40 (88H, m), 0.95 (3H, d, $J = 6.63$ Hz), 0.84 (6H, t, $J = 6.45$ Hz), 0.80 (3H, d, $J = 6.63$ Hz), 0.71 (3H, d, $J = 6.81$ Hz), 0.68 (3H, d, $J = 6.63$ Hz), -0.13 (3H, d, $J = 6.46$ Hz), -0.19 (3H, d, $J = 6.69$ Hz). HRMS (ESI⁺): m/z calcd for C₂₁₇H₂₃₅N₂₁O₂₉ [M+2H]²⁺ 1800.3813 found 1800.3899.

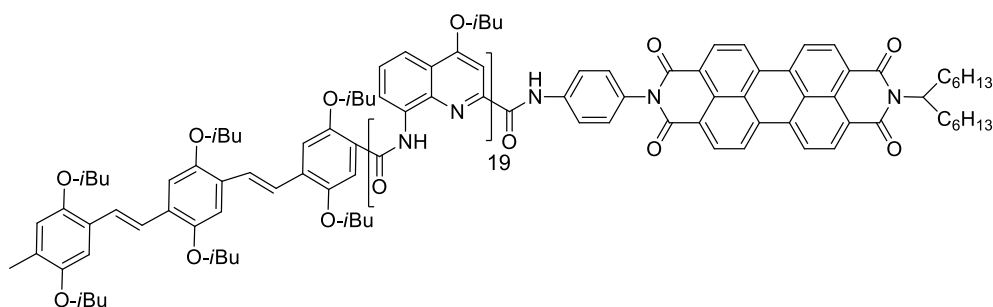
5.2.5 Synthesis of OPV-Q₁₄-PB.



OPV-Q- CO₂H (15 mg, 0.015 mmol) was dissolved in anhydrous CHCl₃ (0.5 mL) under nitrogen. 1-Chloro-*N,N*,2-trimethyl-1-propenylamine (0.006 mL, 0.045 mmol) was added and the reaction mixture was stirred at room temperature for 2 hours and dried under vacuum then dissolved in dry CHCl₃(1 mL) under nitrogen. In another round bottom flask the H₂N-Q₁₃-PB (30 mg, 0.008 mmol) was dissolved in dry CHCl₃ (1 mL) under nitrogen then both DIPEA (0.006 mL, 0.039 mmol) and acid chloride was added drop wise to the amine consequently and stirred at room temperature overnight. Crude product was washed with saturated NaHCO₃, NH₄Cl, brine solution and extracted with chloroform. Product was dried with anhydrous Na₂SO₄ and precipitated in MeOH then purified by GPC to get pure red color solid (20 mg, 53%). ¹H NMR (CDCl₃, 300 MHz) δ ppm = 10.99 (1H, s), 10.86 (1H, s), 10.56 (1H, s), 10.55 (1H, s), 10.52 (1H, s), 10.43 (2H, s), 10.31 (1H, s), 10.28 (1H, s), 10.23 (1H, s), 10.16 (1H, s), 10.13 (1H, s), 10.11 (1H, s), 10.09 (1H, s), 8.56-8.74 (8H, m), 8.52 (1H, s), 7.97-8.04 (2H, m), 7.59-7.85 (15H, m), 7.55 (1H, d, $J = 8.39$ Hz), 7.48 (1H, d, $J = 7.34$ Hz), 7.45 (2H, s), 7.34 (2H, d, $J = 6.81$ Hz), 7.29 (1H, br), 7.12-7.22 (6H, m), 6.98-7.11 (9H, m), 6.79-6.97 (12H, m), 6.74 (1H, s), 6.64-6.72 (5H, m), 6.59 (2H, d, $J = 11.01$ Hz), 6.22 (1H,s), 6.06 (2H, d, $J = 9.86$ Hz), 5.95 (2H, d, $J = 9.86$ Hz), 5.85 (2H, s), 5.76-5.83 (3H, m), 5.66 (1H, s), 5.13-5.25 (1H, m),

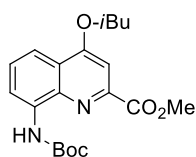
3.48-3.99 (40H, m), 2.08-2.40 (25H, m), 1.82-1.92 (2H, m), 0.99-1.24 (118H, m), 0.88 (3H, d, $J = 6.43$ Hz), 0.83 (6H, t, $J = 6.43$ Hz), 0.74 (3H, d, $J = 6.43$ Hz), 0.66 (3H, d, $J = 6.74$ Hz), 0.62 (3H, d, $J = 6.74$ Hz), -0.23 (3H, d, $J = 6.31$ Hz), -0.29 (3H, d, $J = 6.31$ Hz). HRMS (ESI⁺): m/z calcd for C₂₈₇H₃₀₅N₃₁O₃₉ [M+2H]²⁺ 2406.1468 found 2406.1550.

5.2.6 Synthesis of OPV-Q₁₉-PB.

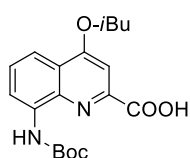


OPV-Q-CO₂H (20 mg, 0.019 mmol) was dissolved in anhydrous CHCl₃ (0.5 mL) under nitrogen. 1-Chloro-*N,N*,2-trimethyl-1-propenylamine (0.008 mL, 0.059 mmol) was added and the reaction mixture was stirred at room temperature for 2 hours and dried under vacuum then dissolved in dry CHCl₃ (0.5 mL) under nitrogen. In another round bottom flask the H₂N-Q₁₈-PB (35 mg, 0.007 mmol) was dissolved in dry CHCl₃ (1 mL) under nitrogen then both DIPEA (0.01 mL, 0.069 mmol) and OPV-Q-COCl was added drop wise to the amine consequently and stirred at room temperature overnight. Crude product was washed with saturated NaHCO₃, NH₄Cl, brine solution and extracted with chloroform. Product was dried with anhydrous Na₂SO₄ and precipitated in MeOH then purified by GPC to get pure red color solid (25 mg, 60%). ¹H NMR (CDCl₃, 300 MHz) δ ppm = 10.91 (1H, s), 10.79 (1H, s), 10.50 (1H, s), 10.46 (1H, s), 10.44 (1H, s), 10.33 (2H, s), 10.17 (1H, s), 10.15 (1H, s), 10.12 (1H, s), 9.99 (1H, s), 9.93 (1H, s), 9.88 (1H, s), 9.86 (1H, s), 9.82 (1H, s), 9.77 (2H, s), 9.75 (2H, s), 8.43-8.74 (9H, m), 7.95 (2H, d, $J = 7.56$ Hz), 7.47-7.78 (21H, m), 7.43 (3H, s), 6.60-7.22 (46H, m), 6.53 (2H, d, $J = 10.11$ Hz), 6.16 (1H, s), 5.97 (2H, d, $J = 12.84$ Hz), 5.87 (2H, d, $J = 5.17$ Hz), 5.57-5.75 (11H, m), 5.12-5.25 (1H, m), 3.36-3.93 (50H, m), 2.05-2.35 (27H, m), 1.72-1.95 (5H, m), 0.95-1.38 (151H, m), 0.80-0.87 (6H, m), 0.70 (3H, d, $J = 6.17$ Hz), 0.56-0.66 (6H, m), -0.26 (3H, d, $J = 6.17$ Hz), -0.32 (3H, d, $J = 6.17$ Hz). HRMS (ESI⁺): m/z calcd for C₃₅₇H₃₇₅N₄₁O₄₉ [M+2H]²⁺ 3011.4106 found 3011.9168.

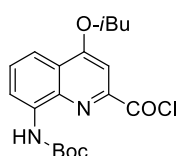
5.2.7 Synthesis of Boc-NH-Q₁₇-OMe



Boc-NH-Q₁-OMe. A mixture of Q₁-NH₂ (2.92 g, 10.6 mmol), (Boc)₂O (6.96 g, 31.9 mmol), DIPEA (5.24 mL, 31.9 mmol) and dioxane (100 mL) was refluxed at 85 °C and monitored by ¹H NMR. Maybe more (Boc)₂O and DIPEA would be added to push the reaction. Subsequent evaporation of dioxane and addition of DCM were followed by washing of water and saturated NaHCO₃ and drying by MgSO₄. Recrystallization in DCM/cyclohexane yielded a pale yellowish solid as product (δ). ¹H NMR (300 MHz, CDCl₃): δ 8.97 (s, 1H), 8.47 (d, *J* = 3.83 Hz, 1H), 7.80 (d, *J* = 4.19 Hz, 1H), 7.55 (d, *J* = 4.01 Hz, 1H), 7.51 (s, 1H), 4.05 (s, 3H), 4.03 (s, 1H), 4.01 (s, 1H), 2.34 – 2.21 (m, 1H), 1.58 (s, 9H), 1.14 (s, 3H), 1.12 (s, 3H). ¹³C NMR (CDCl₃, 75 MHz): δ 166.02, 162.93, 152.81, 146.68, 138.41, 135.91, 128.38, 122.20, 115.43, 114.11, 101.15, 80.66, 75.16, 52.97, 28.42, 28.22, 19.26.

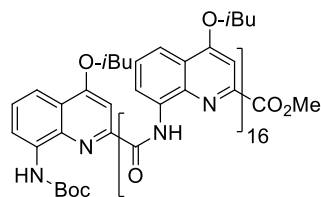


Boc-NH-Q₁-COOH. To a solution of Boc-NH-Q₁-OMe (0.200 g, 0.534 mmol) in 6 mL THF/H₂O (2/1, v/v) was added ground KOH (0.0748 g, 1.34 mmol). The reaction was stirred at room temperature overnight and monitored with ¹H NMR. 5% citric acid was used to quench the reaction and protonate the resulting carboxyl group. After removal of organic solvents, the solid was dissolved into DCM, washed by H₂O and brine, dried by anhydrous Na₂SO₄ and evaporated to produce pale white solid as the product quantitatively. ¹H NMR (300 MHz, CDCl₃): δ 8.73 (s, 1H), 8.48 (d, *J* = 3.54 Hz, 1H), 7.88 (dd, *J* = 3.59, 4.84 Hz, 1H), 7.67 (s, 1H), 7.58 (t, *J* = 8.16 Hz, 1H), 4.09 (s, 1H), 4.06 (s, 1H), 2.36 – 2.23 (m, 1H), 1.61 (s, 9H), 1.15 (s, 3H), 1.13 (s, 3H). ¹³C NMR (CDCl₃, 75 MHz): δ 165.21, 164.02, 153.03, 145.72, 137.42, 135.08, 128.69, 122.77, 116.80, 114.89, 99.90, 81.62, 77.25, 75.60, 28.41, 28.16, 19.21. HRMS (ESI⁺): *m/z* calcd for C₁₉H₂₅N₂O₅ [M+H]⁺ 361.1763 found 361.1769.



Boc-NH-Q₁-COCl. Ghosez Reagent (0.107 mL, 811 μ mol) was added dropwise into a solution of Boc-NH-Q₁-COOH (0.146 g, 406 μ mol) in 1 mL freshly distilled CHCl₃. The reaction was allowed to process at room temperature for approx. 3 h and monitored by ¹H NMR. After removal of solvent and remaining Ghosez Reagent, a pale white solid was obtained as product quantitatively. ¹H NMR (300 MHz, CDCl₃): δ 8.53 (d, *J* = 3.98 Hz, 1H), 8.42 (s, 1H), 7.89 (d, *J* = 4.18 Hz, 1H), 7.66 (s, 1H), 7.61

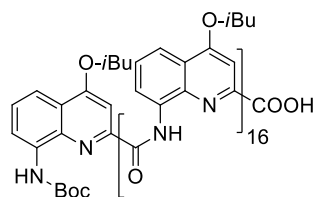
(t, $J = 8.15$ Hz, 1H), 4.10 (s, 1H), 4.07 (s, 1H), 2.37 – 2.24 (m, 1H), 1.61 (s, 9H), 1.15 (s, 3H), 1.13 (s, 3H).



Boc-NH-Q₁₇-OMe. To a mixture of Q₁₆-NH₂ (0.317 g, 81.2 μ mol) and DIPEA (68 μ L, 406 μ mol) in 1.5 mL CHCl₃ was added dropwise a solution of **Boc-NH-Q₁-COCl** in 2.5 mL CHCl₃ at 0 $^{\circ}$ C. The reaction was warmed up, reacted at room temperature

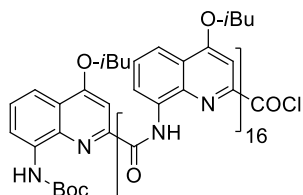
overnight and monitored by ¹H NMR. The resulting reaction crude was worked up with water, 0.1 M HCl, water, saturated NaHCO₃ and brine, and dried by anhydrous NaSO₄. Precipitation of the reaction crude in DCM/MeOH yielded a yellowish solid as product (0.343g, 99.5% yield). ¹H NMR (300 MHz, CDCl₃): δ 11.11 (s, 1H), 11.05 (s, 1H), 10.86 (s, 1H), 10.82 (s, 1H), 10.49 (s, 1H), 10.28 (s, 1H), 10.24 (s, 1H), 10.18 (s, 1H), 10.13 (s, 1H), 10.04 (s, 2H), 9.99 (s, 1H), 9.98 (s, 1H), 9.95 (s, 1H), 9.92 (s, 1H), 9.91 (s, 1H), 7.94 (d, $J = 3.62$ Hz, 1H), 7.90 – 7.53 (m, 20H), 7.40 (d, $J = 4.04$ Hz, 1H), 7.33 (d, $J = 3.65$ Hz, 1H), 7.30 – 6.74 (m, 30H), 6.67 (s, 1H), 6.41 (s, 1H), 6.38 (s, 1H), 6.21 (s, 1H), 6.15 (s, 1H), 6.13 (s, 1H), 5.88 (s, 1H), 5.87 (s, 1H), 5.76 (s, 3H), 5.75 (s, 1H), 5.73 (s, 1H), 5.71 (s, 1H), 5.70 (s, 2H), 3.97 – 3.42 (m, 34H), 2.82 (s, 3H), 2.38 – 2.05 (m, 14H), 1.25 – 1.00 (m, 102H), 0.78 (s, 9H). HRMS (ES⁺): m/z calcd for C₂₄₄H₂₅₂N₃₄O₃₇ [M+2H]²⁺ 2125.948 found 2125.947.

5.2.8 Synthesis of Boc-NH-Q₁₇-perylene.



Boc-NH-Q₁₇-COOH. Ground NaOH powder (0.0536 g, 1.34 mmol) was put into a solution of **Boc-NH-Q₁₇-OMe** (0.285 g, 67.1 μ mol) in 10 mL THF/MeOH (9/1, v/v). The reaction was stirred at room temperature and monitored by TLC (CHCl₃/EtOAc = 40/1). As the reaction completed. It was quenched by 5% citric acid. Evaporation of organic solvents was followed by washing of water and brine, and drying of Na₂SO₄, yielding a yellowish solid (0.270 g, 95.1% yield). ¹H NMR (300 MHz, CDCl₃): δ 10.89 (s, 1H), 10.86 (s, 1H), 10.82 (s, 1H), 10.51 (s, 1H), 10.48 (s, 1H), 10.31 (s, 1H), 10.24 (s, 1H), 10.18 (s, 1H), 10.16 (s, 1H), 10.05 (s, 1H), 10.04 (s, 1H), 10.00 (s, 1H), 9.98 (s, 1H), 9.95 (s, 1H), 9.92 (s, 1H), 9.91 (s, 1H), 8.01 – 7.95 (m, 2H), 7.81 – 7.55 (m, 20H), 7.40 (dd, $J = 3.52, 4.55$ Hz, 1H), 7.33 (d, $J = 3.57$ Hz, 1H), 7.30 – 6.75 (m, 29H), 6.67 (s, 1H), 6.54 (s, 1H), 6.44 (s, 1H), 6.32

(s, 1H), 6.10 (s, 1H), 6.08 (s, 1H), 5.88 (s, 1H), 5.87 (s, 1H), 5.78 (s, 1H), 5.77 (s, 1H), 5.76 (s, 1H), 5.75 (s, 1H), 5.74 (s, 1H), 5.71 (s, 1H), 5.69 (s, 2H), 3.94 – 3.45 (m, 34H), 2.34 – 2.15 (m, 17H), 1.25 – 1.01 (m, 102H), 0.78 (s, 9H). HRMS (ES⁺): *m/z* calcd for C₂₄₃H₂₄₅₀N₃₄O₃₇ [M+2H]²⁺ 2118.940 found 2118.940.



Boc-NH-Q₁₇-COCl. To a solution of **Boc-NH-Q₁₇-COOH** in 2 mL

CHCl₃ was added Ghosez Reagent (16.8 μL, 127 μmol). The reaction was stirred at room temperature and controlled by ¹H

NMR. Removal of solvent and remaining Gholsez Reagent from

the reaction crude provided a yellowish solid as product quantitatively. ¹H NMR (300 MHz,

CDCl₃): δ 10.99 (s, 1H), 10.85 (s, 2H), 10.81 (s, 1H), 10.50 (s, 1H), 10.29 (s, 1H), 10.22 (s,

1H), 10.17 (s, 1H), 10.15 (s, 1H), 10.03 (s, 2H), 9.99 (s, 1H), 9.97 (s, 1H), 9.94 (s, 1H), 9.92 (s,

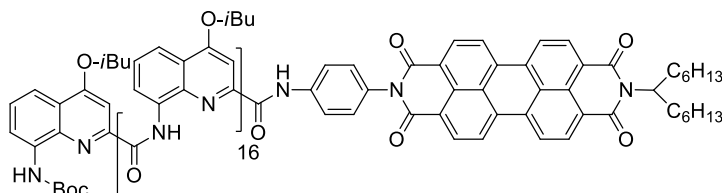
1H), 9.91 (s, 1H), 8.00 (d, *J* = 3.69 Hz, 1H), 7.94 (d, *J* = 3.63 Hz, 1H), 7.81 – 7.55 (m, 20H),

7.40 (d, *J* = 4.11 Hz, 1H), 7.33 (d, *J* = 3.84 Hz, 1H), 7.30 – 6.74 (m, H), 6.66 (s, 1H), 6.49 (s,

1H), 6.42 (s, 1H), 6.12 (s, 1H), 6.11 (s, 1H), 6.07 (s, 1H), 5.88 (s, 1H), 5.87 (s, 1H), 5.77 (s,

1H), 5.76 (s, 1H), 5.75 (s, 1H), 5.74 (s, 1H), 5.73 (s, 1H), 5.71 (s, 1H), 5.69 (s, 2H), 3.93 – 3.41

(m, 34H), 2.38 – 2.14 (m, 17H), 1.22 – 1.01 (m, 102H), 0.77 (s, 9H).



Boc-NH-Q₁₇-perylene. To a

mixture of asymmetrical perylene (0.130 g, 196 μmol)

and DIPEA (27.6 μL, 159

μmol) in 1.5 mL CHCl₃ was added dropwise a solution of **Boc-NH-Q₁₇-COCl** in 3.5 mL CHCl₃

at 0 °C. The reaction was warmed up, reacted at room temperature overnight and monitored by

¹H NMR. The resulting reaction crude was purified by silica gel column (CHCl₃/EtOAc as

eluent.) firstly, and then further purified by recycling GPC, giving a red solid as product (33

mg, 10.6% yield). ¹H NMR (300 MHz, CDCl₃): δ 10.95 (s, 1H), 10.85 (s, 1H), 10.81 (s, 1H),

10.50 (s, 1H), 10.48 (s, 1H), 10.36 (s, 1H), 10.24 (s, 1H), 10.20 (s, 1H), 10.18 (s, 1H), 10.06 (s,

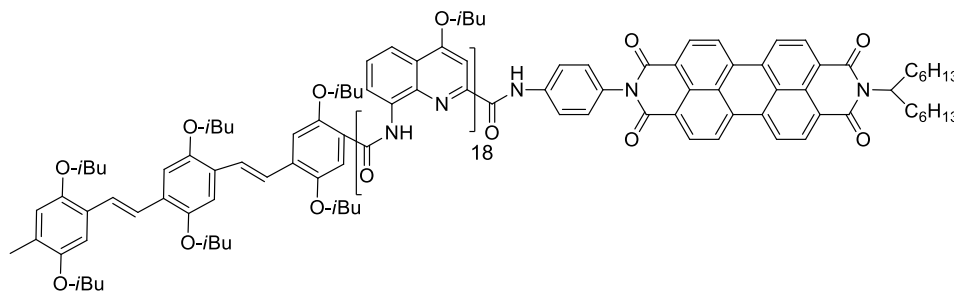
1H), 10.04 (s, 1H), 9.99 (s, 1H), 9.96 (s, 1H), 9.94 (s, 1H), 9.93 (s, 1H), 9.92 (s, 1H), 8.68 –

8.55 (m, 8H), 8.49 (s, 1H), 7.99 – 7.95 (m, 2H), 7.81 – 7.55 (m, 20H), 7.40 (dd, *J* = 3.30 4.51

Hz, 1H), 7.33 (d, *J* = 3.78 Hz, 1H), 7.30 – 6.72 (m, H), 6.68 (s, 1H), 6.67 (s, 1H), 6.65 (s, 1H),

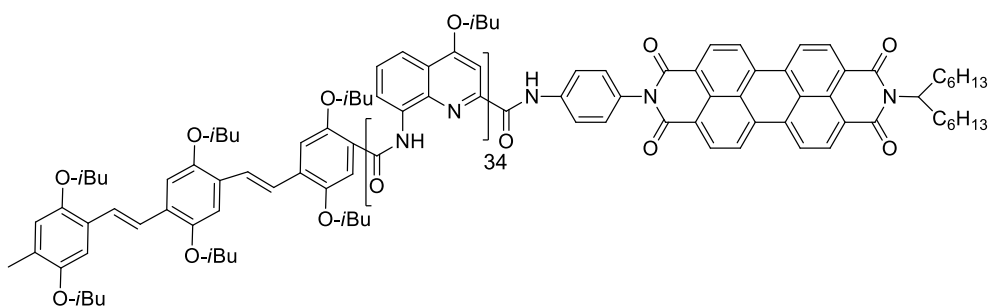
6.64 (s, 1H), 6.63 (s, 1H), 6.19 (s, 1H), 6.03 (s, 1H), 6.00 (s, 1H), 5.89 (s, 1H), 5.87 (s, 1H), 5.76 (m, 4H), 5.73 (s, 1H), 5.71 (s, 2H), 5.69 (s, 1H), 5.24 – 5.14 (m, 1H), 3.97 – 3.42 (m, 34H), 2.37 – 2.10 (m, 19H), 1.89 – 1.82 (m, 2H), 1.32 – 1.01 (m, 118H), 0.83 (t, J = 6.72 Hz, 6H), 0.78 (s, 9H). HRMS (ES⁺): *m/z* calcd for C₂₈₆H₂₈₉N₃₇O₄₀ [M+2H]²⁺ 2442.091 found 2442.096.

5.2.9 Synthesis of OPV-Q₁₈-PB.



OPV-Q-CO₂H (10 mg, 0.009 mmol) was dissolved in anhydrous CHCl₃ (0.5 mL) under nitrogen. 1-Chloro-*N,N*,2-trimethyl-1-propenylamine (0.003 mL, 0.025 mmol) was added and the reaction mixture was stirred at room temperature for 2 hours and dried under vacuum then dissolved in dry CHCl₃(0.5 mL) under nitrogen. In another round bottom flask the H₂N-Q₁₇-PB (20 mg, 0.004 mmol) was dissolved in dry CHCl₃ (1 mL) under nitrogen then both DIPEA (0.006 mL, 0.041 mmol) and OPV-Q-COCl was added drop wise to the amine consequently and stirred at room temperature overnight. Crude product was washed with saturated NaHCO₃, NH₄Cl, brine solution and extracted with chloroform. Product was dried with anhydrous Na₂SO₄ and precipitated in MeOH then purified by GPC to get pure red color solid (8 mg,33%).
¹H NMR (CDCl₃, 300 MHz) δ ppm = 10.92 (1H, s), 10.80 (1H, s), 10.51 (1H, s), 10.47 (1H, s), 10.45 (1H, s), 10.35 (1H, s), 10.34 (1H, s), 10.18 (1H, s), 10.16 (1H, s), 10.13 (1H, s), 10.01 (1H, s), 9.95 (1H, s), 9.90 (1H, s), 9.88 (1H, s), 9.85 (1H, s), 9.82 (1H, s), 9.80 (2H, s), 8.51-8.73 (8H, m), 8.48 (1H, s), 7.95 (2H, d, J = 7.56 Hz), 7.47-7.78 (20H, m), 7.43 (3H, s), 7.29 (1H, s), 7.23 (1H, d, J = 5.66 Hz), 7.05-7.21 (7H, m), 6.82-7.03 (18H, m), 6.60-6.82 (17H, m), 6.54 (2H, d, J = 9.85 Hz), 6.17 (1H, s), 5.99 (2H, d, J = 10.75 Hz), 5.89 (2H, d, J = 5.65 Hz), 5.58-5.78 (10H, m), 5.12-5.25 (1H, m), 3.33-3.96 (48H, m), 2.03-2.37 (27H, m), 1.73-2.01 (4H, m), 0.96-1.36 (145H, m), 0.83 (6H, t, 6.71 Hz), 0.70 (3H, d, J = 6.71Hz), 0.63 (3H, d, J = 6.71Hz), 0.60 (3H, d, J = 6.71Hz), -0.26 (3H, d, J = 6.37 Hz), -0.32 (3H, d, J = 6.74 Hz).
HRMS (ESI⁺): *m/z* calcd for C₃₄₃H₃₆₁N₃₉O₄₇ [M+2H]²⁺ 2890.3579 found 2890.3560.

5.2.10 Synthesis of OPV-Q34-PB.



OPV-Q₁₇-CO₂H (82 mg, 0.016 mmol) was dissolved in anhydrous CHCl₃ (2 mL) under nitrogen. 1-Chloro-*N,N*,2-trimethyl-1-propenylamine (0.006 mL, 0.050 mmol) was added and the reaction mixture was stirred at room temperature for 6 hours and dried under vacuum then dissolved in dry CHCl₃(2 mL) under nitrogen. In another round bottom flask the H₂N-Q₁₇-PB (40 mg, 0.008 mmol) was dissolved in dry CHCl₃ (2 mL) under nitrogen then both DIPEA (0.006 mL, 0.041 mmol) and OPV-Q₁₇-COCl was added drop wise to the amine consequently and stirred at room temperature overnight. Crude reaction mixture was showed by NMR that amine was completely reacted with acid chloride and excess of OPV Q₁₇ acid chloride formed its anhydride. To hydrolyze the OPV Q₁₇ anhydride, DIEA was removed from crude reaction mixture then treated with pyridine/H₂O at 90 °C overnight. Finally pyridine/H₂O was removed under vacuum by azeotrope with toluene. Crude product was dissolved in CHCl₃ and washed with saturated NaHCO₃, NH₄Cl, brine solution and extracted with chloroform. Crude product was dried with anhydrous Na₂SO₄ and purified by GPC and precipitated in MeOH to get pure red color solid (10 mg, 12%). ¹H NMR (CDCl₃, 300 MHz) δ ppm = 10.87 (1H, s), 10.74 (1H, s), 10.46 (1H, s), 10.42 (3H, s), 10.29 (1H, s), 10.26 (1H, s), 9.35-10.16 (24H, m), 8.48-8.73 (10H, m), 8.43 (1H, s), 7.87-8.00 (3H, m), 7.28-7.80 (40H, m), 6.40-7.21 (79H, m), 6.12(1H, s), 5.95 (1H, s), 5.90 (1H, s), 5.81 (2H, s), 5.31-5.76 (23H, m), 5.11-5.23 (1H, m), 3.31-3.98 (3H, s), 3.03-3.91 (77H, m), 1.94-2.35 (43H, m), 1.81-1.93 (4H, m), 0.77-1.38 (m), 0.72 (3H, d, J = 7.55 Hz), 0.66 (3H, d, J = 6.39 Hz), 0.60 (3H, d, J = 6.97Hz), 0.57 (3H, d, J = 6.97 Hz), -0.30 (3H, d, J = 6.39 Hz), -0.36 (3H, d, J = 6.39 Hz). MALDI-TOF MS calcd for C₅₆₇H₅₈₄N₇₁O₇₉ [M+H]⁺ 9650 found 9650.

6 References

- 1 (a) Wasielewski, M. R., Energy, Charge, and Spin Transport in Molecules and Self-Assembled Nanostructures Inspired by Photosynthesis. *The Journal of Organic Chemistry* **2006**, *71* (14), 5051-5066; (b) Kamat, P. V., Meeting the Clean Energy Demand: Nanostructure Architectures for Solar Energy Conversion. *The Journal of Physical Chemistry C* **2007**, *111* (7), 2834-2860; (c) Balzani, V.; Credi, A.; Venturi, M., Photochemical Conversion of Solar Energy. *ChemSusChem* **2008**, *1* (1-2), 26-58; (d) McConnell, I.; Li, G.; Brudvig, G. W., Energy Conversion in Natural and Artificial Photosynthesis. *Chemistry & Biology* **2010**, *17* (5), 434-447; (e) Kärkäs, M. D.; Verho, O.; Johnston, E. V.; Åkermark, B., Artificial Photosynthesis: Molecular Systems for Catalytic Water Oxidation. *Chemical Reviews* **2014**, *114* (24), 11863-12001.
- 2 (a) Fukuzumi, S.; Ohkubo, K.; Suenobu, T., Long-Lived Charge Separation and Applications in Artificial Photosynthesis. *Accounts of Chemical Research* **2014**, *47* (5), 1455-1464; (b) Blumberger, J., Recent Advances in the Theory and Molecular Simulation of Biological Electron Transfer Reactions. *Chemical Reviews* **2015**, *115* (20), 11191-11238.
- 3 (a) Hammarström, L., Accumulative Charge Separation for Solar Fuels Production: Coupling Light-Induced Single Electron Transfer to Multielectron Catalysis. *Accounts of Chemical Research* **2015**, *48* (3), 840-850; (b) Gilbert, M.; Albinsson, B., Photoinduced charge and energy transfer in molecular wires. *Chemical Society Reviews* **2015**, *44* (4), 845-862; (c) Delor, M.; Sazanovich, I. V.; Towrie, M.; Weinstein, J. A., Probing and Exploiting the Interplay between Nuclear and Electronic Motion in Charge Transfer Processes. *Accounts of Chemical Research* **2015**, *48* (4), 1131-1139.
- 4 Emmett, L.; Prentice, G. M.; Pantos, G. D., Donor-acceptor interactions in chemistry. *Annual Reports Section "B" (Organic Chemistry)* **2013**, *109* (0), 217-234.
- 5 (a) Wenger, O. S., Photoinduced electron and energy transfer in phenylene oligomers. *Chemical Society Reviews* **2011**, *40* (7), 3538-3550; (b) Wenger, O. S., How Donor-Bridge-Acceptor Energetics Influence Electron Tunneling Dynamics and Their Distance Dependences. *Accounts of Chemical Research* **2011**, *44* (1), 25-35.
- 6 Daly, B.; Ling, J.; de Silva, A. P., Current developments in fluorescent PET (photoinduced electron

-
- transfer) sensors and switches. *Chemical Society Reviews* **2015**.
- 7 Natali, M.; Campagna, S.; Scandola, F., Photoinduced electron transfer across molecular bridges: electron- and hole-transfer superexchange pathways. *Chemical Society Reviews* **2014**, *43* (12), 4005-4018.
- 8 (a) Wasielewski, M. R.; Niemczyk, M. P.; Johnson, D. G.; Svec, W. A.; Minsek, D. W., Ultrafast photoinduced electron transfer in rigid donor-spacer-acceptor molecules: modification of spacer energetics as a probe for superexchange. *Tetrahedron* **1989**, *45* (15), 4785-4806; (b) Indelli, M. T.; Chiorboli, C.; Flamigni, L.; De Cola, L.; Scandola, F., Photoinduced Electron Transfer across Oligo-p-phenylene Bridges. Distance and Conformational Effects in Ru(II)–Rh(III) Dyads. *Inorganic Chemistry* **2007**, *46* (14), 5630-5641; (c) Ricks, A. B.; Solomon, G. C.; Colvin, M. T.; Scott, A. M.; Chen, K.; Ratner, M. A.; Wasielewski, M. R., Controlling Electron Transfer in Donor–Bridge–Acceptor Molecules Using Cross-Conjugated Bridges. *Journal of the American Chemical Society* **2010**, *132* (43), 15427-15434; (d) Heinz, L. G.; Yushchenko, O.; Neuburger, M.; Vauthey, E.; Wenger, O. S., Tetramethoxybenzene is a Good Building Block for Molecular Wires: Insights from Photoinduced Electron Transfer. *The Journal of Physical Chemistry A* **2015**, *119* (22), 5676-5684.
- 9 Davis, W. B.; Svec, W. A.; Ratner, M. A.; Wasielewski, M. R., Molecular-wire behaviour in p-phenylenevinylene oligomers. *Nature* **1998**, *396* (6706), 60-63.
- 10 Khoo, K. H.; Chen, Y.; Li, S.; Quek, S. Y., Length dependence of electron transport through molecular wires - a first principles perspective. *Physical Chemistry Chemical Physics* **2015**, *17* (1), 77-96.
- 11 (a) Wiberg, J.; Guo, L.; Pettersson, K.; Nilsson, D.; Ljungdahl, T.; Mårtensson, J.; Albinsson, B., Charge Recombination versus Charge Separation in Donor–Bridge–Acceptor Systems. *Journal of the American Chemical Society* **2007**, *129* (1), 155-163; (b) Fukuzumi, S., New perspective of electron transfer chemistry. *Organic & Biomolecular Chemistry* **2003**, *1* (4), 609-620; (c) Griesbeck, A. G.; Hoffmann, N.; Warzecha, K.-d., Photoinduced-Electron-Transfer Chemistry: From Studies on PET Processes to Applications in Natural Product Synthesis. *Accounts of Chemical Research* **2007**, *40* (2), 128-140.
- 12 Ito, A.; Meyer, T. J., The Golden Rule. Application for fun and profit in electron transfer, energy

-
- transfer, and excited-state decay. *Physical Chemistry Chemical Physics* **2012**, *14* (40), 13731-13745.
- 13 Marcus, R. A.; Sutin, N., Electron transfers in chemistry and biology. *Biochimica et Biophysica Acta (BBA) - Reviews on Bioenergetics* **1985**, *811* (3), 265-322.
- 14 Indelli, M. T.; Orlandi, M.; Chiorboli, C.; Ravaglia, M.; Scandola, F.; Lafalet, F.; Welter, S.; Cola, L. D., Electron Transfer Across Modular Oligo-p-phenylene Bridges in Ru(bpy)₂(bpy-phn-DQ)₄⁺ (n = 1–5) Dyads. Unusual Effects of Bridge Elongation. *The Journal of Physical Chemistry A* **2012**, *116* (1), 119-131.
- 15 (a) Dance, Z. E. X.; Ahrens, M. J.; Vega, A. M.; Ricks, A. B.; McCamant, D. W.; Ratner, M. A.; Wasielewski, M. R., Direct Observation of the Preference of Hole Transfer over Electron Transfer for Radical Ion Pair Recombination in Donor–Bridge–Acceptor Molecules. *Journal of the American Chemical Society* **2008**, *130* (3), 830-832; (b) Goldsmith, R. H.; Sinks, L. E.; Kelley, R. F.; Betzen, L. J.; Liu, W.; Weiss, E. A.; Ratner, M. A.; Wasielewski, M. R., Wire-like charge transport at near constant bridge energy through fluorene oligomers. *Proceedings of the National Academy of Sciences of the United States of America* **2005**, *102* (10), 3540-3545.
- 16 Wolffs, M.; Delsuc, N.; Veldman, D.; Anh, N. V.; Williams, R. M.; Meskers, S. C. J.; Janssen, R. A. J.; Huc, I.; Schenning, A. P. H. J., Helical Aromatic Oligoamide Foldamers as Organizational Scaffolds for Photoinduced Charge Transfer. *Journal of the American Chemical Society* **2009**, *131* (13), 4819-4829.
- 17 (a) Jiang, H.; L'éger, J.-M.; Huc, I., Aromatic δ -Peptides. *Journal of the American Chemical Society* **2003**, *125* (12), 3448-3449; (b) Delsuc, N.; Kawanami, T.; Lefeuvre, J.; Shundo, A.; Ihara, H.; Takafuji, M.; Huc, I., Kinetics of Helix-Handedness Inversion: Folding and Unfolding in Aromatic Amide Oligomers. *ChemPhysChem* **2008**, *9* (13), 1882-1890; (c) Qi, T.; Maurizot, V.; Noguchi, H.; Charoenraks, T.; Kauffmann, B.; Takafuji, M.; Ihara, H.; Huc, I., Solvent dependence of helix stability in aromatic oligoamide foldamers. *Chemical Communications* **2012**, *48* (51), 6337-6339; (d) Qi, T.; Deschrijver, T.; Huc, I., Large-scale and chromatography-free synthesis of an octameric quinoline-based aromatic amide helical foldamer. *Nat. Protocols* **2013**, *8* (4), 693-708.
- 18 (a) Huang, Y.; Hu, J.; Kuang, W.; Wei, Z.; Faul, C. F. J., Modulating helicity through

amphiphilicity-tuning supramolecular interactions for the controlled assembly of perylenes. *Chemical Communications* **2011**, *47* (19), 5554-5556; (b) Wicklein, A.; Kohn, P.; Ghazaryan, L.; Thurn-Albrecht, T.; Thelakkat, M., Synthesis and structure elucidation of discotic liquid crystalline perylene imide benzimidazole. *Chemical Communications* **2010**, *46* (13), 2328-2330; (c) Mohamad, D. K.; Fischereder, A.; Yi, H.; Cadby, A. J.; Lidzey, D. G.; Iraqi, A., A novel 2,7-linked carbazole based "double cable" polymer with pendant perylene diimide functional groups: preparation, spectroscopy and photovoltaic properties. *Journal of Materials Chemistry* **2011**, *21* (3), 851-862; (d) Soh, N.; Ariyoshi, T.; Fukaminato, T.; Nakajima, H.; Nakano, K.; Imato, T., Swallow-tailed perylene derivative: a new tool for fluorescent imaging of lipid hydroperoxides. *Organic & Biomolecular Chemistry* **2007**, *5* (23), 3762-3768; (e) Rajaram, S.; Shivanna, R.; Kandappa, S. K.; Narayan, K. S., Nonplanar Perylene Diimides as Potential Alternatives to Fullerenes in Organic Solar Cells. *The Journal of Physical Chemistry Letters* **2012**, *3* (17), 2405-2408; (f) Chen, L. X.; Xiao, S.; Yu, L., Dynamics of Photoinduced Electron Transfer in a Molecular Donor-Acceptor Quartet. *The Journal of Physical Chemistry B* **2006**, *110* (24), 11730-11738; (g) Rajaram, S.; Armstrong, P. B.; Kim, B. J.; Fréchet, J. M. J., Effect of Addition of a Diblock Copolymer on Blend Morphology and Performance of Poly(3-hexylthiophene):Perylene Diimide Solar Cells. *Chemistry of Materials* **2009**, *21* (9), 1775-1777; (h) Wicklein, A.; Lang, A.; Muth, M.; Thelakkat, M., Swallow-Tail Substituted Liquid Crystalline Perylene Bisimides: Synthesis and Thermotropic Properties. *Journal of the American Chemical Society* **2009**, *131* (40), 14442-14453; (i) Balannik, V.; Wang, J.; Ohigashi, Y.; Jing, X.; Magavern, E.; Lamb, R. A.; DeGrado, W. F.; Pinto, L. H., Design and Pharmacological Characterization of Inhibitors of Amantadine-Resistant Mutants of the M2 Ion Channel of Influenza A Virus. *Biochemistry* **2009**, *48* (50), 11872-11882.

VI Conclusion and perspective

With the segment doubling strategy, helical nanosized molecular architectures have been successfully synthesized. Based on the chromatography-free large scale synthesis of quinolone-based octameric starting materials, coupling the oligomer acid chloride with its corresponding amine allowed us to prepare helical nanosized aromatic foldamers, up to approx. 9nm (64mer, 15.6 kDa). The solubility of 64mer, however, limits the further elongation of this series of oligomers. We found that introducing Br on foldameric backbone can give access to increasing the solubility of resulting foldamers. Then various nanosized foldamers containing multi-bromines on the backbones, showing good solubility, have been prepared, and the longest one comes to approx. 14 nm (96mer, 25.7 kDa).

The physicochemical properties of these nanosized foldamers in gas phase and solution have also been explored by using ion mobility mass spectrometry, NMR diffusion ordered spectroscopy and fluorescence anisotropy spectroscopy, respectively, in cooperation with other groups. Ion mobility mass spectrometry was employed to study the rigidity of helical structures of foldamers in gas phase. For bromine-free and brominated foldamers, the CCS results reveal that their helical structures in gas phase are conserved, revealing that these foldameric molecules are rigid enough in gas phase. The similar CCS values between bromine-free and brominated foldamers show that bromination does not affect the structure and the rigidity of foldamers in gas phase. The theoretical calculation for bromine-free foldamers give comparable CCS result as experiments does. Interestingly, for anhydride type of foldamers, three CCS values for one foldamer were observed, indicating that three conformations of this type of foldamers present in gas phase, which is probably caused by the flexible anhydride bond. This interesting phenomenon is now studied in more details. NMR diffusion ordered spectroscopy gave access to estimating the translational diffusion of foldamers in solution and separating spectrally a series of foldamers by their diffusion coefficients. As the number of quinoline monomers increases, their diffusion coefficients decrease. The linear dependences of diffusion coefficients on the reciprocal cubic root of molecular weight and on that of the number of

quinoline unit in foldamer sequence have been revealed. The resulting hydrodynamic radii of these foldamers generally increase with the incremental number of monomers in foldamer sequences. Even though the correction factors are different due to the geometries of the foldamers, the resulting hydrodynamic radii display a linear relationship with their corresponding cubic root of molecular weight and with that of the number of quinoline unit in foldamer sequence. All these experimental results about diffusion coefficient and hydrodynamic radius have been explained by the theoretical derivation. Fluorescence anisotropy revealed the occurrence of rotational diffusion of foldamers in solution and this movement is affected by the viscosity of solvent and the size of foldamers.

Mechanochemistry of foldamers were also investigated with atomic force spectroscopy-based single molecule force spectroscopy (AFM-SMFS). The preliminary results show that plateau-like curves took place, which was attributed to the successive breaking of the non-covalent forces holding the helical structure of the foldamer molecule. The length of this plateau is directly related to the size of the foldamer molecules. The results obtained in freshly distilled (anhydrous) DMF differed from that in water-included DMF, which suggests that the solvent has a significant effect on the structure and stability of these folded secondary structures.

Electron transfer bridged by nanosized foldamers has been studied and disclosed that the rates of charge separation in these studied molecular systems are fast (nanosecond scale) and the rates of charge recombination take place with an extremely slow speed (microsecond scale). The corresponding mechanism of electron transfer is discovered as multiple-step way – the hopping mechanism.

Since the protein-/nano- sized aromatic foldamers have been successfully prepared, the further research into these architectures will give access to the better understanding of their functionality/application and of how nature works. For example, the ‘block foldamers’ in which the bromine-free foldameric segment(s) and brominated foldameric segment(s) are inserted with one another on purpose can be achieved with larger size and good solubility since the solubility of brominated foldamers has been proven as good. Successful synthesis of this series

of 'block foldamers' permits us to investigate the amphiphile^x and self-assembly. The construction of special architectures based on these linear helical foldamers is another approach to expand the field of foldamer research, such as the dumbbell-shape molecule (the existing foldamers as the bar) and the tertiary/quaternary molecular structure – covalently or non-covalently bind the existing helical structure(s) with another structures (e.g., strand, turn and/or coil). The handedness of helix (right-handed, P, and left-handed, M) in these existing and future-prepared nanosized foldamers is also worth the investigation to understand better the physicochemical property of these aromatic foldamers. Applications of these existing and future-designed foldamers to the detection of ambient stimuli, the construction of covalent/metal organic framework, the delivery of molecules/medicines along the foldameric path, the template for self-replication and the construction of artificial muscle are fascinating and worthwhile to be explored. For the photo-induced electron transfer, crossover of mechanism through foldamers (≤ 9 mer) is a very much worthy research topic to be investigated.

^x The amphiphilic property of foldamers also could be achieved by another approaches, e.g. combining the existing foldamers with hydrophilic peptide, DNA sequence or polymer with certain length.

Synthèse et propriétés physiques de foldamères hélicoïdaux de quinolines de taille nanométrique : Structure, Dynamique et transport électronique photo-induit.

Résumé : Ce travail présente la synthèse, la caractérisation et l'utilisation (transfert électronique photo-induit) de foldamères de taille nanométriques constitués d'unités quinolines. Grâce à une stratégie de synthèse de doublement de segment une grande variété d'oligomères (jusqu'à 96 unités) ont pu être préparés à partir du synthon 8-aminoquinoline-2-carboxylate.

Leurs propriétés dynamiques de ces objets ont été étudiées en solution et en phase gazeuse. La spectrométrie de masse de mobilité ionique a permis de déterminer leur conformation en phase gazeuse. Les expériences de RMN DOSY et d'anisotropie de fluorescence ont permis de déterminer leurs propriétés de diffusion (translationnelle et rotationnelle). Ces résultats ont révélé que ces foldamères sont rigides et que leur architecture hélicoïdale est conservée.

Le transport électronique photo-induit à travers ces foldamères de taille nanométrique ont été étudiés et le mécanisme de transfert ainsi que son efficacité ont été déterminés pour une série de composés de tailles variables.

Mots clés : Chimie supramoléculaire, foldamères, quinolone, nanométrique, structure hélicoïdale, spectrométrie de masse de mobilité ionique, RMN DOSY, anisotropie de fluorescence, transport électronique.

Synthesis and Physical Properties of Helical Nanosized Quinoline-based Foldamers – Structure, dynamics and photoinduced electron transport

Abstract : Herein, synthesis, characterization and application (photoinduced electron transport) of nanosized quinoline-based foldamers have been explored. With double segment strategy, a variety of helical nanosized foldamers (up to 96 quinoline units) were successfully prepared based on 8-aminoquinoline-2-carboxylic acid monomer.

The dynamic properties in gas phase and solution were investigated. Ion mobility mass spectrometry afforded access to the conformation state of foldamers in gas phase; DOSY and fluorescence anisotropy assessed the diffusion (translational and rotational, respectively) of foldamers in solution. All of these techniques revealed that quinoline-based foldamers are rigid and that helical conformation is conserved.

Photoinduced electron transport through nanosized foldamer was also studied and the mechanism and the transport ratios were revealed.

Keywords : Supramolecular chemistry, foldamer, quinoline, nanosized, helix, structure, dynamics, ion mobility mass spectrometry, diffusion ordered NMR spectroscopy, DOSY, fluorescence anisotropy, electron transfer.